PROCEEDINGS OF SPIE

SPIE—The International Society for Optical Engineering

Laser Optics '98

Fundamental Problems of Laser Optics

Nikolay N. Rosanov
Editor

22–26 June 1998
St. Petersburg, Russia

Organized by
Institute for Laser Physics, S.I. Vavilov State Optical Institute
General Physics Institute, Russian Academy of Sciences
P.N. Lebedev Physical Institute, Russian Academy of Sciences
Institute for Fine Mechanics and Optics, Technical University
Russian National Center of Laser Physics, St. Petersburg State University
Scientific Council on Coherent and Nonlinear Optics, Russian Academy of Sciences
SPIE—The International Society for Optical Engineering
SPIE Russia Chapter
OSA—Optical Society of America
EOS—European Optical Society
ROS—Rozhdestvensky Optical Society
Government of St. Petersburg

Volume 3685

PROCEEDINGS OF SPIE
SPIE—The International Society for Optical Engineering

Laser Optics '98

Fundamental Problems of Laser Optics

Nikolay N. Rosanov
Editor

22–26 June 1998
St. Petersburg, Russia

Organized by
Institute for Laser Physics, S.I. Vavilov State Optical Institute • General Physics Institute, Russian Academy of Sciences • P.N. Lebedev Physical Institute, Russian Academy of Sciences • Institute for Fine Mechanics and Optics, Technical University • Russian National Center of Laser Physics, St. Petersburg State University • Scientific Council on Coherent and Nonlinear Optics, Russian Academy of Sciences • SPIE—The International Society for Optical Engineering • SPIE Russia Chapter • OSA—Optical Society of America • EOS—European Optical Society • ROS—Rozhdestvensky Optical Society • Government of St. Petersburg

Supported by
Ministry of Science and Technical Policy of Russia • Ministry for Economics of Russia • Ministry for Education of Russia • Russian National Foundation for Basic Research • SPIE—The International Society for Optical Engineering • Lawrence Livermore National Laboratory (USA) • USAF European Office of Aerospace Research and Development • OSA—Optical Society of America

Sponsored by
Technische Zentrum Nord (Germany)
Thomson-CSF (France)
JENOPTIK Technologie GmbH (Germany)

Published by
SPIE—The International Society for Optical Engineering

SPIE PROCEEDINGS SERIES

Volume 3685

Please use the following format to cite material from this book:
Author(s), "Title of paper," in *Laser Optics '98: Fundamental Problems of Laser Optics*, Nikolay N. Rosanov, Editor, Proceedings of SPIE Vol. 3685, page numbers (1999).

ISSN 0277-786X
ISBN 0-8194-3159-1

Published by
SPIE—The International Society for Optical Engineering
P.O. Box 10, Bellingham, Washington 98227-0010 USA
Telephone 360/676-3290 (Pacific Time) • Fax 360/647-1445

Printed in the United States of America.

Contents

Conference Committees

Conference Honorary Chairs

Alexander M. Prokhorov, General Physics Institute, Russian Academy of Sciences
Charles H. Townes, University of California/Berkeley (USA)

Organizing Committee

Arthur A. Mak, *Chair,* Institute for Laser Physics, S.I. Vavilov State Optical Institute
Alexander A. Andreev, *Cochair,* Institute for Laser Physics, S.I. Vavilov State Optical Institute
Vladimir M. Arpishkin, *Cochair,* ROS—Rozhdestvensky Optical Society
E.I. Akopov, SPIE Russia Chapter
T. Fujioka, Tokai University (Japan)
O.D. Gavrilov, Institute for Laser Physics, S.I. Vavilov State Optical Institute
A.S. Gorshkov, Institute for Laser Physics, S.I. Vavilov State Optical Institute
V.B. Kryuchenkov, International Science Technology Center
H. Lowdermilk, Lawrence Livermore National Laboratory (USA)
E.I. Makurov, S.I. Vavilov State Optical Institute
V.B. Smirnov, St. Petersburg State University
E. Spitz, Thomson-CSF (France)
Yu.A. Straus, S.I. Vavilov State Optical Institute
B.S. Zykov, International Science Technology Center

Program Committee

Arthur A. Mak, *Chair,* Institute for Laser Physics, S.I. Vavilov State Optical Institute
Alexander A. Andreev, *Cochair,* Institute for Laser Physics, S.I. Vavilov State Optical Institute
Leonid N. Soms, *Scientific Secretary,* Institute for Laser Physics, S.I. Vavilov State Optical Institute
P.A. Apanasevich, B.I. Stepanov Institute of Physics (Belarus)
S.N. Bagaev, Institute of Laser Physics
N.G. Basov, P.N. Lebedev Physical Institute
V.I. Bespalov, Institute of Applied Physics
F.V. Bunkin, General Physics Institute
Yu.D. Golyaev, Polyus Research and Development Institute
V.M. Gordienko, M.V. Lomonosov Moscow State University
V.P. Kandidov, M.V. Lomonosov Moscow State University
Ya.I. Khanin, Institute of Applied Physics
O.A. Kocharovskaya, Institute of Applied Physics
N.I. Koroteev, M.V. Lomonosov Moscow State University
V.I. Kovalev, P.N. Lebedev Physical Institute

I.B. Kovsh, Laser Association
V.V. Lyubimov, Institute for Laser Physics, S.I. Vavilov State Optical Institute
A.A. Manenkov, General Physics Institute
Yu.T. Mazurenko, S.I. Vavilov State Optical Institute
A.P. Napartovich, TRINITI
A.N. Oraevsky, P.N. Lebedev Physical Institute
V.Ya. Panchenko, NICTL Laser Research Center
P.P. Pashinin, General Physics Institute
G.T. Petrovskiy, S.I. Vavilov State Optical Institute
L.A. Rivlin, Moscow State Institute of Radio Engineering, Electronics and Automation
N.N. Rosanov, Institute for Laser Physics, S.I. Vavilov State Optical Institute
A.S. Rubanov, B.I. Stepanov Institute of Physics (Belarus)
V.A. Serebryakov, Institute for Laser Physics, S.I. Vavilov State Optical Institute
I.A. Shcherbakov, General Physics Institute
V.E. Sherstobitov, Institute for Laser Physics, S.I. Vavilov State Optical Institute
A.P. Shkadarevith, Peleng (Belarus)
V.B. Smirnov, St. Petersburg State University
M.S. Soskin, Institute of Physics (Ukraine)
A.P. Sukhorukov, M.V. Lomonosov Moscow State University
V.I. Ustyugov, Institute for Laser Physics, S.I. Vavilov State Optical Institute
V.V. Valuev, GPO Almaz
E.A. Viktorov, Institute for Laser Physics, S.I. Vavilov State Optical Institute
G.M. Zverev, Polyus Research and Development Institute

American Local Committee

Howard Lowdermilk, *Chair,* Lawrence Livermore National Laboratory (USA)
Sherene Goulart, *Secretary,* Lawrence Livermore National Laboratory (USA)

Asian Local Committee

Sadao Nakai, *Chair,* Osaka University (Japan)
Tomoo Fujioka, *Cochair and Scientific Secretary,* Tokai University (Japan)

European Local Committee

Erich Spitz, *Chair,* Thomson SA (France)
Arnaud Brignon, *Scientific Secretary,* Thomson-CSF (France)
Henri Rajbenbach, *Scientific Secretary,* European Commission (Belgium)

SESSION 1

Laser Dynamics

Vertical Cavity Semiconductor Lasers with Polarization-Controlling Feedback

N.A. Loiko[a], A.V. Naumenko[a], and N. B. Abraham [c]
[a] *Institute of Physics, Academy of Sciences of Belarus, Scaryna ave. 70, 220072 Minsk, BELARUS*
[c] *Department of Physics, Bryn Mawr College, 101 N. Merion Ave., Bryn Mawr, PA 19010-2899, USA*

Abstract

The anisotropy and time-delayed nature of external feedback modify polarization switching thresholds and dynamical phenomena which are studied analytically and numerically for sensitivity to misalignment of the axes of intrinsic and external anisotropies.

Keywords: *light polarization, VCSEL, polarization dynamics, polarization switching.*

I. INTRODUCTION

Linearly polarized light emitted from cylindrical vertical-cavity surface-emitting lasers (VCSELs) is less stable than that of edge emitting lasers. The orientation of polarization can vary from one VCSEL to another, depending on the directions of the crystal axes, stresses and geometrical asymmetries. Polarization switching and polarization selection are governed by the birefringence of the medium and the degree of saturated dispersion as governed by the alpha-factor and the injection current. In various applications of VCSEL's, it is useful to be able to control the polarization of the output light. It has been shown experimentally that switching between linearly polarized states can be achieved by external feedback which enhances one of them [1]. The theoretical description of these experiments has been carried out independently by Stephan and co-workers [2] and in our work [3]. Many similar changes in stability and sustained dynamical switchings have been found. New Hopf instabilities arising from the delay in the feedback loop have been revealed [3].

In the present work we give a detailed analysis of this situation and also consider the practically inevitable experimental situation of a misalignment of the axes of the intrinsic amplitude and phase anisotropies of the VCSEL with the axes of the feedback anisotropy. We assume for the present work that the intrinsic amplitude and phase anisotropies of the VCSEL are diagonalized by the same axes. In the section 2 we present a modification of the model [3] for describing the effects of misaligned polarization-selective feedback. Possible steady-states are found and some aspects of their stability are discussed in section 3. Conclusions are given in section 4. This work is the first step in the development of the general model for consideration of polarization dynamics in VCSEL subjected by the feedback with arbitrary anisotropy axes.

SPIE Vol. 3685 • 0277-786X/99/$10.00

II. MODEL

For our model of the dynamics of semiconductor lasers with polarization-selective feedback such as the VCSEL system , we began with the polarization-sensitive rate equations for a quantum well VCSEL [4,5] and modified them to include external anisotropic feedback in manner similar to [3]:

$$\frac{d}{dt}\bar{E} = \hat{\mathbf{G}}\cdot\bar{E} + \sigma\, e^{-i\omega\tau}\,\hat{\chi}\cdot\bar{E}_\tau \tag{1}$$

$$\frac{d}{dt}\bar{N} = \bar{\mu} + \hat{\mathbf{S}}\cdot\left|\bar{E}\right|^2, \tag{2}$$

Where $N_\pm = N \pm n$, $\gamma = \gamma_a + i\,\gamma_p$, column vectors are denoted by $\bar{\ }$: $\bar{E} \equiv (E_+, E_-)$, $\left|\bar{E}\right|^2 \equiv \left(|E_+|^2, |E_-|^2\right)$, $\bar{N} \equiv (N, n)$, $\bar{E}_\tau = \bar{E}(t-\tau)$, $\bar{\mu} = (\mu - N, -\gamma_s n)$; while matrices $\hat{\ }$ are $\hat{\mathbf{G}} = \begin{pmatrix} k(1+i\alpha)(N_+ - 1) & \vdots & -\gamma \\ -\gamma & \vdots & k(1+i\alpha)(N_- - 1) \end{pmatrix}$, $\hat{\mathbf{S}} = -\begin{pmatrix} N_+ & N_- \\ N_+ & -N_- \end{pmatrix}$ (in the basis $\bar{N}' = (N_+, N_-)$ this matrix is diagonalized $\hat{\mathbf{S}}' = -2\begin{pmatrix} N_+ & 0 \\ 0 & N_- \end{pmatrix}$), $\hat{\chi}$ is the polarization device matrix. For the case of a linear polarizer inserted in the external cavity with the angle of polarization χ in respect to the x-axis, $\hat{\chi} = \frac{1}{2}\begin{pmatrix} 1 & e^{2i\chi} \\ e^{-2i\chi} & 1 \end{pmatrix}$. $E_\pm = \frac{1}{\sqrt{2}}(E_x \pm i\,E_y)$ where E_x and E_y are $\hat{x}$ - and $\hat{y}$ - polarized components of the slowly varying amplitude of the electromagnetic field; ω is the solitary laser frequency; N is the total population difference between conduction and valence bands; n is the difference of the population differences for the two allowed transitions between magnetic sublevels; k is the mean decay rates of the two linearly polarized components of the field while γ_a is the anisotropic field loss rate (positive γ_a gives the $\hat{y}$-polarized component a lower threshold); γ_p represents the effect of linear birefringence (frequency shift) of the medium, such as is commonly caused by anisotropic stress; α is the linewidth enhancement factor; μ is the normalized injection current, which takes the value 1 at the lasing threshold; γ_s is the decay rate for differences in the populations of the different magnetic sublevels, which accounts for their elimination by both spontaneous emission and spin-flip relaxation processes, σ is the feedback strength. The parameters k, γ_a, γ_p and γ_s are normalized to the decay rate Γ of the total carrier population; time t and the delay time τ are normalized to Γ^{-1}.

III. STEADY STATES

The solutions of the system(1)-(2) are found in the form $E_\pm = Q_\pm\, e^{\pm i\psi + i\Omega t}$. We will refer to these as "steady state solutions" (since the intensity and population variables, and the optical frequency, are all constants) and since shifts of the optical frequency are a trivial sort of time dependence. In this case Eqs.(1) can be reduced to:

$$\hat{\rho}\cdot\bar{\varepsilon} = 0, \tag{3}$$

where $\bar{\varepsilon} = (\varepsilon_+, \varepsilon_-)$, $\varepsilon_\pm = Q_\pm\, e^{\pm i\psi}$, and $\hat{\rho} = \hat{\mathbf{G}} + 2\beta\,\hat{\chi} - i\Omega\hat{\mathbf{I}} = \begin{pmatrix} \rho_+ & \alpha_+ \\ \alpha_- & \rho_- \end{pmatrix}$, $\rho_\pm = s(N_\pm - 1) + \beta - i\Omega$, $s = k(1+i\alpha)$, $\beta = \frac{1}{2}\sigma\, e^{-i\tau(\Omega+\omega)}$, $\alpha_\pm = -\gamma + \beta\, e^{\pm i2\chi}$.

The system (3) has a non trivial solution when $\det\hat{\rho}=0$. This condition gives a system of two real equations with respect to N and n: $(N-1)^2-n^2+2(N-1)b-c=0$, where frequency-shift functions b and c are: $b=\frac{1}{s}(\beta-i\Omega)$, $c=d-b^2$, $d=\frac{1}{s^2}\alpha_+\alpha_-$. The system can be resolved with respect to the populations inversions only if $\operatorname{Im}b\neq 0$. In this case expressions for N and n as functions of the frequency shift Ω and the control parameters are obtained: $N(\Omega)-1=\frac{1}{2}\frac{\operatorname{Im}c}{\operatorname{Im}b}=\frac{1}{2}\left(\frac{\operatorname{Im}d}{\operatorname{Im}b}-2\operatorname{Re}b\right)$, $n^2(\Omega)=\frac{1}{4\operatorname{Im}^2 b}\left\{|d|^2-\left(\operatorname{Re}d+2\operatorname{Im}^2 b\right)^2\right\}$.

Eqs. (2) yield the following steady values of field amplitudes as functions of the inversions N, n and therefore frequency Ω: $Q_\pm^2(\Omega)=\frac{\mu-N\mp\gamma_s n}{2N_\pm}$.

The steady frequency-shift Ω can be found from system (3):

$$|\rho_+(\Omega)|^2 Q_+^2(\Omega)=|\alpha_+|^2 Q_-^2(\Omega). \tag{4}$$

The steady field phase difference ψ is also determined from Eqs.(3) (e.g., from $e^{-i2\psi}=-\frac{\rho_+Q_+}{\alpha_+Q_-}$): $\psi=\frac{1}{2}\arg\left(-\frac{\rho_+Q_+}{\alpha_+Q_-}\right)$.

If the control parameters are chosen so that $\operatorname{Im}b=0$ and $\operatorname{Im}c=0$ (or $\operatorname{Im}d=0$) one of the equations of the system $\det\hat{\rho}=0$ is reduced an identity. So we have in this case only one relation between the variables N and n: $(N-1)^2-n^2+2(N-1)\operatorname{Re}b-\operatorname{Re}c=0$, which means it is impossible to find a solution using the above algorithm for these values of the parameters. Equations $\operatorname{Im}b=0$ and $\operatorname{Im}c=0$ results in a co-dimension one restriction on the control parameters and yields polynomial of fourth degree for the frequency Ω. Thus when the frequency is fixed, instead of Eq. (4) an analogous equation for evaluating N (or n) has to be solved.

The stability of the steady solutions of the system (1) is determined by roots of a quasipolynomial having the following form:

$$e^{-2z\tau}\sum_{k=0}^{4}z^k a_k+e^{-z\tau}\sum_{k=0}^{5}z^k b_k+\sum_{k=0}^{6}z^k a_k=0, \tag{5}$$

where the coefficients depend on the steady states values of the variables. We do not give the expressions for the coefficients because they are complicated. We consider here the static (saddle-node and pitchfork) bifurcations ($z=0$) for the most part. At $\chi=0$ this expression is factorized into two separate parts that govern, respectively, the stability of one of two orthogonal linearly polarized solutions and for saddle-node and pitchfork bifurcations [3].

1. Linearly polarized solutions.

Using previous definitions, the linearly polarized solutions ($Q_+=Q_-$) can be found from two conditions: 1) $|\alpha_+|=|\alpha_-|$ which gives $\operatorname{Im}(\gamma\beta^*)\sin 2\chi=0$ and 2) $n(\Omega)=0$ (this requires separate consideration when $\operatorname{Im}b(\Omega)=0$). The specific form of the first condition holds for two types of linearly polarized solutions : (i) - the first type exists only when the polarizer axes are parallel to one of the VCSEL anisotropy axes ($\hat{x}$ or $\hat{y}$) ($\sin 2\chi=0$), and (ii) -the second type exists for any other orientation of the polarizer when $\operatorname{Im}(\gamma\beta^*)=0$.

For case (i) there is the well known structure of external cavity modes (and antimodes) oriented along the polarizer axis ($\hat{x}$-solutions) and one $\hat{y}$-mode orthogonal to the polarizer axis (optical feedback injection is absent in this mode), which appear for each control parameter value. This is a one-codimension solution, if we take into account the one fixed parameter $\chi=\frac{\pi l}{2}$, l - integer.

The second condition is reduced to $\mathrm{Im}\, s^* \left(2\beta - (-1)^l \gamma - i\Omega\right) \mathrm{Im}\, s^* \left((-1)^l \gamma - i\Omega\right) = 0$. Then the frequencies of the external cavity modes and the mode orthogonal to them can be obtained from the following equations, respectively: $(-\alpha\gamma_a + \gamma_p)(-1)^l + \Omega + \sigma\left[\alpha \cos\tau\,(\Omega+\omega) + \sin\tau\,(\Omega+\omega)\right] = 0$ and $\Omega = (-\alpha\gamma_a + \gamma_p)(-1)^l$. These solutions and their stability have been considered in detail in Refs [2,3].

Besides these, for a special choice of feedback parameters there exist additional linearly polarized solutions with arbitrary orientation [3] (the phase shift ψ between E_+ and E_- field components is arbitrary). For them $\rho_+ = \rho_- = \alpha_+ = \alpha_- = 0$ (or in another words $n(\Omega) = 0$, $\mathrm{Im}\, b(\Omega) = 0$ and $d = 0$ - compare these expressions with the solvability of $\det\hat{\rho} = 0$). Conditions for the existence of such solutions are: (1) $\gamma_a^2 + \gamma_p^2 = \frac{\sigma^2}{4}$ (condition on feedback strength σ), and (2) $\alpha\gamma_a - \gamma_p = \Omega_k^0$, where the frequency shift $\Omega_k^0 = -\frac{1}{\tau}(\arg\gamma + \tau\omega \bmod 2\pi + 2\pi k)$ and $k = 0, \pm1, \pm2, \ldots$ (condition on the feedback phase or the feedback delay $(\omega\tau,\, \tau)$). In addition, conditions (3) on the misalignment angle must be satisfied for these states: $\chi = 0$. Thus the co-dimension for these arbitrarily oriented linearly polarized solutions is equal to three.

For arbitrary orientation of the polarizer (case (ii)) the condition ($|\alpha_+| = |\alpha_-|$) reduces to: $2\Lambda\gamma_i(\gamma_i \cos 2\chi - \Omega_k) = \gamma_i^2 - \Omega_k^2$ (or $\cos 2\chi = \frac{\lambda_i^2 - \Omega_k^2 + 2\Omega_k\gamma_i\Lambda}{2\Lambda\lambda_i^2}$), where $\gamma_i = \gamma_p - \alpha\gamma_a$, frequency shift of the solutions $\Omega_k = -\frac{1}{\tau}(\arg\gamma + \tau\omega \bmod 2\pi - \pi k)$, k - is an integer and $\Lambda_k = (-1)^k \frac{\sigma}{2|\gamma|}$. The total population difference of these states is given by $N = 1 - \frac{\gamma_a}{k}\Omega_k$. So we have again as in case (i) the condition on the feedback parameters $(\omega\tau,\, \tau,\, \chi,\, \sigma)$ (a co-dimension one situation). The difference with case (i) lies in the impossibility to fix one of the feedback parameters (e.g., χ) and to move continuously along the branch of linear polarized solutions when some another parameter (σ or τ) is swept. Only simultaneous changes of two control parameters (e.g., χ and σ) keep the system on this branch.

These solutions have a mode structure similar to the structure of the $\hat{x}$-polarized solutions. Figure 1 demonstrates typical features of the linear polarized steady states vs. the feedback time-delay τ. For each value of the delay there are only finite number of the misalignment angles at which these states appear. There are two sets of the solution branches. The modes with number k equal to 2,4,6,..., 1,-1,-3,... - form the first set of branches. Any branch exists in the finite interval of the time delay. Branches of the second set (number k = 3,5,7,..., 0,-2,-4,...) arise approximately at the same values of χ but do not disappear with increasing τ. So when the delay τ is increased, the number of values of the angle χ at which these linearly polarized states exist also increases. Some parts of the branches are stable; some parts are unstable due to static bifurcations (we don't take into account Hopf instabilities here).

Figure 2a presents the corresponding misalignment angle χ vs. feedback strength σ. The linear polarized solutions exist only in a finite interval of σ. However this interval is sufficiently wide that the feedback anisotropy can exceed the VCSEL's anisotropy and the angle of the polarization vector orientation ψ can be changed over a range of values $(0 - \pi/2)$, when the misalignment angle χ is changed in the interval $(0; \pi/2)$ (Fig.2b).

At $\chi = \frac{\pi l}{2}$ this type (case (ii)) of linearly polarized solution intersects the first type $\hat{x}$- and $\hat{y}$-linearly polarized solutions (case (i)). Values of the control parameters in the point of intersection are given by the following equations: $\Omega_k = (-1)^l \gamma_i$ (orientation of these states is orthogonal to the external polarizer axis) and $\Omega_k = \gamma_i\left(2\Lambda - (-1)^l\right)$ (parallel orientation of linearly polarized

solutions and polarizer). These intersection points form a co-dimension-two set. If we introduce an additional restriction on the control parameters (so that the full co-dimension becomes equal to three) such that $\Lambda = (-1)^l$ (i.e. $|\gamma| = (-1)^k (-1)^l \frac{\sigma}{2}$) (this corresponds to the condition $\operatorname{Im} b = 0$) then these linearly polarized solutions coincide with the arbitrary oriented linearly polarized states (see above).

2. Circularly polarized solutions.

The circularly polarized solutions $e_\pm$ ($Q_\mp = 0$ and $Q_\pm \neq 0$) can exist for two restrictions on the control (feedback) parameters (i.e. co-dimension-two solutions). ($Q_\mp = 0 \Rightarrow \alpha_\mp = 0$, $\rho_\pm = 0$). These restrictions lead to: 1) (condition on feedback strength σ) $\gamma_a^2 + \gamma_p^2 = \frac{\sigma^2}{4}$, and 2) (condition on additional feedback parameters ($\omega\tau$, τ, χ)) $\Omega_k^c + |\gamma| \{\alpha \cos\phi_\mp + \sin\phi_\mp\} = 0$; where $\phi_\pm = \pm 2\chi - \arg\gamma$, frequency shift $\Omega_k^c = \frac{1}{\tau}(\phi_\mp - \tau\omega \bmod 2\pi + 2\pi k)$ and k is an integer. The second condition can be satisfied only when $|\Omega_k^c| \leq \sqrt{1+\alpha^2}\,|\gamma|$ and is reduced for $\chi = 0$ to $\alpha\gamma_a - \gamma_p = \frac{1}{\tau}(\arg\gamma + \tau\omega \bmod 2\pi + 2\pi k)$ [3]. The other steady characteristics of the circularly polarized solutions are: $n = \pm p$, $N = \mu - \gamma_s p$, $Q_\mp = \gamma_s p\,(\mu - p\,(\gamma_s + 1))^{-1}$, where $p = (\operatorname{Re} b + \mu - 1)\,(\gamma_s + 1)^{-1}$.

Along with circularly polarized states, at the same control parameter values there also exist elliptically polarized solutions. These possess the same frequencies Ω_k^c. Expressions for other steady characteristics of these solutions can be found from $\rho_\mp = 0$ and $\rho_\pm \neq 0$, which (together with Eq.(4) and relations between Q_+, Q_-, N, n obtained from (2)) lead to a fourth degree polynomial with respect to the populations N or n: $N_\pm |s|^2 n^2 (\mu - N \pm \gamma_s n) = N_\mp |\alpha_\mp|^2 (\mu - N \mp \gamma_s n)$ for $\alpha_+ = 0$ or $\alpha_- = 0$ correspondingly, where $N = 1 - n - \operatorname{Re} b$.

3. Elliptically polarized solutions. The elliptically polarized solutions can be found from the general equation (4) when $\operatorname{Im} b \neq 0$. The condition $n^2(\Omega) > 0$ gives frequency intervals in which Eq.(4) may be resolved with respect to these states. Moreover if $\chi = 0$, the expression $n(\Omega) = 0$ yields linearly polarized solutions. So for this case additional elliptically polarized steady states arise only when a corresponding pair of linearly polarized solutions already has arisen from changing one of the control parameters.

Intrinsic symmetry of the system, elliptical state and dynamics.

We consider in detail the case $\chi = 0$ and static bifurcations of the steady states for this case. Figure 3 demonstrates dependencies of the steady state characteristics of the linearly and elliptically polarized solutions versus the external feedback strength σ. Together with the linearly polarized solutions along the x-axis, forming the usual external-cavity-modes structure ($\hat{x}$-solutions) (light curves) and one mode linearly polarized along y-axis ($\hat{y}$-solution) (light curve 1) there are also elliptically polarized steady states (dark curve). In contrast to the $\hat{x}$-polarized solutions, the number of which is increased when the external feedback strength σ is increased (these solutions only arise by saddle-node bifurcations), elliptically polarized modes exist only in finite interval of σ and can arise or disappear due to both saddle-node bifurcations and pitchfork bifurcations (intersection points of the elliptically and linearly polarized solutions).

System (1) at $\chi = 0$ has a symmetry property with respect to the following changes of the dynamical variables: $E_\pm \to E_\mp$, $n \to -n$, $N \to N$. So any solution with nonzero n has a symmetric paired state with the opposite value of n. For example, a twin elliptically polarized state with exchanged $E_\pm$ always exists for any elliptically polarized steady state, by contrast a linearly polarized state is unique because it is not changed by the variable substitutions. Thus saddle-node

bifurcations of the elliptically polarized states occur also only in pairs, leading to the appearance (or disappearance) of two elliptically polarized modes (nodes) and two antimodes (saddles) with identical stability properties. More details of such bifurcation points are depicted in Fig. 4b,d . As a result of the pitchfork bifurcations, two elliptically polarized states appear in the phase space, splitting from the linearly polarized state (or disappear in colliding with it). A clearer view of the appearance and disappearance of the elliptically polarized solutions as a result of pitchfork bifurcations is presented in Fig. 4a,c. This linearly polarized state changes its stability at the bifurcation point. In the Figure there are both subcritical and supercritical cases of the pitchfork bifurcation. Points of pitchfork bifurcation were found in [3] as the points of bifurcation leading to the instability arises from perturbations of the orthogonal-polarization.

For small values of σ, the elliptically polarized solution is connected with the main $\hat{x}$-polarized mode (the $\hat{x}$-polarized mode existing at $\sigma = 0$) and with the $\hat{y}$-polarized mode and it is stable with respect to static bifurcations. When the feedback strength σ is increased, the new external-cavity $\hat{x}$-polarized modes are born and the elliptically polarized steady states arise from one of the linearly polarized solutions ($\hat{x}$-mode or $\hat{x}$-antimode) and then collide and disappear with another linearly polarized solution belonging to the same external-cavity branch (with $\hat{x}$-antimode or $\hat{x}$-mode correspondingly). Some parts of these elliptically polarized branches can be stable. For large enough σ and τ most of the $\hat{x}$-polarized solutions become unstable with respect to perturbation of the same polarization due to Hopf bifurcations [3]. Some elliptically polarized states (always appearing in pairs) by contrast can be stable and easily observed. The frequencies of the elliptically polarized states are very close to the frequencies of the corresponding linearly polarized modes. This will be discussed further.

Characteristics of the elliptically polarized external cavity modes.

In this section we investigate in detail the elliptically polarized steady states as external cavity modes in their dependence on the feedback time-delay τ. Figure 5 represents dependencies of the steady states from the external cavity delay τ. As the delay τ is increased, the number of the linearly polarized solutions along the $\hat{x}$-axis increases continuously due to saddle-node bifurcations (light curves in the figure). The main $\hat{x}$-polarized mode is node (external cavity mode). The kind of $\hat{x}$-polarized solutions appearing when the delay is increased is determined from the alternation of saddles and nodes on the frequency axis.

In addition to the saddle-node bifurcations, each external cavity branch of $\hat{x}$-polarized solutions undergoes a pitchfork bifurcation as a result of which a pair of elliptically polarized states (dark curves in the figure) arise on the branches with negative frequency shifts Ω (the supercritical case) and disappear on the branches with positive frequency shifts Ω (the subcritical case). In the supercritical case a stable (we do not take into account possible Hopf instabilities) external-cavity-mode becomes unstable with respect to orthogonal perturbations and two stable symmetrical elliptically polarized steady states arise. Obviously, these states (more correctly their basins of attraction if the states is really stable) are separated from each other by a separatrix surface (or a stable manifold) of the bifurcating $\hat{x}$-polarized mode. Moreover, the different twins of elliptically polarized states belonging to different (but adjacent) $\hat{x}$-polarized external-cavity-branches are separated from each other by the separatrix manifolds of the $\hat{x}$-polarized antimode. In the subcritical case, at first two symmetrical pairs of elliptical steady states appear in the phase space of the system as a result of the saddle-node bifurcations. Then with increasing τ the unstable saddle elliptically polarized states

collide with $\hat{x}$-polarized animodes and that leads to an additional loss of stability of the $\hat{x}$-antimodes due to orthogonal perturbations . The stable elliptical mode in both cases (sub- and supercritical) continues to exist for all values of delay $\tau > \tau_{bif}$.

We have already mentioned above that the frequencies of the elliptically polarized states almost coincide with the frequencies of corresponding linearly polarized solutions. This is clearly visible in the figure. The points of pitchfork and saddle-node bifurcations of the elliptical states are connected with points at which linearly polarized $\hat{x}-$polarized modes appear. Thus the elliptically polarized modes form an external-cavity-mode structure similar to the structure of $\hat{x}-$polarized solutions, with approximately the same number of modes and values of frequencies. In the figure the feedback phase $\omega\tau$ is fixed , so only the macro-scale dependence of the steady state frequencies on the delay τ is plotted. Most of the external cavity modes (with linear or elliptical polarization) depicted in the figure are unstable due to Hopf bifurcations excluding, at least, the first two elliptically modes with negative frequency shifts Ω that arise as stable solutions. Nevertheless it is known that unstable states can play a key role in various control problems.

Misalignment and destroying the symmetry.

Let us consider at first what happens with symmetrical states when there is some misalignment in the polarization-selective optical feedback, i.e., when the axes of polarization device in the external resonator are slightly turned with respect to the VCSEL's anisotropy axes (the angle $\chi \neq 0$). The general system of equations (1) with nonzero χ does not have the symmetry described above. (Compare Fig.4c,d and 4e,f). Due to the misalignment, a frequency spliting takes place for the formerly frequency degenerate branches of the elliptically polarized mode. All the pitchfork bifurcations presented in Fig.3,4 are destroyed, transforming into saddle-node bifurcations of two various disjoint branches of solutions. Figs. 6a,b demonstrate pitchfork bifurcations at $\chi = 0$ (a) and corresponding to them saddle-node bifurcations at $\chi \neq 0$ (b) when the pump current μ is increased. The feedback parameters are such that at $\chi = 0$ there are three $\hat{x}$-polarized external cavity modes (curves 1-3), each of them undergoes a symmetry breaking bifurcation. Two $\hat{x}$-polarized steady states (mode (cv.1) and antimode (cv.2)) are connected with each other by one branch of elliptically-polarized solutions. When the misalignment is introduced ($\chi \neq 0$) the pitchfork bifurcations transform into saddle-node bifurcations and steady state branches of the former symmetrical elliptically polarized solutions are split each from other. The $\hat{x}$- and $\hat{y}$- linearly polarized solutions become also elliptically polarized with ellipticity increasing with the misalignment angle χ. These two set of elliptically polarized solutions form new branches of solutions consisting from parts of the old elliptically polarized solutions that exist and at $\chi = 0$ and new ones that appear in result of transformation of the $\hat{x}$- and $\hat{y}$- linearly polarized states (Fig.4e,f).

Figure 7 plots of the steady state values of the variables vs. the misalignment angle χ between polarization device's and VCSEL's anisotropy axes. Small circles at values of the angle equal to $\chi = \frac{\pi m}{2}$, where m is integer, denote the $\hat{x}$- and $\hat{y}$-linearly polarized states. In Fig.7a, the upper solution at $\chi = 0$ in the frequency plot is the $\hat{y}$-polarized mode. Another circle at $\chi = 0$ corresponds to the $\hat{x}$-polarized mode. This solution becomes elliptically polarized with increasing misalignment and disappears soon, colliding with one of the branches of the former symmetrical elliptically polarized solutions. The $\hat{x}$-polarized mode appears again at $\chi = \frac{\pi}{2}$ and disappears colliding with another branch of the former symmetrical elliptically polarized solutions. The orthogonally polarized modes exchange their roles with changing of the feedback phase (Fig. 7c,d). With increasing feedback

strength or delay, when new external cavity modes appear all the linearly polarized modes and elliptically polarized solutions corresponding to one external cavity branch belong to the same closed curve (Fig. 7e,f). So it is enough easy to retrace the mutual transformation of the linearly and elliptically polarized solutions. Points of intersection of the curves with the line $\eta = 0$ correspond to two sets of linearly polarized solutions. Points at which the derivative $d\Omega/d\chi$ is equal to infinity are saddle-node bifurcation points. The type of steady state solutions (saddle or node) depicted in the figure can be retraced from their types at $\chi = 0$. Figure 7 shows that the static stability of the steady state is changed with changes in the misalignment. For parameters determined above (Item 2) elliptically polarized solutions transform into circularly polarized solutions.

IV. CONCLUSION

We have formulated a theoretical model of VCSEL's subject to polarized feedback, including when the polarizer has an arbitrary orientation of its anisotropy axes. Experimentally the misalignment of the axes of the feedback anisotropy can be minimized, but to investigate the possibilities of new and useful dynamics from such misalignments, we have considered both small and large misalignments. As result of the misalignment, when the VCSEL is emitting linearly polarized light aligned with one of the intrinsic axes, the feedback is received by both linearly polarized intrinsic modes of the VCSEL. As a consequence, for almost all angles of misalignment, the steady state solutions of the system are elliptically polarized. Steady state solutions for the aligned and misaligned cases have been determined (linearly polarized, circularly polarized, and elliptically polarized). Conditions governing their static stability (saddle-node and pitchfork) are elucidated. The external feedback shifts the bifurcation points because it introduces additional phase and amplitude anisotropies depending on the time delay, the feedback strength and axes mismatch of the feedback. To get the full information on the stability, possible Hopf bifurcations must be studied more closely. We are doing this presently and the results will be reported elsewhere. The results reported here and previously reported results [3] show that the laser emission can be switched among orthogonally polarized solutions, linearly and elliptically polarized solutions and a variety of time dependent solutions of differing complexity as the feedback parameters are changed. Hence simple electro-optical control of the axes of the feedback might be used to encode information which would be transmitted by the polarization state, optical frequency or pulsation condition of the time dependent polarization of the laser.

V. ACKNOWLEDGEMENTS

The project has been funded in part by the US National Research Council under the Collaboration in Basic Science and Engineering Program. The contents of this publication do not necessarily reflect the view or policies of the NRC, nor does mention of trade names, commercial products or organizations imply endorsement by the NRC.

VI. REFERENCES

[1] Robert F, Besnard P, Chares M-L, Stephan G M 1995 Opt. and Quantum Electron. 27 805; Robert F, Besnard P, Chares M-L, Stephan GM 1996 IEE Proc.-Optoelectron. 143 104.

[2] Besnard P, Robert F, Chares M L and Stephan G M 1997 Physical Review A **56** 3191.

[3] Loiko N A, Naumenko A V and Abraham N B 1998 Quantum Semiclass. Opt. **10** 125.

[4] San Miguel M, Feng Q, and Moloney J V 1995 *Phys. Rev. A* **52** 1728.

[5] Martin-Regalado J, Prati F, San Miguel M, Abraham N B 1997 *IEEE J. Quantum Electron.* **33** 765.

VII. FIGURE CAPTIONS.

Fig. 1. Values of the misalignment angle χ at which the linearly polarized states exist vs. the external cavity delay τ. The unstable states are depicted by circles. The parameters are $\sigma = 3$, $\gamma_a = 0.1$, $k = 300$, $\alpha = 3$, $\gamma_s = 50$, $\mu = 1.2$, $\gamma_p = 3$, $\omega\tau = 1.2\pi$.

Fig. 2. Values of the misalignment angle χ at which the linearly polarized states exist(**a**) and the orientation angle ψ for the states (**b**) vs. the feedback strength σ. The delay $\tau = 0.3$, the mode number k is given at the curves, other parameters are the same as in Fig. 1.

Fig. 3. Three-dimensional representation of characteristics of the steady states (the frequency shift Ω and the population n) vs. the feedback strength σ. The $\hat{y}$-polarized states - light curve **1**,the $\hat{x}$-polarized solutions - other light curves, elliptically polarized states - dark curves). The parameter $\gamma_a = 0$, $\chi = 0$, $\tau = 0.6$, and other parameters are the same as in Fig. 1.

Fig. 4. Projections of steady characteristics vs. the feedback strength σ on the two dimensional planes. (**a,c,e**) -the projection on the plane: the feedback strength σ - the frequency shift Ω; (**b,d,f**) - the projection on the plane: the feedback strength σ - the ellipticity $\eta = \left(Q_+^2 - Q_-^2\right) / \left(Q_+^2 + Q_-^2\right)$. Unstable states are depicted by dark curves. Parameters are: $\gamma_a = 0$, $\gamma_p = 1$, $\tau = 0.1, \chi = 0$ (**a-d**), 0.01 (**e,f**), $\omega\tau/\pi = 0.54$ (**a,b**), 0.64 (**c-f**), others parameters as the same as in Fig. 1.

Fig. 5. The steady frequency shift vs. the external cavity delay τ. Light curves are the linearly polarized solutions (cv.1 - the $\hat{y}$ -polarized state, other curves of this type are $\hat{x}$-polarized states) and dark curves are elliptically polarized states. The parameters are the same as in Fig. 1, $\chi = 0$, $\gamma_a = 0$.

Fig. 6. The steady frequency shift Ω vs. the pump current μ. The misalignment angle $\chi = 0$ (**a**) and $\chi = 0.05\pi$ (**b**), the feedback strength $\sigma = 2$, $\gamma_a = 0$, $\tau = 0.6$. Other parameters correspond to Fig. 1. Curves 1,2,3 (**a**) are the $\hat{x}$-polarized states (cv.1,3 - modes and cv.2-antimode), curve 4 is the $\hat{y}$-polarized state and the other curves in the figure are elliptically polarized solutions.

Fig. 7. The frequency shift Ω (**a,c,e**) and the ellipticity η vs. the misalignment angle χ (**b,d,f**). The feedback strength $\gamma_p = 1$ (**a-d**),3 (**e,f**), $\sigma = 3$ (**a-d**), 2 (**e,f**), $\tau = 0.1$ (**a-d**), 0.6 (**e,f**), $\omega\tau/\pi = 0.48$ (**a,b**), 0 (**c,d**), 1.2 (**e,f**), other parameters are the same as in Fig. 4. Circles at $\chi = \pi l/2$ (l - integer) mark the $\hat{x}$-and the $\hat{y}$-linearly polarized states. Crosses represent linearly polarized solutions of other directions (case ii). Unstable states are marked by dark circles.

Fig.1

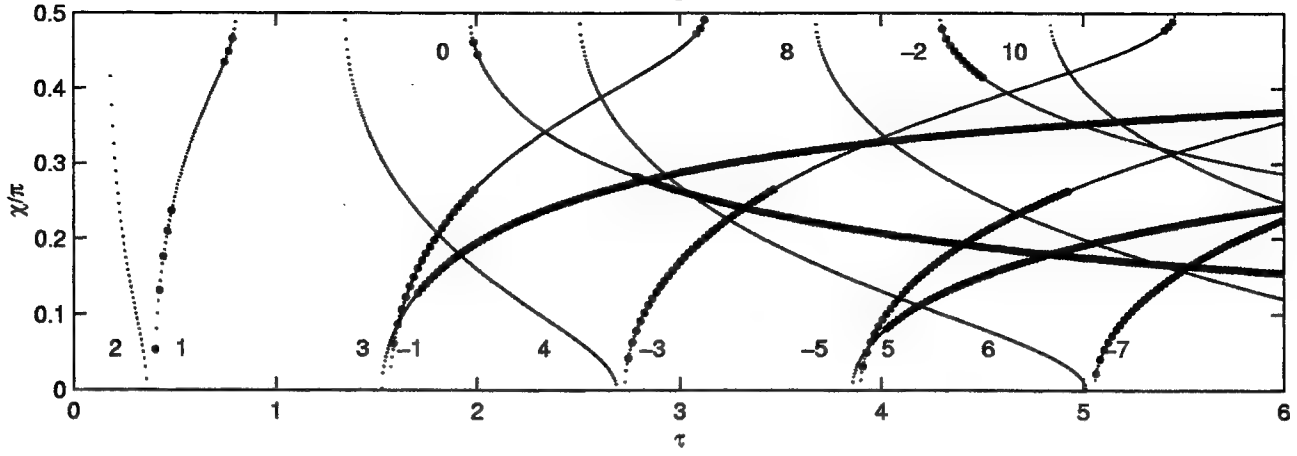

Fig.2a

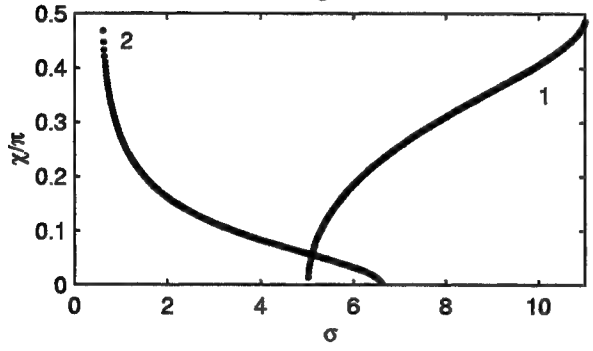

Fig.2b

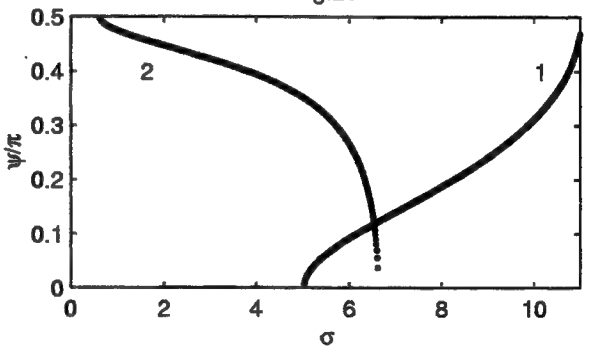

Fig.3

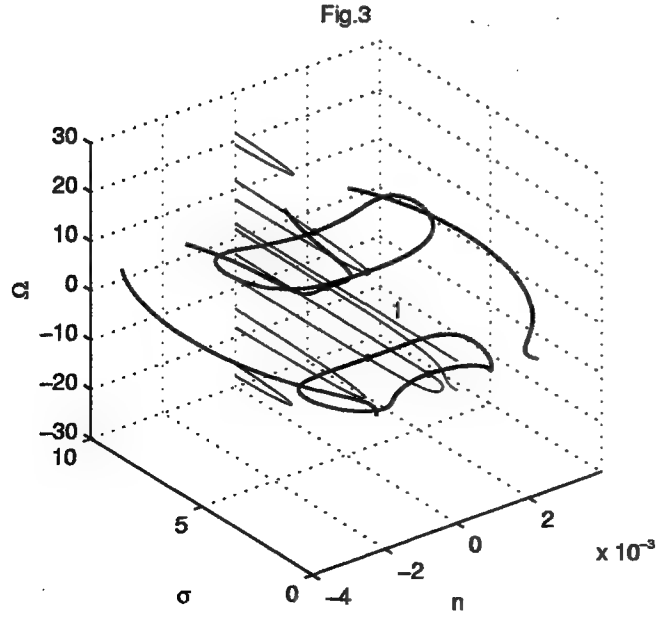

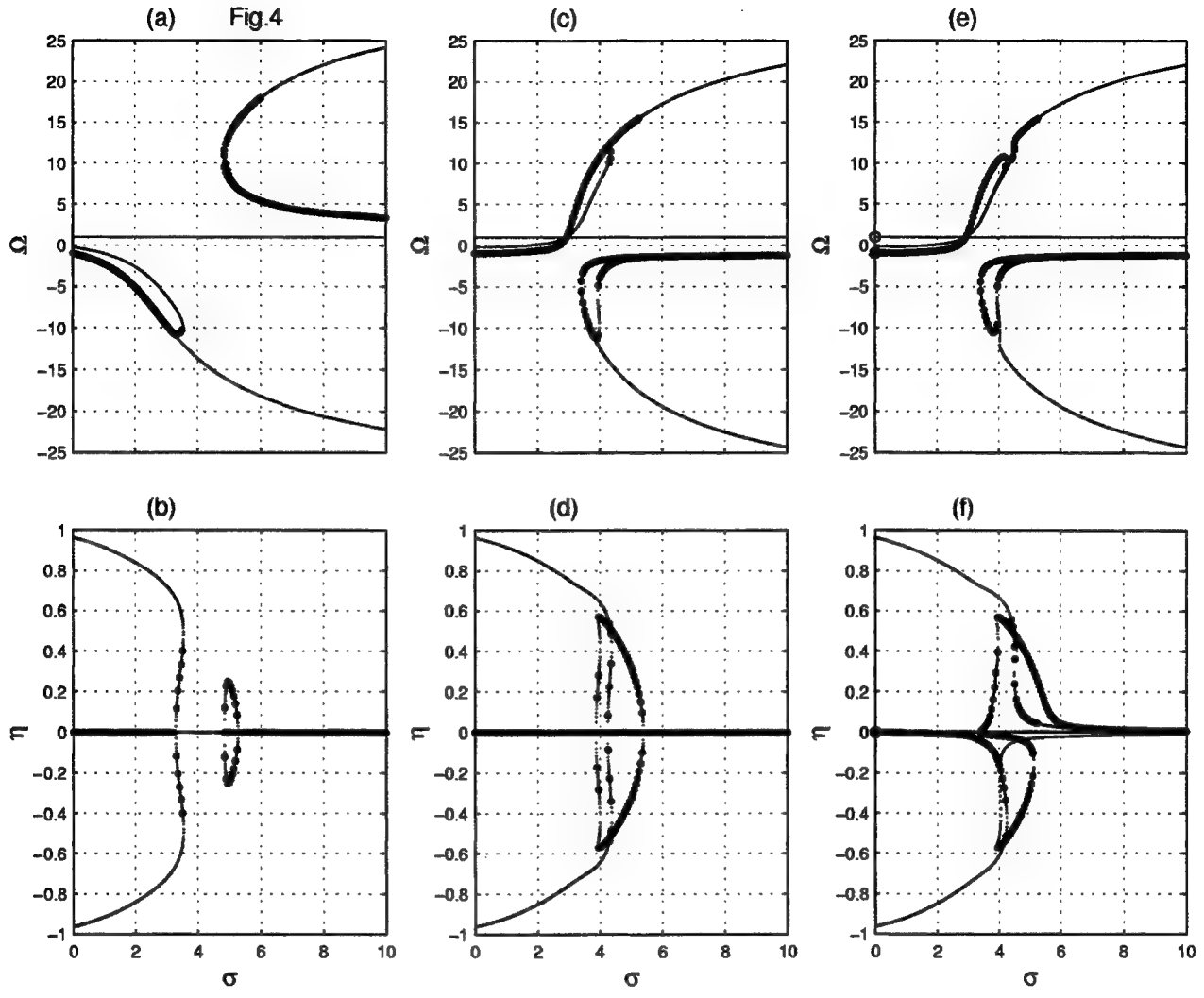

Fig.4

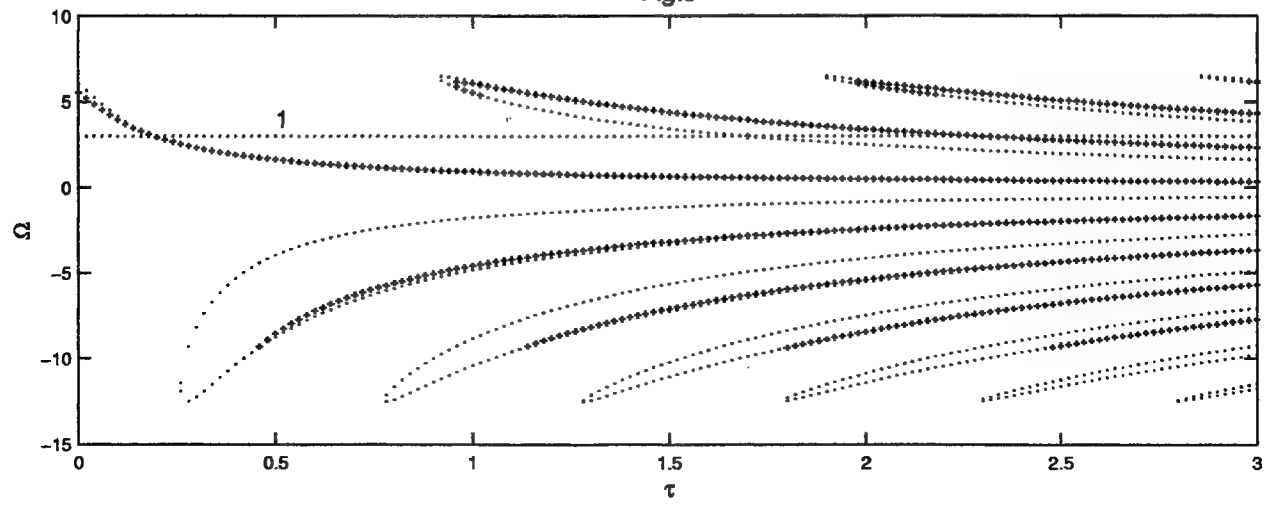

Fig.5

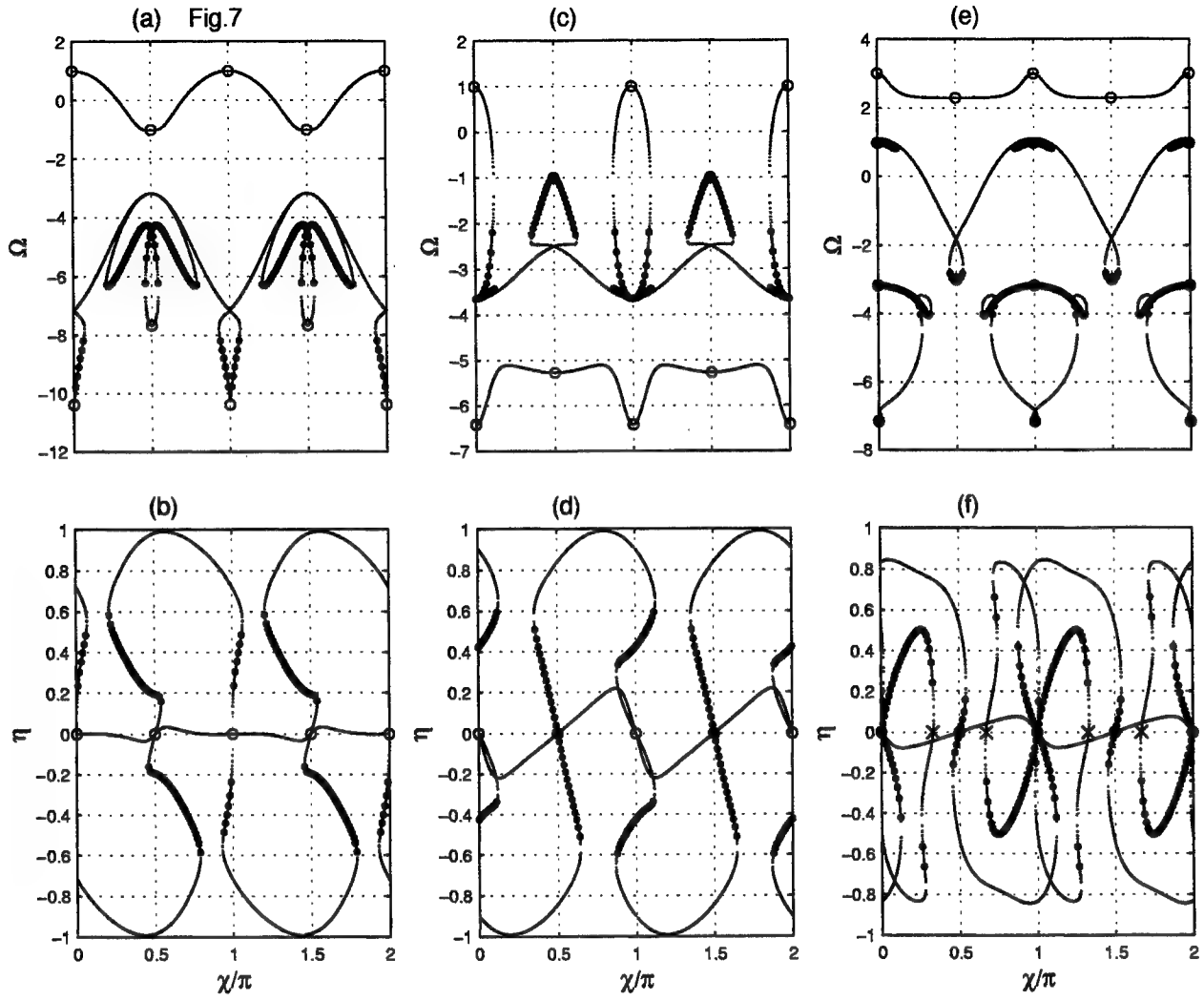
(a) Fig.7
(c)
(e)
(b)
(d)
(f)
Ω
η
χ/π

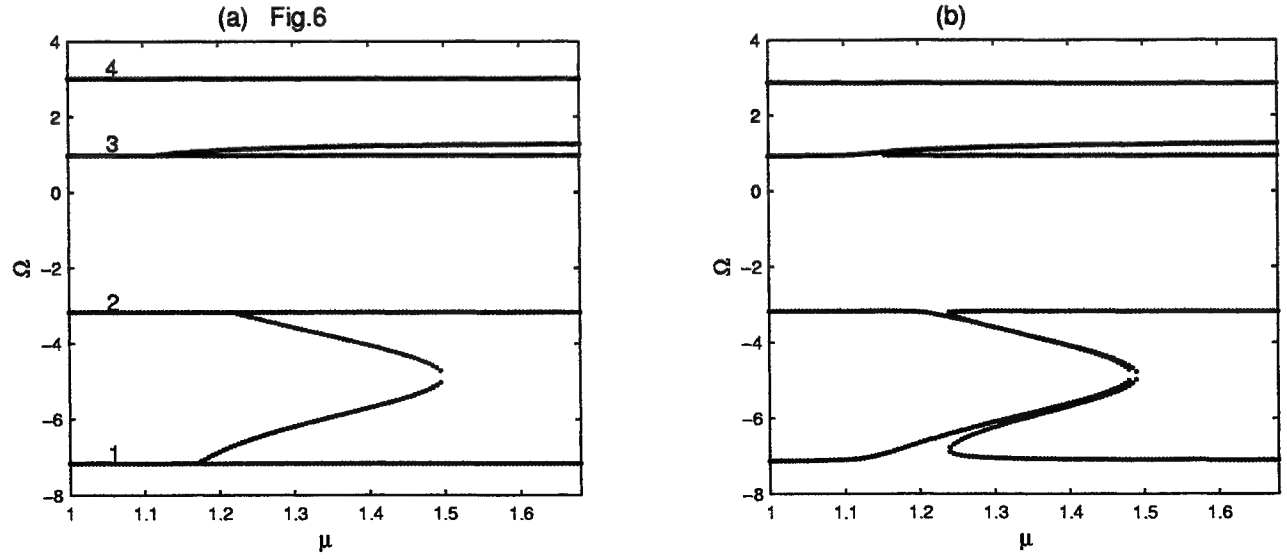
(a) Fig.6
(b)
4
3
2
1
Ω
μ

To the reasons of new types of regular and chaotic operation regimes in CO_2 laser with a saturable absorber

L.A. Kotomtseva, V.V. Nevdakh, O.L. Gaiko, S.G.Rusov
B.I. Stepanov Institute of Physics, Academy of Sciences of Belarus,
Skaryna ave. 70, Minsk, 220072 Belarus

Abstract

Some types of regular and chaotic passive Q switching regimes round several steady points in CO_2 laser with methanol as saturable absorber are obtained experimentally and theoretical model to explain their appearance is proposed. Phase portraits and the first peak intensity return maps are used to analyze them. Complicated regular regimes with some types of dynamics between two or three steady states for two longitudinal modes are considered both with and without intensive giant pulse between oscillations of each of modes. Some kinds of chaos round several points are proposed and reasons for their appearance are discussed.

Keywords: Laser with a saturable absorber, CO_2 laser, regular and chaotic dynamics.

I. INTRODUCTION

Lasers with a saturable absorber (LSA) are known as the systems with rich dynamics due to nonlinearity of both an active and passive media. Thorough experimental and theoretical considerations of CO_2 LSA have been presented for the passive quality switching (PQS) regimes in a great number of publications. Presently regular regimes of PQS with different pulse shapes and various scenarios of the transition to a chaotic regimes have been realized experimentally in such systems, as for example, in [1–7] and references therein. Various theoretical models for description of CO_2 LSA dynamics have been proposed during this period [2–9]. Model of three level system for an active medium and of two levels for an absorber turns out the most effective for the description of the peculiarities of the dynamics in a CO_2 LSA [3,4,7]. Three types of regular regimes are usually distinguished in such lasers, namely, sinusoidally modulated in time intensity, narrow high peaks with constant amplitude of intensity and pulses, which are accompanied by undamped undulation. All such regimes together with a chaotic behavior are qualitatively described in frames of this model. Some specific features of a rotational and vibrational exchange of energy at interactions with intensive light have been considered in [10–13] and their authors explain some discrepancies between experimental and theoretical results due to this exchange. It is necessary to note that main number of results has been described for a single mode LSA where pulsations develop round two steady states of the system with definite constant intensity I and with zero intensity $I_0 = 0$.

Special experiments together with theoretical consideration give us and explain complicated dynamics due to the presence of two transversal modes [14–16] in a CO_2 LSA.

SPIE Vol. 3685 • 0277-786X/99/$10.00

Typical CO_2 LSA acts under pumping energy much more high than the first laser threshold. That is why such system due to wide spectral widths of gain line in the active medium and absorption line in an absorber can have two and more longitudinal modes over the first laser threshold and they can take part in development of the dynamics in such LSA. It has appeared that addition of the second mode to the typical theoretical model of a CO_2 LSA even for incoherent interaction gives us new features in a laser dynamics [17–19]. It appears that experimentally observed radiation with constant intensity after step-wise switching on quality of a laser cavity and after giant pulse emission as it can be seen in [18] corresponds to the unstable steady state of this mode as it has been shown in [19]. Presence of the second mode permits us to explain so called metastable behavior when laser suddenly jumps from regular pulsations to the constant intensity of radiation and it is result of the stability of the steady state of the second mode at the instability of the steady state for the first mode, pulsations of which are interrupted by transition of a laser radiation to the constant in time intensity of the second mode [19].

Some regular and chaotic PQS regimes have been observed in CO_2 laser with methanol as saturable absorber with pulsing round two and more unstable steady states at one transversal mode with different structures of chaotic behavior in [20–22]. We describe below some new experimental results for such regular and chaotic dynamics and propose explanation of the possible reason for their appearance. We consider traditional model of three levels for active medium of CO_2 and two levels for a saturable absorber in a LSA with two longitudinal modes under consideration [17–19,23] and describe pulsations round two or three points.

II. EXPERIMENTAL RESULTS

We experimentally investigate a CW tunable CO_2 laser with a cavity of the length $3.2m$, formed by a diffraction grating (100 lines$/mm$) and a completely reflecting Al mirror. This cavity contains a *GL-501* type sealed-off active element with two Brewster windows, as well as a glass cell of a length of about $1m$ with vapours of a saturable absorber, and an iris diaphragm ensuring that the laser emits the fundamental transverse mode. The intracavity mechanical chopper gives possibility to switch the Q factor of the laser, to observe and investigate the dynamics of the development various PQS regimes and to monitor reliably the zero intensity level. The mirror has been attached to a KP-1 piezoelectric transducer. A stabilized-current power supply has done it possible to vary the discharge current in interval $10-30mA$. The wavelength of a laser emission has been monitored with an SPM-2 monochromator. The measuring system consists of the $GeAu$ photodetector with a time constant $< 1 * 10^{-7}s$, S9-27 digital storage oscilloscope and IBM PC. A more detailed description of the experimental set up has already been given in [18,24]. We use methanol (CH_3OH) vapors as intracavity saturable absorber. It is known (see for example [25]) that methanol molecules have a set of absorption lines characterized by different saturation parameters, as well as different absorption coefficients and offsets of their central frequencies from the centers of CO_2 emission lines of the $00^01 - 02^00$ transition. Owing to these factors CH_3OH represents a valuable object for LSA experiments. We investigate dynamical behavior of the laser output power at fixed discharge current and pressure of a saturable absorber at scanning the laser frequency by change the cavity length with help of piezoelectric transducer. In such way we can change gain in an active medium

and absorption in an absorber simultaneously. Scanning of the frequency of light within the gain profile of each rotational line and changes of the pressure of a vapour of a saturable absorber and the discharge current in the active medium give us possibility to get different PQS regimes both regular and chaotic. These regimes give in laser output as narrow high spikes, so diverging spirals, or alternating diverging and converging spirals, or more complex combinations of different shapes of pulses. Figure 1 gives us one of such experimental results with complicated regular behavior. Two levels in the attraction values of intensity I_0 and I are clearly explicit. We must note that some other regular oscillations not only round two or three points but and round four points have been presented in [20,21].

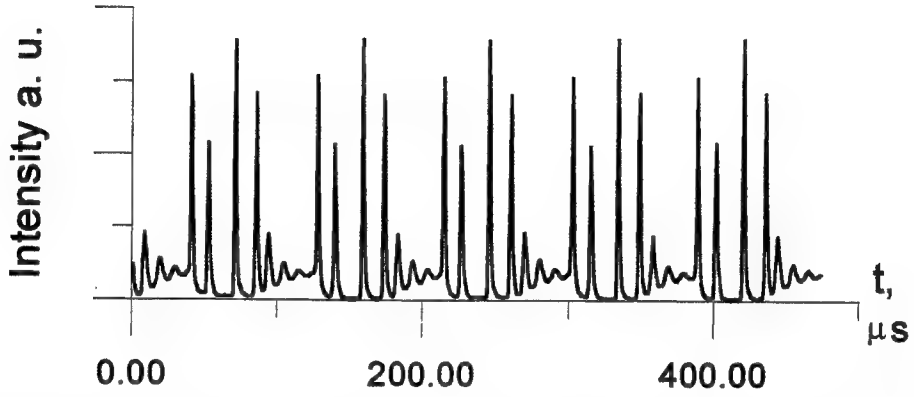

Figure 1. Regular oscillations at line *9P26,* pressure of CH_3OH 210 $mTorr$, discharge current $12mA$.

Some examples of chaotic regimes are seen in figure 2. To analyze a structure of a definite chaotic behaviour we use such standard tool as the phase portrait and the first peak intensity return maps reconstructions [7,9]. The reconstruction of phase trajectories is performed from the temporal evolution of the laser intensity using the time delay technique. Here we represent a chaotic regime that has been observed at $9P26$ line. Chaotic regimes that we have seen may be presented as three groups of behavior:

i) chaotic regimes contain only one unstable fixed point I with intensity different from zero and intensity never falls down to the noise level. Three such chaotic regimes containing one fixed point I with nonzero intensity have been given in [22] and so-called Lorenz-type spiral chaos is among them. Characteristics of this chaos are the monotonic growth of the intensity of pulses in time during individual spirals and the irregular length of these spirals. Intensity return map for this regime has a cusp shape which is inherent to the Lorenz dynamics and differs from the shapes of intensity return maps of other chaotic attractors.

ii) Chaotic regimes contain two fixed points. Figures 2*a* shows chaotic regime with diverging and converging spirals round two fixed points I_1 and I_2 with nonzero intensity. Phase portrait for this behaviour consists of the set of spirals and their intensity never falls down till zero level. The intensity return map resembles cusp shaped set of points as in Lorenz type attractor complicated

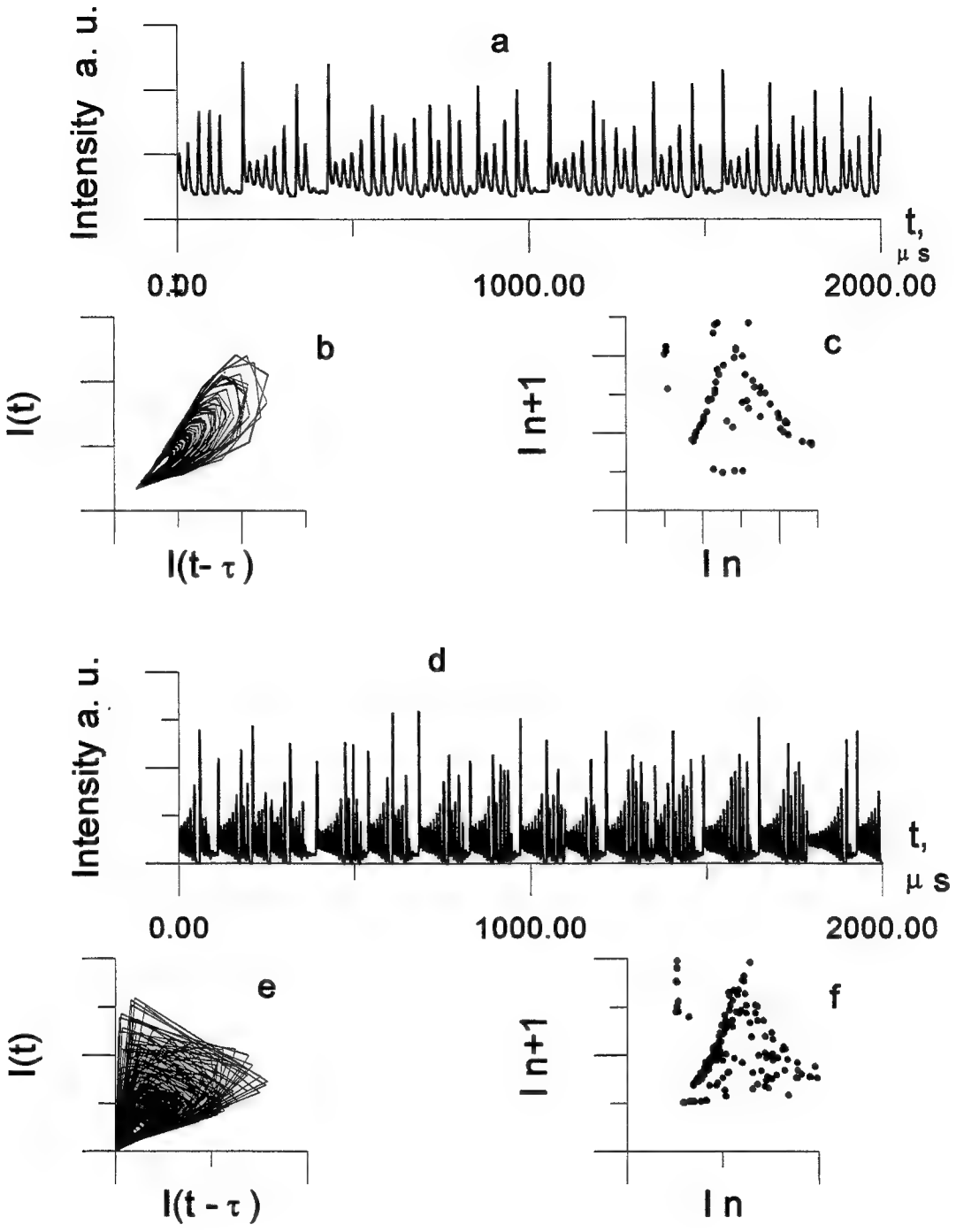

Figure 2. Chaotic dynamics in time (*a, d)*, its phase portrait (*b, e*) and the first return map for the maximal intensity (*c, f*) at line $9P26$ for pressure of CH_3OH 200 (*a-c*), 230 (*d-f*) $mTorr$, discharge current 20 mA, delay time τ=1 μs.

with additional points. In the work [22] we have described two examples of chaos with zero point I_0 and nonzero I. The first return map for intensity of one of them has two groups of points that are symmetric with respect to the diagonal. This symmetric splitting of the map shows us vicinity of a period-doubling bifurcation and looks like one of chaotic homoclinical regimes that have been described in [7]. The intensity return map for the second regime has a shape of a smooth curve with a single extremum and this chaos is similar to chaos in the Belousov-Zhabotinsky chemical reaction.

iii) Chaotic regimes contain three unstable fixed points. Figure 2*b* shows us irregular behaviour with three fixed points $I_0 = 0, I_1$ and I_2. Spirals diverge round point I_2 with the highest value, converging spirals are round the second less in value point I_1 and at the end of diverging spiral after high intensity pulse radiation falls down to the zero intensity level. Phase portrait gives space covered by trajectory and the first return map for the intensity is covered by points in more wide area than in the previous example in figure 2*a*. As to the first maps for intensity in chaotic regimes from [21] they have the different shapes indicating that they all have been produced by the different strange attractors. Thus, we can say that both homoclinic and heteroclinic chaos have been carried out in CO_2 laser with CH_3OH as a saturable absorber.

III. THEORETICAL MODEL AND RESULTS OF COMPUTER SIMULATIONS

Results of consideration of a complicated nonlinear dynamics and reasons for its appearance are proposed on the basis of the next system of equations for the relative inversion of populations Y, population of the lower working level Y_3 and for the intensities of radiation of two longitudinal modes I_1 and I_2:

$$\begin{aligned} &\dot{y} = a_1 - a_2 \cdot y + a_3 \cdot y_3 - (f_1 \cdot I_1 + f_2 \cdot I_2) \\ &\dot{y_3} = b_2 \cdot y - b_3 \cdot y_3 + (f_1 \cdot I_1 + f_2 \cdot I_2) \cdot y/2 \\ &\dot{I_i} = V \cdot \{f_i \cdot y - A \cdot f_{i+2}/[1 + a \cdot (f_3 \cdot I_1 + f_4 \cdot I_2)] - 1\} \cdot I_i + e_i \\ &i = 1, 2 \end{aligned} \tag{1}$$

Equations are written for Y and Y_3 , normalized to the ratio of the loss coefficient to the maximal gain in an active medium, intensities I_j are normalized to the intensity of saturation of an active medium and time is written in units of time of relaxation of populations. Coefficients a_j and b_j are effective rates which take into account for processes of vibration exchange between energy levels in CO_2 and the action of pumping and vibration exchange with molecules N_2. Value A defines maximal unsaturated absorption in a saturable absorber, a - is the parameter of saturation, V - is the ratio of relaxation time of populations in the active medium to the photon lifetime in the cavity, e_i - defines average spontaneous radiation. Coefficients f_j represent spectral properties of media and depend on the shift of frequency of mode from the center of gain profile of active medium or center of absorption line of saturable absorber and have been described in [17,18]. For the first mode value f_1 is near the unity and corresponds to the tuning to the center of the gain line in active medium. The second mode is shifted into the area with less gain $f_2 < f_1$ and absorption in an absorber at the frequency of the second mode is less too ($f_4 < f_3$).

The system (1) can have up to four steady states. The first of them trivial state with $I_{01} = 0$ and $I_{02} = 0$ exists for any parameters and becomes unstable over the first laser threshold when

unsaturated gain in an active medium exceeds sum of unsaturated loss in an absorber and loss of the cavity. Two other steady states, we call them the second and the third, accordingly, correspond to emission of light in one of the modes and absence of it in the another, namely, for the second steady state $I_1 > 0$ and $I_2 = 0$ and for the third one $I_2 > 0$ and $I_1 = 0$. These states exist in the definite rather wide area of parameters. For any of them nonzero intensity is determined as root of the square equation and for some parameters two values of nonzero intensity for the same mode can exist. Below in this paper we consider dynamics for parameters with only one nonzero value of intensity for the second and the third steady states. Finally in the narrow region of parameters the fourth state with simultaneous nonzero intensity values for both modes $I_1 > 0$ and $I_2 > 0$ can exist and linear analysis gives us that it is always unstable. Regions of existence for all these four states can overlap and up to four steady states can coexist.

We consider PQS regimes for the parameters area with coexisting the first, the second and the third steady states at the instability of trivial steady state. Two types of complicated regular regimes are received in computer experiment for some regions of parameters. One of them corresponds to the development of alternating oscillations round the second and the third steady states with short-time interval with zero intensities of both modes. In the second case pulse of radiation with high intensity at both modes is added to such oscillations. We have regimes with pulsations round three steady states.

Figures 3*a*,*b* give us example of regular oscillations round the second and the third steady states. For this case the second steady state with $I_1 > 0$ is stable, has all roots of characteristic equation with negative real parts and the third state with $I_2 > 0$ has one positive real root responsible for the connection with the first mode, other roots - one real and two complex conjugate - have negative real parts. Figure 3*a* gives us oscillations in time of the sum of intensities of both modes $I_1 + I_2$. Converging spiral of the second mode directs to its steady state in accordance with the negative sign of its complex conjugate root and then radiation jumps to the first mode due to connection with it through the real positive root. Oscillations of the first mode I_1 increase in time due to existence of unstable limit cycle round the steady state of this mode. System comes into basin of unstable cycle due to sufficient deviation from the stable second steady state. Phase portrait in Figure 3*b* shows us alternating pulsations of both modes in two perpendicular planes (y, I_1) and (y, I_2). Consideration of difference between gain and loss in each mode - member in main parenthesis of the equations for intensities of both modes - permits us to see interplay of saturations of an active medium and absorber in creation of effective gain for alternating modes. Increase of intensity of oscillations of the first mode leads to decrease of inversion of populations in active medium so that at some moment loss exceeds gain and the total intensity falls down. Permanent action of pumping increases inversion of populations and effective gain (member in parenthesis of equation for the intensity) for the second mode first becomes positive and intensity of the second mode sharply increases. We have connection of oscillations between three steady states: two steady states at each mode with nonzero intensity and one trivial state for both modes.

Figures 3*c*,*d* show us another type of regular dynamics. Parameters for this regime give one distinction — both steady states are unstable. The second steady state for the first mode has a pair of positive complex conjugate roots and for the third state at the second mode signs of the roots remain the same as in previous case. Oscillations on the second mode with decreasing amplitude follow the increasing first mode pulsations. As intensity of the first mode becomes so high that

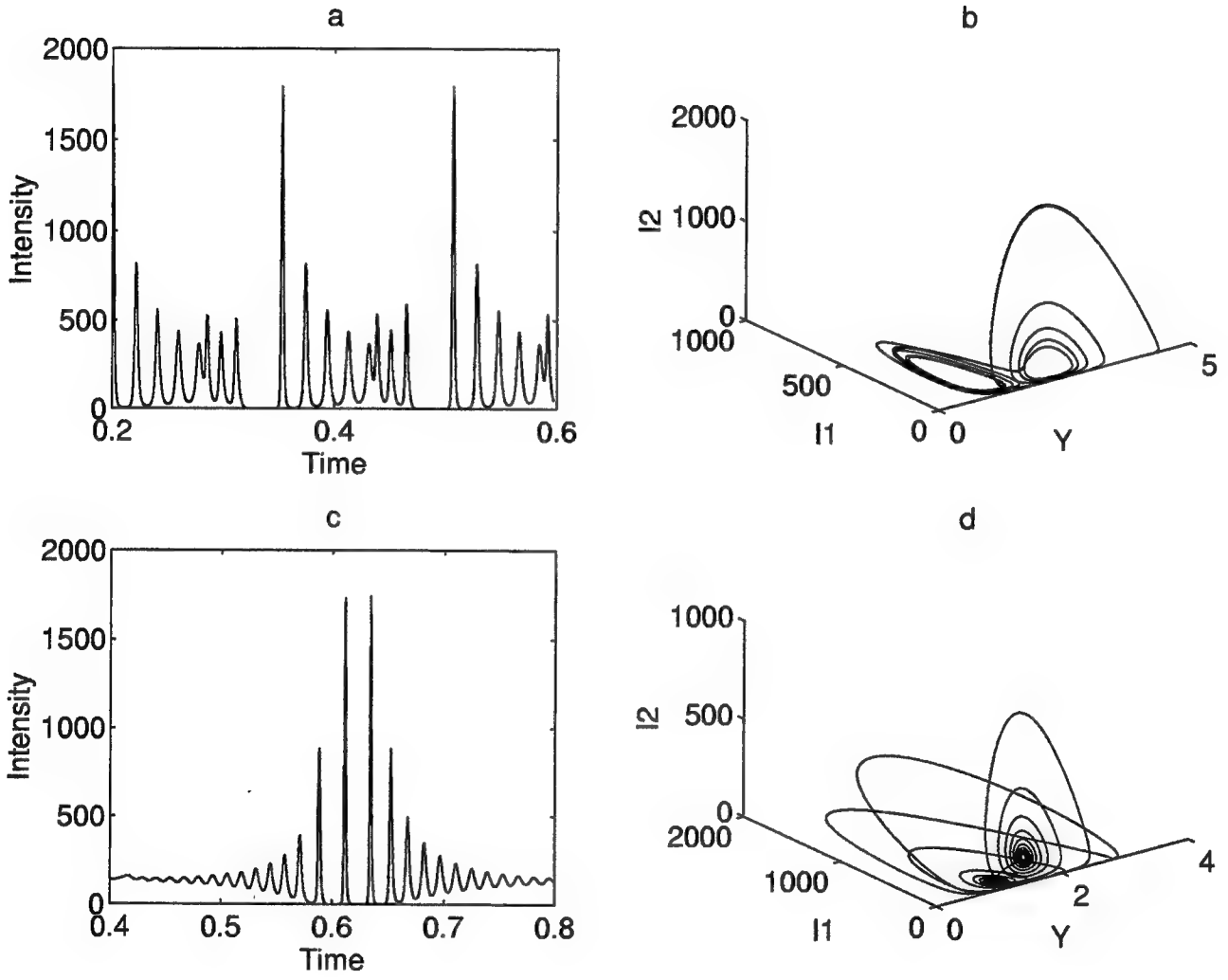

Figure 3. Sum of intensities of both modes (I_1+I_2) vs time (*a, c*) and three-dimensional phase portrait (Y, I_1, I_2) (*b, d*) in a LSA for $a_1=76$, $a_2=0.5$, $a_3=100.5$, $b_2=1.26\cdot10^{-4}$, $b_3=101.5$, $V=2030$, $a=1.11$ (a,b), 0.15(c,d), $A=10.78$ (a,b), 3.2 (c,d), $f_1=0.958$ (a,b), 1.0 (c,d), $f_2=0.410$ (a,b), 0.8 (c,d), $f_3=0.237$ (a,b), 0.368 (c,d), $f_4=0.008$ (a,b), 0.105 (c,d)

inversion of populations decreases till interruption of generation and intensity of both modes falls down to the noise level. Then under the action of permanent pumping intensive single pulse with radiation on both modes develops. We can see in figure 3*d* phase portrait with additional loop in space with simultaneous intensive radiation of both modes.

Both regimes give us examples of heteroclinic connection between modes in our model and correspond to the experimental behavior given in figure 1.

We must note, that domain of the existence of the regime with oscillations round stable steady state of the first mode I_1 (Figure 3*a*,*b*) is relatively narrow. Outside this region laser operates as single mode one with constant intensity on the first mode or with transitions between trivial state and steady state of the second mode. The second regime with both unstable steady states as in figure $3c, d$ exists in more large region. Outside this domain laser operates in different chaotic regimes.

IV. CONCLUSION

Results of experiment give us example of heteroclinic connection in the regular and chaotic dynamics of a CO_2 LSA. They show existence of several, up to four, steady points, round which oscillations take place as for converging so for diverging spirals. Both active medium and absorber are molecular systems with complicated interactions as under action of light so and at heat exchange with the tubes where vapours are embedded. Processes of rotational and vibrational energy exchange can change rates of decay both in active and passive media. Value of pressure in active medium permits us to consider homogeneously broadened line in an active medium. Complicated structure of molecules of absorbers such as CH_3OH, SF_6 and other complicated molecules gives possibility to the coexistence of several lines of absorption of a laser radiation for the set of longitudinal modes. Rather low value of the vapour pressure in a saturable absorber shows that inhomogeneous broadening exists in such media and can bring additional properties into this system..

Comparison of results of our experiment and proposed mechanism of development of complicated behavior in the vicinity of several points gives us foundation to say about important role under the definite conditions of the presence of the second longitudinal modes over the first laser threshold. For the systems with the comparable spectral widths of gain and absorption and between mode spectral interval possibility not only for two but and for several longitudinal modes to appear over the first laser threshold becomes real. That is why we suppose that action of additional longitudinal mode in the laser dynamics is rather typical and has to be taken into account. The same time in the frames of our model for some parameters two values of the steady intensity in the same mode can exist as for the second so for the third steady states and it can become additional reason for the appearance new steady points.

A. Acknowledgments

This work is supported by the Republican Foundation for the Fundamental Investigations of Belarus, Grant No 96-169 and Grant No. F96-117.

B. References

1. Yu.V.Brzhazovsky, L.S.Vasilenko, S.G.Rautian, S.G.Popova, V.P.Chebotayev. "Theoretical and experimental investigation of radiation pulsation from a CO_2 laser with a nonlinear absorbing cell", *Zh. Exp. Teor.Fiz.*, **61**, 500-510, 1971.

2. E.Arimondo, F.Casagrande , L.A.Lugiato, P.Glorieux. "Repetitive passive Q-switching and bistability in laser with saturable absorber", *Appl. Phys.* B **30**, 57-77, 1983.

3. M.Tachikawa, K.Tanii, M.Kajita,T.Shimizu. "Undamped undulation superposed on the passive Q-switching pulse of a CO_2 laser", *Appl. Phys.* B **39**, 83-90, 1986.

4. M.Tachikawa, K.Tanii, T.Shimizu. "Comprehensive interpretation of passive Q switching and optical bistability in CO_2 laser with an intracavity saturable absorber", *JOSA B*, **4**, 387-395, 1987.

5. B.Zambon, F.De Tomasi, D.Hennequin, E.Arimondo. "Investigations of models and experimental studies of a stationary regime for a laser with a saturable absorber", *Phys. Rev. A*, **40**, 3782-3797, 1989.

6. F.De Tomasi, D.Hennequin, B.Zambon, E.Arimondo. "Instabilities and chaos in an infrared laser with saturable absorber: experiments and vibro-rotational model", *JOSA B*, **6**, 45-57, 1989.

7. M.Lefranc, D.Hennequin, D.Dangoisse. "Homoclinic chaos in a laser containing a saturable absorber", *JOSA B*, **8**, 239-249, 1991.

8. V.V.Dembovetskii. "Dynamics of CO_2 laser generation in a passive Q-switch mode of operation", *Optics of Atmosphere* **2**, 100-102, 1989.

9. C.O.Weiss, R.Vilaseca. *Dynamics of Lasers*, VCH Publishers, Cambridge, 1991.

10. G.-L.Oppo, J.R.Tredicce, L.M.Narducci. "Dynamics of vibro-rotational CO_2 laser transitions in a two-dimensional phase space", *Opt. Comm.*, **69**, 393-397, 1989.

11. B.Zambon. "Theoretical investigations of models for the laser with a saturable absorber: a case of homoclinic tangency to a periodic orbit", *Phys. Rev. A*, **44**, 688-702, 1991.

12. M.Ciofini, A.Politi, R.Meucci. "Effective two-dimensional model for CO_2 laser", *Phys. Rev. A*, **48**, 605-610, 1993.

13. M.Ciofini, R.Meucci . "Determination of the effective number of rotational levels affecting the dynamics of CO_2 lasers", *IEEE J. Quant. Electr.*, **31**, 886-893, 1995.

14. K.Tanii, M.Tachikawa, F.-L.Hong, T.Tohei, T.Shimizu. "Multimode instability in a CO_2 laser with saturable absorber", *Nonlinear dynamics in optical systems*, **7**, 389-393, 1990.

15. D.Hennequin, D.Dangoisse, P.Glorieux. "Instabilities in a bimode CO_2 laser with a saturable sbsorber", *Opt. Commun.*, **79**, 200-206, 1990.

16. D.Hennequin, D.Dangoisse, P.Glorieux. "Farey hierarchy in a bimode CO_2 laser with a saturable absorber", *Phys. Rew. A*, **42**, 6966-6968, 1990.

17. O.L.Gaiko, L.A.Kotomtseva, V.V.Nevdakh, L.N.Orlov, A.M.Samson. "Dynamical chaos in a CO_2 laser with a saturable absorber", *J. Appl. Spectr.*, **58**, 287-293, 1993.

18. O.L.Gaiko, L.A.Kotomtseva, V.V.Nevdakh, L.N.Orlov, A.M.Samson. "Dynamics of operation of a CO_2 laser with methanol and ethanol vapours as intracavity saturable absorbers", *Quant. Electr.*, **21**, 603-607, 1994.

19. L.A.Kotomtseva, A.V.Naumenko, A.M.Samson, S.I.Turovets. "Targeting unstable orbits and steady states in class-B lasers by using simple off/on manipulations", *Optics. Commun.*,**136**,

335-348, 1997.

20. V.V.Nevdakh, O.L.Gaiko, L.N.Orlov. "New operation regimes of a CO_2 laser with intracavity saturable absorber", *Optics. Commun.*, **127,** 303-306, 1996.

21. V.V.Nevdakh, O.L.Gaiko, L.N.Orlov. "New regimes in a CO_2 laser with intracavity saturable absorber", *Quant. Electr.*, **23**, 57-58, 1996.

22. V.V.Nevdakh, O.L.Gaiko, Yu.P.Zhurik, L.N.Orlov. "Structure of chaos in a single-mode CO_2 laser with intracavity saturable absorber", *Lithuanian J. Physics,* **37,** 285-290, 1997.

23. L.A.Kotomtseva, S.G.Rusov. "Mechanism of formation of undamped pulsations around several equilibrium states in a laser with a saturable absorber", *Quant. Electr.*, **28**, 155-156, 1998.

24. O.L.Gaiko, V.V.Nevdakh. *Preprint No.561, Institute of Physics,* Academy of Sciences of BSSR, Minsk, 1989.

25. O.L.Gaiko, Ya.I.Nekrashevitch, L.N.Orlov. *Preprint No.417, Institute of Physics,* Academy of Sciences of BSSR, Minsk, 1986.

Long and short wavelength instabilities in an anisotropic dye laser

S.V.Sergeyev
Department of Physics, Belarusian State University, 4 Skorina Ave.,Minsk 220050, Belarus

Abstract
Long and short wavelength spatio-temporal instabilities have been theoretically found in transverse section of an anisotropic dye laser and expression for the pattern sizes, frequencies and amplitudes have been derived as function of the rate of Brownian Rotation.
Key words: laser, instabilities, Brownian Rotation.

1. INTRODUCTION

Spatio-temporal chaos in the transverse section of lasers for large Fresnel numbers is problem of great interest for theoreticians [1] - [8] and experimentalists as well [9] - [12]. It has been recently found for CO_2 laser that transverse dynamics is controlled by two simultaneous instabilities [7], [9]. One is a long wavelength instability appears due to spatio-temporal phase instability and leads to a state uncorrellated in space and time. The next one is a short wavelength instability arises due to a Hopf bifurcation and yields a periodic modulation in space and time.

For an anisotropic multimode dye laser spatio-temporal fluctuations have been experimentally observed depending on solution viscosity [10] - [12]. For methanol solutions of Rhodomine 6G as active medium (high rate of orientational mobility of excited molecules) high- and low - frequency chaotic auto-oscillations and transverse structures with correlation length about $50\mu m$ have been observed [10]-[11]. For Rhodomine 6G solid solution in a copolymer 2 hydroxyethyl methacrylate (HEMA) and methyl methacrylate (MMA) local fluctuations of intensity are considerably less than for the previous case [12]. The objective of this paper consists in filling the gap in theoretical interpretation of the experiments. We use semiclassical approach to describe an anisotropic dye laser taking into account anisotropy of the cavity and Brownian Rotation of excited molecules [8]. In section 2 we build up Maxwell-Bloch equations taking into account cavity anisotropy and Brownian Rotation (BR) of excited molecules. By means of linear stability analysis for short and long wavelength instabilities we derive expression for the pattern sizes, frequencies and amplitudes as function of the solution viscosity. In section 3 based on the theoretical results we explain experimentally observed spatio-temporal instabilities dependence on a solution viscosity.

2. VISCOSITY-DEPENDENT LONG AND SHORT WAVELENGTHS INSTABILITIES

Let us consider ring cavity dye laser with isotropic pumping (flashlamp pumped dye laser) and polarizer inside the cavity. Pumping radiation creates an isotropic distribution of inversion and linearly polarized laser emission burns "hole" in orientational distribution of inversion (fig.1). Brownian Rotation of excited molecules leads to suppression of "hole burning" (fig.1). In experiments [10] - [12] dye laser with flashlamp pumping and Fabry-Perot resonator have been used. This kind of laser emits a continuum of wavelengths (approximately 10^4 modes) corresponding to the set of detunigs $\delta \sim [-1,1]$ [13] (δ is the scaled frequency difference between resonance frequency of the active medium and one of the cavity mode). Resonance frequency denotes here the frequency of the maximum of emission spectrum. As it has been found [8] that approach based on two-level model is quite suitable close to the first threshold . Due to weak modes coupling we can write equations for every mode located within domain $\delta \sim [-1,1]$ [8]:

$$\frac{\partial E}{\partial t} = -k(1-i\delta)E - 3kC\int P(g)(\mathbf{m_e}\cdot\mathbf{e})dg + \frac{iak}{2}\nabla^2 E,$$

$$\frac{\partial P(g)}{\partial t} = -(1+i\delta)P(g) - 3D(g)(\mathbf{m_e}\cdot\mathbf{e})E,$$

$$\frac{\partial D(g)}{\partial t} = -\gamma(-1/2(P(g)^*E + P(g)E^*)(\mathbf{m_e}\cdot\mathbf{e}) + (1-\hat{\mathcal{L}})D(g) - 1), \qquad (1)$$

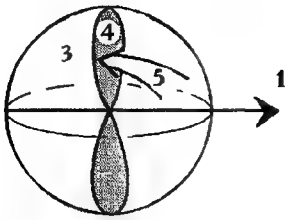

Fig.1

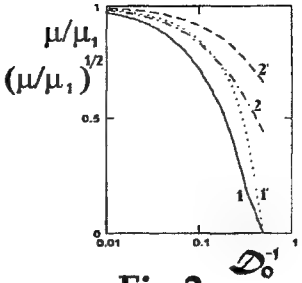

Fig.2

Fig.1 Orientation distribution of inversion $D(g)$. 1 - cavity axis, 2 - linearly polarized dye laser emission, 3 - isotropic distribution by pumping, 4 - hole burning by lasing, 5 - contribution of active molecules with dipoles moments of transitions with emission, oriented close to the cavity axis, into the lasing (Brownian rotation of active molecules.)

Fig.2 Amplitudes of short and long wavelength fluctuations, as function of solvent viscosity $\mathcal{D}_0^{-1}$, 1,1',2,2' - $\delta = 0.01$, 1,1' - $C = 1.2$, 2,2' - $C = 3$, $\mu_1 = \mu|_{\mathcal{D}_0 \to \infty}$.

The lasing electric field amplitude E and the polarization of an active medium P are complex variable, while inversion D is a real one. The scaled pump parameter is denoted by C ($C = 1$ is the laser threshold for $\delta = 0$). Here $k, 1, \gamma$ are the relaxation rates of E, P, D respectively, $\mathbf{e}$ is unit vector oriented along the polarization plane of laser emission, $\mathbf{m_e}$ is unit vector oriented along the dipole moment of transition with emission, ∇^2 is the transverse Laplacian, $a = c\Lambda/(2\pi k)$ (where c is the light speed and Λ is the laser wavelength), $\hat{\mathcal{L}}$ - operator of Brownian Rotation [8]:

$$\hat{\mathcal{L}}x = \mathcal{D}_0\left(\frac{1}{\sin\theta}\frac{\partial}{\partial\theta}\left(\sin\theta\frac{\partial x}{\partial\theta}\right) + + \frac{1}{\sin^2\theta}\frac{\partial^2 x}{\partial^2\phi}\right). \tag{2}$$

It has the following property [15]:

$$\hat{\mathcal{L}}D^l_{m,n} = -l(l+1)\mathcal{D}_0 D^l_{m,n}, \tag{3}$$

where $D^l_{m,n}$-Wigner's functions, $\mathcal{D}_0$ - dimensionless Brownian Rotation factor [15].

Based on substitutions $E = |E|\exp(i\Phi_E)$, $P = |P|\exp(i\Phi_P)$ [7] and using property of Brownian Rotation Operator (3) and approximation of high rate of Brownian Rotation $||\hat{\mathcal{L}}|| \gg 1$ (here $||\hat{\mathcal{L}}||$ is norm of Brownian Rotation Operator [8]) we find uniform steady- states solutions:

$$\tan(\Phi_{E_0} - \Phi_{P_0}) = \delta, \quad |E_0|^2 = \frac{C - (1+\delta^2)}{1 + 2C/5\mathcal{D}_0},$$

$$D_0 = \frac{1+\delta^2}{C}(1 + 2C/5\mathcal{D}_0), \quad |P_0| = 3D_0|E_0|\cos(\Phi_{E_0} - \Phi_{P_0})(\mathbf{m_e}\cdot\mathbf{e}), \tag{4}$$

Linear stability analysis of uniform steady state patterns (4) carried out in [8] for $\delta > 0$ shows: (i) one real positive eigenvalue, associated with phase instability [9] and (ii) complex eigenvalue, associated with Hopf bifurcation for wavenumbers $q > q_0$ [9]:

$$\lambda_1(g) = \delta g - \frac{1+\delta^2}{2\mu k}g^2 + O(g^3),$$

$$\lambda_0(g - g_0) = i\Omega + (i + \frac{2k\delta}{1+\delta^2})(g - g_0) - \sqrt{\frac{\gamma\mu}{2(1+\delta^2)}}\left(\frac{16k\delta}{\gamma\mu(1+\delta^2)} + 3i\right)(g - g_0)^2 + O((g - g_0)^3),$$

$$\Omega = \Omega_0 + g_0 = \sqrt{2k\gamma\mu} + \sqrt{1+\delta^2)\mu\gamma/2} \tag{5}$$

Here $g = akq^2/2$, $\mu = (1 - D_0)/D_0$. It is quite clear from expressions (5) that for $g < g_0$ first type of instability appears. Phase ϕ obeys a Kuramoto-Shivasinsky (KS) type equation [9] and remains chaotic with temporal correlation function $\exp(-t/\tau)$ ($\tau \sim 1/\lambda_{1,max}$) [9]. Thus lasing field displays complex behavior in time,

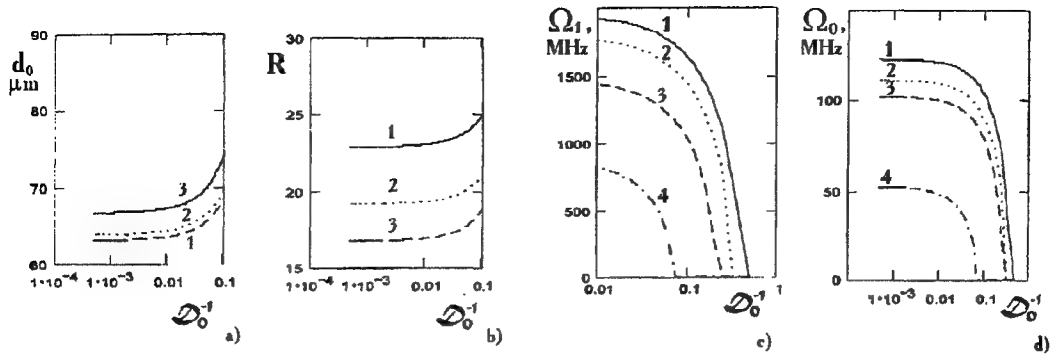

Fig.3

Fig.3 Size of short wavelength patterns (a), (long wavelength)/(short wavelength) patterns size ratio (b), frequencies of short (c) and long wavelength fluctuations (d), as function of solvent viscosity $\mathcal{D}_0^{-1}$, a) 1 - $\delta = 0.01$, 2 - $\delta = 0.1$, 3 - $\delta = 0.2$, b) 1 - $\delta = 0.1$, 2- $\delta = 0.15$, 3 - $\delta = 0.23$, $K_l = 2$, $\Lambda = 5 \cdot 10^{-7} m$, $L = 1m$, $k = \gamma = 10^{-3}$. c) 1 - $\delta = 0.1$, 2 - $\delta = 0.2$, 3 - $\delta = 0.3$, 4 - $\delta = 0.4$, d) 1 - $\delta = 0.1$, 2 - $\delta = 0.2$, 3 - $\delta = 0.25$, 4 - $\delta = 0.4$

but the time averaged value is a space homogeneous pattern [9].For $g > g_0$ two instabilities occur and lasing field displays complex spatio-temporal behavior [9]. Lasing amplitude has instability associated with second eigenvalue producing oscillatory periodic structures and obeys Complex Swift-Hohenberg (CSH) equation [9]. As a result simultaneous arising instabilities (5) obey the coupled KS and CSH equations [9]. Because of derivation of such equations is rather difficult for the case when BR of molecules taken into account, we restrict our consideration to estimations for the dependencies of the patterns sizes, frequencies and amplitudes on the solvent viscosity [8]. As it shown in ref. [7] patterns arising due to phase instability have size $d_1 \sim q_{1,max}^{-1}$ and due to Hoph bifurcation have size $d_0 \sim q_0^{-1}$. By means of expressions (5) we find:

$$d_i = G_i\sqrt{\Lambda L}, \quad G_1 = \sqrt{\frac{1+\delta^2}{2K_l\pi\mu\delta}}, \quad G_0 = \sqrt{\frac{k}{\pi K_l\sqrt{2(1+\delta^2)\mu\gamma}}}, \quad k = \frac{c}{2Ln\gamma_\perp}K_l, \quad (i = 0, 1) \tag{6}$$

where L is cavity length and K_l cavity losses, n is the refractive index, $\gamma_\perp$ $[c^{-1}]$ is the relaxation rate for the medium polarization. Because $\Omega \to \Omega_0$ for $g \to 0$ we find from (5) that long wavelength instability has the characteristic frequency $\Omega_0 = \sqrt{2k\gamma\mu}$ and due to $k, \gamma \sim 10^{-3}$ [10]-[12] for dye laser short wavelength instability has the characteristic frequency $\Omega_1 = \sqrt{(1+\delta^2)\mu\gamma/2}$. It is clear enough that amplitudes of long A_l and short wavelength A_{sh} fluctuations will be proportional to $\lambda_{1,max}, Re(\lambda_{0,max})$ and as it follows from (5):

$$A_l(\mathcal{D}_0)/A_{l,1} = \mu(\mathcal{D}_0)/\mu_1, \quad A_{sh}(\mathcal{D}_0)/A_{sh,1} = \sqrt{\mu(\mathcal{D}_0)/\mu_1}, \tag{7}$$

Here $A_{l,1}$, $A_{sh,1}$ are fluctuations amplitudes for $\mathcal{D} \to \infty$ and $\mu_1 = \mu|_{\mathcal{D}_0 \to \infty}$. Amplitudes of fluctuations as function of the solvent viscosity $\eta \sim \mathcal{D}_0^{-1}$ are found on fig.2.

3. RESULTS AND DISCUSSION

For large viscosity solvents (glycerin for example) molecules with dipole moments, oriented close to the cavity axis, do not participate in lasing (fig.1). Therefore for this case amplitudes of short and long wavelength fluctuations are small (fig.2, curves 1,1'). For small viscosity (methanol for example) there is significant contribution of these molecules in lasing by means of Brownian rotation (fig.1). It leads to increasing the fluctuations amplitudes (fig.2, curves 1,1'). With increasing the pumping parameter the fluctuations dependence on solvent viscosity is reduced (fig.2, curves 2,2') due to expanding of "hole" in orientational distribution of inversion $D(g)$ (fig.1). In the frameworks of the model it is not possible to determine the contribution of every mode into the lasing, i.e. dependence of fluctuation amplitude on detuning. But for the frequencies and pattern sizes it is possible to determine this dependence. The patterns sizes and frequencies as function of viscosity $\eta \sim \mathcal{D}_0^{-1}$ for different

detunigs are found on fig.3. As it follows from fig.3 (a,b) short wavelength instability has the pattern sizes $d_0 \sim 60 \div 70\mu m$ and long wavelength instability has the pattern sizes $d_1 \sim 1 \div 1.5mm$. The sizes of both types of instabilities are practically viscosity-independent that corresponds to the experiments [12]. Pattern sizes for short wavelength instabilities are detuning-independent as well (fig.3(a)). On the other hand pattern sizes of the long wavelength instability reveal strong dependence on detuning (fig.3(b)).

It has been found experimentally that spectrum of chaotic auto-oscillations has the maxima at $16MHz$ and $50MHz$ [10] - [12] and amplitude of high-frequency fluctuations decreases with increasing the solvent viscosity more rapidly than amplitude of low-frequency fluctuations [12]. Based on fig.3 (c,d) we find that these frequencies are present in the spectrum of chaotic auto-oscillations, but due to the approximation of uncoupled modes we couldn't determine the maxima of spectrum. As it follows from fig.3(c,d) spectrum is shifted into the low-frequency region with increasing the solvent viscosity. Therefore the amplitude of low-frequency auto-oscillations goes down more slowly than amplitude of high-frequency auto-oscillations.

Inspite of influence of boundary conditions have been neglected, theoretical results are in a good correspondence with experiments [10]-[12]. It is well known that including different types of boundary conditions into considerations leads only to shift in thresholds parameters [7]. For example long and short wavelength instability can arise for $\delta < 0$ as well.

References

[1] P.Coullet, L.Gil, and J.Lega, "Defect-Mediated Turbulence", ***Phys. Rev. Lett.*** 62 1619-1622 (1989).

[2] L.Gil, "Vector Order Parameter for an Unpolarized Laser and its Vectorial Topological Defects", ***Phys. Rev. Lett.*** 70 162-165 (1993).

[3] G.K.Harkness, W.J.Firth, J.B.Geddes, J.V.Moloney, E.M.Wright, "Boundary effects in large-aspect-ratio lasers", ***Rhys. Rev. A*** 50 4310-4317 (1994).

[4] J.Lega, J.V.Moloney, A.C.Newell, "Swift-Hohenberg Equation for Lasers", ***Phys. Rev. Lett.*** 73 2978-2981 (1994).

[5] K.Staliunas, C.O.Weiss, "Titled and standing waves and vortex lattices in class-A lasers", ***Physica D*** 81 79-93.

[6] Q.Feng, J.V.Moloney, and A.C.Newell, "Transverse patterns in lasers", ***Phys. Rev. A*** 50 3601-3604 (1994).

[7] G. Huyet, S.Rica, "Spatio-temporal instabilities in the transverse patterns of lasers", ***Physica D*** 96 215-229 (1996).

[8] S.V.Sergeyev, "Orientational relaxation-dependent spatio-temporal instabilities in an anisotropic dye laser", ***JEOS (Quantum and Semiclassical Optics)*** (1998) to be published.

[9] G.Huyet, M.C.Martinoni, J.R.Tredicce, and S.Rica, "Spatio-temporal chaos in the transverse section of lasers", ***Physica D*** 96 209-214 (1995).

[10] V.M.Pér,ez-García and J.M.Guerra, "Weak turbulent behavior and dynamical frequency locking in a high-Fresnel-number laser" ***Phys. Rev. A*** 50 1646-1663 (1994).

[11] V.M.Pér,ez-García, I.Pastor, J.M.Guerra, "Order-disorder transitions in the dynamics of a dye laser", ***Phys. Rev. A*** 52 2392-2400 (1995).

[12] O.G.Calderón, J.M.Guerra, A.Costela, I.García-Moreno, and R.Sastre, "Laser emission of a flash-lamp pumped Rhodamine 6 G solid copolymer solution", ***Appl. Phys. Lett.*** 70 20-27 (1997).

[13] L.G.Nair, "Dye lasers" ***Prog. Quant. Electr.*** 7 153-268 (1982).

[14] ***Dye Lasers***, edited by F.P.Schäfer, p.32,33, Topics in Applied Physics, Springer-Verlag, 1990.

[15] D.A.Varshalovich, A.H.Moskalev, V.K.Hersonsky, ***Quantum theory of angular momentum***, (Rus) Leningrad, 1975.

Phase modulation instability of passive mode-locking of solid-state lasers

A.K.Komarov, K.P.Komarov[1)], A.S.Kuch'yanov

Institute of Automation and Electrometry, the Russian Academy of Sciences, the Siberian Branch, Universitetskii Pr. 1, 630090, Novosibirsk, Russia

ABSTRACT

Nonlinear dynamics due to the phase modulation instability and resulting in the bistability for the regime of formation of ultrashort pulses is investigated. We studied the regime of breathing ultrashort pulse due to this instability. Other possible established regime connects with an increase in the number of stable stationary ultrashort pulses in laser cavity. It is shown that type of established regime depends on initial conditions.

Keywords: passive mode-locking, bistability, propagation of ultrashort pulses through nonlinear dispersion media, stability of stationary ultrashort pulses

1. INTRODUCTION

This paper is a continuation of earlier reports of our studies of passive mode-locking in solid state lasers[1–6].

The evolution of the radiation in the ring laser cavity is described by the following equation in dimensionless variables[1,2,4]:

$$\frac{\partial}{\partial t}E = (1+id)\frac{\partial^2}{\partial z^2}E + \frac{1}{2}\left(\frac{1+a}{1+b\int_V |E|^2\,dz} - 1 - \frac{p}{1+|E|^2} + iq\,|E|^2\right)E, \qquad (1)$$

where E is the slow field amplitude; t and z are time and coordinate variables; d is the frequency dispersion of refractive index. The first term in parentheses defines the saturated amplifier gain in active medium, the third term determines the saturable absorber loss, and the last term describes the refractive index nonlinearity. The integration is performed over the cavity volume V.

Eq. (1) is used for description of passive mode-locking of solid-state lasers with negative feedback loop preventing Q-switching instability[6].

If the intracavity medium is free from the frequency dispersion and nonlinearity of refractive index ($d = 0$, $q = 0$) we can obtain the following equation for the Lyapunov functional of eq. (1)[3]:

$$\frac{d}{dt}\left\{\int_V \left[2\left|\frac{\partial E}{\partial z}\right|^2 + |E|^2 + p\ln\left(1+|E|^2\right)\right]dz - \frac{1+\alpha}{b}\ln\left(1+b\int_V |E|^2\,dz\right)\right\} = \qquad (2)$$

$$= -4\int_V \left|\frac{\partial E}{\partial t}\right|^2 dz.$$

[1)]e-mail: komarov@iae.nsk.su

From this relation one can see that in this case irrespective of the initial conditions the passive mode-locking always pass into the stationary state ($\dot{E} = 0$) which is the state of single stationary ultrashort pulse[3].

It is amply clear that this property of system retains if the frequency dispersion and nonlinearity of refractive index are sufficiently small ($d \ll 1$, $q \ll 1$).

In the case of small intensity ($|E| \ll 1$) we determined steady-state solution of eq. (1) describing the equilibrium ultrashort pulse with regard to the frequency dispersion and the nonlinearity of refractive index ($d \neq 0$, $q \neq 0$)[1,2]:

$$E_s = E_0 \sec^{1+i\alpha} \beta z, \tag{3}$$

where the peak amplitude E_0, the reciprocal length of pulse β, and the self-phase modulation parameter α are determined by algebraic equations obtained by substitution of (3) into (1). For this approximation the latter takes the form:

$$\frac{\partial}{\partial t} E = (1 + id) \frac{\partial^2}{\partial z^2} E + \frac{1}{2} \left(\frac{1 + \alpha}{1 + b \int_V |E|^2 \, dz} - (1 + p) + (p + iq) |E|^2 \right). \tag{4}$$

On occasion the eq. (4) is named the Ginzburg-Landau equation.

The stability of steady-state solution (3) of eq. (4) was analysed by us[1,2]. We determined the condition of its instability. In the case of $d = 0$ the criterion of phase-modulation instability has the form[1]:

$$|q| > 3p. \tag{5}$$

What regime of passive mode-locking will be realized in the case of the initiation of the phase-modulation instability?

In our recent paper[4] we have established that the phase-modulation instability produces splitting of the initial pulse into several pulses. In such a manner after transient evolution the regime with the same several stationary pulses (3) is realized for wide region of parameters of system described by eq. (1). The number of stable stationary pulses in established regime depends on the pump a and the nonlinearity of refractive index q.

In this paper we report about another passive mode-locking regime due to the phase-modulation instability.

2. BREATHING PULSES AND BISTABILITY OF PASSIVE MODE-LOCKING

Using computer simulation we have investigated in detail the dependence of regime for passive mode-locking on initial conditions. We have established that the passive mode-locking regime realizing after transient evolution depends on length of initial ultrashort pulse. If the initial length is sufficiently large then after transient evolution regime of several stationary pulse is realized. Fig. 1 illustrates this regime in the case of two established stationary pulses (the frequency dispersion of refractive index d is assumed below to equal zero). The established regime changes radically if the length of initial pulse is sufficiently small. Fig. 2 demonstrates this change.

As one can see in fig. 2, the established regime becomes periodical. There exist two periods of temporal changes. The first period (≈ 10) corresponds to fast oscillations of wings of ultrashort

pulse. The second period (≈ 40) is connected with repetitive slow build-up and suppression of the pulse wings.

Thus, the established regime depends on initial conditions, that is, passive mode-locking described by eq. (1) is bistable.

Fig. 3 illustrates the transient evolution for length of initial pulse closed to borderline length, which separates two areas of initial conditions corresponding first and second established regimes. One can see, that in the transient process wings considerably increase, central part of the pulse is almost suppressed. The initial pulse almost splits into two pulses. However, then the central part of the pulses increases and the regime of the breathing pulse is established.

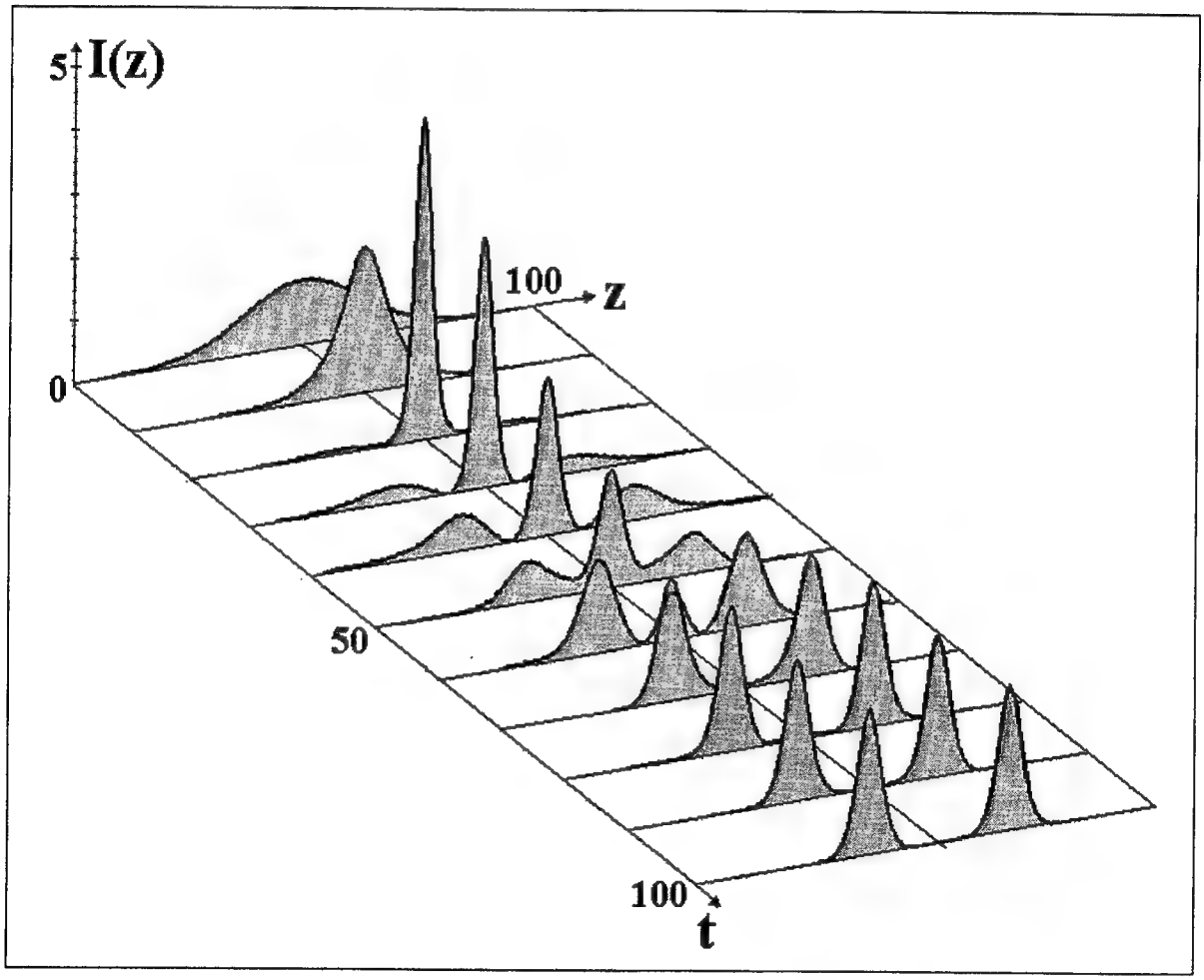

Fig. 1. Transient process with $a = 4$, $b = 0.1$, $p = 0.3$, and $q = 0.3$.
The length of the initial Gaussian pulse is 30.

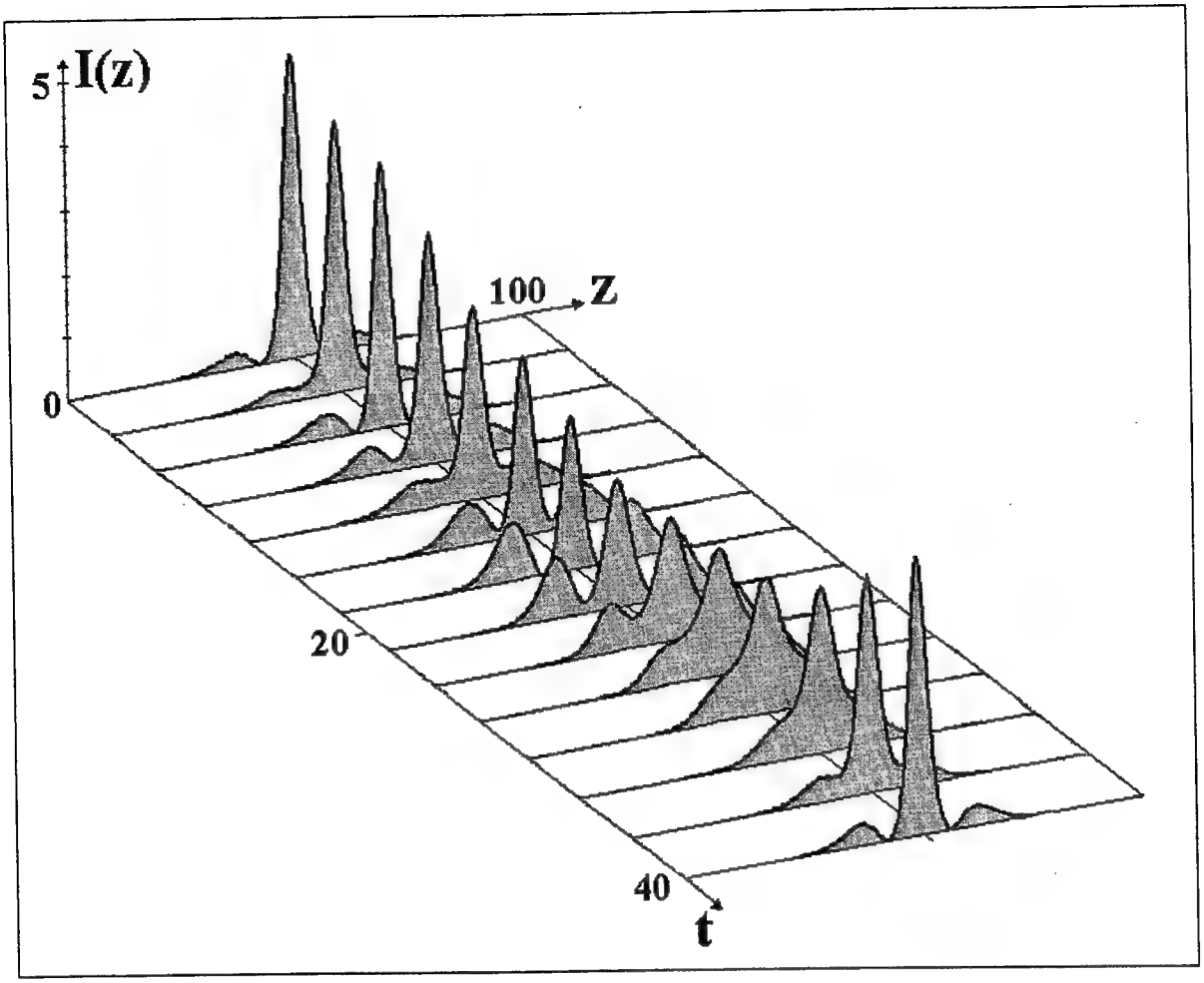

Fig. 2. The established regime with $a = 4$, $b = 0.1$, $p = 0.3$, and $q = 0.3$. The length of the initial Gaussian pulse is 15.

3. DISCUSSION

Any solution of eq. (1) ($d = 0$) can be decomposed into eigenfunctions determined from the following problem:

$$\frac{\partial^2}{\partial z^2}\Psi + \frac{1}{2}\left(\frac{1+\alpha}{1+b\int_V |E|^2\,dz} - 1 - \frac{p}{1+|E|^2} + iq\,|E|^2\right)\Psi = \lambda\Psi. \tag{6}$$

The spatial configuration of field described by Ψ_k will be named by us as k-th supermode. If $q = 0$ then all eigenvalues λ_k are real. As consequence of the oscillatory quantum-mechanical theorem the increments λ_k depends monotonically on k. For principal supermode ($k = 0$) λ_0 is maximum. This supermode with maximum increment remains after transient evolution, but all

other supermodes are suppressed. As a result, after transient evolution the established field has the form (3) ($\alpha = 0$) corresponding the principal supermode (see also (2)).

In the case of $q \neq 0$ eigenvalues become complex. The frequencies of individual supermodes $\mathrm{Im}\lambda_k$ differ. If the refractive index nonlinearity q is sufficiently large the dependence of increment $\mathrm{Re}\lambda_k$ on k is not monotone. There is critical value of the nonlinearity q, for which $\mathrm{Re}\lambda_2 = \mathrm{Re}\lambda_0$. As a result the 2nd supermode is built up. In fig. 2 this build-up manifests itself in the build-up wings of ultrashort pulse. We interpret the fast oscillations as the interference oscillations of intensity with the frequency spacing of principal and second supermodes ($\mathrm{Re}\lambda_2 - \mathrm{Re}\lambda_0$). The slow oscillations are interpreted by us as oscillations of intensities of principal and second supermodes due to their nonlinear interaction. Similar type of undamped oscillations is well-known for cavity modes of solid-state lasers[7–9].

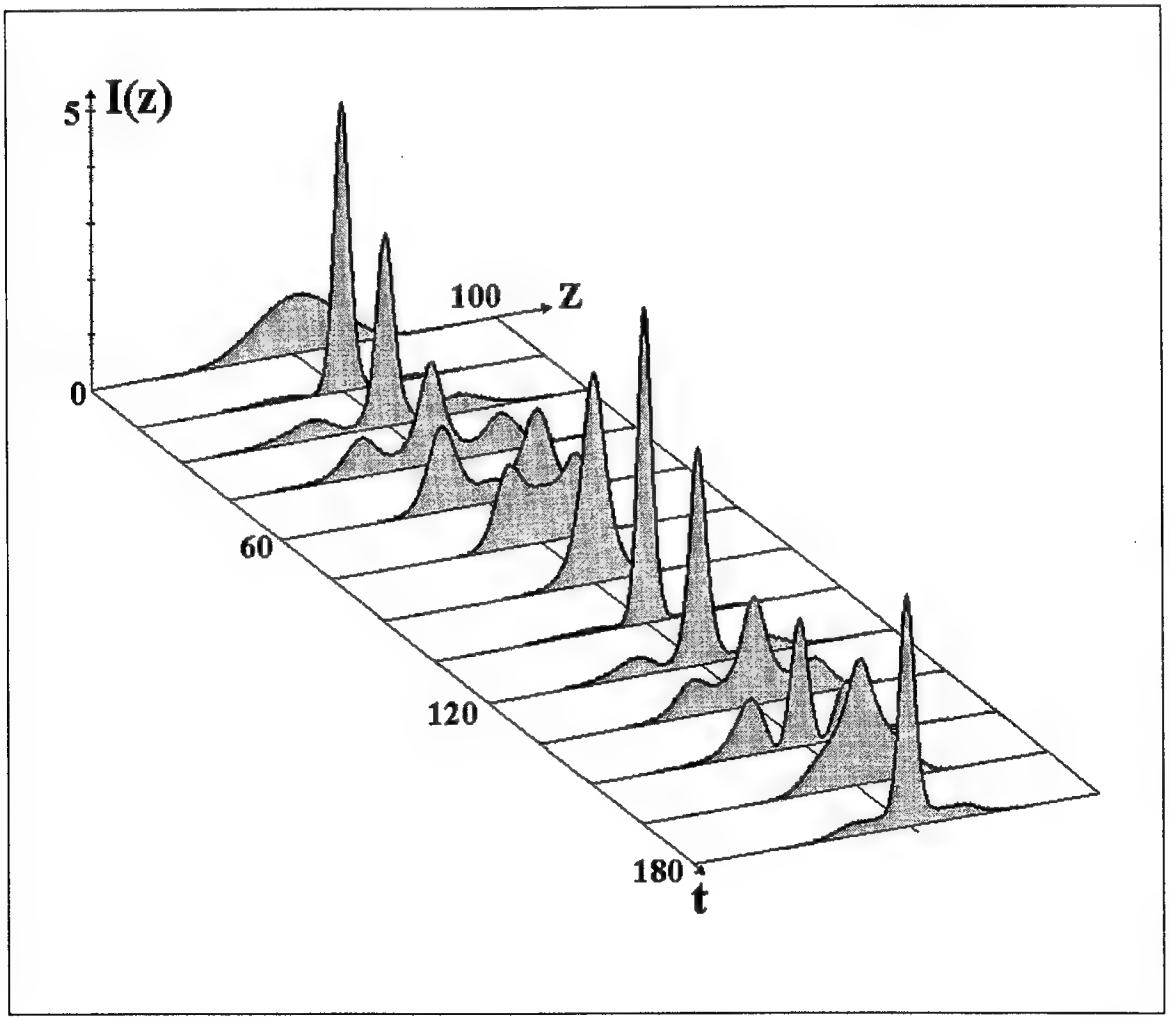

Fig. 3. Transient process with $a = 4$, $b = 0.1$, $p = 0.3$, and $q = 0.3$.
The length of the initial Gaussian pulse is 25.

4. CONCLUSION

Thus, the phase modulation instability due to nonlinearity of refractive index results in the change for the regime of passive mode-locking. For investigated model in the established regime either the number stable stationary pulses increases or the regime of breathing pulse is realized. That is, the established regime depends on initial conditions.

5. ACKNOWLEDGMENTS

This work has been supported by the Russian Fund for Fundamental Research (Grant 98–02–17791) and the State Science and Technology Program "Laser Physics" (Grant 3.20).

6. REFERENCES

1. K.P.Komarov, "Steady-state pulses in nonlinear dispersive medium with complex permittivity. Passive mode-locking of lasers", preprint № 247 Institute of Automation and Electrometry, Siberian Branch of the USSR Academy of Sciences, 1984.

2. K.P.Komarov, "On the theory of steady-state ultrashort pulses in passively mode-locked lasers", *Opt. Spektrosc. (USSR)*, Vol.60, № 2, pp.231-235, 1986. (Optika i spektroskopiya, Vol.60, № 2, pp.379-383, 1986.)

3. K.P.Komarov, "On the theory of transient evolution of the passive mode-locking", *Optics Communications*, Vol.54, № 4, pp.233-235, 1985.

4. A.K.Komarov, K.P.Komarov, A.S.Kuch'yanov, "On phase-modulation bifurcation during passive mode-locking in lasers", *JETP Letters*, Vol.67, № 4, pp.280-283, 1998. (Pis'ma Zh. Eksp. Teor. Fiz., Vol.67, № 4, pp.261-264, 1998.)

5. A.K.Komarov, K.P.Komarov, A.S.Kuch'yanov, "Phase modulation instability of passive mode-locking of solid-state lasers with inertial saturable absorber", *Quantum Electronics*, Vol.25, № 7, 1998. (Kvantovaya Elektronika, Vol.25, № 7, 1998.)

6. K.P.Komarov, A.S.Kuch'yanov, V.D.Ugozhayev, "Generation of stationary ultrashort pulses by a passive mode-locking solid-state laser", *Optics Communications*, Vol.57, № 4, pp.279-284, 1986.

7. D.Pieroux, P.Mandel, "On the rate equation approximation for free-running multimode lasers", *Quantum & Semiclass. Opt.*, Vol.9, pp.L17-L22, 1997.

8. D.Pieroux, P.Mandel, "Transient dynamics of a multimode laser: oscillation frequencies and decay rates", *Optics Communications*, Vol.107, pp.245-248, 1994.

9. A.K.Komarov, A.S.Kuch'yanov, "Bistability of solid-state laser generation", *Optoelectronics, Instrumentation and Date Processing*, № 2, 1998. (Avtometriya, № 2, pp.50-52, 1998.)

Generation dynamics of laser array with diffraction coupling.

V.P.Kandidov, A.V.Kondrat'ev

International Laser Center, Moscow State University, Moscow, Russia
E-mail: kandidov@fort.phys.msu,su; avk@fort.phys.msu.su

ABSTRACT.

The studies on transients in waveguide 1D and 2D laser arrays with the diffraction coupling in Talbot cavities are presented. The transient behavior essentially depends on the selectivity of an external cavity which are determinated by the number of lasers, dimensionality and filling configuration of arrays involved. Probabilities of the in-phase generation as a result of transient are calculated. The possibility of the in-phase generation forming during the transient is discussed. Keywords: ***laser array, external cavity, in-phase mode, out-of-phase mode, transient, selectivity.***

INTRODUCTION.

We consider a dynamics of collective generation of laser arrays with a diffraction coupling. The main purpose of such system creation is a high-power radiation with low angular divergence under in-phase generation of lasing channels.

The principle of diffraction coupling is simple. The radiation from each channel diffracts, reflects from coupling mirror and is injected into the other channels. It is usual to employ the Talbot effect to minimization of diffraction losses. This is the effect of Fresnel diffraction. Periodic field, diffracting, is self-reproduced at the Talbot distance equals to $2a^2 / \lambda$ (a is array period, λ is wavelength) . In the cavity coupling mirror is placed at a half of the Talbot distance from the channel's output apertures.

Experiments with laser arrays in Talbot cavity have been done in many scientific groups: of Napartovich[1] and Apollonov[2] in Russia, of Leger[3], Waarts[4] in USA, of Lescroart[5] in France and others.

The fundamental difficulty of a Talbot-cavity technique consists in a nearness of the diffraction losses of the in-phase and out-of-phase collective modes, which makes it complicate to obtain a desired in-phase generation. To achieve effective mode selection spatial filters[5,6], mode-selecting mirror[7] or even liquid crystals control display[8] can be placed in a Talbot cavity.

In theoretical works on the dynamics the in-phase mode stability is usually discussed. Wang and Winful[9,10] did it for semiconductor laser array with evanescent coupling. The "continuum" model with transversal phase diffusion[11,12] was offered for arrays of a large number of lasers. Likhanskii with colleagues employed the method of average field[13,14]. At the certain conditions the field of laser array can be demonstrate a complex behavior, in particular, the chaotic regimes of generation[15,16].

The approach to study diffraction coupling by means of a coupling matrix had been formulated, it seems, in the well known work of Golubentsev, Likhanskii and Napartovich[11]. We found the analythical expression for the complex elements of matrix of diffraction coupling at the assumptions wide enough[17].

The main subject of this report is a transient from spontaneous radiation of lasing channels of array to the collective generation regime.

SPIE Vol. 3685 • 0277-786X/99/$10.00

1. DYNAMICS MODEL OF THE COLLECTIVE GENERATION.

So, we consider one and two dimensional array of waveguide lasers with diffraction coupling in the external cavity (fig.1) Output windows of lasers are enlightenment and an independent generation of one channel is impossible. We assume that all the channels are identical and that each of them emits a same axial mode.

The field on the output aperture of an array can be written as the sum of the products of complex amplitude and the channel transverse mode f(x,y):

$$u(x,y,0,t) = \sum_n E_n(t) f_n(x,y) e^{i\omega t}, n = 1,2,\ldots,N.$$

We imply the validity of the constant mode approximation, according to which the collective generation does not alter the transverse field distribution in the lasing channels. We normalize time to the round trip time.

Then, the field gain in channels in tandem with diffraction field exchange in an external cavity defines the evolution of the complex amplitudes E:

$$E_n(t+1) = \sum_m M_{nm}\left(1 + \frac{g}{1+|E_m(t)|^2}\right)\cdot E_m(t), \quad m,n = 1,2,..,N.$$

Notice, the terms describing these processes appears in the equation multiplicatively. For a gain model we use the model of fast relaxation medium, neglecting by the possible frequency detunings. Here g is a small signal gain and the amplitudes E are normalized to the saturation field. A complex matrix of the coupling describes the diffraction field exchange. An element of matrix equals to projection of the field of one channel, diffracted after a round trip in the cavity onto the mode of other channel. We supposed that each channel emits a Gaussian beam with the dimensions σ_x, σ_y; the array periods equal to a_x, a_y and a coupling mirror is placed at distance L from the output aperture.

At these assumption we obtain the general expression for the diffraction coupling coefficients:

$$M_{nm} = \frac{1}{\sqrt{1-iD_x}}\frac{1}{\sqrt{1-iD_y}} exp\left\{-\frac{a_x^2}{2\sigma_x^2}\frac{(n_x-m_x)^2}{1-iD_x} - \frac{a_y^2}{2\sigma_y^2}\frac{(n_y-m_y)^2}{1-iD_y}\right\}, \quad D_{x,y} = \frac{2L}{k\sigma_{x,y}^2}.$$

Hence n_x, n_y and m_x, m_y are the numbers of the columns and rows in which the nth and mth lasers are located. The formula describes the linear array if $n_y - m_y = 0$ for any n_x, n_y.

We simulate the transient to the collective generation by the numerical solving of the dynamic equation system with initial conditions corresponding to the spontaneous radiation. It is a random set of statistically independent distribution of complex amplitudes over the channels:

$$\tilde{E}_n(t=0) = \left|\tilde{E}_n\right| exp(i\tilde{\varphi}_n), \quad \left\langle \tilde{E}_n^* \tilde{E}_m \right\rangle = \sigma^2 \delta_{nm}$$

The absolute values of amplitudes are distributed by Rayleigh law, the phases are uniformly:

$$w(|E|) = \frac{|E|}{\sigma^2} exp\left(-\frac{|E|^2}{2\sigma^2}\right), \qquad w(\varphi) = \frac{1}{2\pi}.$$

Further in our calculations, the dispersion σ^2 of Rayleigh distribution equals to 10^{-10}. After that, the distance between the output aperture and the coupling mirror will be equal to a half of the Talbot distance.

2. TRANSIENTS IN A LASER ARRAYS. COLECTIVE MODES.

Consider, for example, the transient to the in-phase generation in a linear array of twenty-five lasers at a small gain (fig.2a). We notice how collective generation develops from a field noise with random phase over the laser set. The tone image of phase dynamics is given nearly. The spots correspond to initial random phases. In the steady state we can see the uniform gray tone. The early life of absolute values of complex amplitudes is hidden from view because of small variety. The amplitude and phase decays on the array edges are explained by diffraction losses. The emitted field is shown as tone photos for initial noise at the time equal to zero and for the steady state. The white tone corresponds to positive real part of the field, the dark does to negative one.

To take the other possible situation when the out-of-phase mode depresses others at a rather large gain (fig.2b). In the steady state the phase changes from one channel to the next on pi. Respectively, on the tone image the dark and white fringes alternate each other.

It is convenient to use collective modes for analysis of dynamics of collective generation. The spectrum of collective modes of a laser array in an external cavity is the set of eigenvectors of the matrix of diffraction coupling:

$$\gamma_j e_n^{(j)} = M_{nm} e_n^{(j)}, \qquad j = 1,2,..,N$$

In essence, the collective modes $e_n^{(j)}$ are the field configurations which are supported by an external cavity as a selecting element. When the matrix is known the eigenvectors $e_n^{(j)}$ as easily as eigenvalues γ_j can be calculated numerically. Represent the complex amplitude E as the superposition of collective modes:

$$E_n(t) = \sum_m A_j(t) \cdot e_n^{(j)}$$

Far from saturation $(|E| << 1)$ the following linear equation defines the evolution of the complex amplitudes:

$$E_n(t+1) = \sum_m M_{nm}(1+g)E_m(t)$$

For this reason the amplitude of jth mode in one round-trip changes in $\gamma_j(1+g)$ times. Therefor, the condition of jth mode excitation requires g to be greater than jth mode threshold G_j:

$$G_j \equiv -1 + \frac{1}{|\gamma_j|}.$$

For the small diffraction losses these thresholds equal to $-ln|\gamma_j|$. It is alike the expression for transverse mode threshold in the usual laser.

Take for example the linear array of slab lasers (fig.4a). As we might expect, the difference between thresholds of the in-phase and out-of-phase modes is relatively small and decreases with the number of lasers. The next modes are far apart. Notice, if a gain is small the difference between losses leads usually to depression of the out-of phase mode by the in-phase mode.

For two-dimensional square arrays (fig4b) of lasers with symmetrical apertures the thresholds of four modes are closely related, namely, of the in-phase, two degenerate "fringe" modes and of the out-of-phase mode. Of course, the difference between thresholds vanishes with number of lasers. The transients in such arrays refer to competition of in-phase and "fringe" modes..

Fig. 5 shows the tone images of real part of the field over the apertures of square array of twenty-five lasers at initial "noise" state (fig.5a) and at the steady states. In one case (fig. 5b), the in-phase mode depresses the higher modes. For other realization (fig. 5c) two degenerate modes depress the in-phase and out-of-phase modes. The steady state is a superposition of the "fringe" modes.

3. EFFECT OF SELECTIVITY. STATISTICAL TESTS.

In this way the selectivity of a Talbot cavity may be defined as difference of thresholds of the in-phase and next modes. Threshold of the in-phase mode G_1 and selectivity S decrease with a number of lasers due to a decline of edge losses and these equalization for the lowest modes. In two-dimensional arrays the selectivity falls slowly as one dimensional array owing to the system geometry.

The effect of the selectivity of a Talbot cavity on transients in laser arrays is born by statistical tests. We computed the probabilities of the in-phase generation as a result of transient from the exceeding of a gain g over the in-phase mode threshold (fig.6). At the small exceeding Δg the in-phase generation will most probably. The probability decreases away from the threshold because the selectivity S becomes low-significant in comparison with a gain g. For the arrays of large elements the probability cuts down more quickly. Here the result of transient in large extent is dictated by initial conditions. Asymptotically, at the exceeding more greater than the selectivity, the in-phase or out-of-phase generation are equally liked.

In two-dimensional arrays where the selectivity for the same number of lasers is better, the probability falls more slowly. At $\Delta g >> S$ it's value is less than 50 per cents on account of the competition of the four lowest modes.

4. TRANSIENT CONTROL.

The high probability of in-phase generation at a small gain opens an avenue for transient control and obtaining of the in-phase generation even at high powers.

To this end we can use gain-variation during the course of transient. The results may be different at the same initial conditions. As example a linear array of twenty-five lasers is shown (fig.7).

For the first case (fig7a) a small gain makes possible to select the in-phase mode from out-of-phase to the 700th round trip. The later gain increasing bring up output power, retaining the desired profile of in-phase collective generation.

When the gain is large from the outset, the out-of-phase mode which prevailed in initial stage depresses the in-phase mode. We have the out-of-phase generation.

5. CONCLUSIONS.

The suggested dynamic model of the collective generation of laser arrays accounts for the sequential gain in lasing channels and diffraction exchange in an external cavity. Complex matrix of diffraction coupling describes amplitude and phase relationships of the fields of channels in the plane of these apertures. For linear array the transient refers to competition of the in-phase and out-of-phase modes, for square array it does to four lowest modes. Relation between selectivity of an external cavity and exceeding over the threshold of the in-phase mode brings the probability of in-phase generation as a result of transient. At a small gain the probability significantly greater than 50 per cents. The gain-variation from small to large values during the course of transient allows to obtain the in-phase generation at high out-put energy.

REFERENCES.

1.O.R.Kachurin, F.V.Febedev, A.P.Napartovich. "Properties of the Radiation from an Array of Phase-Locked CO_2 Lasers". *Quantum Electronic*, 15, 1808 (1988).
2. V.Apollonov et al. // Quantum Electronics, 25, 1808 (1998)
3.Leger et al. // Appl.Phys.Lett., 55, 334 (1989)
4.R.Waats, D.Mehuys, D.Nam, D.Welch, W.Steifer, D.Seifres *Appl. Phys. Lett.* 58, 2586, (1991).
5. G.Lescroart, R.Miller, G.L.Bourdet. "Phase Filter design for Efficient Side Lobe Suppression in Phase Coupled CO_2 Waveguide Lasers Array". *Optics Comm.*, 115, №3,4, 223, (1995).
6. A.F.Glova, S.Yu.Kurchatov, V.V.Likhanskii, A.Yu.Lysikov, A.P.Napartovich. "Coherent emission of a linear array of CO_2 waveguide lasers with a spatial filter". *Quantum Electronic*, 23, 515 (1996).
7. J.R.Leger, G. Mowry // Appl. Phys. Lett. 63, 2884 (1993)
8. S.Sandlers, D.Waarts, D.Nam et al., *Appl. Phys. Lett.*, 64, №12, 1478-80, (1994).
9. S.S.Wang, H.G.Winful. "Dynamics of phase-locked semiconductor laser arrays". Appl. Phys. Lett. 53, 1894 (1988).
10. H.G.Winful, *Phys. Rev.*, A, 46, 6093, (1992).
11. A.A.Golubyentsev, V.V.Likhansky, A.P.Napartovich. "Theory of phase synhronization of laser sets". *JETF*, 93, 1199 (1987).
12. Z.Jiang, M.McCall //Proc. SPIE, v.2099, p.40
13. S.Yu.Kourtchatov, V.V.Likhanskii, A.P.Napartovich, F.T.Arecchi, A.Lapucci, "Theory of phase locking of globally coupled laser arrays". *phys. Rew.*, A, 52, 4089 (1995).
14. S.N.Kozlov, V.V.Likhanskii. "Field dynamics of optically coupled lasers with random fluctuations of eigenfrequencies" *laser physics*, 3, 1067 (1993).
15. K.Otsuka, "SelfInduced Phase Turbulence and Chaotic Itinerancy in Coupled Laser Systems". *Phys. Rev. Lett.*, 65, 329 (1990).
16. D.Merbach, O.Hess, H.Herznel, E.Schoell. "Injection-induced bifurcations of transverse spatiotemporal patterns in semiconductor laser arrays". *Phys. Rev.* E, 52, 1571 (1997).
17. V.P.Kandidov, A.V.Kondrat'ev. "Collective modes of laser arrays with diffraction coupling in Talbot cavities of various geometries". Quantum Electronics, 24, 240 (1997).

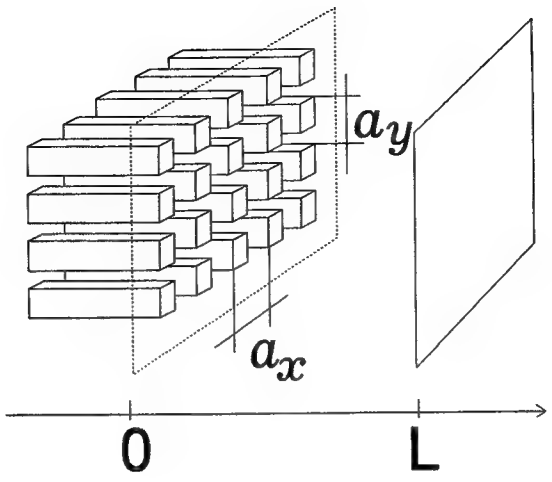

Fig.1. Scheme of 2D laser array in an external cavity.

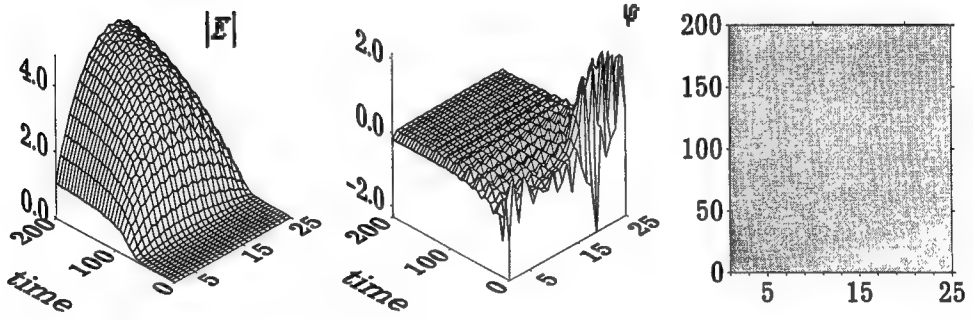

Fig2a

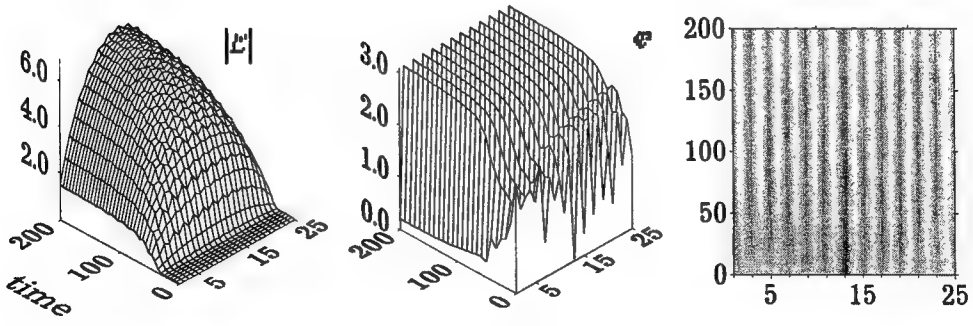

Fig.2b

Fig.2. Dynamics of the absolute values and phases (profile and tone images) of the complex amplitudes. Linear array of 25 slab lasers in a Talbot cavity at a small gain -fig.2a- (g=0.1) and large gain -fig.2b- (g=0.4).

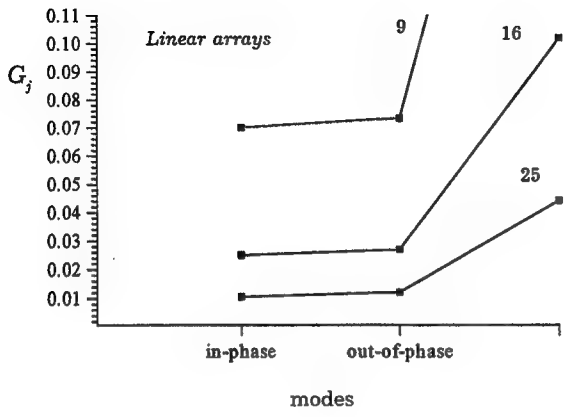

Fig.3a

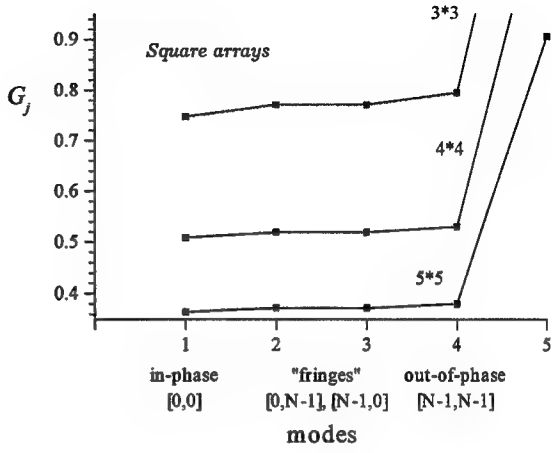

Fig3b

Fig.3. Thresholds of collective modes of linear arrays of slab lasers (fig. 3a) and square arrays (fig 3b) in Talbot cavities. $(a / \sigma = 4, L = 0.5z_t)$

Fig.4a

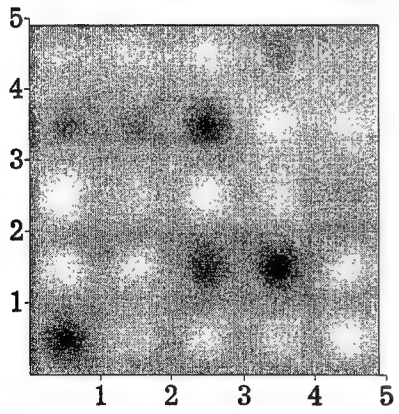

Fig.4b

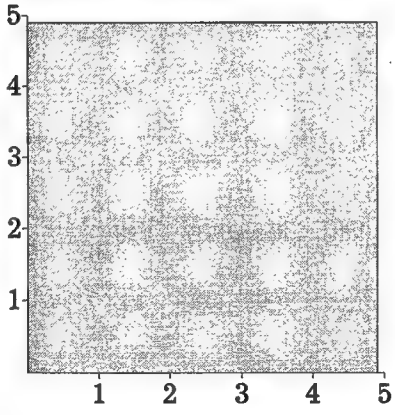

Fig.4c

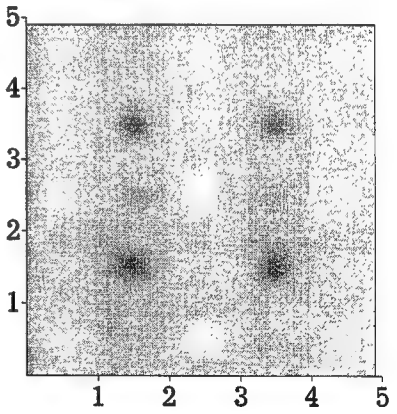

Fig4. Tone images of real part of the field over the apertures of square array of 5*5 lasers. Initial "noise" state (fig.4a) and the possible steady states: in-phase mode ([0,0]) -fig.4b; sum of two degenerate "fringe" modes ([0,4]+[4,0]).

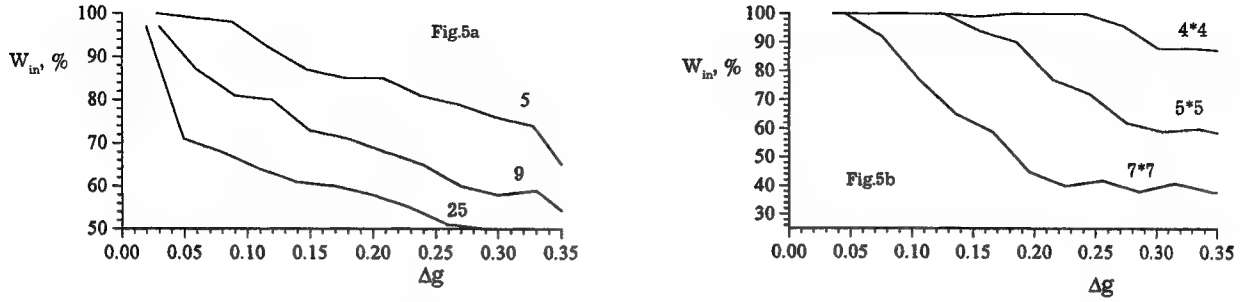

Fig.5 The probabilities of in-phase generation as a result of transient in linear laser arrays and square arrays.

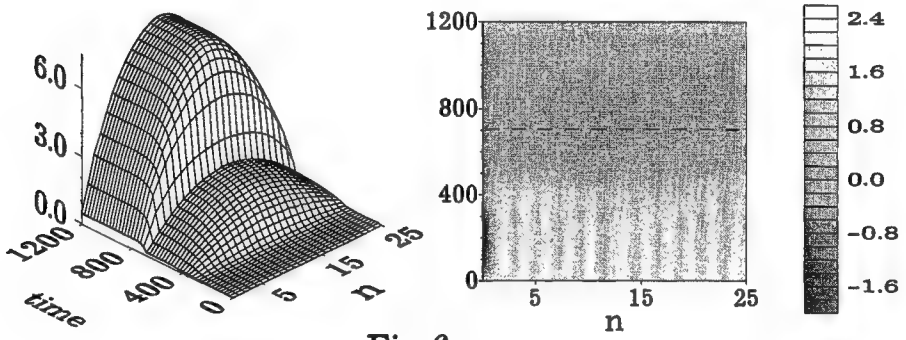

Fig.6a

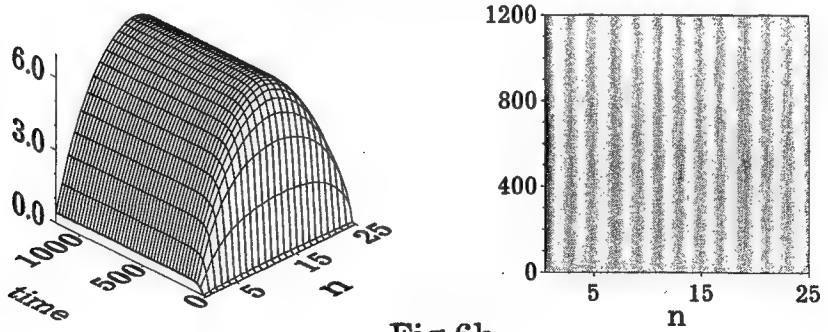

Fig.6b

Fig.6. Transient control. Linear array of 25 slab lasers ($a / \sigma = 4$) in a Talbot cavity. Gain-variation (t=1..700: g=0.05, t=700...1200: g=0.4) -fig.6a. Invariable gain (t=1..1200: g=0.4) -fig. 6b.

Electrodynamic resonances and ultimate pump intensities for microsphere and microdisk resonators

V.Gruzdev* , and M.Libenson*

State Research Center "S.I.Vavilov State Optical Institute"
Birzhevaya Liniya, 12, St.-Petersburg 199034 Russia

ABSTRACT

The problem of initiating of laser-induced damage of ideal microspherical and microdisk resonators and nature of processes limiting ultimate pump intensity of the resonators are considered in this paper. Electrodynamic processes are supposed to play major role in initiating of laser-induced damage of the resonators and theoretical model to describe local increasing of high-power electromagnetic field in passive microresonator is presented to study the processes. It is based on idea of formation of unstable field structure in resonant dielectric microcavity connected with formation of positive feedbacks resulting in light-induced variation of quality factor and its spectrum. Possibility for field instability to arise is estimated making use of model of diffraction of high-power plane wave on sphere and microdisk resulting in formation of resonant whispering-gallery mode. Field instability is shown to be threshold-like phenomenon. There are estimated ultimate amplitude of incident pump wave and field amplification in the microsphere and microdisk.

Keywords: microsphere resonator, microdisk resonator, whispering-gallery mode, field instability, positive feedback, high-power laser field, laser-induced damage

1. INTRODUCTION

Theoretical and experimental investigation of recently developed microspherical (MS) and microdisk (MD) resonators is one of new and fast developing areas of laser physics. Great attention has been attracted to the resonators since lasing has been observed in microdroplets[1-4], solid microspheres[5-7] and microdisks[8]. This attention is connected with unusually high quality factor and finesse of whispering-gallery modes of MS and MD resonators which can exceed 10^9 and is 10 - 1000 times higher than those for similar Fabry-Perot resonators[9]. For example, ordinary Fabry-Perot resonator with mirrors of R=0.99 reflectivity has record[10] finesse $F=\pi R^{1/2}/(1-R)\cong Q/L=10^5$ (L - distance between plane mirrors) while finesse of MS resonator of 100-μm-diameter[9] exceeds 10^6.

Such high-Q resonators can confine large electromagnetic field in small volumes while high Q can result in formation of both positive and negative feedbacks. In this connection problem of radiation-induced damage of MS and MD resonators becomes important because optical damage limits both output radiation power and intensity of optical pumping.

Processes in microresonators and problem of their optical damage differs from that of ordinary macroresonators. In macro-resonator increasing of amplitude of high-power internal laser radiation results in laser-induced damage (LID) of mirrors, lenses, optical coatings and other optical elements of the resonator. In this case LID is determined by processes (which are connected with local high-absorbing inclusions) in the single optical elements and focusing conditions in the resonator. Moreover, special methods allows to exclude laser-induced increasing of Q-factor and field instability due to various negative feedbacks. Developing of manufacturing technology is able to increase LID thresholds of single optical elements. Together with introduced negative feedbacks and safe focusing arrangements inside the resonator it can result in increasing of total LID threshold of macro-resonator.

Our paper is devoted to investigation of physical processes underlying LID of microresonators and determining their ultimate pump power. The problem of ultimate parameters differs from that of macroresonators and requires specific

*Tel. (812)218-0231, e-mail: photphys@dost.bcam.ifmo.ru

theoretical consideration. We present a model describing sharp increasing of high-power laser field inside non-amplifying (passive) microresonator which material has Kerr-like nonlinear optical response. Field self-action through nonlinear variation of refractive index is shown to result in laser-induced variation of quality factor, in particular, variations of its spectrum leading to formation of unstable field structure inside the resonator through involving of pump radiation of near-resonant wavelengths into formation of quasi-resonant mode. Possible processes of formation of positive and negative feedbacks are discussed.

2. FIELD INSTABILITY IN MICRORESONATOR: GENERAL IDEA AND FORMALISM

The aim of this section is to show possibility of laser-induced formation of unstable field structure from high-Q eigenmode inside microresonator. There are studied some characteristics of this process and the mechanism of formation of positive feedback resulting in the instability.

2.1. General idea of developing of field instability

On the one hand, it is well known that dielectric microcavities, for example, sphere or disk, can accumulate large amount of electromagnetic-field energy by forming of resonant eigenmodes[11]. On the other hand, nonlinear interaction of matter with high-power laser field which is capable to induce considerable addition to refractive index can result in variation of quality factor Q of the microresonators. That can be followed by formation of specific quasi-eigenmode and its resonant excitation. Thus, combination of resonant properties with nonlinear self-action through laser-induced variation of refractive index can lead to formation of positive feedback. The feedback can result in changing of rates of some processes inside the resonator and even in field instability inside the resonator if stabilizing negative feedback are dominated by the positive one. It is shown below that in the most general case (with no respect to geometry of the microresonator and type of resonant mode) the instability comes through the following[12]: field amplitude E_{in} inside the microresonator tends to some limited value and its derivation with respect to incident field amplitude E_0 tends to infinity while incident field amplitude approaches finite threshold value E_0*:

$$E_{in} \to E_{in}^{*}, \qquad \frac{\partial E_{in}}{\partial E_0} \to \infty \quad \text{with} \quad E_0 \to E_0^{*}. \tag{1}$$

Let us consider mechanisms of developing of the mentioned positive feedback. Surface whispering-gallery eigenmodes of MS and MD microresonator are well known to be formed only for certain combinations of wavelengths of incident pump field and microcavity's size and refraction index which are referred to as resonant parameters. Optical pumping of such microlasers is usually provided with rather wide-spectrum source, so, only radiation of few single wavelengths corresponding to resonant parameters can form eigenmodes. Such pumping is not very efficient because of high filtering properties of the microresonators due to narrow peaks of Q-factor spectrum. Most of pumping radiation has parameters close to resonant.

On the other hand, amplitude of resonant mode can reach very large values even for linear scattering[11] and can tend to infinity according to (1) in nonlinear case. Then field-induced variations of Q-factor of the microresonator can play major role in evolution of field inside the resonator. The variations can result in developing of either positive or negative feedbacks (Fig. 1) which can either contribute to developing of field instability or stopping of field increasing and stabilization of its amplitude. In the first case the positive feedback can be formed through laser-induced variations of Q spectrum - its broadening and shift of resonant frequency (Fig. 5). This results in involving of pump radiation of near-resonant wavelengths in formation of quasi-resonant mode. The possible mechanism of this process is as follows.

If field's and microresonator's parameters are not exactly resonant but do not differ from them very much and light flux density is high enough to induce positive addition to refraction index then light-induced variation of refraction index can result in making conditions for an eigenmode to be formed with pump radiation of near-resonant parameters. Small initial increasing of near-resonant pump field inside the resonator is followed by small variation of refraction index. The matter of fact is that pump field induces distribution of refraction index which is adjusted with distribution of field inside the microcavity. This implies increasing of field amplitude inside the resonator due to field-induced variation of refraction index. Variations of Q-factor spectrum induced by electric field of resonant whispering-gallery mode can contribute to this

process too. Resonant excitation of the quasi-eigenmode for near-resonant wavelengths results in amplitude increasing inside the microcavity which in turn results in inducing of greater variation of refraction index. Thus, self-induced formation of quasi-eigenmode establishes positive feedback (Fig. 1) resulting in radiation-induced variation of Q-factor spectrum and resonant increasing of total amplitude and field instability inside the microresonator if incident pump field amplitude exceeds instability threshold.

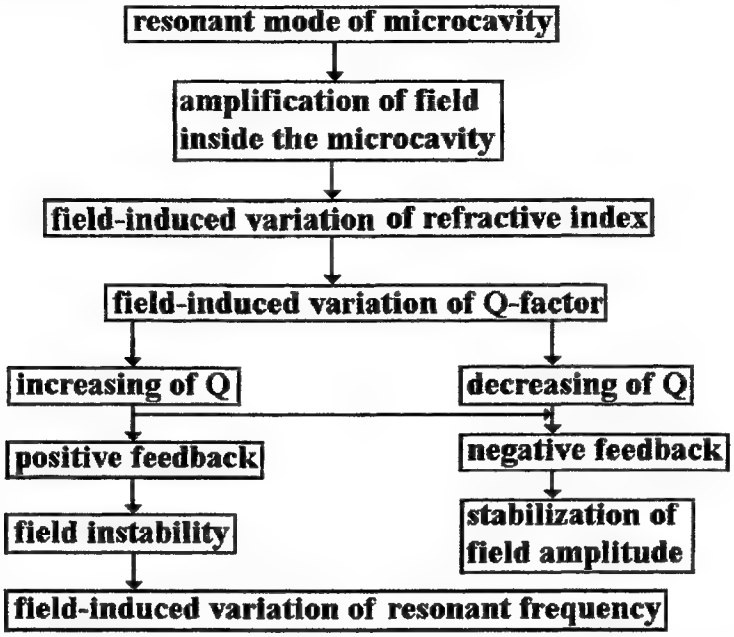

Fig. 1. General idea of formation of field instability inside microresonator accompanied by field-induced variations of Q-factor, in particular, variations of its spectrum and resonant frequency.

It should be mentioned that we consider passive resonators, so, we do not take into account negative feedbacks connected with space distribution of inversion and its variation during lasing. Competition between the negative feedbacks and described positive feedbacks can result in stopping of increasing of field inside the resonator and stabilization of its amplitude at a certain level. Nevertheless, the discussed below formation of unstable field mode in the microresonator can play important role in many processes in the resonator, in particular, laser-induced damage.

2.2. General formalism

Surface whispering-gallery eigenmodes seems to be the most probable modes for developing of this type of instability due to their super-high Q-factor[5, 8, 9]. For this reason to obtain general description of the proposed type of instability in microresonators let us consider microcavity (spherical or microdisk) of radius a consisting of isotropic nonabsorbing homogeneous dielectric with refractive index n_{in} being placed in homogeneous transparent dielectric with refractive index n_{ex} (Fig. 2). We neglect nonlinear properties of the external medium. The microresonator is pumped by plane linearly polarized wave of amplitude E_0 and wave number k. We suppose that

$$n = n_{in} / n_{ex} = m + \delta n, \tag{2}$$

where $m=const$ and field-induced addition has the following form for isotropic Kerr-like nonlinear medium:

$$\delta n = n_2 \cdot E_{in}^2, \tag{3}$$

E_{in} is total electric field inside the microcavity. Let us consider a single whispering-gallery mode of the microresonator. According to exact solution of diffraction problem field amplitude in the microresonator can be represented in the following form[13, 14]:

$$E_{in} = \sqrt{|E_r|^2 + |E_\theta|^2 + |E_\varphi|^2} \approx E_{in0} + \delta n \cdot E_{in0} \cdot S(r, \theta, \varphi, x) = S_0 \cdot E_0 \cdot (1 + \delta n \cdot S(r, \theta, \varphi, x)), \tag{4}$$

where E_{in0} is electric field amplitude inside the resonator in linear approximation (i.e., amplitude of the resonant whispering-gallery mode in linear case), $\delta n \cdot S < 1$, $S(r, \theta, \varphi, x)$ is dimensionless function which value is determined by geometric parameters of the microcavity, $S_0 = const$ is amplification of field amplitude in linear case. This function describes space field distribution in microresonator and its maximum value depends in resonant manner on size parameter $x = 2\pi a n_{in} / \lambda_0$. Thus, solution for linear case is expanded with respect to small perturbation and only first terms are taken into account to estimate influence of optical nonlinearity onto behavior of laser field inside the microcavity and variations of Q-factor.

Substituting (3) and (2) into (4), one gets equation for real positive value of field amplitude inside the microresonator

$$E_{in} \cong S_0 \cdot E_0 + n_2 \cdot S \cdot S_0 \cdot E_0 \cdot E_{in}^2 . \quad (5)$$

Let us consider maximum value of field amplitude in the microcavity. Solution to equation (5) has the following form:

$$E_{in} = \frac{1}{2 n_2 E_0 S_m S_0} \left[1 - \sqrt{1 - 4 n_2 S_m S_0^2 E_0^2} \right], \quad (6)$$

where S_m is maximum value of $S(r, \theta, \varphi, x)$. The solution exists under the condition

$$E_{in0} \le E_{in0}^* = [4 n_2 S_m S_0^2]^{-1/2}, \quad (7)$$

where at the edge of solution-existence interval ($E_0 = E_0^*$)

$$E_{in} \to E_{in}^* = \sqrt{\frac{1}{n_2 S_m}} ; \frac{\partial E_{in}}{\partial E_{in0}} \to \infty . \quad (8)$$

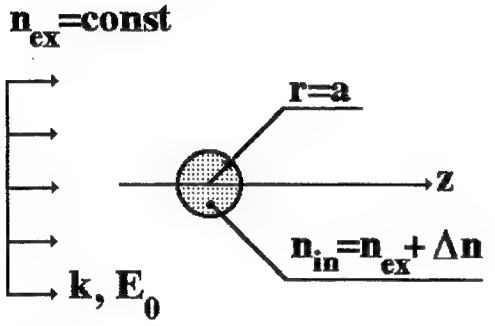

Figure 2. Geometry of the problem for obtaining of general formalism.

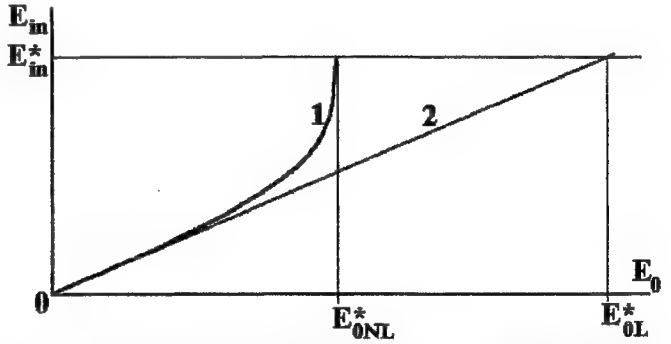

Figure 3. Typical dependence of field amplitude inside microcavity E_{in} on pump field E_0 for nonlinear (curve 1) and linear (curve 2) cases.

Dependence of field amplitude inside the microcavity on amplitude of pump field for both linear and nonlinear cases is depicted in Fig. 3. Instability threshold E_0^* is determined by material parameters of the sphere and its geometry (through the value S_m). Linear dependence between field amplitude inside the microcavity and that of pump field is depicted in Fig. 3 for references.

The developed formalism allows to get detailed information about instability characteristics and their dependence on parameters of microresonator of arbitrary shape. Influence of the shape and geometrical size on instability threshold comes through the value of S_m.

Thus, nonlinear dependence of microresonator's refractive index on electromagnetic field amplitude can result in electrodynamic field instability of the determined above type (1). In case of MS resonator it can be referred to as field collapse. The described instability can affect processes in microcavity through radiation-induced variations of various parameters, in particular, variations of Q-factor. To investigate this problem one should obtain connection of the Q with field amplification inside the microresonator for unstable mode.

3. PASSIVE AMPLIFICATION OF FIELD IN MICROCAVITY AND ITS QUALITY FACTOR

We consider influence of amplitude of resonant mode on Q-factor and its spectrum in this section. Our aim is to determine type of feedback (positive or negative) developing with the variations of Q and role of spectrum variations in formation of field instability. For this purpose we find connection of field amplification inside the resonator with Q for nonlinear case.

In linear case amplification of pump power of resonant wavelength is connected with Q-factor of microresonator (see for example, appendix A) in the following way:

$$\frac{P_{0MAX}}{P_{pump}} = \frac{\omega_0^2}{\gamma\ \omega_{res}} \cong \sqrt{3}Q_0 \tag{A4}$$

where $\omega_{res}^2 = \omega_0^2 - \gamma^2/4 \cong \omega_0^2$ is resonant frequency for lossy microcavity and Q_0 is quality factor for the case of linear interaction of laser radiation with matter. Amplification of field amplitude for resonant mode with quality factor Q can be estimated as follows

$$\frac{E_{in}^{MAX}}{E_0} \cong \sqrt{\sqrt{3}Q_0} \cong 1.316\sqrt{Q_0} \tag{A6}$$

This estimate is used for particular case of MS resonator to obtain threshold pump amplitude and dependence between Q-factor and field amplification. Estimating threshold pump amplitude or power, one should take into account that different modes of one and the same microcavity have different Q (for example, in microsphere[11, 15-18]), so, every mode has its specific instability threshold.

On the other hand, amplification of field amplitude inside microspherical resonator can be estimated using general expressions (4), (7), (8):

$$\left(\frac{E_{in}^*}{E_0^*}\right)_{\max} = 1.316\sqrt{Q} = S_0(1+\delta n \cdot S_m) \le 2 \cdot S_0 \tag{9}$$

where Q is quality factor for nonlinear case. Flux density amplification is given by

$$\left(\frac{I_{in}^*}{I_0^*}\right)_{\max} = 1.732Q = 4S_0^2 \tag{10}$$

According to our estimates for resonant wavelength 1.06 μm S_0=7250 (corresponding to $Q_0 = 10^8$). Using the obtained formulas one can get the estimates for:

$$\left(\frac{E_{in}^*}{E_0^*}\right)_{\max} = 14500; \left(\frac{I_{in}^*}{I_0^*}\right)_{\max} = 2.1 \cdot 10^8 \tag{11}$$

$$S_0 = 0.658 \cdot Q^{1/2} \tag{12}$$

Absolute value of threshold amplitude can be got utilizing data from[19]. Assuming threshold of LID in 10-μm-diameter silica MS resonator to be $E^*_{in}=10^7$ V/cm and $I^*_{in}=10^{12}$ W/cm^2, nonlinear coefficient of refraction index $n_2=10^{-12}$ esu, one can get the following estimate of ultimate pump amplitude, fluence and power:

$$E^*_0 = 380 \text{ V/cm}, \qquad I^*_0 = 2.887 \text{ kW/cm}^2, \qquad P_{pump} = I^*_0 \cdot \pi r^2 = 226.75 \text{ μW} \tag{13}$$

One can see that field-induced variations of refraction index in the microcavity are much less than linear part of the refraction index even for near-damage field value. This implies that field-induced variations of all parameters can be considered as small additions proportional to field intensity or squared electric field.

One of important questions which should be touched is how field-induced variation of quality factor influences decay rate. To study this problem one should consider equation describing decay of field intensity I inside the resonator[21]:

$$\frac{dI}{dt} = -\frac{I}{\tau} = -\frac{\omega}{Q} I \tag{14}$$

where τ is photon life-time, ω is resonant frequency,

$$Q = Q_0 + \beta \cdot I \tag{15}$$

is intensity-dependent quality factor, Q_0 is quality factor of the resonant mode for linear case, β describes laser-induced variation of Q. In general case it can be either positive (corresponding to positive feedback) or negative (negative feedback).

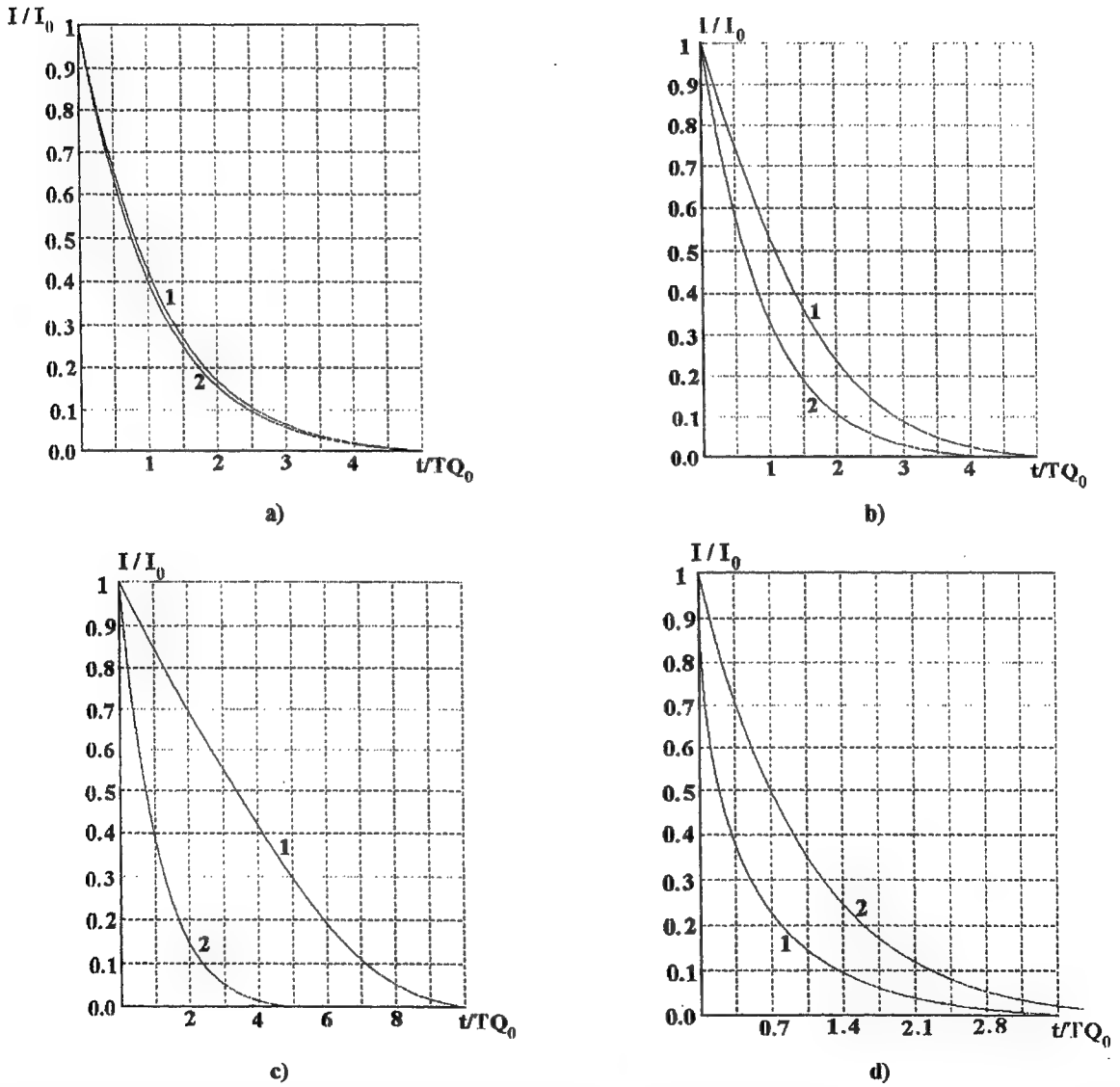

Fig. 4. Decay of laser intensity for several cases of field-induced variations of Q-factor (curve 1) as compared with exponential field decay for linear case (curve 2). a) $a = \beta I_0 / Q_0 = 0.1$ - weak positive feedback; b) $a = \beta I_0 / Q_0 = 1.0$ - medium positive feedback; c) $a = \beta I_0 / Q_0 = 5.0$ - strong positive feedback; d) $a = \beta I_0 / Q_0 = -1.0$ - negative feedback.

Integrating of (15) gives the following

$$\ln\frac{I}{I_0}+\frac{\beta I_0}{Q_0}\left(\frac{I}{I_0}-1\right)=-\frac{\omega}{Q_0}(t-t_0) \tag{16}$$

This dependence is depicted in Fig. 4 for several parameters Q_0 and $a=\beta \cdot I_0/Q_0$. As one can expect positive feedback ($a>0$) results in slower decreasing of field intensity I with time (Fig. 4 a, b, c) while negative one leads to faster decay of field intensity (Fig. 4 d) as compared with linear exponential decay. As one can see, the more field-induced variation of Q-factor, the more deviation from exponential decay characteristic of linear case. In the limiting case of $a>>1$ field intensity decays linearly (Fig. 4 c). This implies that much power of resonant mode stays inside the resonator for rather long time.

Thus, decreasing of power of resonant (in linear approximation) mode slows down due to field self-influence. That is equivalent to increasing of Q-factor due to positive addition. Now determining of sign of β is very critical for our model. It can be done using estimations (9), (10):

$$\left(\frac{E_{in}}{E_0}\right)_{\max}=\left(\frac{E_{in0}+\Delta E}{E_0}\right)_{MAX}=S_0+\delta\, nS_mS_0=1.316\sqrt{Q_0+\beta\, I}\cong 1.316\left(\sqrt{Q_0}+\frac{\beta\, I}{2\sqrt{Q_0}}\right), \tag{17}$$

what allows to determine the constant β:

$$\beta=\frac{\delta n\cdot S_m\cdot S_0\cdot 2\sqrt{Q_0}}{I_0} \tag{18}$$

As one can see here $\Delta E>0$ and $\delta n>0$ what implies that $\beta>0$ too, so, developing of field instability in the resonator with positive nonlinear coefficient of refraction index is accompanied by positive feedback in field-induced variations of Q-factor. That agrees well with the model described in section 2.1.

It is not difficult to show that generation frequency increases with developing of field instability. Really, assuming field-induced variations of the frequency to be small, we can consider the following dependence on radiation intensity:

$$\omega=\omega_{RES}+\eta\cdot I \tag{19}$$

where ω_{RES} is resonant frequency of whispering-gallery mode for linear case. Field-induced increasing of Q-factor is equivalent to decreasing of losses described by value γ in (A5):

$$\omega_{RES}^2=\omega_0^2-\gamma^2/4. \tag{A5}$$

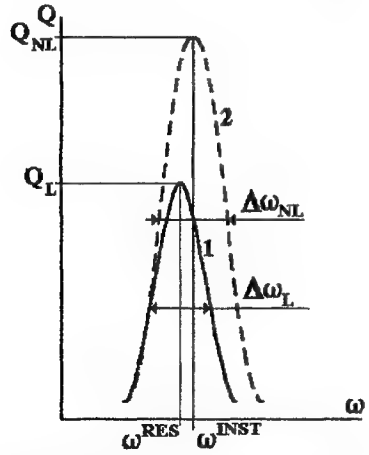

Fig. 5. Laser-induced variation of Q-factor spectrum of passive microresonator which can accompany developing of field instability. 1 - spectrum of Q-factor for linear resonant case; 2 - that for nonlinear case. There are shown variation of resonant frequency and broadening of Q-factor spectral line for linear (L) and nonlinear (NL) optical response. ω^{RES} is resonant frequency for linear passive resonator, ω^{INST} is generation frequency at which field instability develops.

So, resonant frequency of unstable mode is higher than that of initial whispering-gallery mode and $\eta>0$. This feature can be used to check the presented model and to detect developing of field instability prior to LID.

Similar consideration can show that field-induced variation of width of Q-factor spectral line described by the dependence

$$\Delta\omega_{NL} = \Delta\omega_L + \rho \cdot I \tag{20}$$

results in increasing of full width at half maximum, i.e., $\rho > 0$.

4. FIELD INSTABILITY IN MICRODISK RESONATOR

An example with MS resonator was used to illustrate the presented ideas. Similar calculations can be carried out for MD resonator which can define the values S_0 and S_m in general expressions from section 2.

One important feature of MD resonators should be taken into account when one considers the problem of field instability in microdisks: there can be distinguished three types of eigenmodes for passive microdisk (Fig. 6). The eigenmode of the first type is formed by reflections at plane edges and is a standing wave similar to that in ordinary Fabry-Perot resonator. The eigenmode of the second type is a whispering gallery mode. Analytical and numerical calculations[20] have shown many similarities between whispering-gallery modes of microsphere and those of cylinder. The modes of the third type can be called hybrid and are formed by multiple reflections at both plane and side boundaries of the microcavity. Whispering-gallery modes have the highest Q among all the described modes, so, they are the most probable candidates to start developing of field instability in MD resonators. In the first approximation, the presented model can be applied to this kind of modes.

For example[20], it follows from (9) that field amplification in linear case S_0 is about 68.2 for whispering-gallery mode of glass cylinder (refraction index 1.530, diameter 8.733 μm for radiation wavelength 0.600 μm). That corresponds to Q_0 = 10743 according to (A6). Field amplification in nonlinear case is $2S_0$=136.4 according to (9) what implies threshold of field instability 73 kV/cm according to (7), (8) and (9).

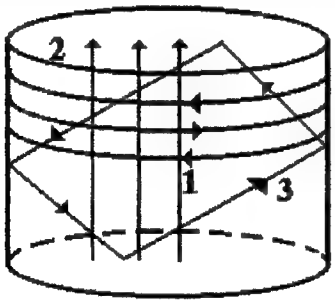

Fig. 6. Sketch of space structure of modes of microdisk resonator in approximation of geometric optics. 1 - mode formed by reflections at plane edges (standing wave); 2 - whispering-gallery mode (surface waves; 3 - hybrid mode (reflected at both plane and side surfaces).

Nevertheless, except the considered processes there are possible other processes accompanying developing of field instability in MD cavities which are connected with multiple peaks in Q-factor spectrum - the distance between two neighboring peaks corresponding to modes of different types is much less than in case of MS resonator (modes of MS resonator are well-known to be degenerated). This can result in coupling of neighboring modes leading to mode beating and other effects. Considering this problem, one should take into account also nonlinear mode coupling through variations of refractive index and mode competition in active medium. In general case this problem is too much complicated while simple estimations are given by the developed theory.

5. CONCLUSIONS

Model describing developing of field instability in passive microsphere and microdisk resonators has been considered. Physical reason for developing of the instability has been considered and shown to be connected with formation of positive feedback arising with light-induced variation of quality factor of microresonators' eigenmodes through formation of field-induced distribution of refraction index. Field amplitude tends to infinity in the framework of presented model. But we have considered the simplest model just to show possibility of developing of the instability. In real situation field amplitude can be stabilized at a certain value by laser-induced processes resulting in dominating of negative feedback. In particular, that can be connected with laser-induced variation of inversion.

There have been considered field-induced variations of spectral characteristics which follow developing of field instability. In particular, variations of resonant frequency and spectrum of Q-factor have been studied and shown to contribute to developing of positive feedback resulting in field instability through involving of pump radiation of near-resonant wavelengths in formation of quasi-resonant mode. Resonant frequency of passive microresonator is shown to increase with developing of field instability inside the resonator. This feature can be used to test the presented model and detect developing of LID in the resonator.

The presented models can be applied to analysis of problem of laser-induced damage of dielectric microresonators and increasing of their damage thresholds.

6. APPENDIX A

Here we derive several important results used for consideration of the problem of field-induced variations of Q-factor. Let the microcavity of arbitrary form and size to be pumped with optical radiation of P_{pump} power for resonant wavelength. Let $(1-\delta)$ be a part of pump power lost due to scattering. Then time variation of power inside the cavity if described by equation[21]

$$\frac{d^2P}{dt^2} + \gamma \frac{dP}{dt} + \omega_0^2 P = \delta \cdot P_{pump} \cdot \omega_0^2 \cdot \exp(i\omega t) \tag{A1}$$

where γ determines losses, ω_0 is eigenfrequency of the microcavity with zero losses and δ gives the effectiveness of pumping. Having been integrated, this equation gives time variation (exponential decay together with harmonic variations) of radiation power inside the resonator after the pumping has been switched off. Then amplitude value of field power inside the cavity is given by

$$P_0 = \frac{P_{pump}\omega_0^2}{\sqrt{(\omega_0^2 - \omega^2) + (\gamma \cdot \omega)^2}} \tag{A2}$$

Assuming $\gamma << \omega$ one can show that full width of resonant peak at half of maximum is $\Delta\omega \cong 3^{1/2} \cdot \gamma$. On the other hand, $\Delta\omega / \omega_0 = Q$ what implies

$$\gamma = \frac{\omega_0}{\sqrt{3}Q} \tag{A3}$$

Then it follows from (A2) that amplification of power at resonance can be estimated as follows

$$\frac{P_{0MAX}}{P_{pump}} = \frac{\omega_0^2}{\gamma\ \omega_{res}} \cong \sqrt{3}Q_0 \tag{A4}$$

where

$$\omega_{res}^2 = \omega_0^2 - \gamma^2 / 4 \cong \omega_0^2 \tag{A5}$$

is resonant frequency for lossy microcavity. Amplification of field amplitude for resonant mode with quality factor Q can be estimated as follows

$$\frac{E_{in}^{MAX}}{E_0} \cong \sqrt{\sqrt{3}Q_0} \cong 1.316\sqrt{Q_0} \tag{A6}$$

7. REFERENCES

1. K.Sasaki, H.Misawa, N.Kitamura, R.Fujisawa, and H.Masuhara, "Optical micromanipulation of a lasing polymer particle in water", *Jpn. Journal of Appl. Phys.*, v. **32**, pp. L1144-L1147, 1993.
2. H.-M.Tzeng, K.F.Wall, M.B.Long, and R.K.Chang, "Laser emission from individual droplets at wavelengths corresponding to morphology-dependent resonances", *Opt. Lett.*, v. **9**, pp. 499-501, 1984.
3. H.-B.Lin, J.D.Eversole, C.D.Merritt, and A.J.Campillo, "Cavity-modified spontaneous-emission rates in liquid microdroplets", *Phys. Rev.*, v. **A 45**, pp. 6756-6760, 1992.

4. H.B.Lin, A.L.Huston, B.L.Justus, and A.J.Campillo, "Some characteristics of a droplet whispering-gallery-mode laser", *Opt. Lett.*, v. **11**, pp. 614-616, 1986.
5. L.Collot, V.Lefevre, M.Brune, J.M.Raimond, and S.Haroche, "Very high-Q whispering-gallery mode resonances observed on fused silica microspheres", *Europhys. Lett.*, v. **23**, pp. 327-334, 1993.
6. T.Baer, "Continuous-wave oscillation in a Nd:YAG sphere", *Opt. Lett.*, v. **12**, pp. 392-394, 1987.
7. S.C.Ching, H.M.Lai, and K.Young, "Dielectric microspheres as optical cavities: Einstein A and B coefficients and level shift", *Journal of the Opt. Soc. Am.*, v. **B 4**, pp. 2004-2009, 1987.
8. S.L.McCall, A.F.J.Levi, R.E.Slusher, S.J.Pearton, and R.A.Logan, "Whispering-gallery mode microdisk lasers", *Appl. Phys. Lett.*, v. **60**, pp. 289-291, 1992.
9. V.B.Braginsky, M.L.Gorodetsky, and V.S.Ilchenko, "Quality-factor and nonlinear properties of optical whispering-gallery modes", *Phys. Lett.*, v. **A 137**, pp. 393-397, 1989.
10. R.Drever in: *Gravitational radiation*, Eds. N.Druelle and T.Piran, North-Holland, Amsterdam, 1983.
11. P.Chylek, J.D.Pendleton, R.G.PInnick, "Internal and near-surface scattered field of a spherical particle at resonant conditions", *Applied Optics*, v. **24**, N 23, pp. 3940-3942, 1985.
12. V.E.Gruzdev,. M.N. Libenson, "Electrodynamic instability as a reason for bulk and surface optical damage of transparent media and thin films", *Proc. SPIE*, v. **2714**, pp. .595-603, 1995.
13. M.Born, E.Wolf, *Principles of Optics*, 4-th ed. Pergamon Press, New York,1968, Ch.1.6
14. M.Kerker, *The scattering of Light*, Academic Press, New York, 1969.
15. A.L.Aden, M.Kerker, "Scattering of electromagnetic waves from two concentric spheres", *Journal of Applied Physics*, v. **22**, N 10, pp. 1242-1246, 1951.
16. G.J.Rosasco, H.S.Bennet, "Internal field resonance structure: implicatiobs for optical absorption and scattering by microscopic particles", *Journal. of the OSA*, v. **68** N 9, p. 1242-1250, 1978.
17. A.Ashkin, J.M.Dziedzic, "Observation of optical resonances of dielectric spheres by light scattering", *Applied Optics*, v. **20**, N 10, pp. 1803-1814, 1981.
18. A.Ashkin, J.M.Dziedzic, "Observation of Resonances in the Radiation Pressure on Dielectric Spheres", *Phys. Rev. Lett.*, v. **38**, N 23, pp. 1351-1354, 1977.
19. M.J.Soileau, W.E.Williams, N.Mansour, E.W.Van Stryland, "Laser-induced damage and the role of self-focusing", *Optical Engineering*, v. **28**, N 10, pp. 1133-1144, 1989.
20. J.F.Owen, R.K.Chang, P.W.Barber, "Internal electric field distributions of a dielectric cylinder at resonance wavelengths", *Optics Letters*, v. **6**, N. 11, pp. 540-542, 1981.
21. O.Svelto, *Principles of Lasers*, 3-d edition, Plenum Press, New York, 1989, Ch. 4.3.

Backward light scattering in fiber lasers

Andrei A.Fotiadi[a] , Roman V.Kiyan[a], and Stanislav V.Chernikov[b]

[a]A.F.Ioffe Physico-Technical Institute, St.-Petersburg 194021, Russia
[b]Imperial College, Prince Consort Road, London SW7 2BZ, UK

ABSTRACT

Backward light scattering processes always take place in fiber lasers. They create additional feedback in laser resonator changing qualitatively the laser operation. We have described for the first time the mechanisms of their influence on lasing in number of fiber configurations. The understanding of the mechanisms allows us to get several important scientific results suitable for rapid practical applications in the process of elaboration of new fiber sources of light.

Keywords: optical fiber, fiber lasers, Brillouin scattering, Rayleigh scattering, Q-switch, gyro, fiber sensors, distributed feedback

1. INTRODUCTION

Nowadays rare-earth-doped fiber lasers are widely used. One can see the way of further important developments in fiber lasers. Apart from the population inversion for light amplification we may use others mechanisms of laser energy conversion in fibers such as linear and non-linear light scattering processes[1]. This greatly expands the possibilities of fiber lasers for many applications and lead to creation of new high technology light sources in which standard fiber elements with use of diode pumping are compactly included.

In this paper we consider for the first time the cooperative dynamics of the linear Rayleigh backscattering (RS) and the most low-threshold nonlinear process of Stimulated Brillouin Scattering (SBS) in different fiber configurations and describe the mechanisms of their influence on lasing. We have considered three mechanisms.

1. For lasing the RS creates additional feedback in laser resonator leading to very effective line-narrowing thus creating conditions for SBS generation. The rise of SBS causes series of avalanche processes changing qualitatively the laser operation, and, in particular, leading to Q-switching. Generation of short, 2-15 ns pulses with peak powers up to ~10 kW at a repetition rate 1-20 kHz caused by the mechanism remarkably differs from relaxation oscillation pulsation commonly observed with fiber lasers.

2. For SBS in optical fiber double Rayleigh scattering of the Stokes field forms the distributed interferometer in fiber causing SBS lasing. It qualitatively narrows SBS spectrum and changes statistics. Such SBS laser with distributed Rayleigh mirrors can be used for fiber sensor applications.

3. For light generation in ring fiber lasers the processes of light backscattering lead to geometric coupler of resonators for the waves propagating in the opposite directions thus preventing laser operating in stable bi-directional single mode. The elimination of the backward scattering allows us for the first time to obtain such generation in the ring fiber Er-laser.

2. PASSIVE Q-SWITCHING OF FIBER LASERS WITH USE OF A DYNAMIC RS-SBS COOPERATIVE PROCESS IN FIBER.

Recently a new and rather extraordinary Q-switching mechanism taking place in Fiber lasers have been reported [2] . The passive Q-switching was observed in an all-optical fiber configuration for both ytterbium operating around 1μ and erbium at 1.5 μ. The configuration employed a linear cavity with a high rejecting mirror on one side and distributed back-reflection from a piece of single mode silica fiber or a fiber ring interferometer on the other side, while feedback from the output Fiber end was suppressed by use of an angled cleave (Fig.1,a). Generation of short, 2-15 ns pulses was observed at a repetition rate 1-20 kHz remarkably different from relaxation oscillation pulsation commonly observed with Fiber lasers. In a self-Q-switched ytterbium Fiber laser, the prelasing pulse with duration about ~50 ns and peak power ~40W (Fig1.,b) followed by gigantic 2-ns pulses with record high peak powers exceeding 10 kW from a single-mode. Such extremely high powers followed after ~20 ns by the secondary echo in single-mode fiber produced extreme spectral broadening from 0.8 to 2.3 μ. With the involvement of literally all possible nonlinear processes in silica optical Fiber, including parametric four-wave mixing, Raman scattering, harmonic generation, etc. Such a unique and practically attractive source has considerable potential for many applications as a result of its super broad spectrum in conjunction with high spectral brightness.

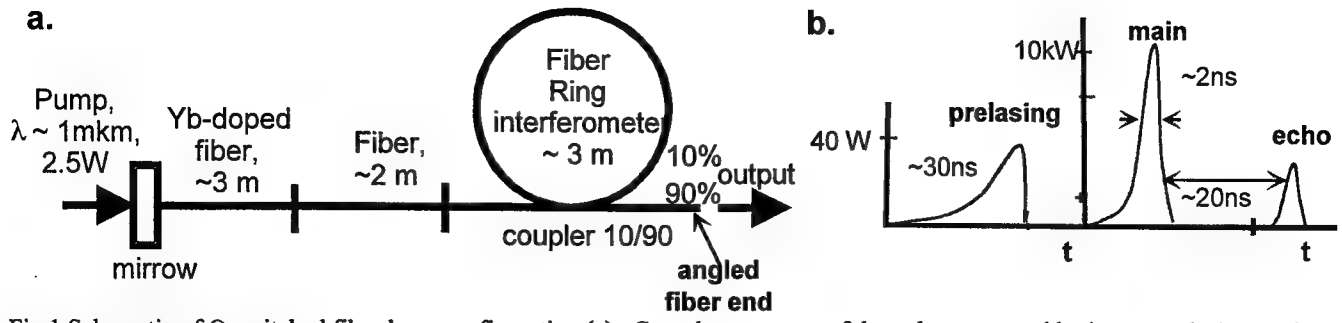

Fig.1.Schematic of Q-switched fiber laser configuration (a). Complex structure of the pulse generated by laser : prelasing, main pulse and echo pulse(b).

We suggest a theoretical model to explain the Q-switching mechanism in the fiber laser. The model is based on dynamic cooperative RS-SBS process in the fiber configuration[3]. There are three main stages of the process (Fig.2).

1. At the beginning of the cycle (Fig.2), the population inversion builds up, however, suppression of feedback from the fiber end prohibits lasing (field A). Feedback can arise from Rayleigh scattering (field~A) enhanced by the ring interferometer at its resonance frequencies. Although the Rayleigh scattering coefficient of the loop is rather low, the double pass dynamic gain of the fiber amplifier is sufficiently high for threshold to be reached. Lasing (field A) occurs on one or a few resonance modes of the ring interferometer ω_A which are also resonance modes for the linear fiber cavity. The lasing power builds up exponentially, and field A has very narrow linewidth suitable for pumping SBS in the ring.

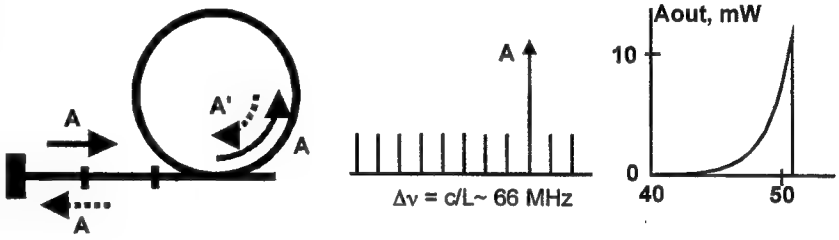

Fig.2. Stage I. Initial lasing caused by Rayleigh backscattering in the ring.

2. At a certain power level the threshold of SBS in ring interferometer is reached generating a Stokes pulse (field B) of hundreds nanosecond duration that is fed back into the cavity (Fig.3). The frequency of the pulse is shifted to Stokes side by the frequency of hypersound wave in media Ω ($\omega_B = \omega_A - \Omega$, Ω ~ 16GHz for λ~1μm), and it also should be one of the resonant frequencies of the ring interferometer. The pulse experiences strong double pass amplification and results in both suppression of the Rayleigh feedback (i.e. depleting of the field A') and pumping new SBS process in the cavity fiber (Fig.4).

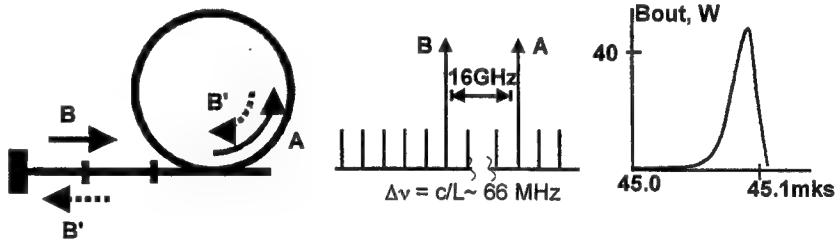

Fig.3. Stage II. SBS generation in the ring.

3. For the last SBS process the pulse B is depleted and leaves the fiber as prelasing (B_{OUT}) with the duration of about tens nanoseconds and peak power of tens Watts. New Stokes pulse C ($\omega_C = \omega_A - 2\Omega$) is formed in the fiber from the noise and represents SBS amplified noise fluctuations with characteristic time determined by SBS spectrum[4]. As rule there are two initial peaks of Stokes pulse, which experiences strong double pass amplification depleting the pump signal all over the fiber configuration and extracting most of the energy stored in the cavity. Its leave the laser as a double peaks pulse (C_{OUT}) . There are the first Q-switching main pulse with duration of ~5nS, peak power of ~10 kW and secondary echo pulse that was always delayed by ~20 ns

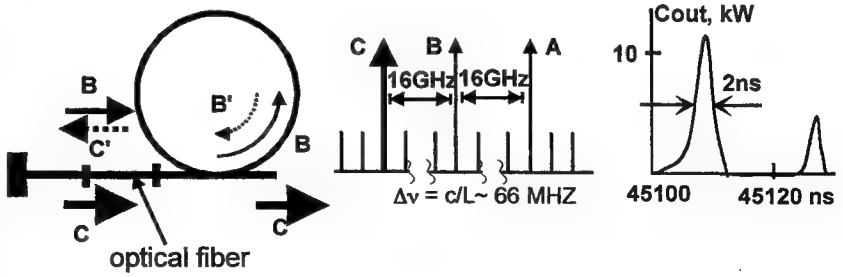

Fig.4. Stage III. Second Stokes SBS generation in the cavity fiber.

is determined by characteristic hypersound lifetime in silica fibers. The last stage process turn the system to initial state and lasing repeats periodically.

So, our model explains the prelasing, the main pulse and echo pulse (Fig.1,b) which are always present in experiment. This structure did not depend on the pump power and remained so for different geometries and composition of the fibers used suggesting that the mechanism is determined by a described RS-SBS processes. Numerical simulations based on this model excellently reproduce the experimentally observed pulse shapes.

3. SBS LASING EFFECT CAUSED BY DOUBLE RAYLEIGH SCATTERING DYNAMIC FEEDBACK IN OPTICAL FIBER.

We consider SBS process in optical fiber at the presence of additional feedback caused by double Rayleigh scattering. Rayleigh backscattering of SBS-amplified Stokes waves in fibers always takes place (fig.5).

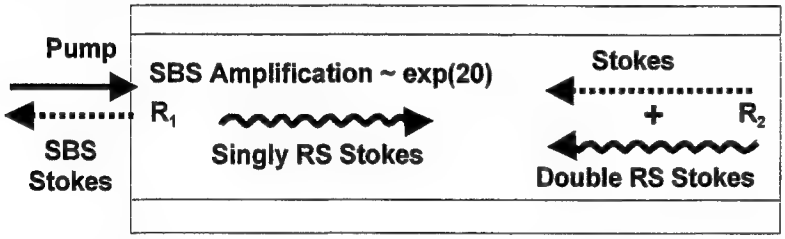

Fig.5. Schematic of SBS-RS cooperative process.

Singly backscattered Stokes wave does not participate in SBS process. However when it is also scattered backward (Double RS Stokes wave), that provides a feedback. By the way interferometer with two distributed Rayleigh mirrors (with effective reflectivities R_1 and R_2) is formed in the fiber. This interferometer demonstrates strong spectral selectivity, its feedback coefficient strongly depends on distribution of the Stokes field along the fiber.

The reflection coefficient of the distributed Rayleigh mirror in single-mode optical fiber is very small (reflected intensity is about 1/600 part of Rayleigh losses in fiber). However, the extremely high SBS amplification (~ e^{20} times) compensates the losses caused by small reflection coefficient. Feedback for some spectral components inside SBS line may be high enough to provide their primary SBS amplification and lasing (it happens if $R_1R_2\exp\{20\} \sim 1$).

In the experiment the radiation of single-frequency Nd:YAG laser (1.06μm, linewidth ~50 kHz) was launched into 300 m silica singlemode optical fiber (~17 dB/km losses). From the first, pump radiation was sinusoidally modulated with period ~20 μs. As a result, the feedback caused by double Rayleigh scattering was suppressed. In the second case the fiber was pumped by 600 μs pulses (the pulse growth time was 25 μs). That guaranteed quasi-stationary pump mode and allowed double Rayleigh scattering feedback.

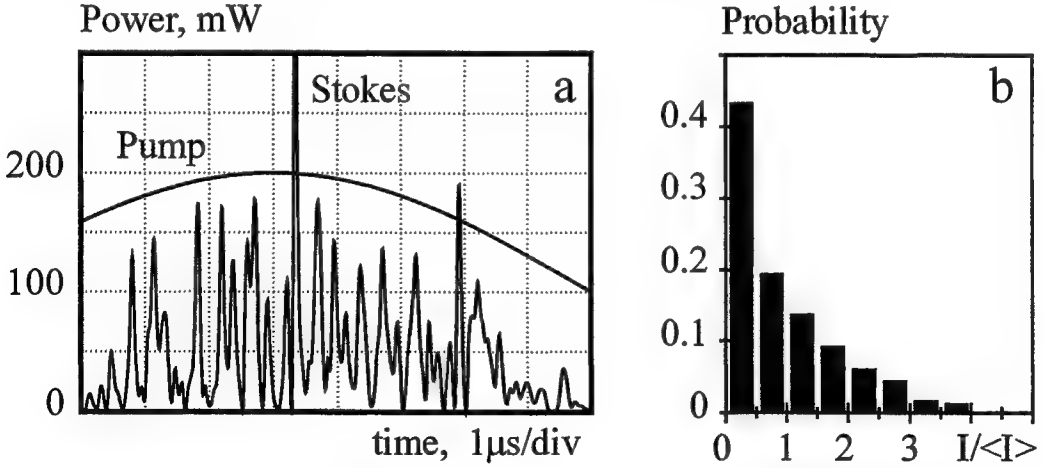

Fig.6. Experimental oscilloscope traces of the input pump and output Stokes signal for SBS with suppressed Rayleigh feedback (a). The histograms of the Stokes power statistical distribution for SBS calculated from experimental data (b).

The experimental oscilloscope traces for SBS with suppressed Rayleigh feedback is shown in Fig.6, a. The intensity of the Stokes wave exhibits 100% temporal fluctuations. The characteristic time of the Stokes radiation fluctuations is 100-200 ns. Intensity correlation function is described by Gaussian curve with correlation time of ~50ns. The normalized standard deviation of

the Stokes intensity is estimated to be about unity. The Stokes energy spectrum linewidth reproduced from the correlation function is about 10 MHz. Histogram of the statistical distribution of the Stokes intensity fluctuations calculated from the digitized Stokes radiation oscilloscope trace (Fig.6,b) also points to nearly Gaussian statistic of the Stokes field fluctuations. Such SBS parameters correspond to the well-known SBS mode in long fibers, when the time of the light trip in the fiber is much longer than the hypersound wave relaxation time[1].

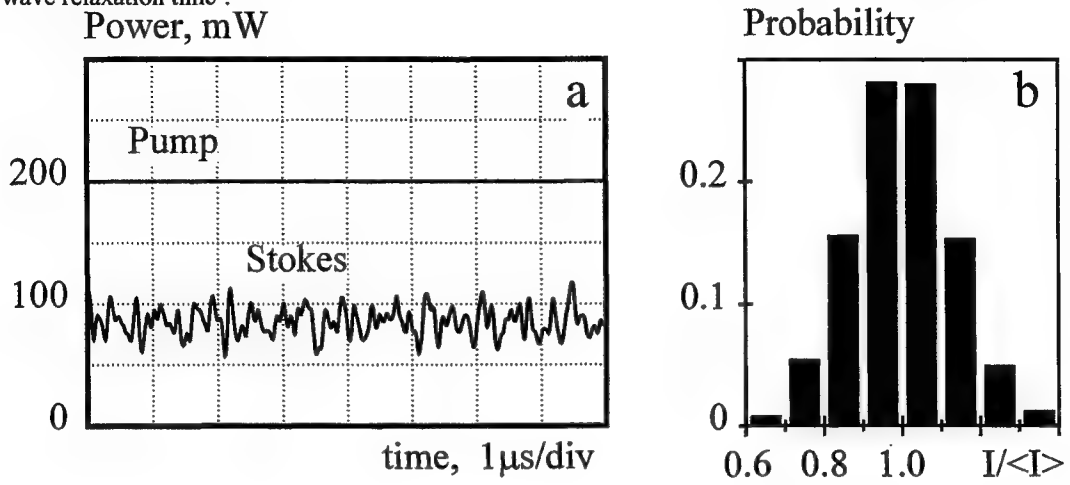

Fig.7. Experimental oscilloscope traces of the input pump and output Stokes signal for SBS with effective Rayleigh feedback (a). The histograms of the Stokes power statistical distribution for SBS calculated from experimental data (b).

Qualitatively different oscilloscope traces presented in Fig.7,a are obtained in the experiment without Rayleigh feedback suppression. In that case the modulation depth of the Stokes signal temporal fluctuations is less then 50%. The correlation function for Stokes intensity is also correspond Gaussian shape with the same correlation time, but the normalized standard deviation of the Stokes intensity is estimated to be 0.1. It means that the main energy Stokes spectrum lies in a very narrow line. The linewidth of the modified Stokes radiation spectrum is to be smaller then 0.1 MHz. The histogram of the statistical distribution of Stokes intensity fluctuations also is calculated from experimental data (Fig.7,b). In this case, Stokes intensity (but not field) fluctuations are in Gaussian statistics that points to SBS lasing process in the fiber.

Numerical simulation of the SBS in the optical fiber with Rayleigh scattering was performed. The following equations for complex amplitudes of pump $E_P(z,t)$, Stokes $E_S(z,t)$, Rayleigh backscattered Stokes $E_R(z,t)$ waves and the hypersound wave $\rho(z,t)$ were used for simulation:

$$\frac{n}{c}\frac{\partial E_P}{\partial t}+\frac{\partial E_P}{\partial z}=-K_1\rho E_S-\mu E_P$$

$$\frac{n}{c}\frac{\partial E_S}{\partial t}-\frac{\partial E_S}{\partial z}=K_1\rho^* E_P+\eta_1(z)E_R-\mu E_S$$

$$\frac{n}{c}\frac{\partial E_R}{\partial t}+\frac{\partial E_R}{\partial z}=\eta_2(z)E_S-\mu E_R$$

$$T_2\frac{\partial \rho}{\partial t}+\rho=K_2 E_P E_S^*+f(z,t)$$

where K_1 and K_2 are Brillouin coupling constants, μ is the linear loss coefficient, $\eta_1(z)$ and $\eta_2(z)$ are the Rayleigh backscattering coefficients. These scattering coefficients are δ-correlated Gaussian random complex functions with zero mean and dispersion $\langle \eta_1\eta_1^*\rangle=\langle \eta_2\eta_2^*\rangle=k\mu$, where k is backward Rayleigh capture fraction, which is determined by fiber geometry and stimulated to be about 1/600. The Langevin noise source $f(z,t)$ is δ-correlated in space and time Gaussian random process with

zero mean. It describes the thermal fluctuations of the medium density that lead to spontaneous Brillouin scattering.

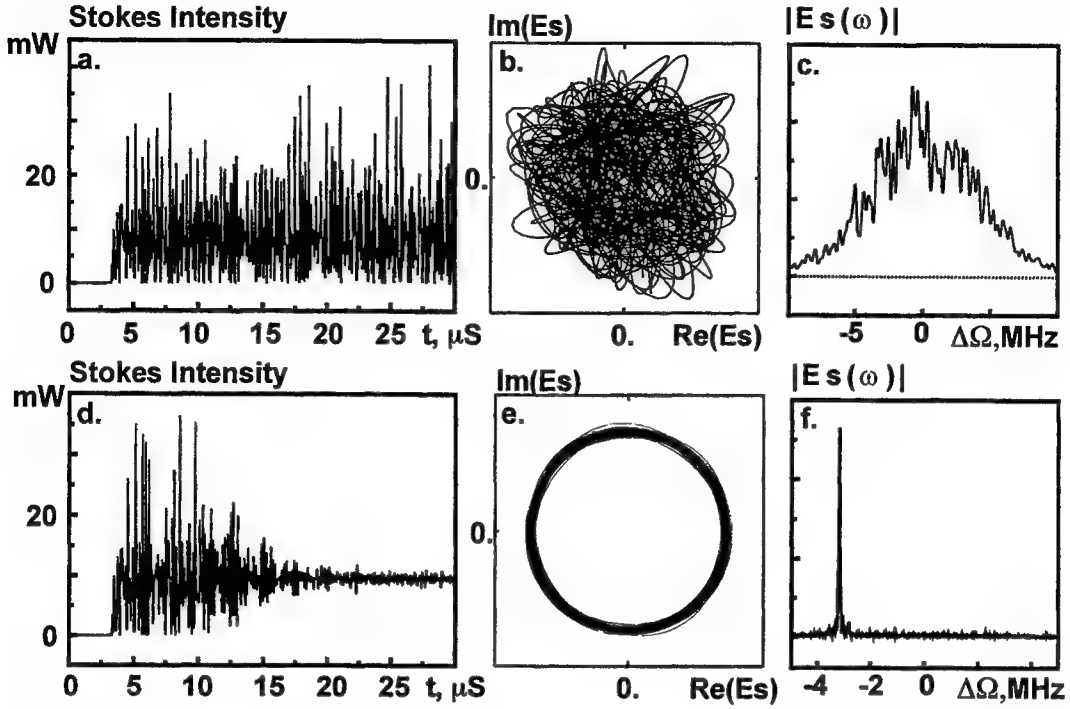

Fig.8. Numerical simulations of SBS without Rayleigh feedback (a-c) and SBS-RS cooperative process(d-f): the Stokes power behavior (a, d), the settle Stokes phase portrait (b, e) and the Stokes power spectrum (c, f).

The results of the numeric simulation of the cooperative RS-SBS process in the optical fiber are in good agreement with the experimental results. Fig.8 shows the difference of Stokes behavior for both experimental realizations in the case of weak pump depletion. One can see Rayleigh feedback causes the Stokes field phase matching and leads to SBS lasing.

4. SINGLE-MODE BI-DIRECTIONAL ER-DOPED RING FIBER LASER.

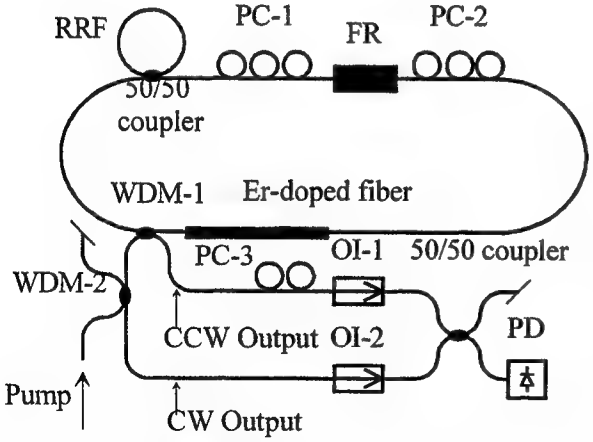

Fig. 9. Configuration of the Er-doped bi-directional ring fiber laser.FR - 90° Faraday Rotator; RRF – ring resonator filter; WDM1,2- fiber couplers;OI-1, OI-2 – optical isolators; PD – photo detector.

The ring laser gyroscope (RLG) gives information on the rotation rate in the most convenient form of the frequency difference between the counter-propagating waves, that is guarantee of the extremely high sensitivity and the widest dynamic range of measured rotation rate. The successful applications of Er-doped silica fibers in optical amplifiers and lasers[5] make attractive the idea to develop RLG based on Er-doped bi-directional ring fiber laser (EDBRFL). It is possible if stable single-longitudinal mode bi-directional operation of the laser is achieved and lock-in phenomena originated from parasitic back-scattering in the laser resonator is eliminated. However, because of very wide homogeneous line in Er-doped silica fibers, the waves counter-propagating in the resonator of EDBRFL are strongly coupled through the amplification medium, and stable bi-directional single mode generation without lock-in becomes impossible. In recent experiment[6] this obstacle was successfully overcome by introduction of 45° Faraday Rotator (FR) into the resonator of Er-doped ring fiber laser. The only evident disadvantage of the FR presence in the laser resonator is increased sensitivity of the nonreciprocal frequency bias produced by FR to fluctuations of the fiber ring resonator birefringence and FR rotation angle. The results of the theoretical and experimental investigation of the EDBRFL with 90° FR in resonator are presented in this report.

Configuration of the laser is shown in Fig. 9. It is demonstrated, that parasitic sensitivity of the nonreciprocal frequency bias to fluctuations of the fiber ring resonator birefringence can be strongly suppressed if 90° FR is used as phase nonreciprocal element in the resonator of the EDBRFL.

From the theoretical analysis presented in the report, in the Er-doped bi-directional ring fiber laser with ideal 90° FR in resonator generation of either orto-conjugated or complex conjugated counter-propagating modes pair can be obtained. In the upper case, the nonreciprocal frequency bias depends continuously on the resonator birefringence. On the contrary, it does not depend on the laser resonator birefringence and is equal to the half of the laser resonator free spectral range in the latter case. Detail investigation of these regimes was carried out. In particular, it is shown that polarization-dependent losses in laser resonator allow to separate complex conjugated and orto-conjugated counter-propagating modes pair generation regimes.

In despite of the rotation angle of the real FR is different from ideal value 90°, presented experimental results confirm the theoretical conclusions. Single-longitudinal mode bi-directional generation of the orto-conjugated or complex conjugated counter-propagating modes pairs were obtained in experiment separately. To confirm the theoretical conclusions concerning properties of these operational regimes the laser was investigated under perturbation by airflow that resulted in random fluctuations of the laser resonator birefringence. The radio frequency (RF) spectra of the CW-CCW outputs beat signals recorded by RF spectrum analyzer with 1000 video-averaging for orto-conjugated and complex conjugated counter-propagating modes generation regimes are shown in Fig.10,a and Fig.10,b, respectively. The beat signal frequency fluctuations about 7 kHz and below 800 Hz respectively were observed in these operational regimes. That demonstrates the significant suppression of the sensitivity of the nonreciprocal frequency bias to fluctuations of the laser resonator birefringence in complex conjugated counter-propagating modes pair generation regime.

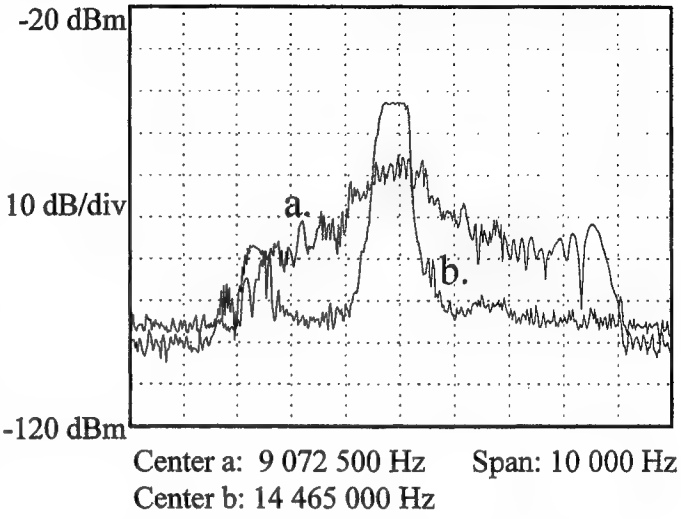

Fig. 10.Radio frequency spectra of the CW-CCW output beat signals. Resolution: 37 Hz, Measurement time: 40 ms.
a) The orto-conjugated counter-propagating modes pair generation regimes
.b) The complex conjugated counter-propagating modes pair generation regimes.

5. CONCLUSION

Thus understanding of the mechanisms of backward light scattering allows us to get several important scientific results suitable for rapid practical applications in the process of elaboration of new fiber sources of light. We believe that further detailed investigations will extend the possibilities of the laser radiation control and allow creation of new light sources with the given characteristics such as new fiber sensors.

6. REFERENCES

1. E.A.Kuzin, M.P.Petrov and A.A.Fotiadi. «Phase conjugation by SMBS in optical fibers», *Optical phase conjugation,* ed. by M.Gower, D.Proch, pp.74-96, Springer-Verlag, 1994.
2. S.V.Chernikov, Y.Zhu, J.R.Taylor, V.P.Gapontsev, «Supercontinuum self-Q-switched ytterbium fiber laser», *Opt.Lett.*, Vol.**22**, N5, pp.298-301, 1997.
3. S.V.Chernikov, A.A.Fotiadi, «Passive Q-switching of fiber lasers with use of a dynamic SBS silica fiber mirror», *Conference on Laser and Electro-Optics, 1997 Technical Digest Series*, pp.477-478, Optical Society of America, Washington, D.C., 1997.
4. A.A.Fotiadi, E.A.Kuzin. «Noise modulations of the scattered radiation intensity during stimulated Brillouin scattering in a single-mode optical fiber with strong pump depletion', *Tech.Phys.*, v.**40**, N7, pp.740-742, 1995.
5. E. Desurvire, Erbium-Doped Fiber Amplifiers, *A Wiley-Interscience publication*, 1994.
6. R. Kiyan, S.K. Kim, B.Y. Kim, «Bidirectional single-mode Er-doped fiber-ring laser», *IEEE Photonics Technol. Lett*, v.**8**, p.1624-1626, 1996.

SESSION 2

Optical Patterns

Transverse quasi-periodic structure of optical fields in a wide - aperture laser with a saturable absorber

N.E. Molevich, A.P. Zaikin

P.N.Lebedev Physical Institute, Samara branch, Samara, Novo- Sadovaya 221

ABSTRACT

A theoretical investigation was made of the dynamics of generation of an optical field in a Fabry -Perot cavity with an active medium and a bleachible filter, considered in the limiting case of an infinitely large aperture and in the case of realy laser. Self- similar wave solutions were obtained in the first case, wave velocity and frequency were determined. For the second case it is created the spatiotemporal numerical model which permits to find the states of the optical field $E(x,z,t)$ at the every cavity round-trip time. Using this model we investigated the formation of the transverse structure of laser fields at the different parameters of active media and saturable absorber. It is found the stationary quasi-periodic waves travelling across the finite aperture at a slow response time of an active medium. Their structure and the conditions of their excitation are considered.

Keywords: laser, saturable absorber, optical field, self- wave, bifurcation

1. INTRODUCTION

Distributed nonlinear optical systems can generate optical field structures. Formation of these structures is of interest in a general theory of self- organising system and in practical application, particularly in information processing. Intensive investigations are going on of, for example, laser autosolitons in the wide- aperture laser containing the instantly relaxating active medium (AM) and the additional saturable absorber (SA) with the instantaneous response[1]. Autosolitons appear at the excitation of the laser generation in the "hard" regime when the difference between the unsaturated values of the gain and of the absorption coefficient m<0. In the present work such laser system is investigated analytically and numerically at m>0 for the finite relaxation times of an active medium and saturable absorber. It is shown the existense of the regimes with a periodic autowave transverse profile of optical fields

2. DIMENSIONLESS EQUATIONS

A model of the investigated system is shown in Fig. 1. The basic equations governing the dynamical behaviour of the laser, under the slowly varying envelope and paraxial approximations, were the Maxwell -Bloch equations:

$$\begin{aligned} &\frac{\partial E}{\partial t} - i\frac{\partial^2 E}{\partial x^2} = \frac{\nu}{2}E(N - N_f - 1) \\ &\frac{\partial N}{\partial t} = N_e - N(1 + I) \\ &\tau\frac{\partial N_f}{\partial t} = N_{fe} - N_f(1 + I\delta). \end{aligned} \qquad (1)$$

where the dimensionless time t and the coordinate x are related to dimensional quantities t_d and x_d by the expressions $t= t_d/T_i$, $x= x_d(2k/T_i c)^{1/2}$; k is the wave number; c is the velocity of light; T_i and T_f are the relaxation times of levels in the AM and the SA; $\tau=T_f/T_i$; $E=E_d/E_s$ and $I=I_d/I_s$ are the dimensionless amplitude and the intensity of the optical field; $I_d=|E_d|^2$; Is is the saturation intensity; $\delta=\sigma_f\sigma/\sigma$ is the ratio of the saturation intensities in the AM and in the SA; σ and σ_f are the cross sections describing the emission from the AM and the absorption in the SA; g, χ and g_t are respectively, the gain of the AM, the absorption coefficient of the SA, and the loss factor, all averaged over the cavity length; g_e and χ_e are unsaturated values of the gain and of the absorption coefficient; ; $N=g/g_t$, $N_e=g_e/g_t$, $N_f=\chi/g_t$, $N_{fe}=\chi_e/g_t$ are the values of the gain and of the absorption coefficient normalised to the loss factor g_t; $\nu=cT_i g_t$ is the ratio of the relaxation time of the populations in the AM to the photon lifetime in the cavity.

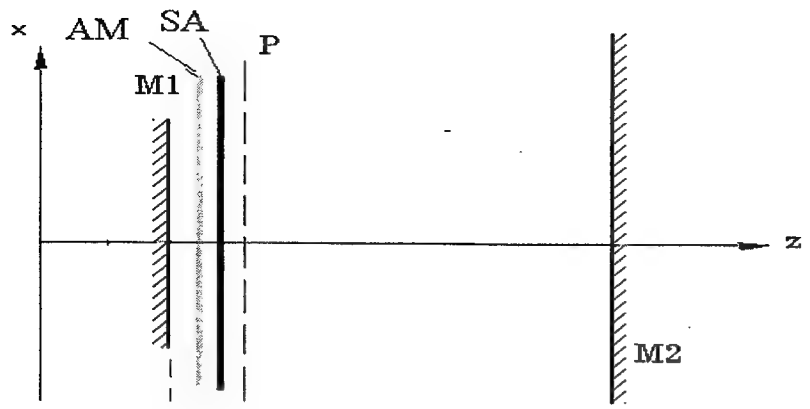

Fig.1. Model used in calculations (the line P is the reference plane)

3. BIFURCATION ANALYSIS

We consider the solution of the system of equations (1) in the wave- travelling form

$E(x,t)=E_c[1+e(\xi)]$, $N(x,t)=N_c[1+n(\xi)]$, $N_f(x,T)=N_{fc}[1+n_f(\xi)]$,

where $\xi=t-\beta x$ is the automodel variable; e, n, n_f are periodic function; $w=1/\beta$ is the self-wave propagation velocity; $E_c=\sqrt{I_c}$, N_c, N_{fc} are steady state values. In terms of this notation, the system of equations (1) becomes

$$\begin{aligned}
&\frac{de}{d\xi} - i\beta^2 \frac{d^2e}{d\xi^2} = \frac{\nu}{2}(1+e)\left[\frac{N_e}{1+I_c} n - \frac{N_{fe}}{1+I_c\delta} n_f\right],\\
&\frac{dn}{d\xi} = -n[1 + I_c(1+e)(1+e^*)] - I_c(e + e^* + ee^*),\\
&\tau \frac{dn_f}{d\xi} = -n_f[1 + I_c\delta(1+e)(1+e^*)] - \delta I_c(e + e^* + ee^*).
\end{aligned} \tag{2}$$

We shall now write down a complex perturbation of the field in the form

$e = Z + iY$,

and introduce new variables

$P = dZ/d\xi$, $Q = dY/d\xi$. (3)

Then the system of equations (2) transforms to

$$\begin{aligned}
&\beta^2 \frac{dQ}{d\xi} = -P + \frac{\nu}{2}(1+Z)\left(\frac{N_e}{1+I_c} n - \frac{N_{fe}}{1+I_c\delta} n_f\right),\\
&\beta^2 \frac{dP}{d\xi} = Q - \frac{\nu}{2} Y\left(\frac{N_e}{1+I_c} n - \frac{N_{fe}}{1+I_c\delta} n_f\right),\\
&\frac{dn}{d\xi} = -n[1 + I_c(1 + 2Z + Z^2 + Y^2)] - I_c(2Z + Z^2 + Y^2),\\
&\frac{dn_f}{d\xi} = -n_f[1 + \delta I_c(1 + 2Z + Z^2 + Y^2)] - \delta I_c(2Z + Z^2 + Y^2).
\end{aligned} \tag{4}$$

The characteristic equation corresponding to the linearised system of equations (3) and (4) is

$$(\lambda\tau+1+I_c\delta)[(\lambda+1+I_c)(\lambda+\beta^4\lambda^3)+I_c\nu N_e/(1+I_c)]- \\ -\nu N_{fe}I_c\delta(\lambda+1+I_c)/(1+\delta I_c)=0, \tag{5}$$

The condition of instability of the steady state in the case of plane waves can be found by applying the Routh-Hurwitz criterion to the equation (5). It is simple to find that if $N_{fe}/N_e > \tau^2/\delta$, the Routh- Hurwitz criterion is not satisfied only for

$$\beta^4 > \mu_{cr}' = \frac{(N_{fe}\delta-\tau^2 N_e)a_2}{A_1\tau a_1(1+I_c)^3(1+\delta I_c)^3}. \tag{6}$$

where

$$a_1 = \frac{1+\delta I_c}{\tau}+1+I_c,$$

$$A_1 = \frac{N_e}{(1+I_c)^2}-\frac{\delta N_{fe}}{(1+\delta I_c)^2}.$$

$$a_2=[(1+I_c\delta)+\tau(1+I_c)](1+I_c)(1+I_c\delta)-\nu I_c(\delta N_{fe}-\tau^2 N_e)>0.$$

We shall analise the nature of this instability by considering the case of a filter which has a relatively fast response and is defined by condition $\lambda\tau<<(1+\delta I_c)$. Then condition (6) simplifies and we obtain the next equation

$$\beta^4 A_1/b_1 > \delta N_{fe}/(1+I_c)^3/(1+\delta I_c)^2. \tag{7}$$

where

$$b_1=1+I_c-\frac{\nu\delta I_c N_{fe}}{(1+I_c\delta)^2}\left[1-\frac{\tau(1+I_c)}{1+I_c\delta}\right].$$

Periodic waves may appear for bifurcations of a complex focus, which exists if

$$b_1>0, A_1>0,$$

$$\beta^4=\mu_{cr}=\frac{\delta b_1 N_{fe}}{A_1(1+I_c)^3(1+\delta I_c)^2},$$

where $\mu_{cr}'\to\mu_{cr}$ in the limit $\tau\to 0$.

Two roots of the characteristic equation are then purely imaginary [2]:

$$\lambda_{1,2}=\pm i\omega_0, \\ \omega_0=(1+I_c)(1+\delta I_c)\sqrt{A_1/\delta N_{fe}}. \tag{8}$$

The other two roots have nonzero real parts. The form of this roots depends on the sign of the difference

$$\Delta=\frac{(1+I_c)^2}{4}\left[\frac{4A_1 I_c\nu}{b_1}-1\right].$$

If $\Delta>0$, then $\lambda_{3,4}=P\pm Qi$, where $P = -\frac{(1+I_c)}{2}, Q = \sqrt{|\Delta|}$. If $\Delta<0$, then $\lambda_{3,4} = P\pm Q$, and for $A_1>0$ and $b_1>0$ the real parts of this roots are negative. Therefore the first requirement of the Andronov -Hopf theorem is satisfied: $\mathrm{Re}\,\lambda_{1,2}(\mu_{cr}) = 0, \mathrm{Re}\,\lambda_{3,4}(\mu_{cr}) < 0$ [3]. We shall show that the second requirement

$$\frac{d}{d\mu}[\mathrm{Re}\,\lambda_{1,2}(\mu)]_{\mu_{cr}} \neq 0. \tag{9}$$

is also satisfied. We shall do this by finding $\lambda_{1,2}$ in the direct vicinity of the bifurcation parameter $\mu = \beta^4 = \mu_{cr}(1+\varepsilon)$, where $\varepsilon<<1$. We shall apply the method of successive approximations to characteristic Eq. (5), i.e. we shall write down $\lambda = \omega_0(i+\Delta\lambda), \Delta\lambda << 1$, substitute this quantity in Eq. (5) and collect terms of the same order of smallness. If the terms of the second order of smallness in respect of the parameter ε and $\Delta\lambda$ are ignored, then algebraic transformations give

$$\mathrm{Re}\,\lambda = \frac{vA_1b_1I_c(1+I_c)}{2\{b_1^2+\omega_0^2[b_2\beta^4-2b_1/(1+I_c)]^2\}}\frac{\mu-\mu_{cr}}{\mu_{cr}}. \tag{10}$$

where

$$b_2 = [1 + N_{fe}I_c\delta\tau v/(1+I_c\delta)^3]/\beta^4.$$

Such a dependence of a real part λ on the bifurcation parameter μ satisfies the second requirement, given by expression (9). Since the conditions of the Andronov -Hopf theorem imposed on creation of a limit circle are satisfied, it follows directly that a family of periodic small- amplitude plane waves, parametrised with the help of μ, can exist [4].. The bifurcation parameter μ_{cr} governs the velocity of propagation of small- amplitude waves $w\sim\mu_{cr}^{-1/4}$, and the frequency ω_0, descriebed by formula (8), determines the period $T\approx 2\pi/\omega_0$ of this waves. The existence of such small-amplitude waves requies "soft" creation of a stable limit cicle for $\mu>\mu_{cr}$. This is possible only if the first Lyapunov parameter L_1 of the system of equations (2) is negative. Numerical simulation of this system of equations given below confirms the existence of such a mechanism of the loss of stability of the equilibrium state.

4. SELF- SIMILAR SOLUTIONS

The system of equations (1) was simulated numerically by self- similar substitution of variables $\xi=t-\beta x$, $\beta=\mu^{1/4}$. The initial conditions correspond to small deviations of E,N and N_f from the steady -state values. The main results of numerical modelling are as follows.

1. Periodic self- similar solutions exists only if the nontrivial homogeneous steady state is stable, i. e. when the conditions $b_1>0$, $A_1>0$ are satisfied and there is no unstable limit circle around this equilibrium state $(v<v_1)$.

2. Steady state periodic solutions exists if $\mu>\mu_{cr}$ (supercritical bifurcation). The equilibrium state then becomes unstable in a "soft" regime with creation of a stable limit circle of amplitude $\sim\sqrt{\Delta\mu/\mu_{cr}} = \sqrt{(\mu-\mu_{cr})/\mu_{cr}}$ and with period $T\approx 2\pi/\omega_0$. The numerical solution shows that the deviations of the oscillation period and normalised amplitude from their values obtained on the basis of the Andronov -Hopf bifurcation theorem do not exceed 5 % for small values $\Delta\mu$ $(\Delta\mu/\mu_{cr}<0.1)$.

3. As $\Delta\mu$ increases, the self- similar solution becomes irregular - Fig. 2. When the response time of a filter is long, i.e. $\tau > (\delta N_{fe}/N_e)^{1/2}$, the steady -state finite self- similar solutions are no longer obtained.

4. If $\Delta\mu$ is small, the time for establishment of periodic solutions is proportional to $(Re\,\lambda)^{-1}$.

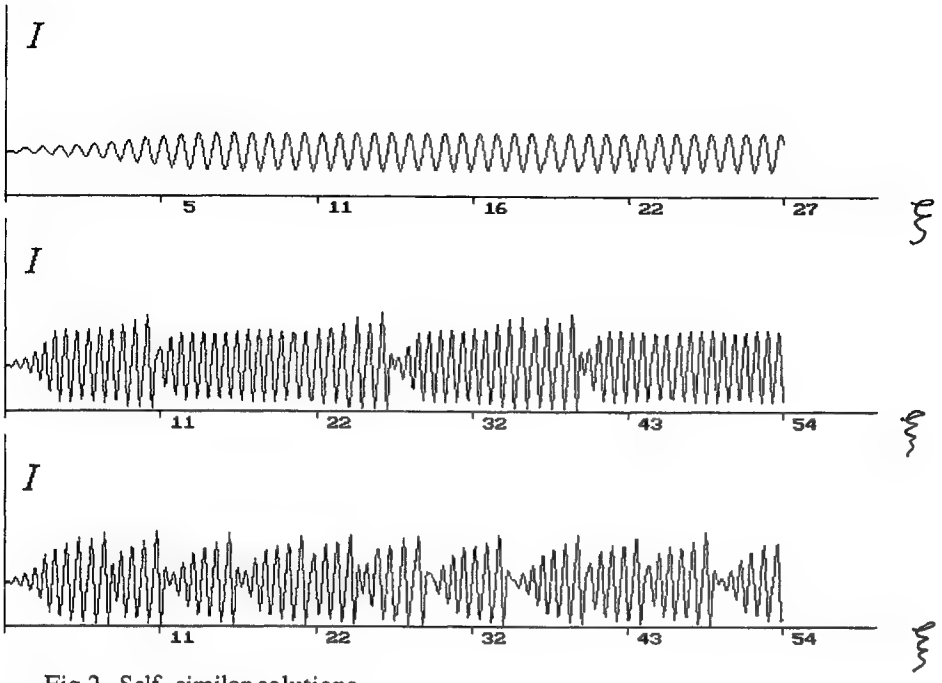

Fig.2. Self- similar solutions

5. SPATIOTEMPORAL STRUCTURE OF THE OPTICAL FIELD IN A FABRY- PEROT CAVITY

It was conducted the numerical investigation of the forming of the spatiotemporal structure of optical field $E(x,z,t)$ in a Fabry- Pertot cavity with the inertial AM and the SA at m>0. The reflection of the mirror edges was smoothed. An optical field was defined by the Fresnel formula at every cavity round- trip time τc. Then the equations for an active medium and a saturable absorber were integrated. Thus we obtained the laser system states at every τc.

The numerical simulation showed the existence of two types of the stationary transverse patterns. The first pattern with standing "hillock" (bright spot) in the aperture center (Fig. 3) is the mode of an active cavity at large Fresnel numbers N_f. At the weak slope of mirror the "hillock" is displaced on the mirror edge. The self-waves are practically absent here.

The other pattern of the optical field is more complex (Fig.4). It is the modulated spot in the center of an aperture and the travelling system of self- waves propagating from the center to the mirror edges. The dependence of their velocity and frequency on laser system parameters is in a good coincidence with the bifurcation analysis of the Maxwell -Bloch equations.

The self- wave pattern appears only at $G=2Re\lambda a/w_{cr} >>1$, where $a \sim N_f^{1/2}$ is the aperture dimension. At constant parameters of the saturable absorber the amplification factor G depends strongly on the relaxation time of an active medium T_i and the gain coefficient N_e. The increase of T_i (or ν) is accompanied by the increase of G and, hence, by more sharp self- wave patterns. The more value N_e, the more T_i necessary for the self- wave patterns observing. Further increase of T_i leads to unstable regimes of laser generation. The transverse profile is strongly irregular and very contrast near the border of instability of the laser system point model, that is near the pulsing generation regime.

Separately we considered the influence of the reflection smoothing. It was shown that at more smoth change of the reflection on the mirror edges the self- wave patterns appeared at higher value of G.

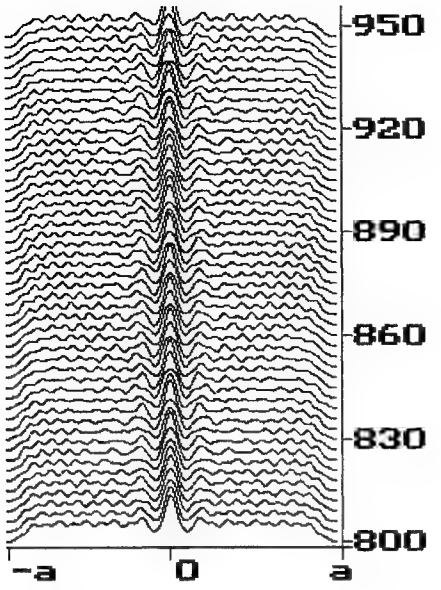

Fig. 3

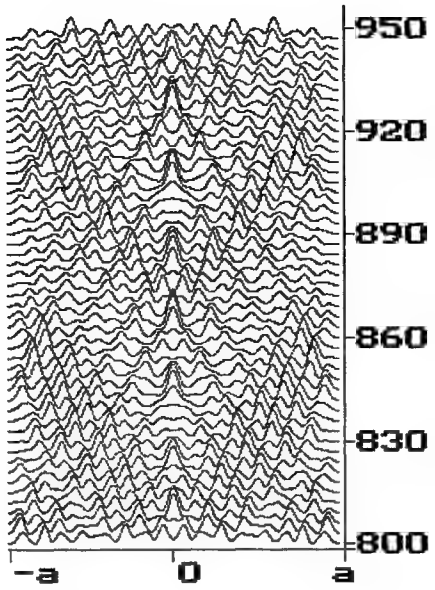

Fig. 4

Laser optical field profile at the various time for the cases of small and large self- waves amplification

6.CONCLUSION

When the broadaperture laser contains a bleachable filter then it can generate an optical field modulated with self-wave profile. The nonlinear oscillations theory let us the appearance conditions and main properties of these autowaves. Self- similar solutions were determined: pure garmonic , many- frequences and chaotic.

The numerical calculations give the optical field form influenced by all nonlinearities and by mirrors form. It was shown that self- wave velocity and frequency are near to the bifurcation result, and the wave amplitude and regularity are determined mainly by an self- wave amplification along the whole aperture.

7.REFERENCES

1. Rosanov N.N. *Optical Bistability and Hysteresis in Distributed Nonlinear Systems* , Nauka, Moscow,:1997.

2. Bautin N.N., Leontovich E.A. *Metody i Priemy Kachestvennogo Issledovaniya Dinamicheskikh Sistem na Ploskosti* (Methods and Procedures in Qualitative Investigation of Dynamic Systems in a Plane) Nauka, Moscow, 1976.

3. BautinN.N. *Povedenie Dinamicheskikh Sistem Vblizi Granits Oblasti Ustoichivosti* (Behaviour of Dynamic Systems Near Boundary Instability Regions) Nauka, Moscow, 1976.

4. Hassard D.B., Kasarinoff N.D., Wan Y.H. *Theory of Applications of Hopf bifurcation,* Cambridge University Press, Cambridge, 1981.

On instability development of counter propagating light waves with unequal amplitudes

Konstantin Y. Nikitenko, Vyacheslav A. Trofimov

Lomonosov Moscow State University
Department of Computational Mathematics & Cybernetics
Vorobyovy Gory, Moscow 119899, Russia

ABSTRACT

Nonlinear interactions of counter propagating waves take place in various nonlinear optical processes attracting attentions of investigators for many years. This is due to problems having a practical importance (for example, wave front conjugation). However, a number of factors that influence on processes quality were exposed by investigators. There is an instability appearance in the system of counter propagating waves among them. An analytical solution for the scheme of two wave have been obtained by now only for strict counter interaction.

In the present report some instabilities development is demonstrated by the examples obtained from the mathematical simulation experiments. As an explanation of the some reasons of instability, the question of convective instability (along the interaction region) in the system of counter propagating noncollinear plane waves with unequal amplitudes is studied.

Keywords: wave-front conjugation, four-wave mixing, nonlinear interaction, optical bistability, instability.

1. BASIC EQUATIONS. NUMERICAL EXPERIMENTS

Process of wave-front conjugation by noncollinear four-wave mixing (WFC FWM) is described by the following system of equations.

$$L_j A_j + i\gamma_j (F_{sj} + F_{cj}) = 0, \quad j = 1-4, \tag{1}$$

where A_j are the complex amplitudes of waves normalized on a pump wave amplitude maximum, $A_{1,2}$ are the pump waves, $A_4 \equiv A_{conj}$, $A_3 \equiv A_{signal}$, L_j is the linear operator that is determined by the interaction geometry and expresses in our case as following:

$$L_j = \frac{\partial}{\partial t} + v_j \frac{\partial}{\partial z} + \beta_j \frac{\partial}{\partial x} + iD_j \frac{\partial^2}{\partial x^2}, \; t > 0, 0 < x < L_x, 0 < z < L_z. \tag{2}$$

Here, t is a normalized time, z is the longitudinal coordinate measured in the diffraction length $L_D = 2ka^2$, a is an initial radius, k is a wave number, x is the transverse coordinate normalized on a, β is the angle being measured in the diffraction divergence units of a beam in a linear medium $\beta_D = \frac{1}{2} k a$ and characterizing the angle between the direction of the incident beam at the nonlinear medium outlet ($z = 0$) and z-axe, D_j is a diffraction coefficient, v_j is a coefficient determining the direction of the j th wave ($v_{1,3} = 1, v_{2,4} = -1$), $L_{x,z}$ are the longitudinal and transverse region values accordingly. As we are interested in nonstationary effects then we will limit to the case of the plane geometry ((X, Z) coordinates).
Items F_{sj} in Eq. (1) with form

$$F_{sj} = A_j \left(\sum_{m=1}^{4} |A_m|^2 - 0.5 |A_j|^2 \right), \; j = 1 - 4, \tag{3}$$

describe the self-acting of a light beam under conditions of equality of the dielectric gratings permeability (a dispersion lack) in a transparent medium, and

$$F_{cj} = \frac{\partial}{\partial A_j^*} \left(A_3 A_4 A_1^* A_2^* + A_1 A_2 A_3^* A_4^* \right), \; j = 1 \div 4, \tag{4}$$

describe the j^{th} wave generation in the lack of dispersion.

Taking into account of a time in Eq. (1) is conditioned by the nonstationary nature of the interaction process in our case. It is principle here and allows to describe adequate all processes in the system.

Boundary and initial conditions for the system (1) are

$$A_j(z,x,t=0)=0, \quad j=1\div 4;$$

$$A_j(z=0,x,t)=(1-exp(-\tau t))\,exp\{-(x-x_{cj})^2\}, \quad j=1,3;$$

$$A_j(z=L_Z,x,t)=R_0 A_{j-1}(z=L_Z,x,t)\,exp(i(x-x_{cj})^2/R_m), \quad j=2,4. \tag{5}$$

Here x_{cj} is the initial center position of the j th beam, R_m is the curvature radius of a reflecting mirror, R_0 is the reflection coefficient on amplitude, τ is a parameter characterizing achievement of a stationary state.

The analysis of the counter noncollinear interaction of beams was performed by using a numerical simulation method. At such conditions, the investigation of the interaction characteristics dynamic shown the possibility of an instability occurrence of different physical natures. As an example of such an effect, the intensity maximum of the conjugated signal wave

$$MaxI_4(z,t)=\max_x |A_m(z,x,t)|^2 \tag{6}$$

is shown on figure 1.
Note that the energetic center value of the reflected waves

$$X_c(z,t)=\int_0^{L_X}(x-X_c(0,t))|A(z,x,t)|^2 dx/P(z,t),$$
$$P(z,t)=\int_0^{L_X}|A(z,x,t)|^2 dx, \tag{7}$$

can be lower the energetic centers of the incident waves (fig. 2).

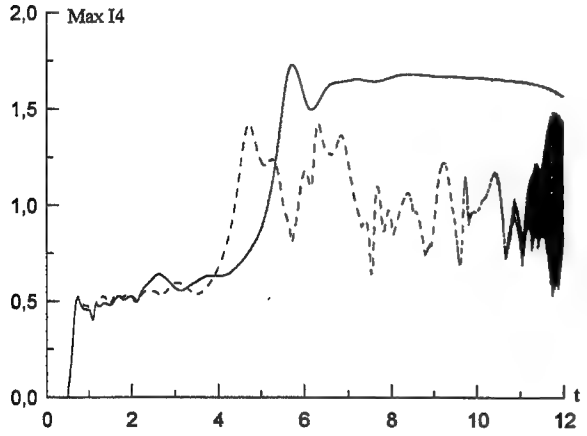

Fig. 1. Evolution of the maximum intensity of the conjugated wave for $\beta = 0$ (solid line), $\beta = 0.5$ (dotted line) with interaction parameters: $\beta = 0.5, \gamma = -17, D = 0.1, L_z = 0.25, L_x = 9$

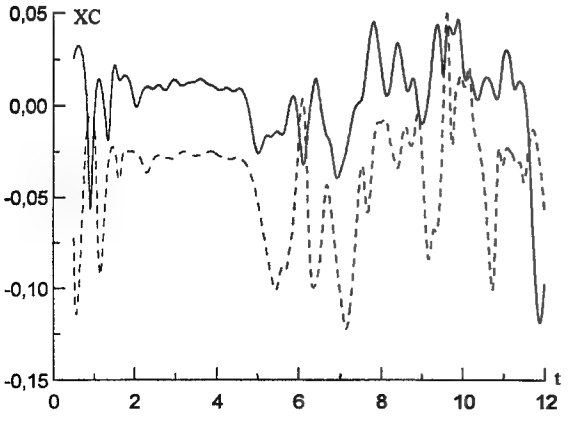

Fig. 2. Evolution of the energetic center of the signal wave (in a mirror section) (solid line) and the conjugated wave (in a nonlinear medium outlet) (dotted line) with interaction parameters: $\beta = 0.5, \gamma = -17, D = 0.1, L_z = 0.25, L_x = 9$

Also, we obtained the results of instability development investigating an optical bistable scheme based on counter two-wave interaction at a condition that one of two waves was formed by the reflection of the other wave from a mirror with a hole in the center. Originally, such scheme was offered and described in references [1,2]. Later in reference [3] this scheme was modified to decrease its dimension by placing the mirror directly at the nonlinear medium outlet ($z = L_Z$). This scheme is described by the following system of equations.

$$\frac{\partial A_+}{\partial t} + \frac{\partial A_+}{\partial z} + \beta \frac{\partial A_-}{\partial x} + iD \frac{\partial^2 A_+}{\partial x^2} + i\gamma \{0.5|A_+|^2 + |A_-|^2\} A_+ = 0,$$

$$\frac{\partial A_-}{\partial t} - \frac{\partial A_-}{\partial z} + \beta \frac{\partial A_-}{\partial x} + iD \frac{\partial^2 A_-}{\partial x^2} + i\gamma \{0.5|A_-|^2 + |A_+|^2\} A_- = 0, \qquad (8)$$

All parameters are described above.

Boundary and initial conditions for the system (8) are

$$A_{+|_{z=0}} = A_0(t) exp\left\{-\left(\frac{x - x_c}{r_p}\right)^6\right\},$$

$$A_{out} = A_{+|_{z=L_z}} exp\left\{-\left(\frac{x - x_c}{R_a}\right)^2\right\},$$

$$A_{-|_{z=L_z}} = A_{+|_{z=L_z}} R_0 \left(1 - exp\left\{-\left(\frac{x - x_c}{R_a}\right)^2\right\}\right) exp\left(\frac{i(x - x_c)^2}{R_m^2}\right),$$

$$A_0(t) = \begin{cases} 1.05 - exp(-\tau_1 t), & t < \tau_{on} \\ 1.05 + A_s\, exp\left\{-\left(\frac{t-\tau_c}{\tau_s}\right)^2\right\}, & \tau_{on} \le t \prec \tau_{off}, \\ 1.05, & \tau_{off} \le t \le L_t, \end{cases} \qquad (9)$$

with the pulse parameters $A_s = 0.19$, $\tau_1 = 50$, $\tau_{on} = 3$, $\tau_{off} = 25$, $\tau_c = 12 + \tau_{on}$, $\tau_s = 0.1$, $L_t = 30$, and interaction parameters $\gamma = -17$, $\beta = 0.5$, $D = 0.1$, $L_z = 0.25$, $L_x = 6$, $R_0 = 1$, $x_c = 3$, $R_a = 0.15$, $R_m = 100$, $r_p = 1$.

Here R_a is the radius of the reflecting mirror hole.

We were interested in investigation of such a model because of possibility of obtaining an optical bistability (OB) properties of the system by characteristics of an incident wave part that passed through the hole in the reflecting mirror at the medium outlet [4]. Such an OB element could be used, for example, as switching one in a optical computer units. However, detailed analysis of this scheme exposed features of instability by characteristics registered with some sets of parameters.

On figure 3, the power of the incident wave part

$$P_{out} = \int_0^{L_x} |A_{out}|^2 dx, \qquad (10)$$

that passed through the hole is shown.

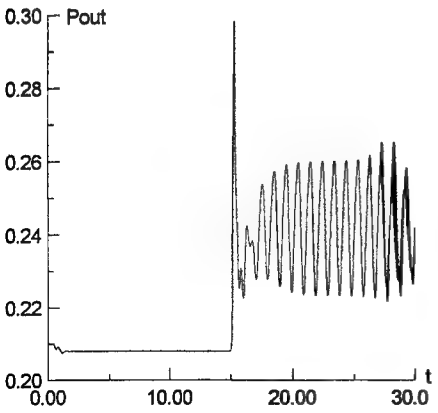

Fig. 3. Evolution of the outcome power of the incident waves

Summing up all above mentioned, we must be pointed out that effects of instability development are caused by many factors. One of these factors is the influence of inequality of counter propagating waves amplitudes.

2. CONDITIONS OF INSTABILITY DEVELOPMENT BY NONCOLLINEAR INTERACTION OF TWO COUNTER WAVES

2.1 Statement of a problem and the solution for the system of two counter noncollinear waves

Possibility of convective instability development must be taken into consideration equally with absolute instability in the WFC FWM problems. Also, in this case, inequality of the counter propagating waves amplitudes can play an essential role for the appearance of such instability.

By analogy with the method offered in reference [5], where the instability of two counter collinear waves in reactive nonlinear medium is investigated, we obtained the conditions of the instability development in the case of noncollinear interaction [6]. This process is described by the following system of the dimensionless equations:

$$\begin{aligned}
&\frac{\partial A_+}{\partial z}+\beta\frac{\partial A_+}{\partial x}+iD\frac{\partial^2 A_+}{\partial x^2}=-i\gamma(0.5|A_+|^2+|A_-|^2)A_+,\\
&\frac{\partial A_-}{\partial z}-\beta\frac{\partial A_-}{\partial x}-iD\frac{\partial^2 A_-}{\partial x^2}=i\gamma(0.5|A_-|^2+|A_+|^2)A_-,
\end{aligned} \tag{11}$$

where A_+ is an incident wave amplitude, A_- is a counter wave amplitude. The rest parameters are the same as described above.

It must be pointed out that each wave goes into the medium independently from opposed one, that is at $z=0$ section and $z=L_z$ accordingly.

For further analysis it is convenient to introduce new functions $A_\pm=\tilde{A}_\pm exp(i\frac{\beta}{2D}x)$. Then equations (11) are transformed to the following form:

$$\begin{aligned}
&\frac{\partial\tilde{A}_+}{\partial z}+\frac{i\beta^2}{4D}\tilde{A}_++iD\frac{\partial^2\tilde{A}_+}{\partial x^2}=-i\gamma(0.5|\tilde{A}_+|^2+|\tilde{A}_-|^2)\tilde{A}_+,\\
&\frac{\partial\tilde{A}_-}{\partial z}-\frac{i\beta^2}{4D}\tilde{A}_--iD\frac{\partial^2\tilde{A}_-}{\partial x^2}=i\gamma(0.5|\tilde{A}_-|^2+|\tilde{A}_+|^2)\tilde{A}_-.
\end{aligned} \tag{12}$$

2.2 Solution of the equations relatively to an instability increment

We will take the solution of Eq. (12) in the form of the plane waves perturbation.

$$\begin{aligned}
&\tilde{A}_+=A_+^0\,exp(-0.5i\gamma(I_++2I_-)z)\;\;(1+u(x,z)),\\
&\tilde{A}_-=A_-^0\,exp(0.5i\gamma(I_-+2I_+)z)\;\;(1+v(x,z)),
\end{aligned} \tag{13}$$

where $A_\pm^0$ - is the incident waves amplitudes, $I_\pm=|A_\pm^0|^2$, $u(x,z),v(x,z)$ are perturbations ($u,v<<1$).

Using Eqs. (12), (13) and transformed the equations to a linear form, we obtain, in the first approximation, the following equations relative to the perturbations:

$$\begin{aligned}
&\frac{\partial u}{\partial z}+iD\frac{\partial^2 u}{\partial x^2}+\frac{i\beta^2}{4D}(u+1)=-0.5i\gamma\{I_+(u+u^*)+2I_-(v+v^*)\},\\
&\frac{\partial v}{\partial z}-iD\frac{\partial^2 v}{\partial x^2}-\frac{i\beta^2}{4D}(v+1)=0.5i\gamma\{2I_+(u+u^*)+I_-(v+v^*)\},
\end{aligned}$$

and a couple of equations conjugated to them.
Further, assuming that

$$u = \tilde{u} + C_1, \quad u^* = \tilde{u}^* + C_2,$$
$$v = \tilde{v} + C_3, \quad v^* = \tilde{v}^* + C_4,$$

where C_i are the constants determined in the assumption of the homogeneity of the system obtained and expressed as following

$$C_{1,2} = -\frac{i\beta^2(i\beta^2 - 4i\gamma I_- D)}{-\beta^4 - 4\gamma D\beta^2 I_+ - 4\gamma D\beta^2 I_- + 48\gamma^2 D^2 I_+ I_-},$$
$$C_{3,4} = -\frac{i\beta^2(i\beta^2 - 4i\gamma I_+ D)}{-\beta^4 - 4\gamma D\beta^2 I_+ - 4\gamma D\beta^2 I_- + 48\gamma^2 D^2 I_+ I_-},$$

we get:

$$\begin{aligned}
&\frac{\partial\tilde{u}}{\partial z} + iD\frac{\partial^2\tilde{u}}{\partial x^2} + \frac{i\beta^2}{4D}\tilde{u} = -0.5i\gamma\{I_+(\tilde{u} + \tilde{u}^*) + 2I_-(\tilde{v} + \tilde{v}^*)\},\\
&\frac{\partial\tilde{v}}{\partial z} - iD\frac{\partial^2\tilde{v}}{\partial x^2} - \frac{i\beta^2}{4D}\tilde{v} = 0.5i\gamma\{2I_+(\tilde{u} + \tilde{u}^*) + I_-(\tilde{v} + \tilde{v}^*)\},
\end{aligned} \tag{14}$$

and a couple of the equations conjugated to Eq. (14).
For further analysis of the perturbation development we take the solutions of Eq. (14) in the form:

$$\begin{aligned}
&\tilde{u}(x,z) = U_0 \exp(iqx + i\mu z + i\varphi),\\
&\tilde{v}(x,z) = V_0 \exp(iqx + i\mu z + i\varphi),\\
&\tilde{u}^*(x,z) = U_0^* \exp(iqx + i\mu z + i\varphi),\\
&\tilde{v}^*(x,z) = V_0^* \exp(iqx + i\mu z + i\varphi),
\end{aligned} \tag{15}$$

Here $U_0 = (p + ih), V_0 = (m + in)$ are the perturbation amplitudes, μ is an instability increment, q is a transverse wave number, φ is an initial phase.
After a simple transformation of Eq. (11), the system of the equations relative to the perturbation amplitudes is obtained.

$$\begin{aligned}
&i\mu U_0 - iq^2 DU_0 + \frac{i\beta^2}{4D}U_0 = -0.5i\gamma\{I_+(U_0 + U_0^*) + 2I_-(V_0 + V_0^*)\},\\
&-i\mu V_0 + iq^2 DV_0 - \frac{i\beta^2}{4D}V_0 = 0.5i\gamma\{2I_+(U_0 + U_0^*) + I_-(V_0 + V_0^*)\},\\
&-i\mu U_0^* + iq^2 DU_0^* - \frac{i\beta^2}{4D}U_0^* = 0.5i\gamma\{2I_+(U_0 + U_0^*) + I_-(V_0 + V_0^*)\},\\
&i\mu V_0^* - iq^2 DV_0^* + \frac{i\beta^2}{4D}V_0^* = -0.5i\gamma\{I_+(U_0 + U_0^*) + 2I_-(V_0 + V_0^*)\}.
\end{aligned} \tag{16}$$

Note that with $\mu = 0$ it is following from Eq. (14) that for $q^2 D = \frac{\beta^2}{4D}$ h, n can have any values (otherwise the amplitudes are equal to zero). In this case, we deal with the process of the selfoscillation development with the finite amplitude. Consequently, noncollinearity of propagation cause the selfoscillation regime at a spatial frequency q defined by β and D.

Having transformed Eq. (16) with $q^2 D \neq \frac{\beta^2}{4D}$, we obtain the following system:

$$\left\{\frac{\beta^2}{4D}+\gamma I_+ - q^2 D - \left(\frac{\beta^2}{4D}-q^2 D\right)^{-1}\mu^2\right\}p + 2\gamma I_- m = 0,$$
$$-2\gamma I_+ p - \left\{\frac{\beta^2}{4D}+\gamma I_- - q^2 D - \left(\frac{\beta^2}{4D}-q^2 D\right)^{-1}\mu^2\right\}m = 0, \tag{17}$$

which for $\beta = 0$ turns into equations analyzed in reference [5].

The condition of existence of a nontrivial solution of a homogeneous system (17) is equality to zero its determinant.

$$\begin{vmatrix} \left\{\frac{\beta^2}{4D}+\gamma I_+ - q^2 D - \left(\frac{\beta^2}{4D}-q^2 D\right)^{-1}\mu^2\right\} & 2\gamma I_- m \\ -2\gamma I_+ & -\left\{\frac{\beta^2}{4D}+\gamma I_- - q^2 D - \left(\frac{\beta^2}{4D}-q^2 D\right)^{-1}\mu^2\right\} \end{vmatrix} = 0. \tag{18}$$

2.2.1 The case of equal amplitudes

In the particular case, when $I_+ = I_- = I$, relative to the increment μ, the fourth order equation follows from Eq. (18).

$$-\left\{\frac{\beta^2}{4D}+\gamma I - q^2 D - \left(\frac{\beta^2}{4D}-q^2 D\right)^{-1}\mu^2\right\}^2 = 4\gamma^2 I^2. \tag{19}$$

For the case of a focusing medium ($\gamma \succ 0$) the equation (19) is equivalent to

$$\mu^2 = \left(\frac{\beta^2}{4D}-q^2 D\right)^2 + 3\gamma I\left(\frac{\beta^2}{4D}-q^2 D\right),$$
$$\mu^2 = \left(\frac{\beta^2}{4D}-q^2 D\right)^2 - \gamma I\left(\frac{\beta^2}{4D}-q^2 D\right), \tag{20}$$

and for the focusing one ($\gamma \prec 0$) it is equivalent to

$$\mu^2 = \left(\frac{\beta^2}{4D}-q^2 D\right)^2 - 3|\gamma| I\left(\frac{\beta^2}{4D}-q^2 D\right),$$
$$\mu^2 = \left(\frac{\beta^2}{4D}-q^2 D\right)^2 + |\gamma| I\left(\frac{\beta^2}{4D}-q^2 D\right). \tag{21}$$

2.2.1.1 Propagation in focusing medium ($\gamma \succ 0$)

For a convenience of analyses we express

$$\mu^2 = x^2 - ax,$$
$$x = q^2 D - \frac{\beta^2}{4D},\ a = 3\gamma I, -\gamma I \tag{22}$$

on the figure. 4.

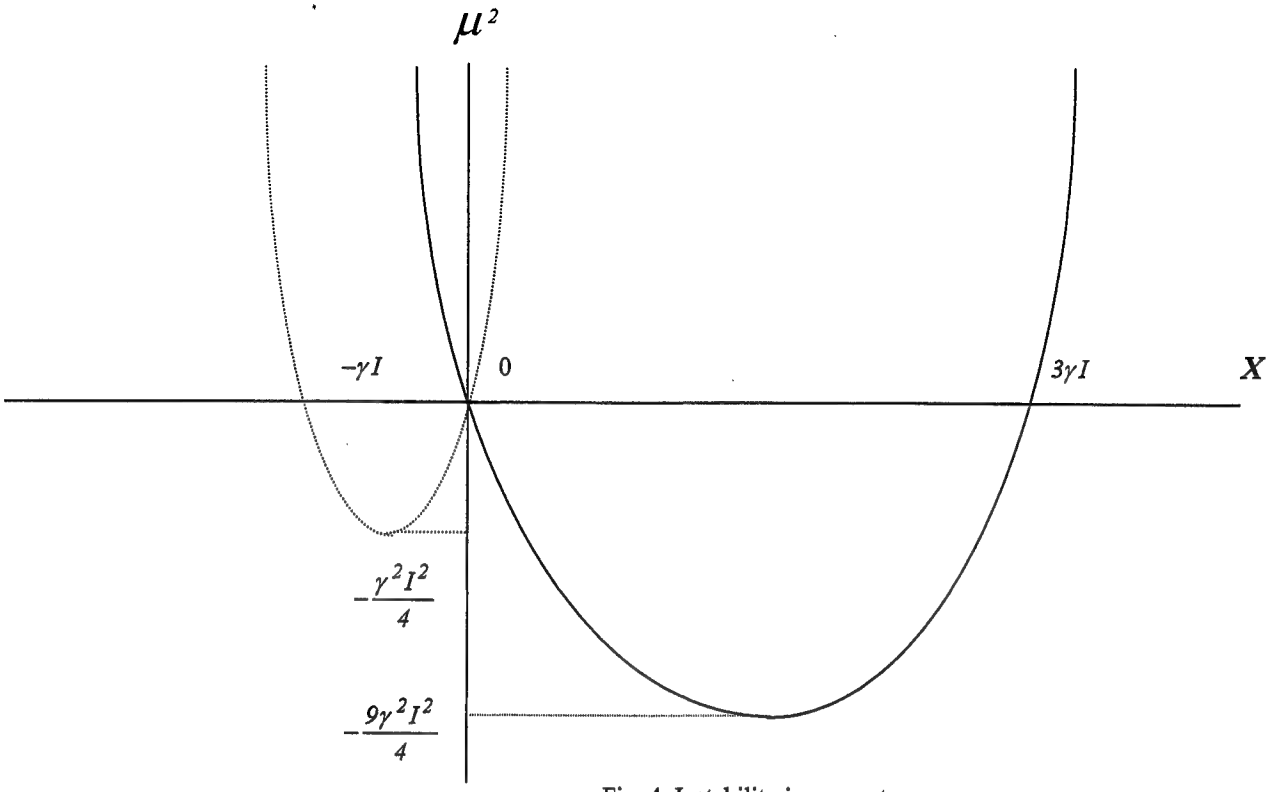

Fig. 4. Instability increment

One can see from fig. 4 that it is possible to exit of two region of instability. These regions are correspondent with the values of the parameters lying on X-axe. Noncollinearity yields the additional diapason of spatial frequencies at which noises can develop. Also, it shifts the diapason of spatial frequencies of the absolute instability to upper level. Generally, a minimum frequency q^2_{min} is defined by the angle of incidence of a light beam on nonlinear medium and an initial beam power. Summing up the results shown on fig. 4, we have

$$q^2 = \begin{cases} \left(0; \frac{\beta^2}{4D^2}\right), \beta^2 \prec 4\gamma \quad ID, \\ \left(\frac{\beta^2}{4D^2} - \frac{\gamma I}{D}; \frac{\beta^2}{4D^2}\right), \frac{\beta^2}{4D^2} \neq q^2 D, \beta^2 \succ 4\gamma ID, \\ \left(\frac{\beta^2}{4D^2}; \frac{\beta^2}{4D^2} + \frac{3\gamma I}{D}\right), \frac{\beta^2}{4D^2} \neq q^2 D. \end{cases} \tag{23}$$

It must be pointed out that a maximum instability increment differs in 3 times for the different regions. It is defined by the incident beam power.

2.2.1.1 Propagation in defocusing medium ($\gamma \prec 0$)

Analogous to the case described above, we obtained results for the defocusing medium.

The main difference of these two cases is in changing of diapason of spatial frequencies at which maximum amplifier coefficient is achieved. Also, with some values of an angle, the spectrum diapason for the focusing medium can be both

shorter and longer in comparison with the defocusing medium. The total diapason of instability development in the defocusing case is following:

$$q^2 = \begin{cases} \left(0, \dfrac{\beta^2}{4D^2}\right), \beta^2 \prec 12|\gamma| \quad ID, \\ \left(\dfrac{\beta^2}{4D^2} - \dfrac{3|\gamma|I}{D}; \dfrac{\beta^2}{4D^2}\right), \dfrac{\beta^2}{4D^2} \neq q^2 D, \beta^2 \succ 12|\gamma|ID, \\ \left(\dfrac{\beta^2}{4D^2}; \dfrac{\beta^2}{4D^2} + \dfrac{|\gamma|I}{D}\right), \dfrac{\beta^2}{4D^2} \neq q^2 D. \end{cases} \tag{24}$$

Note that in the defocusing case the perturbations develop at the diapason $0 \prec q \prec \dfrac{\beta}{2D}$, that is for the lower values of wave vectors in comparison with collinear interaction.

2.2.2 Case of unequal amplitudes

In the general case, when $I_+ \neq I_-$ we obtain from Eq. (18) following expressions.

$$\mu^2 = x^2 - \frac{\gamma x}{2}(c \pm d),$$
$$x = q^2 D - \frac{\beta^2}{4D}, \tag{25}$$
$$c = I_- + I_+, \; d = \sqrt{I_+^2 + I_-^2 + 18 I_+ I_-}.$$

On the grounds of Eq. (25), the graph characterizing influence of amplitudes inequality of counter propagating waves on a value of the instability increment is shown in fig. 5.

It is following from fig. 5 that inequality of supporting waves amplitudes may result in both increasing and decreasing of instability for different solutions of Eq. (25).

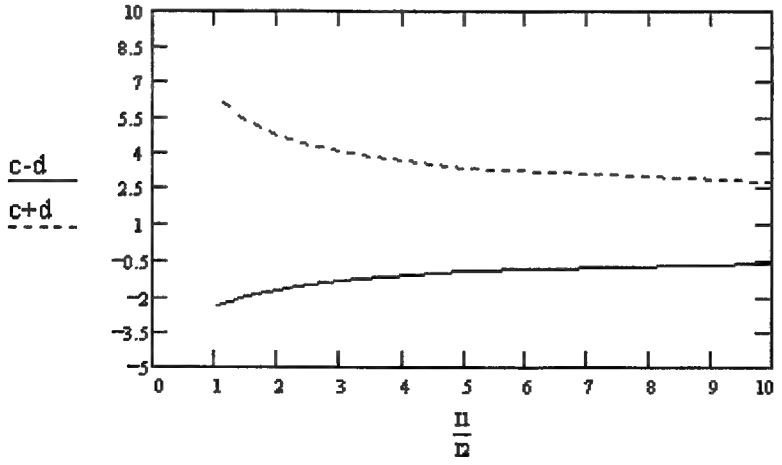

Fig. 5. Influence of amplitude inequality on the instability increment

3. CONCLUSION

Instability development takes place in various processes based on counter interactions of laser beams. In connection with this fact, it is important to note that noncollinearity of interaction as well as inequality of amplitudes of interacting waves have an important role in such an instability development.

Summing up the results obtained, we may come to conclusion that noncollinearity widens the spectrum interval of the instability development and changes the diapason of the maximum amplifier coefficient appearance. Enrichment of the spectrum interval depends on the sign of self-acting. In the case of defocusing for the noncollinear interaction the maximum instability increment is achieved at frequencies for which, in the collinear case, instability does not appear. Inequality of amplitudes can play an essential role in instability development. It may cause both shifting of the spectrum interval of the instability development and changing of the instability increment value.

REFERENCES

1. Bjorkholm J.E., Smith P.W., Tomlinson W.J., "Optical bistability based on self-focusing: an approximate analysis", IEEE J. Of Quantum Electronics, V. QE-18, № 12, pp. 2016-2022, 1982.
2. Borsch A.A., Brodyn M.S., Semashko V.I., Pisma v GTF *(In Russian)*, **12** (6), 345-349 (1986).
3. Zacharova I.G., Trofimov V.A., "On realization of optical bistability by two-wave counter interaction", Pisma v GTF *(In Russian)*, **22** (1), 79-84 (1997).
4. Nikitenko K.Y., Trofimov V.A., "Optical bistability and nonstationary processes with counter noncollinear wave interaction", Proc. Of 4th Int. Symp. On Optics of Atmosphere and Ocean, Tomsk, 91 (1997).
5. Zeldovich B.J., Pilipecky I.F., Shkunov V.V., *Wave front conjugation*, 240 p, Nauka publishers, Moscow, 1985.
6. Nikitenko K.Y., Trofimov V.A., "Instability and wave front conjugation by counter four-wave mixing", Optica i spectroscopia *(In Russian)*. (Sent to the journal.)

Laser bullets

N.N.Rosanov, N.A.Kaliteevkii, S.V.Fedorov

Institute of Laser Physics,
Research Centre "S.I.Vavilov State Optical Institute"
St. Petersburg 199034 RUSSIA

ABSTRACT

We present results of direct computer simulations of formation of laser bullets – 3D localised (soliton-like) structures of coherent radiation in media with saturable optical absorption and amplification and frequency dispersion. Stable stationary symmetric and pulsing asymmetric laser bullets are demonstrated. Superstability of these dissipative solitons and absence of drift of their main parameters give good reason to believe that these structures are promising for applications in the field of optical information processing.

1. INTRODUCTION

The term "laser bullets" means three-dimensional localised (nonwidening) structures of radiation propagating through continuous medium with nonlinear gain and absorption. Practically, unbounded medium can be replaced by ring and sufficiently long cavity filled in by the medium with similar characteristics.

The laser bullets are soliton-like formations, but they differ greatly from more familiar "conservative" optical solitons propagating in transparent nonlinear media (without optical absorption and amplification) [1]. The conservative solitons have a continuous spectrum of their main characteristics, e.g. peak intensity and width. Small fluctuations result in (small) change of these parameters. By this is meant that drift of the main parameters is unavoidable for the conservative solitons.

As for the laser bullets, they belong to a family of dissipative (not conservative) optical localised structures. It means that radiation energy exchange is important for them. Concurrent optical gain and losses are balanced only for some fixed levels of radiation intensity. Therefore the spectrum of the main parameters of the dissipative solitons is not a continuous, but a discrete one. Small initial fluctuations dissolve with time, and this feature leads to especial stability and robustness of the dissipative solitons. For this reason the dissipative optical solitons are promising for optical information processing.

The dissipative optical solitons were predicted 10 years ago for driven nonlinear interferometers [2,3]; their first experimental demonstrations were given by

SPIE Vol. 3685 • 0277-786X/99/$10.00

Rakhmanov and Schmalhausen [4,5]. Similar solitons were also forecast in lasers with saturable absorption [6,7] and found in experiments [8,9]. The results of subsequent studies of the dissipative optical solitons can be found in monograph [10]; a review of dissipative solitons – "autosolitons" – in systems of different physical nature was given by Kerner and Osipov [11]. Note that these solitons are one- or two-dimensional. Three-dimensional laser bullets in continuous media with saturation of gain and losses and frequency dispersion were predicted in the frames of approximate analytical method of momenta [12]; this prediction was recently borne out by direct computer simulations [13,14]. In this paper we give more detailed presentation of these simulations.

2. THE MODEL

For the radiation we will use approximation of slowly varying amplitudes, or parabolic equation. It is valid for the radiation packages with spatial sizes much exceeding the light wavelength [10]. As for the medium, we suppose that it is composed from two types of two-level particles, the first corresponding to radiation amplification and the second – to radiation absorption. Additionally to this resonant response we take into account a bulk constant (nonresonant) absorption and linear in the field amplitude and quadratic in frequency medium dispersion. Now we restrict ourselves by the case of very fast nonlinearity (saturation) and neglect any frequency detunings in the medium.

Under these assumptions the initial parabolic equation for the field envelope E has the form

$$\frac{\partial E}{\partial z} - i\Delta_\perp E + iD\frac{\partial^2 E}{\partial \tau^2} = f(|E|^2)E. \tag{1}$$

Here z is the longitudinal coordinate, $\Delta_\perp = \partial^2/\partial x^2 + \partial^2/\partial y^2$ is the transverse Laplacian, x and y are transverse coordinates, D is the coefficient of frequency dispersion, $\tau = t - z/v_g$ is time in moving with group velocity v_g system of coordinates, t is time. Nonlinear function f represents balance of the total losses and gain:

$$f(|E|^2) = -1 + \frac{g_0}{1 + |E|^2/I_g} - \frac{a_0}{1 + |E|^2}. \tag{2}$$

In this equation g_0 is the coefficient of linear gain, a_0 is the coefficient of linear resonant absorption, I_g is intensity of gain saturation while by the field amplitude scaling we can set that intensity of absorption saturation $I_a = 1$. Coefficient before the Laplacian in Eq. (1) is omitted because of scaling of transverse coordinates, scale for axis z is determined by the value of constant (nonresonant) absorption, and we can suppose $|D| = 1$ by scaling time τ. The sign of the coefficient D is not so important here as in the case of conservative solitons. For definiteness sake we take D = -1 (anomalous dispersion). Then we can rewrite Eqs. (1),(2) in the form

$$\frac{\partial E}{\partial z} - i\Delta_3 E + iD\frac{\partial^2 E}{\partial \tau^2} = \left(-1 + \frac{g_0}{1+|E|^2/I_g} - \frac{a_0}{1+|E|^2}\right), \qquad (3)$$

where $\Delta_3 = \partial^2/\partial x^2 + \partial^2/\partial y^2 + \partial^2/\partial \tau^2$ is three-dimensional Laplacian. Note that the scheme considered is cavityless and we do not use any approximation like a mean field limit. Effect of medium finite relaxation time and finite width of amplification and/or absorption spectral lines can be taken into account by introduction before the Laplacian in Eq. (3) a complex multiplier.

In all simulations presented we use values $a_0 = 2$ for linear resonant absorption and $I_g = 10$ for saturation intensity. As an initial condition, distributions of the field envelope for $z = 0$ were given.

3. RESULTS OF SIMULATIONS

Eq. (3) has "a spherical symmetry" (in coordinates x, y and τ). Therefore, it is natural to start from the search of "spherically symmetric" light bullets setting the envelope initial distribution with this symmetry. Calculations show formation of stationary spherically symmetric distributions of the field for linear gain g_0 in the range from 2.153 to 2.17. An example of such dynamics is given in Fig. 1. A set of stationary radial profiles is given in Fig. 2 for different values of g_0. If we introduce sufficiently small asymmetry in the initial distribution, it decreases with time, providing stability of stationary symmetric laser bullets (Fig. 3).

However, if the initial asymmetry exceeds some critical value, new type of laser bullets is formed with field distribution, which is periodic in time and asymmetric in space. One can see from Fig. 4 that after introduction of perturbation, depth of modulation of maximum intensity and average width gradually increases and then stabilizes. Some periods of these bullets dynamics are given at Fig. 5, and one can see that dynamics of the bullet width in the two transverse directions w_x and w_y is approximately antiphase. The periodically oscillating bullets exist in more narrow range of parameter g_0 than the stationary ones. There are also evidences of existence of high-order localised structures with more complex field distribution.

Hence, in the laser system considered there are stable stationary and oscillating 3D-localised structures of radiation – the laser bullets. Discrete spectrum of their main parameters and absence of drift of these parameters are the properties that may recommend the laser bullets for optical information processing.

4. ACKNOWLEDGMENTS

This research was supported by International Science and Technology Center, grant No 666.

5. REFERENCES

1. V.E.Zakharov, S.V.Manakov, S.P.Novikov and L.P.Pitaevskii, *Theory of Solitons: Inverse Problem Method*, Nauka, Moscow, 1980 (in Russian).

2. N.N.Rosanov and G.V.Khodova, "Autosolitons in bistable interferometers," *Opt. Spectr.*, Vol. 65, pp. 761-763, 1988.

3. N.N.Rosanov, A.V.Fedorov and G.V.Khodova, "Effects of spatial distributivity in semiconductor optical bistable systems," *Phys. Stat. Sol.*, Vol. B150, pp. 545-555, 1988.

4. A.N.Rakhmanov, *Opt. Spectr.*, Vol. 74, p. 1184, 1993.

5. A.N.Rakhmanov and V.I.Schmalhausen, *Proc. SPIE*, Vol. 2108, p. 428, 1993.

6. N.N.Rosanov and S.V.Fedorov, "Diffraction waves of switching and autosolitons in a saturable-absorber laser," *Opt. Spectr.*, Vol. 72, pp. 1394-1399, 1992.

7. S.V.Fedorov, G.V.Khodova and N.N.Rosanov, "Solitonlike field transverse structures in passive and active optical bistable systems," *Proc. SPIE*, Vol. 1840, pp. 208-215, 1992.

8. M.Saffman, D.Montgomery and D.Anderson, "Collapse of a transverse-mode continuum in a self-imaging photorefractively pumped ring resonator," *Opt. Lett.*, Vol. 19, pp. 518-520, 1994.

9. V.B.Taranenko, K.Staliunas and C.O.Weiss, *Phys. Rev.*, Vol. A56, p. 1582, 1997.

10. N.N.Rosanov, *Optical Bistability and Hysteresis in Distributed Nonlinear Systems,* Nauka, Physmatlit, Moscow, 1997 (in Russian).

11. B.S.Kerner and V.V.Osipov, *Autosolitons – a new approach to the problems of self-organization and turbulence,* Kluver, Dordrecht, Boston, London, 1994.

12. N.N.Rosanov, "The characteristics of laser autosolitons within the framework of the method of moments," *Opt. Spectr.*, Vol. 81, pp. 276-280, 1996.

13. N.A.Kaliteevskii, N.N.Rosanov and S.V.Fedorov, "Formation of laser bullets," submitted to *Opt. Spectr.*, 1998.

14. A.G.Vladimirov, S.V.Fedorov, N.A.Kaliteevskii and N.N.Rosanov, "Numerical investigation of laser localised structures," submitted to *Quant. Semiclass. Optics*, 1998.

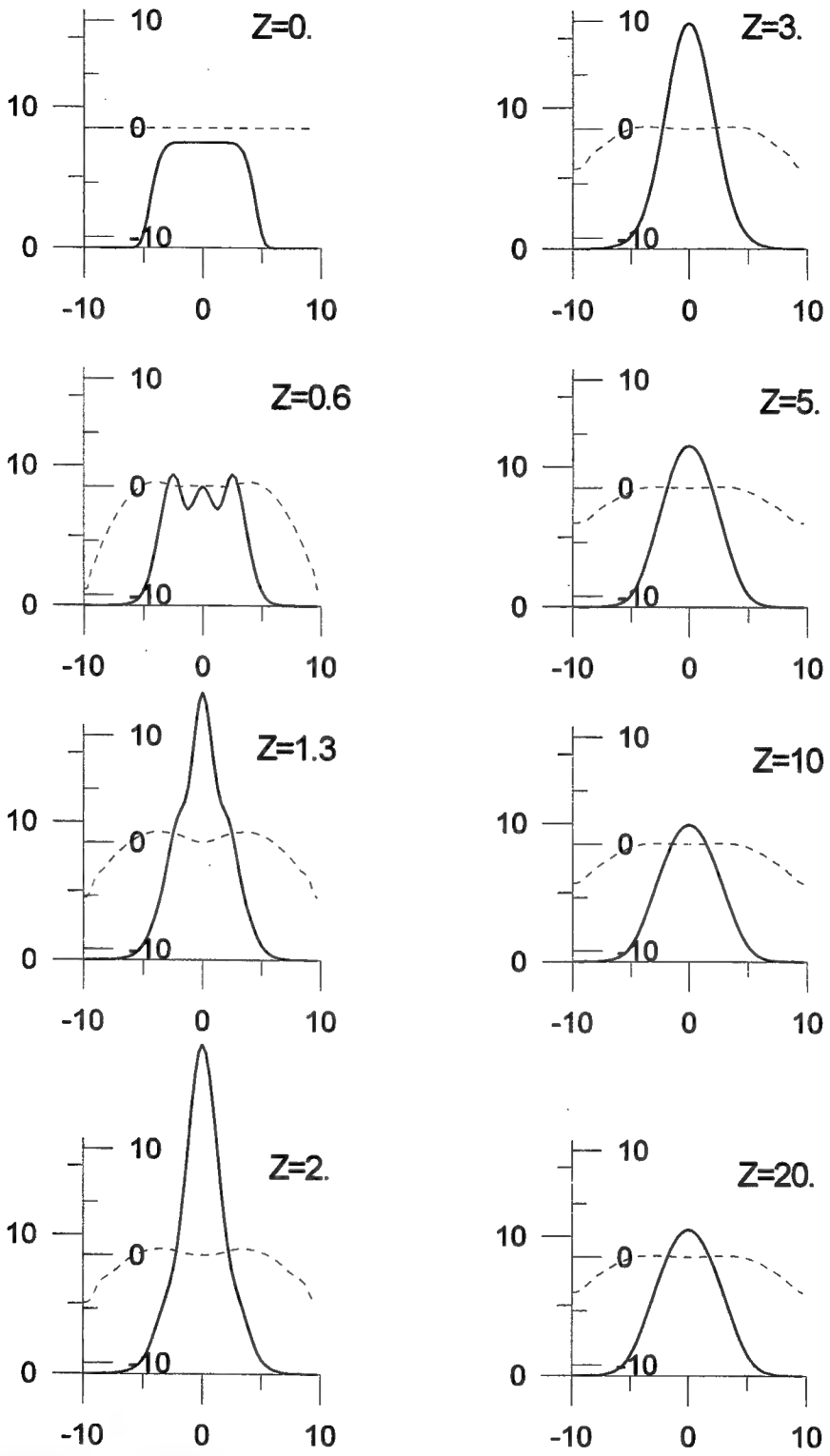

Fig.1 Formation of stable state of symmetric laser bullet.
Consequent profiles of light intensity (1) and phase (2) for laser bullet in process of its formation. Initial spot of light with radial symmetry is narrowing and approaching to stationary distribution.

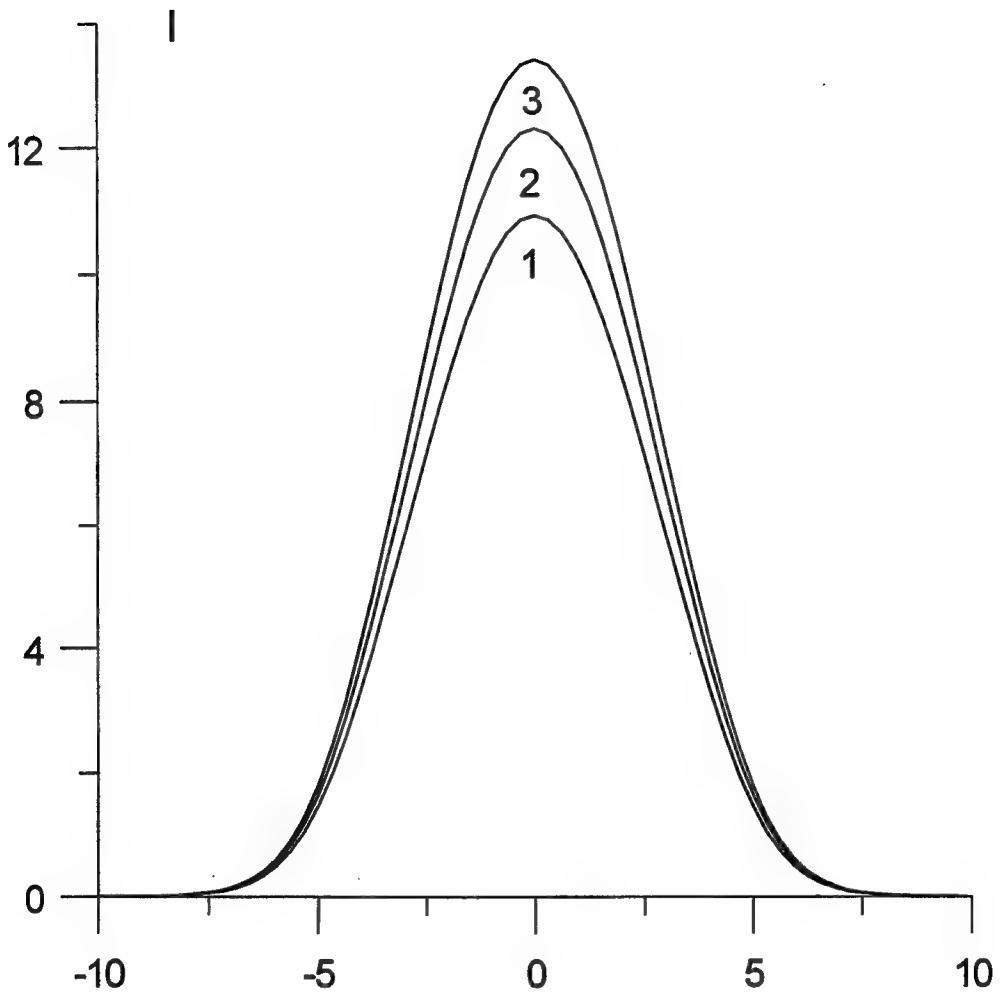

Fig.2 Light intensity profiles for laser bullets with radial symmetry.
Maximal intensity in center of bullet growths width gain
of active medium: $g_0 = 2.153,\ 2.16,\ 2.17$ for curves (1,2,3) consequently.

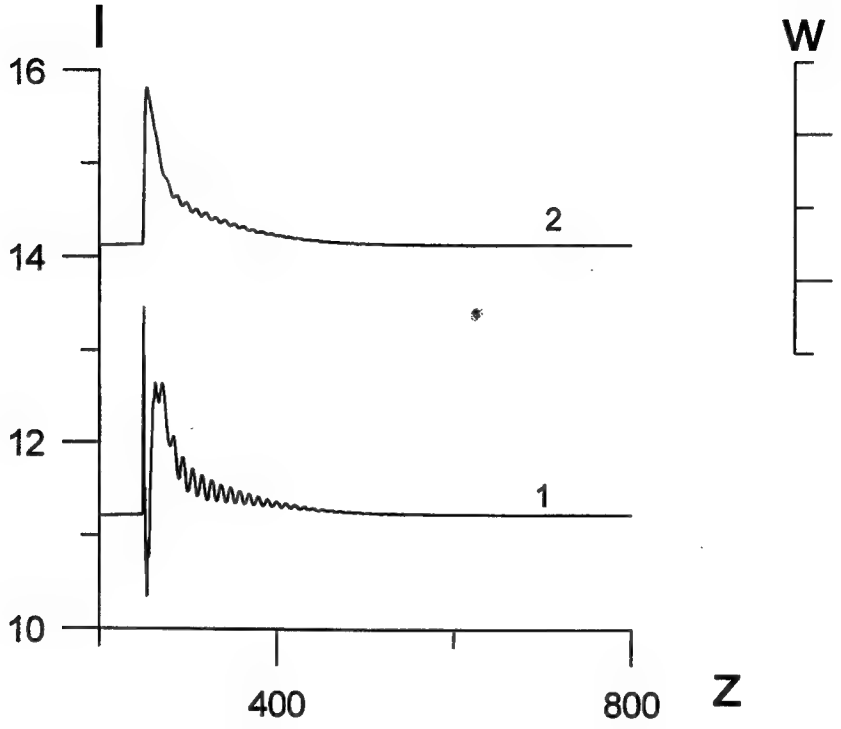

Fig.3 Demonstration of laser bullet stability
Evolution of maximal intensity (1) and averaged width (2)
for laser bullet in active medium ($g_0 = 2.154$) and saturable absorber.
Asymmetric initial perturbation of intensity
(the half of value for previous figure) is dissolving.
Symmetric profile and previous stable values of width
and maximal intensity are setting up.

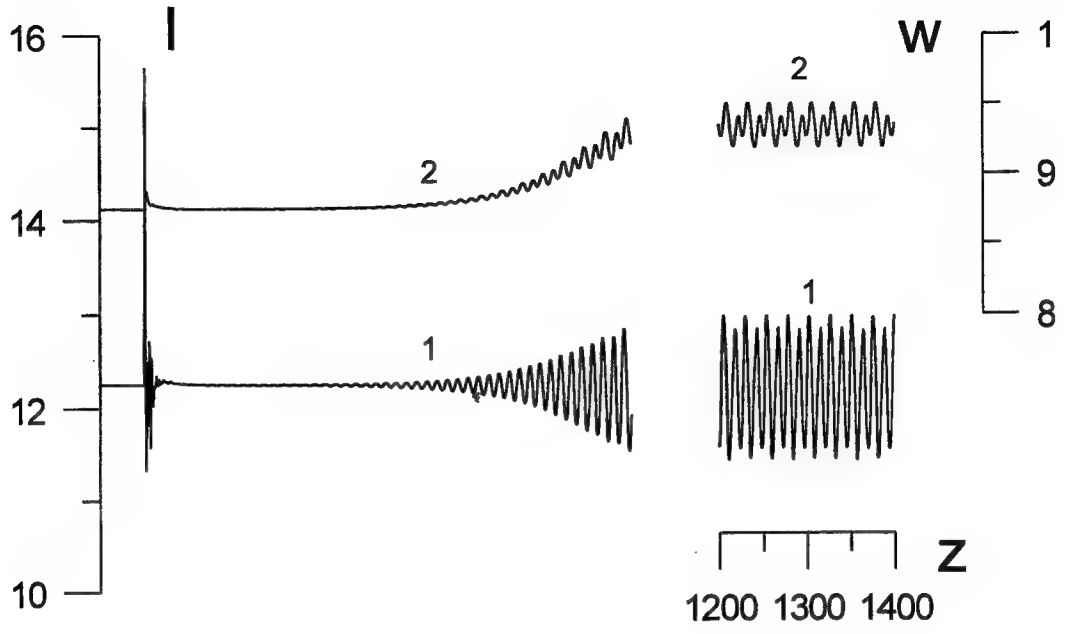

Fig.4 Formation of oscillating laser bullet
The swing of maximal intensity (1), and averaged width (2) for laser bullet in active medium ($g_0 = 2.16, I_g = 10$) and saturable absorber ($\alpha_0 = 2.$).
Asymmetric initial perturbation of intensity leads to excitation of periodically oscillating state.

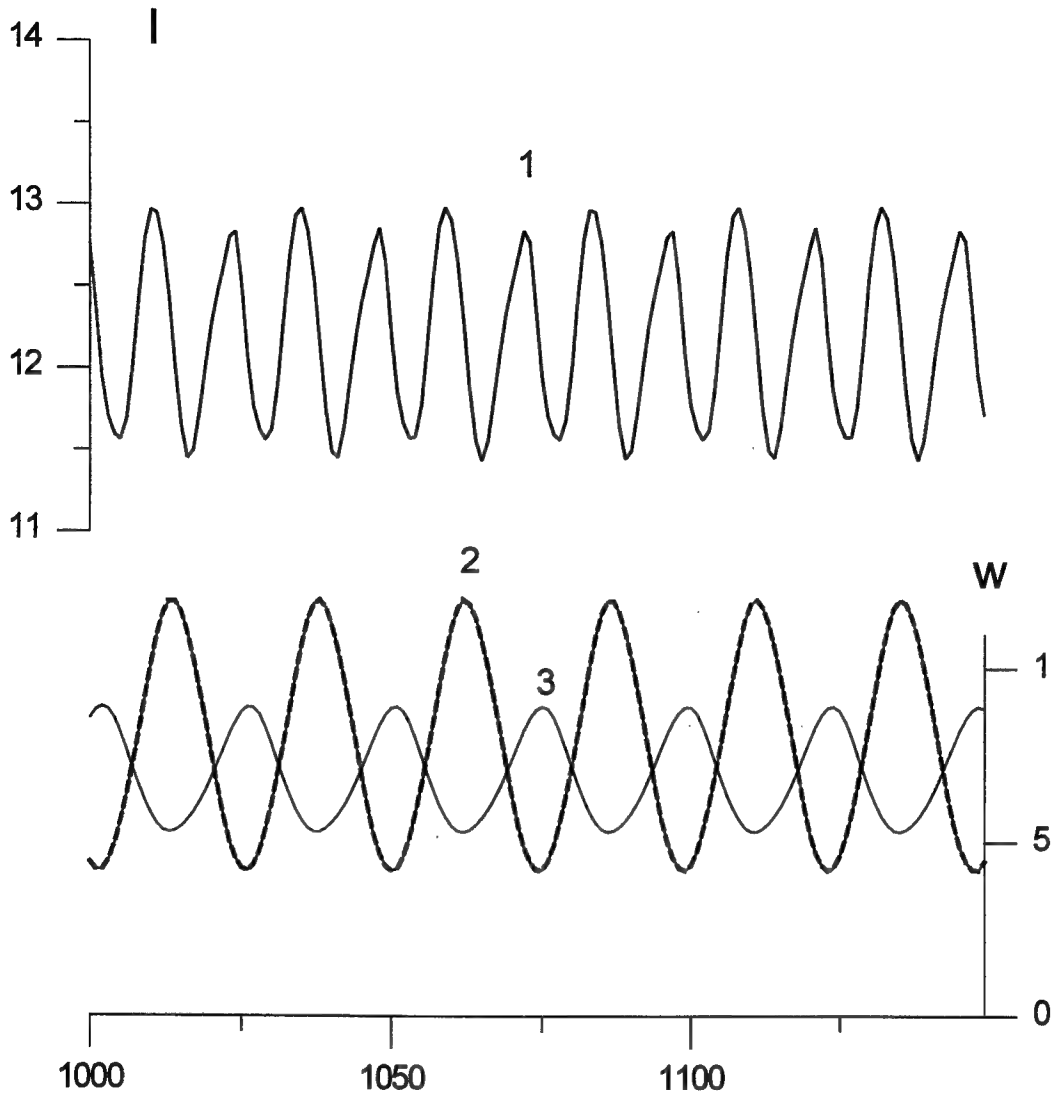

Fig.5 The oscillating laser bullet

Periodic oscillation of maximal intensity (1), and widths along first (2) & second (3) axes in stable, periodically oscillating laser autosoliton ($g_0 = 2.16, I_g = 10, \alpha_0 = 2.$).

The frequency of oscillation of intensity is doubled relatively frequencies of oscillation of axis widths.

SESSION 3

Second-Order Nonlinear Interactions

Advanced numerical simulation models for second-order nonlinear interactions

Gunnar Arisholm

Forsvarets forskningsinstitutt
(Norwegian Defence Research Establishment)
PO Box 25, N-2007 Kjeller, Norway

ABSTRACT

A general model for nonlinear optical frequency conversion devices based on second-order parametric processes is presented. The main emphasis is on optical parametric oscillators (OPOs). First, the model allows propagation in any direction in uniaxial or biaxial crystals, and diffraction and walk-off are included. Alternative numerical methods for solving the equations for the nonlinear interaction in the birefringent crystal are compared. Second, techniques for modeling temporal walk-off are considered. This is important in devices operating with short pulses or wide spectra. Third, initiation of parametric oscillation from spontaneous emission noise is modeled by adding random noise to the signals. The random nature of the noise initiation process leads to pulse to pulse fluctuations in energy, spectrum, and transverse beam shape. The fluctuations in transverse shape are small for narrow pump beams, but for wide pump beams they can be significant. Finally, thermal effects are considered. In devices with high average power, even a small absorption of one of the interacting beams can cause a temperature gradient in the nonlinear crystal. This temperature gradient leads to thermal lensing and spatially varying phase matching.

Keywords: Optical parametric oscillators, optical parametric amplifiers, beam propagation, quantum noise, thermal effects

1. INTRODUCTION

The great interest in optical parametric frequency conversion, combined with the continually increasing performance of computers, has led to extensive numerical modeling of optical parametric processes in recent years. Good computer models are useful tools for efficient design of high-performance devices, and they can also improve understanding by bringing out details that are difficult to measure in experiments. Detailed modeling of parametric processes poses many challenges, and some relevant effects are diffraction, spatial walk-off, temporal walk-off, thermal effects, and quantum noise effects. The model to be presented here combines all these effects.

Most materials with second-order nonlinearity are birefringent. If noncritical phase matching or quasi phase matching is used, birefringence can often be neglected, but if critical phase matching is used, there will be walk-off, and correct modeling of the birefringence is important. A general model for propagation with parametric interaction in birefringent crystals is discussed in Section 2. The performance of two alternative numerical methods for this problem is compared.

In short pulse devices, group velocity dispersion, leading to temporal walk-off of the interacting pulses, is important. This effect is also important in other devices operating with wide-band signals, because it is the temporal walk-off that limits the phase matching bandwidth, and hence determines the output signal spectra, of such devices. Modeling of these effects is discussed in Section 3.

Harmonic generation and sum- and difference-frequency mixing can be modeled classically because two beams are input to the nonlinear crystal and the third beam is deterministically generated from them. However, in parametric oscillators and generators, where the input is a single pump beam and signal beams grow from spontaneously emitted noise, the random nature of the spontaneous parametric emission process leads to pulse to pulse fluctuations in energy, spectrum, and transverse shape of the signals. Section 4 treats modeling of these effects.

A final problem, which becomes increasingly important when devices are scaled to higher powers, is related to thermal effects. In many nonlinear frequency conversion processes, at least one of the beams involved experiences some

Other author information:
E-mail: Gunnar.Arisholm@ffi.no

absorption in the nonlinear crystal. If the average power is high, the absorption leads to a significant temperature gradient in the crystal. This has two effects: First, the temperature dependence of the refractive index leads to thermal lens effects. Second, the temperature dependence of the birefringence leads to spatially varying phase mismatch, in other words, different parts of the crystal are temperature tuned to operate at different wavelengths. Both these effects can affect the efficiency, beam quality, and spectral quality of the conversion process. An iterative approach to modeling thermal effects is described in Section 5.

2. PARAMETRIC AMPLIFICATION IN BIREFRINGENT CRYSTALS

This section deals with modeling of the parametric interaction of three beams propagating in a birefringent crystal. For simplicity, temporal effects are neglected, so the equations presented in this section apply to the steady-state situation. (If the interacting beams have identical group velocities v_g, the time t can be replaced by $\tau = t - z/v_g$, and the equations are also valid for time dependent beams.) The method is based on previous work,[1–4] but it is generalized to include asymmetric diffraction and arbitrary propagation direction in biaxial crystals, except along the optic axes. This restriction on propagation direction is not a problem in practice, because phase matching is not possible for propagation along the optic axes. A brief explanation and an example are given here, and more details can be found in Ref. 5.

2.1. Mathematical Basis

Consider first the propagation of a single beam. In an optical beam with transverse variation, the electric field must necessarily have a nonzero longitudinal component. When working with beam propagation in isotropic media, this field component is usually ignored. By restricting attention to one of the transverse polarizations, the vector equations can be reduced to scalar equations, greatly simplifying the problem. In birefringent media, even plane waves have nonzero longitudinal field components if they have an extraordinary polarization. Birefringence, and the associated phenomena of beam walk-off and asymmetric diffraction, are intimately related to the vector nature of the electric field and the tensor properties of the dielectric medium.[6] However, the longitudinal field component is uniquely determined by the transverse part of the field and the dielectric tensor, so it is possible to model propagation in birefringent media without representing the longitudinal field component explicitly. The method is a generalization of the plane-wave expansion used for beam propagation in isotropic media[7]: Given a beam propagating in the z-direction, with transverse part of the field $\mathbf{E}_\mathrm{T}(x, y, z)$, the transverse distribution at $z = 0$ can be decomposed in terms of the plane wave eigenmodes of the birefringent medium. The eigenmode amplitudes are scalars, and each eigenmode can be propagated exactly using its correct refractive index. The dielectric tensor of the medium must be used for finding the plane wave eigenmodes and their refractive indices, but after that the vector nature of the field is automatically taken care of by the eigenmode expansion. If required, the longitudinal field components can be reconstructed from the eigenmode expansion using the known longitudinal field components for each eigenmode.

Mathematically, the transverse field of a single frequency component at $z = 0$ is written as $\mathcal{E} = \mathbf{E}_\mathrm{T} \exp(-i\omega t) + \text{c.c.}$, where

$$\mathbf{E}_\mathrm{T}(x, y, 0) = \int\int dk_x\, dk_y \sum_{j=1,2} \bar{E}(j, k_x, k_y, 0)\mathbf{u}(j, k_x, k_y) \exp(i(k_x x + k_y y)), \tag{1}$$

k_x and k_y are the transverse components of the wave vector, the sum is over the two polarization eigenmodes for each propagation direction, $\mathbf{u}(j, k_x, k_y)$ are polarization unit vectors, and $\bar{E}(j, k_x, k_y, 0)$ are the expansion coefficients, or the amplitudes of the eigenmode components. Bars denote Fourier amplitudes and $\mathcal{E}$ is the physical field oscillating at an optical frequency. Each mode propagates according to

$$\frac{\partial \bar{E}(j, k_x, k_y, z)}{\partial z} = -\alpha \bar{E}(j, k_x, k_y, z) + ik_z(j, k_x, k_y)\bar{E}(j, k_x, k_y, z), \tag{2}$$

where

$$k_z(j, k_x, k_y) = \sqrt{k^2(j, k_x, k_y) - k_x^2 - k_y^2}, \tag{3}$$

$$k(j, k_x, k_y) = 2\pi n(j, k_x, k_y, k_z)/\lambda, \tag{4}$$

λ is the vacuum wavelength of the light, α is the absorption coefficient, and n is the refractive index. Note that n depends on the direction specified by k_x, k_y, and k_z, so Eqs. (3) and (4) are implicit equations for k_z. All birefringence effects are represented by the dependence of n on the propagation direction. If n is expanded in a power series in k_x

and k_y, the first order terms describe walk-off, and higher order terms describe diffraction. In isotropic media, the diffraction terms in k_x and k_y are equal, but in birefringent media they differ, giving rise to asymmetric diffraction.

In practical nonlinear devices, the polarizations are chosen such that each beam has a well-defined linear polarization, corresponding to $j = 1$ or $j = 2$. Therefore, the sum over j can be eliminated, and the j argument in n, k, $\bar{E}$, and $\mathbf{u}$ can be suppressed. If the sum over j is kept, and the exact eigenmodes and polarization unit vectors are used in the decomposition of the beam, the formalism can also handle propagation along the optic axis. This approach has been used to study conical refraction.[8,9]

Now turn to the situation with three interacting beams with amplitudes E_1, E_2, and E_3, and frequencies ω_1, ω_2, and ω_3 such that $\omega_1 + \omega_2 = \omega_3$ and $\omega_1 \leq \omega_2$. The fields are represented by $\mathcal{E}_3 = E_3 \mathbf{u}_3 \exp(-i\omega_3 t) + \text{c.c.}$ etc., where $\mathbf{u}_3$ is a polarization unit vector and E_3 is an amplitude that is taken to be time independent. In the equations for each beam, the nonlinear driving polarization caused by the other two beams must be included. For generality, polarization terms due to a spatially varying refractive index are also included. The spatially varying refractive index can represent thermal effects. Taking beam 3 as example, the additional polarization is given by

$$P_3(x,y,z) = P_3^{(2)}(x,y,z) + P_3^{(T)}(x,y,z), \tag{5}$$

where $P_3^{(2)}$ is the second order polarization at ω_3 caused by beams 1 and 2. It is given by

$$P_3^{(2)}(x,y,z) = 2\epsilon_0 \chi_{\text{eff}} E_1(x,y,z) E_2(x,y,z), \tag{6}$$

where χ_{eff} is the effective susceptibility of the second order interaction.[10] $P_3^{(T)}$ is the additional polarization caused by the spatial variation of the refractive index, $\Delta n(x,y,z)$. Mathematically it is given by

$$P_3^{(T)}(x,y,z) = 2\epsilon_0 n_3 \Delta n(x,y,z) E_3(x,y,z), \tag{7}$$

where n_3 is the refractive index for beam 3. The small variation of the index for different plane wave components is not important in this expression, so n_3 can be taken to be constant.

2.2. Numerical Methods

The nonlinear polarization (5) can be included in the propagation equation (2) by adding its Fourier transform as a driving term. Again taking beam 3 as example, the equation becomes

$$\frac{\partial \bar{E}_3(k_x,k_y,z)}{\partial z} = ik_{3,z}(k_x,k_y)\bar{E}_3 - \alpha_3 \bar{E}_3 + \frac{i\mu_0 \omega_3 c}{2n_3} \mathcal{F}(P_3), \tag{8}$$

where the arguments to $\bar{E}_3$ were suppressed on the right hand side, and $\mathcal{F}$ is the Fourier transform, i.e.

$$\mathcal{F}(P_3) = \frac{1}{(2\pi)^2} \int\int dx\, dy \exp(-i(k_x x + k_y y)) P_3(x,y,z). \tag{9}$$

Now the rapid variation in the z-direction is factored out, and the amplitudes in Fourier-space and real space are written $\bar{E}_m(k_x,k_y) = \bar{e}_m(k_x,k_y)\exp(ik_m z)$ and $E_m(x,y) = e_m(x,y)\exp(ik_m z)$, respectively, where $k_m = 2\pi n_m/\lambda_m$. The equation for the slowly varying amplitude $\bar{e}_3$ becomes

$$\frac{\partial \bar{e}_3(k_x,k_y,z)}{\partial z} = i\delta k_{3,z}(k_x,k_y)\bar{e}_3 - \alpha \bar{e}_3 + i\frac{\omega_3}{n_3 c}[\exp(-i\Delta k z)\chi_{\text{eff}} \mathcal{F}(e_1 e_2) + \mathcal{F}(n_3 \Delta n e_3)], \tag{10}$$

where

$$\delta k_{3,z}(k_x,k_y) = k_{3,z}(k_x,k_y) - k_3 \tag{11}$$

and $\Delta k = k_3 - k_2 - k_1$ is the phase mismatch of the central beam components. The equations for $\bar{e}_1$ and $\bar{e}_2$ are similar. This method is denoted the Fourier-space method because Eq. (10) is solved in Fourier-space. When Eq. (10) is solved numerically, the integrals in Eqs. (1) and (9) are replaced by sums. This method has been implemented using an adaptive, 4th order Runge-Kutta method[11] for the resulting set of ordinary differential equations.

An alternative method of solution is the split-step method. In this method, propagation and linear loss are handled in Fourier-space using Eq. (2), which can be solved exactly. The nonlinear polarization term is handled in real space using the equation

$$\frac{\partial E_3(x,y,z)}{\partial z} = \frac{i\mu_0\omega_3 c}{2n_3} P_3(x,y,z). \tag{12}$$

Computation is carried out alternately in real space and Fourier-space, and Eq. (12) is solved separately for each transverse position. The simple split-step method, which first propagates a whole step and then solves the nonlinear equations for the whole step (or vice versa) is accurate to second order in the step size. The symmetrized split-step method, which propagates half a step, solves the nonlinear equations for the whole step, and then propagates the second half step, is accurate to third order,[12] and is therefore preferred in practice. The split-step method was implemented using the same 4th order Runge-Kutta method for Eq. (12).

The Fourier-space method turned out to be more efficient than the split-step method for solving the equations with high accuracy. This efficiency can be ascribed to the high order of the differential equation solver used. Another advantage of the this method is that adaptive step-size control can be implemented with little extra cost. The split-step method, on the other hand, turned out to be more efficient when low accuracy was sufficient. The point of equal performance corresponded to accuracies of 10^{-3} or better, which was found to be adequate for most practical OPO simulations. A further advantage of the split-step method is that it requires much less memory, and this is an important point when the model is extended to handle multiple longitudinal modes. Note that birefringence is represented by k_z, computed from Eqs. (3) and (4). Since k_z needs to be computed only once for each simulation, the additional computational cost of including birefringence, compared to a model with only diffraction, is negligible.

2.3. Example

To demonstrate simulation of propagation outside the principal planes of a biaxial crystal, type 2 parametric amplification in $KNbO_3$ was simulated (See Fig. 1). Although type 2 interaction in $KNbO_3$ has small χ_{eff}, it may be the desired interaction mode due to the smaller line width near degeneracy.[13] In the example, the propagation vector (our z-axis) had an angle $\theta = 52°$ with respect to the crystal Z-axis, and its projection on the crystal XY-plane made the angle $\phi = 45°$ with respect to the X-axis. The crystal was 1.5 cm long and $\chi_{\text{eff}} = 3\,\text{pm/V}$. The vacuum wavelengths of the interacting fields e_1, e_2, and e_3 were $\lambda_1 = \lambda_2 = 2.128\,\mu\text{m}$, and $\lambda_3 = 1.064\,\mu\text{m}$. Beams 1 and 3 had the fast polarization, and beam 2 had the slow polarization. Beams 1 and 3 were incident, while beam 2 was generated in the crystal. The incident beams were Gaussian with beam radii $w = 0.5\,\text{mm}$ and power 192 kW. The transverse resolution was 128 points on a $25\,\mu\text{m}$ grid. When both incident beams had plane wave fronts, the power of the generated beam (beam 2) was 18.5 kW. When the incident beam 3 had a converging wave front with 60 mm radius of curvature, the power of beam 2 was 4.4 kW. Although the intensity in the crystal increased somewhat because of the converging beam, the power of the generated beam was reduced. This is because the $\approx 1°$ divergence of the input beam leads to phase mismatch. This example shows the importance of detailed modeling when beams are divergent and angular acceptance is small. Fig. 1 shows the interaction geometry and the contours of input and output beams for the case when the incident pump was converging. The peaks of beams 1 and 3 are shifted relative to each other although these beams have the same polarization. They have slightly different walk-off because of dispersion, but most of the shift is caused by the transfer of energy in the nonlinear interaction.

3. TEMPORAL EFFECTS

The signals interacting in a nonlinear crystal usually have different group velocities. This leads to temporal walk-off between the envelopes of the interacting signals. In devices with picosecond pulses, temporal walk-off can limit the effective interaction length. However, temporal walk-off is also important in devices with longer pulses because it is related to the phase matching bandwidth. This can be seen by the following argument: Consider a device with a single pump frequency ω_3, signal frequencies $\omega_1 + \omega_2 = \omega_3$, and corresponding wave numbers k_1, k_2, and k_3. The phase mismatch is given by $\Delta k = k_3 - k_2 - k_1$, and its variation with signal frequency is

$$\frac{d\Delta k}{d\omega_1} = -\frac{dk_1}{d\omega_1} + \frac{dk_2}{d\omega_2} = \frac{n_{g,2} - n_{g,1}}{c} = t_w/L, \tag{13}$$

where $t_w = L(n_{g,2} - n_{g,1})/c$ is the temporal walk-off of the signals, $n_{g,i}$ are the group indices, c is the speed of light in vacuum, L is the length of the nonlinear crystal, and the sum $\omega_1 + \omega_2$ was held constant in the differentiation. Thus,

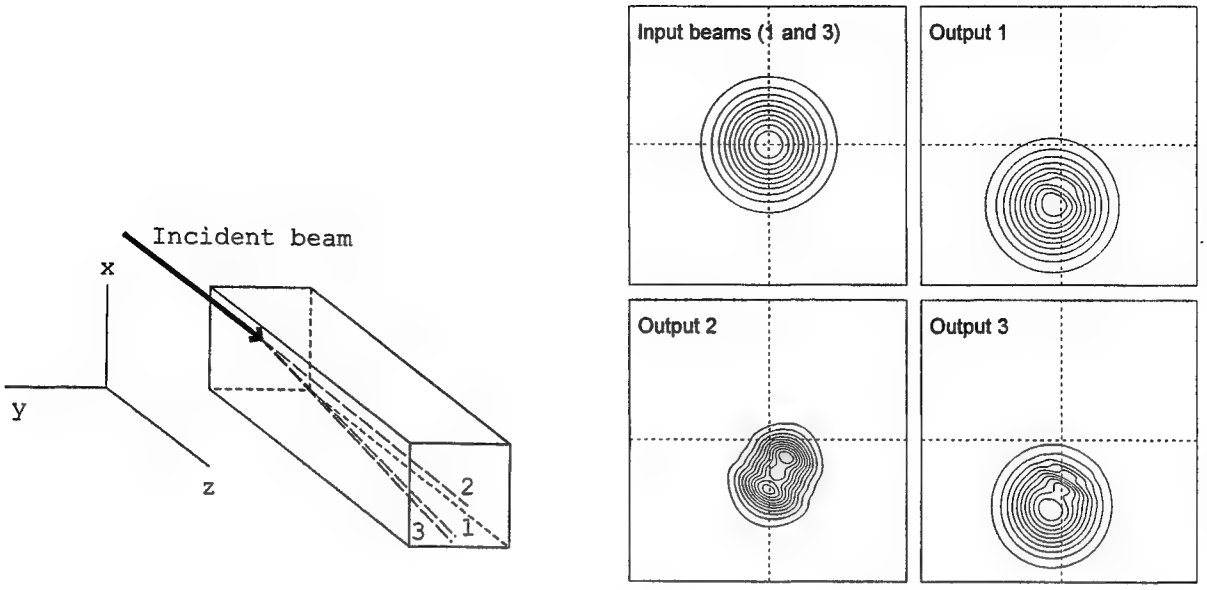

Figure 1. $KNbO_3$ parametric amplifier. Left: Interaction geometry. Note that all the beams have walk-off, and that they walk in different directions. Right: Contours of the magnitudes of the field amplitudes of the beams before and after the parametric amplifier. Beams 1 and 3 were incident, and they had the same intensity profiles. Beam 2 was generated in the interaction. The sides of the squares containing the beams are 3.2 mm.

temporal walk-off can be seen as a time domain description of phase matching bandwidth. In optical propagation, there is an analogy between spatial and temporal effects,[14] where spatial walk-off corresponds to temporal walk-off, and diffraction corresponds to pulse broadening by group velocity dispersion. It follows that temporal walk-off and pulse broadening can be handled in the frequency domain, with methods analogous to those used for the spatial effects in Section 2. In other words, multiple spatial and temporal modes can be handled by similar methods. Corresponding to Eq. (3), each temporal mode will have a wave number $k_z(\omega)$ depending on its frequency ω. A linear dependence of k_z on ω is related to the group velocity, and determines the temporal walk-off. Higher order dependences are related to pulse broadening (or narrowing).

There is, however, one important problem in the implementation of transform-based methods. In Section 2, the area over which the spatial Fourier transforms were taken was tacitly assumed to be large enough to contain the whole beam. In the spatial domain, this can in principle always be satisfied. In the temporal domain, the analogous condition is that the time interval over which Fourier transforms are taken must be long enough to contain the whole pulse. This can be satisfied in single pass devices, like parametric generators and frequency mixers, where the input signals are given in advance. In OPOs, however, the input signal in one round trip depends on the output from the previous round trip. Therefore, the complete signals are not known in advance, and calculations have to proceed one round trip at a time. If the pulse length is shorter than the round trip time, round trips can be treated independently, and the condition on the transform interval can be met.

In typical nanosecond OPOs, on the other hand, the pulse length is longer than the round trip time, and because of temporal walk-off, the round trip time is different for each wave. The result is that the pulse cannot be divided in independent round trips, because temporal walk-off would mix signals from adjacent round trips. To explain this problem in another way, suppose the transform interval is taken equal to the round trip time for one of the waves. Using a finite transform interval is equivalent to representing the signal by a periodic signal. This is no problem if the signal pulses in adjacent periods are well separated, but as explained above, this is not the case for typical nanosecond OPOs. Temporal walk-off, which should be represented by shifting the real signals along the time axis, is instead represented by shifting the periodic signals, which is equivalent to cyclic shifts within each transform interval. In practice, this approximation is often good because the temporal walk-off is small compared to the round trip time. Thus, only small parts of the signals, near the ends of the transform intervals, are affected by the approximation. Moreover, it is intuitively clear that if the signal changes little from one round trip to the

next, the error in the approximation will be small. Temporal walk-off can be modeled more accurately by working directly in the time domain, solving the coupled wave equations for short steps and shifting the signals with respect to each other between the steps. The disadvantage of this approach is that it requires higher temporal resolution because the temporal walk-off is introduced in discrete steps. Results using exact temporal walk-off and the cyclic approximation are compared in Section 4.

To conclude, short-pulsed OPOs (pulse time shorter than round trip time) can be modeled with Fourier transform methods, taking care of both temporal walk-off and pulse broadening. Long-pulsed OPOs (pulse time longer than round trip time) can be modeled approximately by the same method. Alternatively, temporal walk-off can be modeled more exactly in the temporal domain. Pulse broadening is small for pulses longer than a few picoseconds,[15] so this effect can be neglected in long-pulsed OPOs.

In real OPOs, both the temporal effects and the spatial effects from Section 2 can be present. These effects can readily be combined, giving the equation

$$\frac{\partial \bar{e}_3(\omega, k_x, k_y, z)}{\partial z} = i\delta k_{3,z}(\omega, k_x, k_y)\bar{e}_3 - \alpha\bar{e}_3 + i\frac{\omega_3}{n_3 c}[\exp(-i\Delta kz)\chi_{\text{eff}}\mathcal{F}(e_1 e_2) + \mathcal{F}(n_3 \Delta n e_3)], \tag{14}$$

where $\bar{e}_3(\omega, k_x, k_y, z)$ denotes the amplitude of a plane-wave component with transverse wave vector components k_x and k_y and frequency $\omega_3 + \omega$, where ω_3 is the center frequency of the wave. The Fourier transforms on the right hand side operate both in time and space. The functions $k_{m,z}(\omega, k_x, k_y)$ include the effects of birefringence, diffraction, and group velocity. If necessary, they can also include group velocity dispersion and higher order dispersion effects.

4. QUANTUM NOISE INITIATION OF PARAMETRIC OSCILLATION

Unless it is injection seeded, an OPO starts from spontaneous parametric emission, which can be regarded as a result of quantum noise. The randomness in this initiation process results in pulse to pulse fluctuations in the signal parameters. Fluctuations in the energy and spectrum of OPOs have been studied theoretically and experimentally.[16,17] There were large pulse to pulse fluctuations in the spectra, with approximately 100% standard deviation of the energy in individual modes. There were also significant fluctuations in the total pulse energy. The numerical model in that work was based on classical equations with random noise terms, but it did not include diffraction and multiple pump modes. The problem of simulating quantum noise initiation can be circumvented by simulating injection seeded OPOs, and very good agreement between simulation and experiment has been obtained for this case.[4] In this section, a model that combines the quantum noise effect with the full spatial and temporal modeling of Sections 2 and 3 is discussed. The quantum effects are investigated from the point of view of frequency conversion, so emphasis is placed on fluctuations in macroscopic signal properties, not on squeezing or correlation between the two signals.

4.1. Mathematical Basis

A full quantum model of the system would be very complicated because it would involve nonlinear operator equations. To avoid this, a two-step simulation model is used. In the first step, the signals are treated quantum optically whereas the pump is treated classically and is taken to be undepleted. In the second step, all fields are treated classically and pump depletion is included. These two models complement each other because the first is valid until pump depletion becomes significant. When this happens, the signals must necessarily have grown to macroscopic levels, and the rest of the OPO pulse can be simulated classically. The model neglects quantum effects when the signals are strong, so it does not include phenomena like the fundamental line width of a continuous wave OPO. This limit is so small[18] that it can be ignored compared to the inherent line width in nanosecond pulsed OPOs.

Because the spontaneously emitted noise has a wide bandwidth, the model must include multiple longitudinal modes, or equivalently, multiple sample points per round trip. Even if the pump source has a single frequency, the pump beam will also acquire a wider band width when it is depleted by a temporally varying signal. Because of the bandwidth of the signals, temporal walk-off, as discussed in Section 3, must be included. The starting point for the model is Eq. (14) for the evolution of multi-mode signals. This equation is just what is needed for the second, classical, step of the model. In step one, the quantum part of the model, the field amplitudes become operators. In absence of absorption, the operator equations for propagation of the fields through the nonlinear crystal are exactly like the classical equations with the field amplitudes replaced by the corresponding operators.[19] Since the pump is taken to be classical and undepleted, the operator equations are linear, and the output amplitudes after a pass through the crystal are a linear combination of the input amplitudes. The quantized equations for the mirrors differ

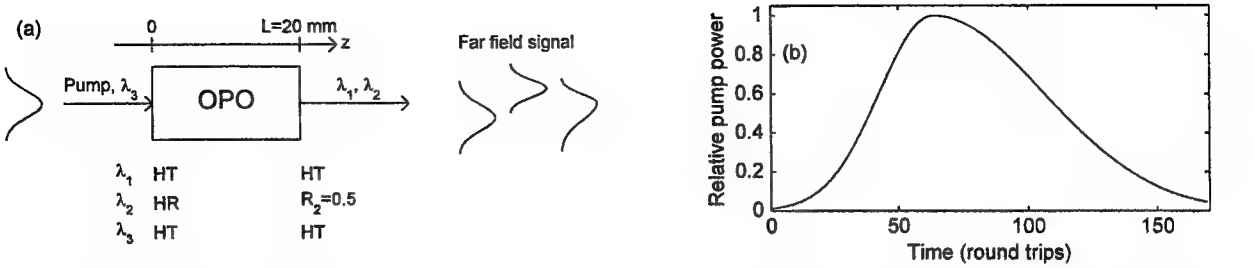

Figure 2. (a) The OPO model. The plane mirrors are placed directly at the ends of the nonlinear crystal. The reflectance for each wavelength is indicated below the mirrors. The different far-field signal profiles indicate fluctuations in beam shape and pointing direction. (b) Pump pulse envelope. One round trip time is $\approx 0.24\,\text{ns}$. The envelope is asymmetric Gaussian with 10 ns rise time and 20 ns fall time, measured between the e^{-2} points.

from their classical counterparts because vacuum noise enters from outside,[20] but these equations are also linear. The net result is that the signal operators after a number of round trips can be expressed as linear combinations of the initial signal operators and the noise operators entering through the mirrors in each round trip. Output signal amplitudes with the correct probability distribution can be obtained simply by inserting amplitudes with the appropriate distribution for all the initial and input noise operators. It is not even necessary to compute this linear combination explicitly: The correct output amplitudes can be computed simply by solving Eq. (14) for each pass through the OPO, starting with random field amplitudes and adding random noise terms for each reflection off the mirrors. When computing random amplitudes for the initial signal operators and input noise operators, their joint distribution must be taken into account. It turns out that they are independent with Gaussian distributions, corresponding to operators in the vacuum state. This can be shown by expressing all these operators in terms of eigenmode operators of a composite system consisting of the OPO cavity and the space outside. This approach has been used in one dimension,[21,22] and it can easily be extended to 3 dimensions.

4.2. Examples

Although the qualitative signal fluctuations can be expected to be independent of the particular OPO, a specific physical example was chosen for definiteness. This also makes it clear that the results seen in the examples correspond to experiments with realistic parameters. The example chosen was an OPO converting $1.064\,\mu\text{m}$ pump light to a $1.57\,\mu\text{m}$ signal and a $3.3\,\mu\text{m}$ idler in a noncritically phase matched $KTiOPO_4$ (KTP) crystal. The crystal is 20 mm long, with mirrors directly on its end faces, as shown in Fig. 2(a). The relevant nonlinear coefficient, d_{24}, was 3 pm/V. The pump pulse envelope is shown in Fig. 2(b). In most of the examples, the pump was taken to be single frequency, but there are also some examples with a multi-mode pump. The multi-mode pump signals had a Lorentzian average spectrum with 200 MHz mode spacing and a width of 70 modes (FWHM). These parameteres are typical of a Q-switched Nd:YAG laser. In the present examples, absorption is not included. This assumption is not correct for the $3.3\,\mu\text{m}$ idler, but the examples are nevertheless realistic because there are other crystals, like $KTiOAsO_4$, that have small absorption at this wavelength and otherwise approximately the same parameters as KTP.

4.2.1. Plane-wave modeling

Running simulations with multiple longitudinal modes and two transverse dimensions is very time consuming. Therefore, a plane wave model was used for investigating effects that are present regardless of the transverse beam shape. Various results from the plane wave simulations are shown in Fig. 3. Part (a) shows distributions of signal fluence for 4 different pump fluences and single- or multi-mode pump. The lowest pump fluence, $W_0 \approx 0.8\,\text{J/cm}^2$, corresponds to a peak intensity $I_0 \approx 44\,\text{MW/cm}^2$ for the single frequency pump. This intensity would give 100% conversion efficiency in steady state. The other pump fluences were $1.5\,W_0$, $2\,W_0$, and $3\,W_0$. The fluence W_0 is about 1.05 times above threshold for the single-mode pump, where threshold corresponds to 1% conversion to the signal. As expected, the random fluctuations in the multi-mode pump pulses lead to much wider energy distributions for the signals. The signal energies with the multi-mode pump are lower than with the single mode pump. For both pumps,

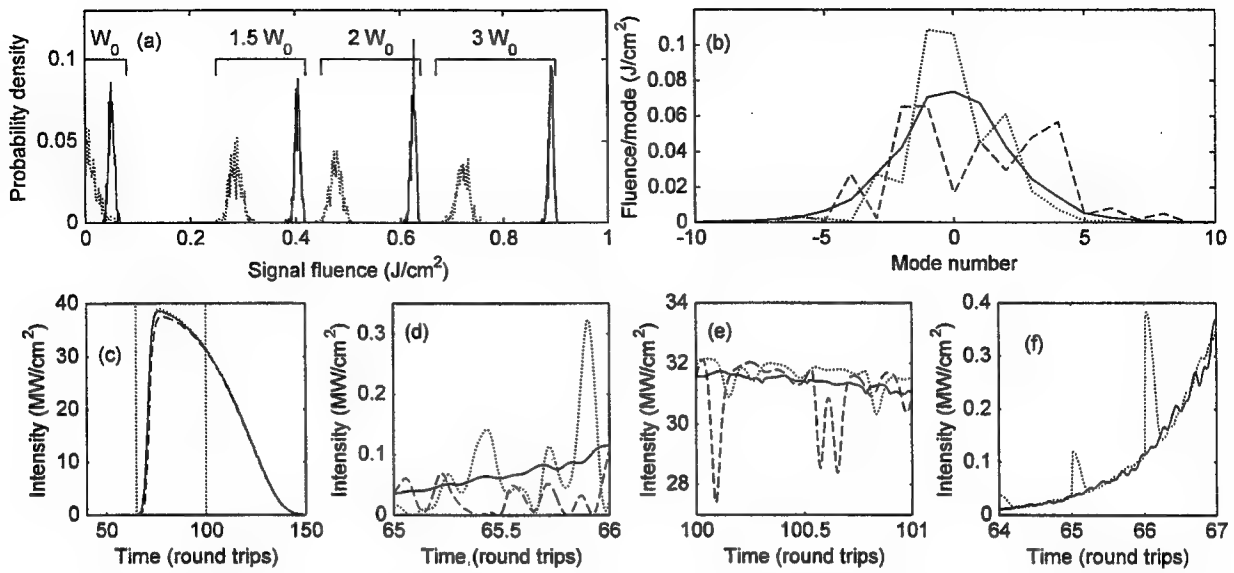

Figure 3. Results from plane wave simulations with quantum noise initiation. In parts (b-f), the pump is single frequency with fluence $1.5\,W_0$. (a) Distribution of signal fluence for 4 different pump fluences. The solid lines apply to single frequency pumps, while the dotted lines apply to multi-mode pumps. Pump fluences (see text) are shown above the graphs. (b) Mean spectrum (solid) and two individual examples (broken). (c) Mean signal power (solid) and two individual examples (broken). The power was averaged over each round trip, so the rapid variation within each round trip cannot be seen. The two vertical lines indicate the positions of the round trips seen in detail in (d) and (e). (d, e) Mean signal (solid) and example signals (broken) in round trips 65 and 100, computed with exact temporal walk-off. In round trip 65, the signals have not yet been smoothed by pump depletion. (f) Mean signals computed with exact temporal walk-off (solid) compared to cyclic temporal walk-off (dotted).

the relative width of the energy distribution decreases with increasing pump energy. Parts (b) and (c) show signal spectra and power, respectively, of two individual example signals together with the mean values over many pulses. The power curves are close to the mean, while the spectra fluctuate widely. Part (d) shows two example signals, and the mean signal, in round trip 65. The rapid variation is caused by the multi-mode nature of the spontaneous noise. Part (e) shows the same signals in round trip 100. Now modulation is much smaller because the signals have been smoothed by pump depletion. The spatially varying depletion of the pump tends to smooth out power fluctuations in the signal and leads to phase modulated light.[23] Part (f) shows the mean signal in round trips 64–66 computed with both exact temporal walk-off and the cyclic temporal walk-off approximation described in Section 3. The strong modulation of the latter signal is an artefact of the approximation. However, when the signal grows to full power, the modulation is damped by pump depletion, so the modulation is near maximum at the time shown in the figure. Apart from this difference in the detailed shape of the signals, the two models give almost identical results for energy distributions, spectra, and round trip averaged signals.

4.2.2. Transverse effects

Two different pump beams were used in simulations with transverse effects: Gaussian with $w_0 = 0.5\,\text{mm}$ and super-Gaussian of order 6 and $w_0 = 2\,\text{mm}$. The temporal profile of the pump was the same as above, and the peak intensity was $1.5\,I_0$. This corresponded to pump energies of 4.7 mJ and 106 mJ, respectively, for the two beams. With the narrow pump beam, the fluctuations in the spatial properties of the signal beam were small. The far-field pointing angle fluctuated by a few μrad, and both near-field and far-field distributions were almost identical in each pulse. The beam quality was good with $M^2 \approx 1.1$. With the wide pump beam, on the other hand, there were significant fluctuations in the beam shape and pointing direction, as shown in Fig. 4. The beam quality was much reduced with $M^2 \approx 6$. The reason for this qualitative difference is that, with the narrow pump beam, gain guiding causes strong spatial filtering of the signal. With the wide pump, multiple transverse modes can run.

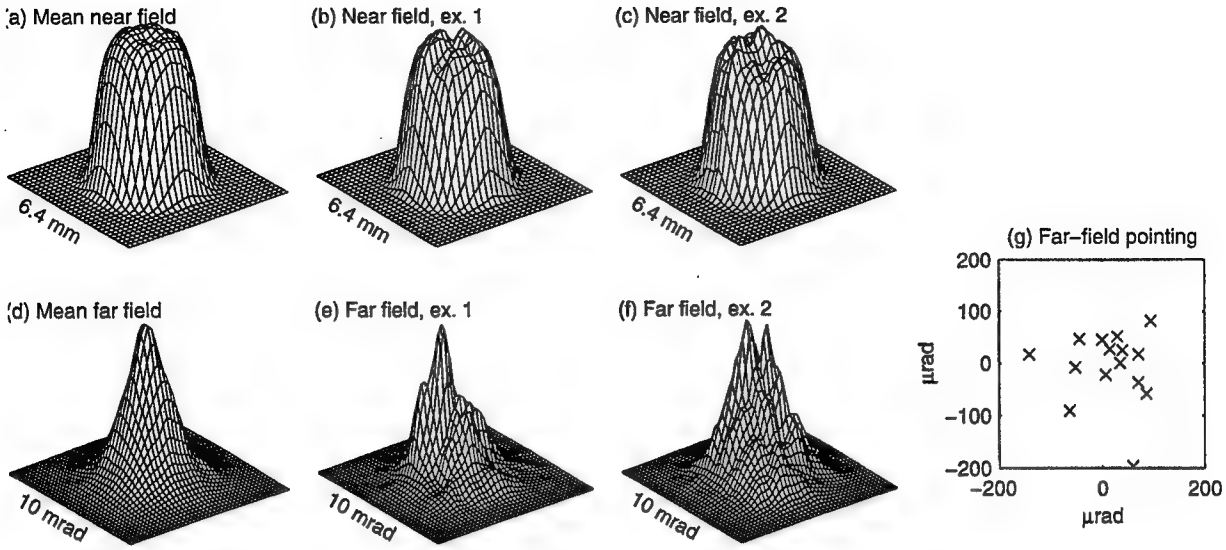

Figure 4. Simulation results with super-Gaussian $w_0 = 2\,\text{mm}$ pump beam. (a) Mean near-field signal fluence. (b, c) Near-field signal fluence in two individual examples. (d) Mean far-field signal fluence. (e, f) Far-field signal fluence in the same two examples as in parts (b) and (c). (g) Distribution of far-field pointing directions, computed from the centroids of the far-field fluence distributions.

4.2.3. Comparison with a classical model

A simple approch to OPO simulation is to use a model with a single longitudinal mode and start it with a seed signal corresponding to a single photon in the cavity. It is interesting to check the usefulness of such a model by comparing its results to the multi-mode model. It turns out that signal fluence and round trip average signals for plane waves (as shown in Fig. 3(c)) are predicted quite well with the simple model. The fluence from the single-mode model is in the upper end of the fluence distribution from the multi-mode model because the seed signal is always on the line center, while the multi-mode spectrum is sometimes dominated by off-center frequencies. When transverse effects are included, near-field and far-field beam profiles agree well for the 0.5 mm pump beam. For the 2 mm pump beam, near-field profiles agree farily well, but the deterministic single-mode model can obviously not reproduce the irregular and fluctuating far field-profiles. If an OPO runs on multiple transverse modes with significantly different frequencies, as may happen with critical phase matching, the multi-mode model is required.

5. THERMAL EFFECTS

There are presently strong efforts to scale OPOs and other frequency conversion devices to higher power.[24] With high average power, even a small absorption in the nonlinear crystal can lead to a temperature gradient that severely affects the performance of the device. Consequently, modeling of thermal effects is important in the design of high average power OPOs. The model of Dreger and McIver[2] allowed an arbitrary transverse refractive index variation, which could represent a nonuniform temperature distribution, but their model did not actually compute that temperature. Komine et.al.[25] modeled thermal lensing in a KTP OPO, but they did not give much details of their model, and it did not seem to include thermally induced phase mismatch.

The model to be presented here is a generalization of the multi-longitudinal mode, 3-dimensional model of the previous section. The nonlinear crystal is divided in a number of longitudinal slices, and during modeling of a single pulse, the transverse distribution of absorbed energy in each slice is computed. Based on this energy, the pulse repetition rate, the thermal properties of the crystal, and its thermal boundary conditions, the steady state temperature distribution in the crystal is computed. Then a new OPO pulse is simulated with this temperature distribution, and a new distribution of absorbed energy is found. This procedure is iterated until the results converge, which typically happens after only a few iterations. Transient thermal effects, that is, the heating of the crystal during a single pulse, are also included. This heating is simply proportional to the absorbed energy, as heat conduction can

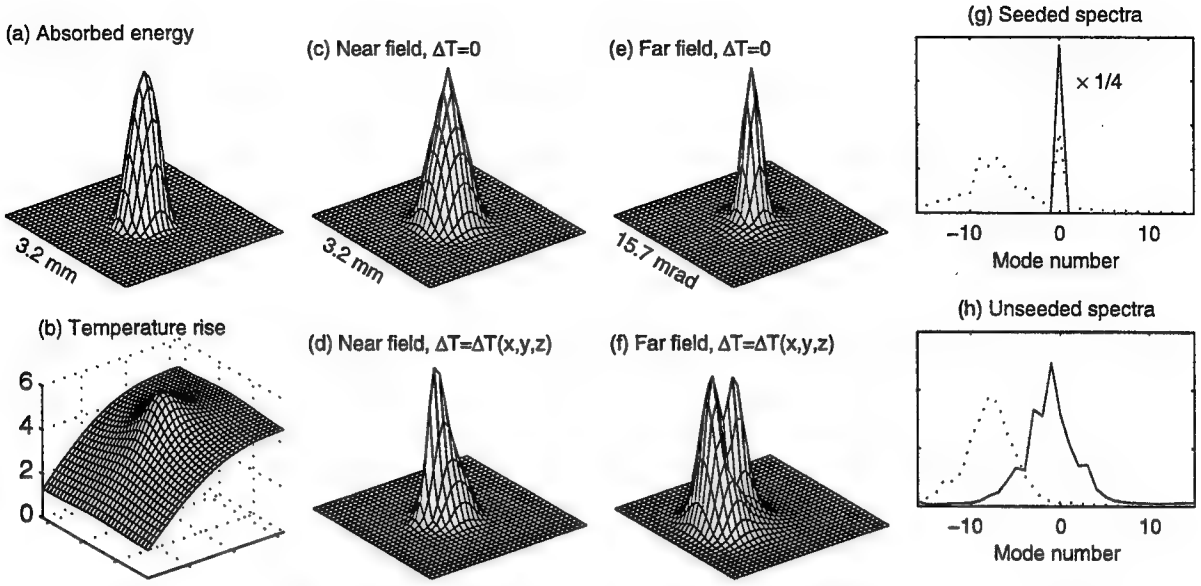

Figure 5. Modeling of thermal effects. (a) Transverse distribution of the energy absorbed in a single pulse. (b) Temperature rise in the 5th crystal slice at 500 Hz repetition rate. (c, d) Mean near-field signal fluence without and with thermal effects. (e, f) Mean far-field signal fluence without and with thermal effects. (g) Spectra for seeded OPO with (dotted) and without (solid) thermal effects. The solid curve was divided by 4 to fit in the same graph. (h) Spectra for unseeded OPO with (dotted) and without (solid) thermal effects.

be neglected because the pulse duration (on the order of 10 ns) is so small compared to the thermal time constant of the crystal. The sum of the steady-state and transient temperature distributions is used for computing the spatially varying index change, Δn in Eq. (14). Since this term is included in the spatial integration of the equations, both thermally induced phase mismatch and thermal lensing are taken into account.

5.1. Examples

The same example OPO as in Section 4 was used, except that the absorption coefficient of 0.5 cm^{-1} for the 3.3 μm idler was now included. The thermo-optic coefficients were taken from Ref. 26, and the thermal conductivity was taken to be 0.03 W/(cm K).[27] The small anisotropy of the thermal conductivity was negelcted. The Gaussian pump beam with $w_0 = 0.5$ mm was used, and the pump energy was 10 mJ. The transverse dimensions of the crystal were 3.2 by 3.2 mm. One side of the crystal was assumed to be mounted on a heat sink with fixed temperature and heat transfer coefficient of 0.5 W/(Kcm^2) between the crystal and heatsink. Thermal convection from the other three sides and the end faces was ignored. For a temperature rise of a few K, the heat lost through convection is two orders of magnitude smaller than that conducted to the heat sink. The crystal was divided in 8 axial slices for the thermal modeling.

Both seeded and unseeded operation were modeled. Without thermal effects, the signal energy from the seeded OPO was 3.8 mJ, and the total energy absorbed in the crystal was about 1 mJ. The transverse distribution of the total absorbed energy is shown in Fig. 5(a). The steady-state temperature distribution corresponding to a repetition rate of 500 Hz was computed. The temperature rise in the hottest slice is shown in Fig. 5(b). Transient thermal effects were small in this example. With thermal effects present, the signal energy of the seeded OPO dropped to 2.8 mJ. For the unseeded OPO, the energy dropped from 3.4 to 3.0 mJ. The nonuniform temperature also changes the shape of the signal beam. Fig. 5(c-f) show near-field and far-field signal fluences with and without thermal effects. Results without thermal effects correspond to operation at low repetition rate. The near field is seen to be focused by the thermal lens, while the far field is deflected by the wedge shape of the temperature distribution. The far field also becomes double-peaked, and this indicates reduced beam quality. Fig. 5(g,h) show spectra for seeded and unseeded operation with and without thermal effects. For the unseeded OPO, the spectrum is shifted because of temperature tuning. With the seeded OPO, the peak gain is shifted away from the seed frequency. This allows

other modes to grow, and the resulting spectrum looks more like that for unseeded operation. The fact that the seeded OPO no longer operates on a single frequency indicates that detailed modeling of OPOs with thermal effects may require multiple longitudinal modes and quantum noise initiation. The reason for this is that when different parts of the crystal are effectively temperature tuned to different wavelengths, it is not possible to tell in advance which mode will have the highest gain. Therefore, it is necessary to include multiple modes.

6. CONCLUSION

Methods for detailed modeling of second order nonlinear interactions have been discussed and illustrated by examples. Propagation in arbitrary directions in biaxial crystals, except along the optic axes, and including nonuniform diffraction, can be handled with small additional computational cost compared to methods including only diffraction. Modeling of temporal walk-off exactly and with a cyclic approximation was compared in a nanosecond regime OPO, and although there were clear differences in the details of the signals, macroscopic pulse properties like energy and spectra were not significantly affected. Fluctuations in the spontaneous parametric emission initiating OPO operation lead to fluctuations in energy and spectra of OPO pulses. For wide pump beams, there are also large fluctuations in transverse beam shape. Finally, modeling of thermal effects was considered. An example demonstrated the importance of modeling such effects in the design of high average power OPOs, and it also indicated that realistic modeling of thermal effects may require multiple longitudinal modes and statistically correct noise initiation.

ACKNOWLEDGMENTS

Thanks to Knut Stenersen and Halvor Ajer for useful discussions and suggestions.

REFERENCES

1. E. Lalor, "The angular spectrum representation of electromagnetic fields in crystals. II. Biaxial crystals," *J. Math. Phys.* **13**, pp. 443–449, 1972.
2. M. Dreger and J. McIver, "Second-harmonic generation in a nonlinear, anisotropic medium with diffraction and depletion," *J. Opt. Soc. Am. B* **7**, pp. 776–784, 1990.
3. A. Smith and M. Bowers, "Phase distortions in sum- and difference-frequency mixing in crystals," *J. Opt. Soc. Am. B* **12**, pp. 49–57, 1995.
4. A. Smith, W. Alford, T. Raymond, and M. Bowers, "Comparison of a numerical model with measured performance of a seeded, nanosecond KTP optical parametric oscillator," *J. Opt. Soc. Am. B* **12**, pp. 2253–2260, 1995.
5. G. Arisholm, "General numerical methods for simulating second order nonlinear interactions in birefringent media," *J. Opt. Soc. Am. B* **14**, pp. 2543–2549, 1997.
6. A. Yariv and P. Yeh, *Optical waves in crystals*, ch. 4. Wiley, 1984.
7. A. Siegman, *Lasers*, ch. 16. University Science Books, 1986.
8. E. Lalor, "An analytical approach to the theory of internal conical refraction," *J. Math. Phys.* **13**, pp. 449–454, 1972.
9. A. Schell and N. Bloembergen, "Laser studies of internal conical diffraction. I. quantitative comparison of experimental and theoretical conical intensity distribution in aragonite," *J. Opt. Soc. Am.* **68**, pp. 1093–1098, 1978.
10. V. Dmitriev, G. Gurzadyan, and D. Nikogosyan, *Handbook of nonlinear optical crystals*, ch. 2.8. Springer-Verlag, Heidelberg, 1991.
11. W. Press, S. Teukolsky, W. Vetterling, and B. Flannery, *Numerical recipes in C*, ch. 16. Cambridge university press, second ed., 1992.
12. G. Agrawal, *Nonlinear fiber optics*, ch. 2.4. Academic press, San Diego, second ed., 1995.
13. W. Bosenberg and R. Jarman, "Type-II phase matched $KNbO_3$ optical parametric oscillator," *Opt. Lett.* **18**, pp. 1323–1325, 1993.
14. A. Siegman, *Lasers*, ch. 9. University Science Books, 1986.
15. D. Reid, M. Ebrahimzadeh, and W. Sibbett, "Design criteria and comparison of femtosecond optical parametric oscillators based on $KTiOPO_4$ and $RbTiOAsO_4$," *J. Opt. Soc. Am. B* **12**, pp. 2168–2179, 1995.

16. T. Schröder, K. Boller, and R. Wallenstein, "Spectral properties and numerical modelling of a critically phase-matched nanosecond LiB_3O_5 optical parametric oscillator," *Appl. Phys. B* **58**, pp. 425–438, 1994.
17. A. Fix and R. Wallenstein, "Spectral properties of pulsed nanosecond optical parametric oscillators: Experimental investigation and numerical analysis," *J. Opt. Soc. Am. B* **13**, pp. 2484–2497, 1996.
18. R. Graham and H. Haken, "The quantum-fluctuations of the optical parametric oscillator. i," *Z. Phys.* **210**, pp. 276–302, 1968.
19. E. Merzbacher, *Quantum mechanics*, ch. 15.7. Wiley, New York, 1970.
20. L. Mandel and E. Wolf, *Optical coherence and quantum optics*, ch. 12.12. Cambridge University Press, 1995.
21. R. Lang, M. Scully, and W. Lamb, "Why is the laser line so narrow? a theory of single-quasimode laser operation," *Phys. Rev. A* **7**, pp. 1788–1797, 1973.
22. B. Abbott and S. Prasad, "Quantum noise and squeezing in an optical parametric oscillator with arbitrary output-mirror coupling," *Phys. Rev. A* **45**, pp. 5039–5051, 1992.
23. D. Armstrong and A. Smith, "Tendency of nanosecond optical parametric oscillators to produce purely phase-modulated light," *Opt. Lett.* **21**, pp. 1634–1636, 1996.
24. S. Velsko and P. Kryukov, "Applications of high-average power nonlinear optics," in *Nonlinear frequency generation and conversion*, M. Gupta, W. Kozlovsky, and D. MacPherson, eds., vol. 2700 of *Proc. SPIE*, pp. 6–17, 1996.
25. H. Komine, J. Fukumoto, W. Long, and E. Stappaerts, "Noncritically phase matched mid-infrared generation in $AgGaSe_2$," *J. Select. Top. Quantum Electron.* **1**, pp. 44–49, 1995.
26. W. Wiechmann, S. Kubota, T. Fukui, and H. Masuda, "Refractive-index temperature derivatives of potassium titanyl phosphate," *Opt. Lett.* **18**, pp. 1208–1210, 1993.
27. J. Bierlein and H. Vanherzeele, "Potassium titanyl phosphate: properties and new applications," *J. Opt. Soc. Am. B* **6**, pp. 622–633, 1989.

Peculiarities of parametric frequency conversion at pumping by a Bessel light beam.

Belyi V.N., * Khilo N.A.

Institute of Physics, * Department for Optical Problems in Information Technologies of the National Academy of Sciences of Belarus. 220072, Minsk, Belarus.

ABSTRACT

Parametric generation of light at pumping by Bessel light beam has been investigated. Advantages of such pumping over the use of Gaussian light beams have been revealed. A theory of azimuth-matched nonlinear interaction of Bessel light beams has been developed. It is shown that at such an interaction in the parametric generator the maximum coupling coefficient is realized and no destruction of the spatial structure of introcavity fields at high coefficients of conversion occurs. This opens up the possibility of increasing the energy conversion coefficient of the input Bessel beam compared to the Gaussian beam.

***Key words**: parametric light generator, Bessel light beams.*

1. INTRODUCTION

In present practice, nonlinear-optical frequency converters and optical parametric oscillators (OPO) use mainly Gaussian type light beams [1]. At the same time, their use is associated with a number of limitations. First, because of the specific structure of Gaussian beams the maximum overlap integral of interacting modes is not realized [2]. This leads to a decrease in the conversion efficiency. Another limitation on the efficiency of nonlinear conversions using parametric interaction with Gaussian pump beams is due to the distortions in the spatial profile of wave in the process of nonlinear conversion. In this case, because of the formation of super-Gaussian profiles there appears instability towards the generation of higher spatial modes. In turn, this leads to the broadening of the converted radiation spectrum as well as to a decrease in the conversion efficiency. The above limitations can be eliminated by using non-traditional Bessel light beams (BLB) in the processes of nonlinear-optical conversion. The specific structural peculiarity of Bessel beam is that a manifold of wave vectors of its Fourier spectrum lies on the cone surface. Therefore, in the cross-section of Bessel beams a standing light wave is formed which does not diffract in the case of an unrestricted beam. The spatially restricted Bessel beam is characterized by an extended focus, i.e. by suppressed diffraction divergence of the central part of the beam.

During the past few years have seen sharply increasing interest in the nonlinear properties of nondiffracting Bessel beams [5-11].The operation of an OPO pumped by a coherent and incoherent BLB is demonstrated for the first time in Refs [12-14]. It is proved that the OPO output has a caracteristic spatial profile caused by noncollinear phase matching and consists of a central spot with ring around it. In Refs [5-14] some peculiarities of using BLBs compared to the traditional Gaussian beams have been established. At the same time these works have not revealed the principal advantage of BLBs which consists in the possibility of their nonlinear-optical conversion without destructing the spatial structure. This leads to a limitation of potentialities of using Bessel light beams in nonlinear optics.

SPIE Vol. 3685 • 0277-786X/99/$10.00

In [15,16] a new kind of nonlinear interaction which does not destruct the Bessel beams at arbitrary conversion coefficients have established. This kind of nonlinear interaction is realised due to azimuth-matched interaction of the spatial spectral components of BLBs. The kind of interaction established in above mentioned works is realised in both sum-frequency and difference-frequency mixing as in parametric interactions. The predicted azimuth-matched interaction, which does not destruct the spatial structure of Bessel beams has been demonstrated experimentally by other authors in a recent work devoted to Raman scattering of Bessel light beams [17]. A particular case of azimuth-matched interaction is the interaction of the Bessel beam with a quasi-plane wave or a Gaussian-type field.

In the present paper, a theory of azimuth-matched interaction of BLBs in the optical cavity is developed. The influence of the transverse and the longitudinal mode structure of the cavity on parametric generation is investigated. Analysis is carried out of interaction conditions under which realization of maximum overlap integrals of BLBs is possible.

2. PARAMETRIC CONVERSION OF BESSEL BEAMS IN A CAVITY WITH LONGITUDINAL AND TRANSVERSE MODE STRUCTURE

Let us consider a parametric interaction of three BLBs in an anisotropic crystal placed in an optical cavity. To illustrate the approach described below, we choose an X-cut KTP crystal in which frequency conversion is realized under the conditions of noncritical phase synchronism for interaction of the type $o_3 \rightarrow o_3 e_1$ when the fast pump wave at frequency ω_3 is converted to a fast signal wave (ω_1) and a slow idler wave (ω_2). Such a scheme of an OPO on an X-cut KTP crystal is promising, for example, for Nd:YAG laser $\lambda_3 = 1.064\,\mu m$ radiation conversion into an eye-safe range of wavelengths $\lambda_1 \approx 1.54\,\mu m$ [18]. The above type of interaction is also characterized by the maximum coefficient of effective nonlinearity $d_{32} = 3.4\,pm/V$.

We consider an optical cavity whose transverse modes are described by Bessel functions. The simplest geometry of such a cavity consist of two spherical mirrors one of which is annular.

To describe the nonlinear interaction of BLBs, we represent them as a superposition of plane waves with wave vectors lying on the surface of a cone. Thus, in the general case, the interaction of these plane-wave components will be vectorial depending on the fulfillment of the conditions of spatial synchronism

$$k_3 \cos\theta_3 = k_1 \cos\theta_1 + k_2 \cos\theta_2, \tag{1}$$

$$q_3 = q_1 \cos(\Delta\varphi_1) + q_2 \cos(\Delta\varphi_2), \tag{2}$$

$$q_1 \sin(\Delta\varphi_1) = q_2 \sin(\Delta\varphi_2), \tag{3}$$

where $k_i = 2\pi n_i(\lambda_i)/\lambda_i$ are wave numbers, θ_i - half-angles at the vertex of cones of the wave vector of three BLBs, ($\varphi_3 = 0$ is assumed), $q_i = k_i \sin(\theta_i)$ - transverse components of wave vectors (see Fig. 1 a,b). In (1)-(3) it is assumed that subscripts 1,2,3 correspond, respectively, to the signal wave, the idler wave, and the pump.

We consider a single- cavity model of OPO for the signal wave. The wave vectors of the signal BLB are determined from the conditions of longitudinal and transverse resonances:

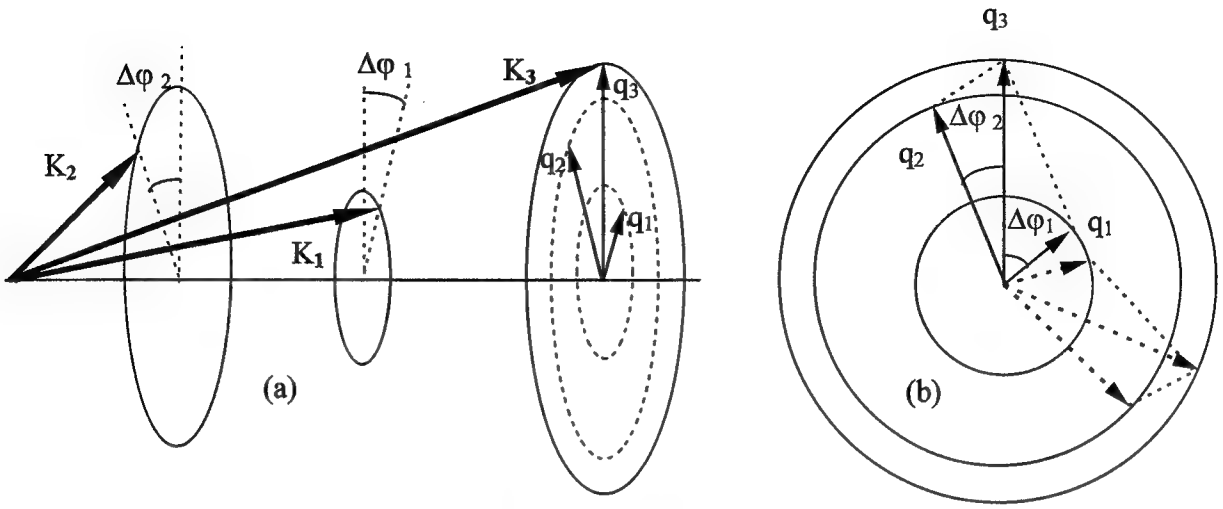

Fig.1. Cones of the wave vectors of Bessel light beams representing the pump (3), signal (1), and idler (2) waves (a); Azimuth-matched interaction geometry (b).

$$k_1\cos(\theta_1) = s\pi \ , \ J_0(q_{1m}R) = 0, \tag{4}$$

where R is the output mirror radius, m is the zero number of the Bessel function or the transverse mode index, s is the longitudinal mode index. Using the known relation for Bessel function zeros $\chi_m \approx (m-0.25)\pi$, where $\chi_m = q_{1m}R$, we obtain

$$q_{1m} = \frac{(m-0.25)\pi}{R}. \tag{5}$$

Then the wave number of the signal wave is

$$k_1(m,s) = \left(\frac{\chi_m^2}{R^2} + \frac{s^2\pi^2}{L^2}\right)^{\frac{1}{2}}. \tag{6}$$

Using further the Sellmeier equation for the refractive index $n_1(\lambda_1)$ in the KTP crystal [19] $n_1(\lambda_1) = A_1 + B_1/(1 - C_1/\lambda_1^2) - D_1\lambda_1^2$ from the relation $k_1(m,s) = 2\pi n_1(\lambda_1)/\lambda_1$ we obtain the biquadratic equation

$$\lambda_1^4\left[\left(\frac{k_1}{2\pi}\right)^2 + D_1\right] + \lambda_1^2\left[A_1 + B_1 + C_1 + \left(\frac{k_1}{2\pi}\right)^2 + D_1\right] + A_1C_1 = 0, \tag{7}$$

from which we calculate the length $\lambda_1(m,s)$ of the generated signal wave. The wave number of the idler wave is found by the known value of the wavelength $\lambda_2(m,s) = \lambda_1(m,s)\lambda_3/(\lambda_1(m,s) - \lambda_3)$ and the refractive index $n_2(\lambda_2) = A_2 + B_2/(1 - C_2/\lambda_2^2) - D_2\lambda_2^2$. Thus, the wave number $k_2(m,s)$ and the

length $\lambda_2(m,s)$ of the idler wave are unambiquously determined by specifying the mode indices m and s.

Then, from (5) and (6) we find the half-angle $\theta_1(m,s)$ at the cone vertex of wave vectors for the Bessel beam of the signal wave

$$\theta_1(m,s) = \sin^{-1}\left(1+\left(\frac{Rs\pi}{\chi_m L}\right)^2\right)^{-1/2}. \tag{8}$$

In turn, the half-angle $\theta_2(m,s)$ at the cone vertex of wave vectors for the Bessel beam of the idler wave can be calculated from the condition of longitudinal phase synchronism (1):

$$\theta_2(m,s) = \cos^{-1}\left(\frac{k_3\cos\theta_3 - s\pi/L}{k_2(m,s)}\right). \tag{9}$$

The azimuth angles φ_1 and φ_2 are determined then from the conditions of transverse phase synchronisms (2), (3):

$$\varphi_1(m,s) = \cos^{-1}\left(1-\frac{q_2^2\sin^2(\varphi_2)}{q_1^2}\right)^{1/2}, \varphi_2(m,s) = \cos^{-1}\left(\frac{q_3^2-q_1^2+q_2^2)}{2q_1q_3}\right)^{1/2}. \tag{10}$$

From the obtained expressions (8)-(10) it follows that the setting of mode indices m and s of the signal wave in the cavity defines unambiquously the cone angles θ_1, θ_2 of the generated waves and the azimuth angle $\varphi_1 + \varphi_2$ between the effectively interacting plane-wave components of Bessel beams of the signal and the idler wave. From thus it follows that in the specific case of a single-mode cavity each plane-wave component of the pump BLB will interact effectively with a particular pair of plane-wave components of the BLB of the signal and the idler waves. Such a mode of interaction was considered first in [16] and named azimuth-matched interaction.

Let us make a more detailed study of the dependence of angles θ_1, θ_2, φ_1 and φ_2 on mode indices m and s. In so doing, we presume that the conditions of longitudinal and transverse phase synchronism (1) - (3) are fulfilled. This question was investigated by numerical analysis of expressions (8) - (10) at the following parameters of the cavity: $L = 2.9\,cm$, $R = 2\,mm$ and of the pump BLB: $\lambda_1 = 1.064\ \mu m$, $\theta_3 = 0.2$ deg.

Fig.2. gives the quantity $\cos(\varphi_2)$ as a function of the longitudinal mode index s. It is seen that to the condition of spatial synchronism there satisfies a set of ~ 40 longitudinal modes.

Fig.3. gives the values of azimuth angles φ_1 and φ_2 corresponding to this range of the mode index s. As seen, the azimuth angle φ_1 varies within the range of ~ 80 deg while the range of angle φ_2 variation is ~ 25 deg. From Fig.3 it is also seen that at the boundaries of the interval of the existence of phase- synchronous interaction the azimuth angles φ_1 and φ_2 vanish. This indicates that here the azimuth - degenerate interaction is realized.

Fig. 4 gives the angles at the cone vertex of wave vectors of the signal θ_1 and the idler θ_2 wave versus the longitudinal mode index s. It is seen that the angle θ_1 is fixed and the angle θ_2 varies within the range of ~0.5 deg. The angle θ_1 is invariable due to the fact that unlike the idler wave, the signal wave is the transverse mode of the cavity.

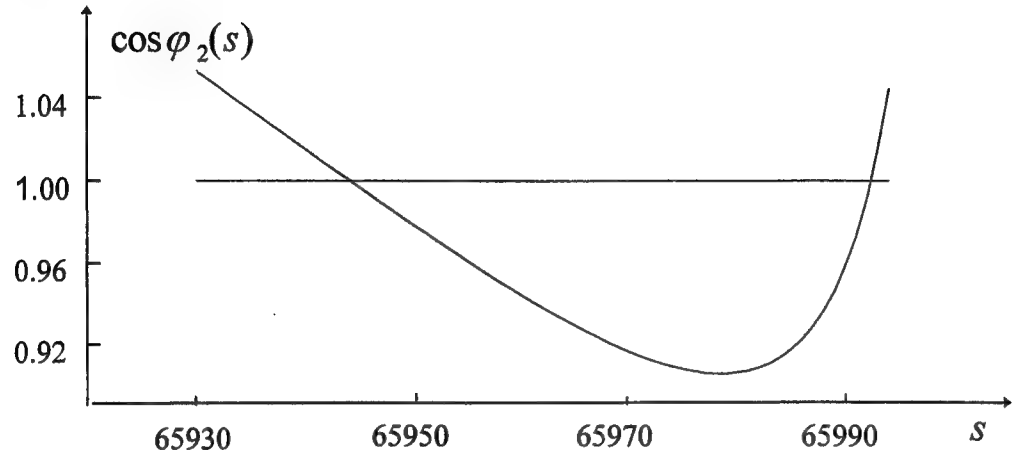

Fig.2. The range of the longitudinal mode index s for the case of the azimuth-matched interaction.

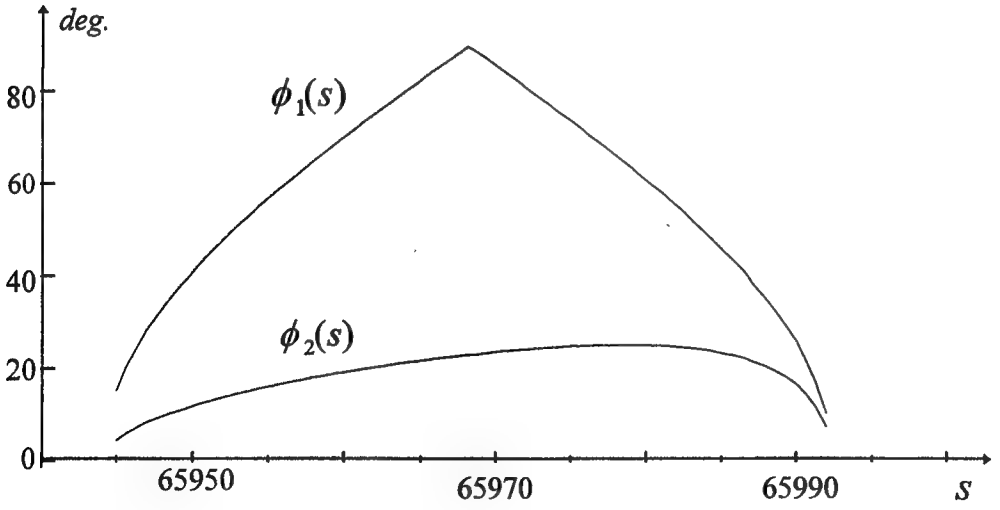

Fig.3. The values of azimuth angles of the signal ϕ_1 and idler ϕ_2 waves versus longitudinal mode index s.

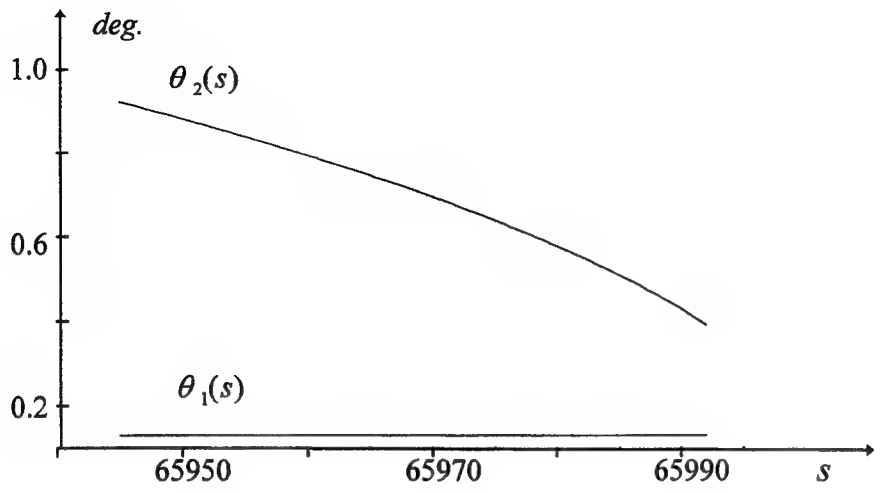

Fig.4. The angles at the cone vertex of wave vectors of the signal θ_1 and idler θ_2 waves versus longitudinal mode index s.

The results presented point to the existence of a difference between the parametric generation by BLBs and by Gaussian beams. As is known, even in the case of the fundamental Gaussian mode the conditions of spatial synchronism are satisfied by a unique solution [2]. This is due to the fact that in determining the conditions of synchronism for Gaussian beams, their real transverse spatial structure is ignored. Therefore the conditions of spatial synchronism for Gaussian beams and plane waves actually coincide. At the same time, such a simplified approach is not applicable to BLBs. Account of the transverse structure of a BLB appears as the possibility of the existence of various sinchronous vectorial interactions of plane - wave components of the beams. This leads to the fact in the general case that the conditions of spatial synchronism are satisfied in some range of mode indices m and s. Nevertheless, as numerical analisis has shown, by selecting the parameters of the cavity and the pump BLB we can considerably limit the range of m and s values down to a few modes.

3.THEORY OF AZIMUTH- MATCHED INTERACTIONS OF BESSEL LIGHT BEAMS

Let us formulate the general approach to the description of azimuth - matched interactions of BLBs. We consider, as we did above, the $o_3 \rightarrow o_1 e_2$ type of nonlinear conversion of Bessel beams propagating along the X_1-axis of the KTP crystal. Within the range of small angles θ at cone vertices of BLB wave vectors, the surface of the refractive indices in the first approximation will be spherical. As mentioned in [16], this is a necessary condition for propagation of circular BLBs in this direction. At propagation in the vicinity of the X_1-axis the BLB polarization is linear. Specifically, the pump and signal BLBs are polarized along the X_2-axis and the beam of the idler wave is polarized along the X_3-axis, where X_1,X_2,X_3 are crystallophysical axes which for the KTP crystal coincide with crystallographic axes. Then, when describing BLB propagation, it is convenient to introduce a system of coordinates

XYZ with axes $Z \parallel X_1$ and $Y \parallel X_2$. In the paraxial approximation considered here, the components E_y of the electric vector of the pump and the signal wave are of the form

$$E_y(R,t) = A_{3,1} J_m(q_{3,1}\rho)\exp[i(m_{3,1}\varphi + \phi_{3,1})], \tag{11}$$

where $\phi_{3,1} = k_{3,1}z - \omega_{3,1}t$, $R = (\rho,\varphi,z)$. The idler wave field is of the form

$$E_z(R,t) = A_2 J_m(q_2\rho)\exp[i(m_2\varphi + \phi_2)]. \tag{12}$$

To describe the interaction of BLBs, it is necessary to concretize the kind of nonlinear polarization. To this end, we separate in the amplitudes of interacting fields the multipliers depending on the transverse coordinate ρ which contain Bessel functions. Using then integral representation of Bessel functions, we introduce angular spectral components $\Psi^e_{1,2,3}(\rho,\varphi)$ of interacting waves. So for the signal wave field

$$E_y(\omega_1) = \frac{A_1(-i)^{m_1}\exp(i\varphi_1)}{2\pi} E_y(\omega_1,\rho), \quad E_y(\omega_1,\rho) = \int_0^{2\pi} \Psi^e_1(\rho,\varphi)d\varphi \ , \tag{13}$$

where

$$\Psi^e_1(\rho,\varphi) = \exp(i q_1 \rho\cos\varphi + i m_1 \varphi) \tag{14}$$

and, in a simular manner, for the pumping and the idler wave.

In accordance with the results presented in section 2 we assume that the angular spectral components $\Psi^p_{1,2,3}(\rho,\varphi)$ of nonlinear polarization are formed as the result of multiplying together the corresponding spectral components of the field, i.e.

$$\begin{aligned}
\Psi^p_1(\rho,\varphi) &= \Psi^e_3(\rho,\varphi)\Psi^e_2(\rho,\varphi+\Delta\varphi_2))^*, \\
\Psi^p_3(\rho,\varphi) &= \Psi^e_1(\rho,\varphi+\Delta\varphi_1)\Psi^e_2(\rho,\varphi+\Delta\varphi_2), \\
\Psi^p_2(\rho,\varphi) &= \Psi^e_3(\rho,\varphi)\Psi^e_1(\rho,\varphi+\Delta\varphi_1))^*.
\end{aligned} \tag{15}$$

Using the explicit form of the spectral components given by (14), we obtain, for example, for the first relation of (15)

$$\Psi^p_1(\rho,\varphi) = \exp[i\rho(q_3\cos\varphi - q_2\cos(\varphi+\Delta\varphi_2)) + i(m_3 - m_2)\varphi]. \tag{16}$$

The complete spatial function of nonlinear polarization is formed by integration with respect to the azimuth angle φ of the spectral components given by (13). Then, using (16), for the linear polarization at the signal frequency we obtain

$$P_y(\omega_1,\rho) = \int_0^{2\pi} \exp[i\rho(q_3\cos\varphi - q_2\cos(\varphi+\Delta\varphi_2)) + i(m_3 - m_2)\varphi]d\varphi. \tag{17}$$

Expression (17) has the Bessel function structure when the relation $q_3\cos\varphi - q_2\cos(\varphi+\Delta\varphi_2) = q_1\cos(\varphi+\Delta\varphi_1)$ holds. From this relation the conditions of transverse

synchronism (2), (3) follow. Then the nonlinear polarization at the signal wave will have the form of the Bessel function with the conicity parameter q_1

$$P_y(R,t) = C_1 J_{m_3-m_2}(q_1\rho)\exp[i(m_3-m_2)\varphi + i(k_{z3}-k_{z2})z - i\omega_1 t]. \quad (18)$$

This polarization will generate in the cavity a Bessel beam with the same conicity parameter q_1 and the overlap integral equal to unity.This follows from the known property of orthogonality of Bessel functions satisfying relation (4).

$$\int_0^R J_p(q_m\rho)J_p(q_n\rho)\rho\, d\rho = \frac{R^2}{2}(J_{p+1}(q_m R))^2\delta_{mn}, \quad (19)$$

where δ_{mn} is a Kronecker delta.

Thus, it has been found above that adequate description of parametric interaction of BLBs proceeding in the conditions of fixed mutual orientation of interacting plane- wave components of pump beam, the signal and idler waves should be carried out on the basis of introduction of angular spectral functions of fields and the formation of nonlinear polarization in accordance with expression (15). Note that the azimuth - matched regime of conversion is stable to the process of pump wave depletion, namely, depletion of the pump wave is not attended by distortion of the spatial structure of Bessel beams. This follows from the above demonstrated complete coincidence of the spatial structures of the nonlinear polarization wave and the light field generated by it. And the truncated equations of slowly varying amplitudes $A_{1,2,3}(z)$ are reduced to the form known for plane waves (see, for example, [1]). At the same time in the OPO on the basis of Gaussian beams the process of pump depletion leads to a distortion in its spatial profile and a decrease in the conversion efficiency.

Note also that the proposed theoretical description is valid for the specific case of phase-matched parametric generation. If the wave detuning $\Delta k_z = k_3\cos\theta_3 - k_1\cos\theta_1 - k_2\cos\theta_2$ is taken in account, the above theoretical approach holds good. The difference is in that azimuth- matched interactions will take place within some small range of azimuth angles which is determined by the maximum value of Δk_z.

The form of nonlinear polarization (17) differs significantly form the traditional expression

$$P^{NL} \sim J_m(q_1\rho)\, J_n(q_2\rho)\exp[i(k_{2z}+k_{1z})z]. \quad (20)$$

The writing of nonlinear polarization in the form of (20) actually means the taking into account of interactions of all the spectral components of the BLB. And the wave detuning turns out to be independent of a specific set of three interacting spectral components. At the same time, as follows from the results presented in section 2, such a description of nonlinear polarization is incorrect.

4. CONCLUSIONS

The investigations have shown that the parametric interaction of Bessel beams differs essentially from the parametric interaction of Gaussian beams. The principal difference is in the possibility of realizing the high- efficiency regime of nonlinear optical conversion of BLBs without

destructing the spatial structure. And the overlap integral of interacting beams can approach the highest possible value equal to unity. This regime of parametric conversion of BLBs is attained at azimuth - matched interaction of spatial spectral components of beams in an optical cavity whose transverse mode structure has the form of Bessel functions. The possibility of realizing the regime of azimuth - matched interaction has been demonstrated by an example of parametric generation in a KTP crystal. A general approach to the description of azimuth - matched interactions of BLB has been developed.

Thus, the optimum use of the specific space - frequency structure of Bessel beams offers possibilities of increasing the efficiency of parametric conversion of light.

5. REFERENCES

1. For example, see A.Yariv, " Quantum Electronics", (Wiley, New York,1989); Y.R. Shen "The principles of Nonlinear Optics", (Willey, New York,1984).
2. S.E. Harris, Proc IEEE, Vol.57, p.2096, 1969.
3. J. Durnin, JOSA, Vol.2A, p.110, 1985; 4A, p.651, 1987.
4. G.Scott, N. Mc Ardle, Opt.Engin., Vol.31, p.2640, 1992.
5. T. Wulle, S.Herminghaus, Phys.Rev.Lett., Vol.58 , p.1499, 1987.
6. B. Glushko, B.Kryzhanovsky, D.Sarkisyan, Phys.Rev.Lett., Vol.71, p.243, 1993.
7. S.P. Tewari, H. Huang, R.W. Boyd, Phys.Rev., Vol. A71, p.R2707, 1995.
8. I. Golub, Opt. Lett., Vol.20, p.1847, 1997.
9. S. Klewitz, P. Leiderer, S.Herminghaus, S. Sogomonian, Opt. Lett., Vol. 21, p.248, 1996.
10. K. Shinozaki, C-Q Xu., H. Sasaki, T Kamijoh, Opt. Commun., Vol.113, p.300, 1997.
11. M.K. Pandit, F.P. Payne, Opt. Quantum Electron, Vol.29, p.35, 1997.
12. A.P. Piskarskas, V. SmilgeviČius, A.P. Stabinis, Appl. Opt., Vol.36, p.7779, 1997.
13. A.P. Piskarskas, V. SmilgeviČius, A.P. Stabinis, Opt. Commun., Vol.143, p.72, 1997.
14. R. Gadonas, A. MarcinkeviČius A. Piskarskas, V. SmilgeviČius, A. Stabinis, Opt. Commun., Vol.146, p.253, 1997.
15. N.S. Kazak, N.A. Khilo, V.K. Pavlenko, Kovariant. Metody Opt. Akust., N.4, p.24, 1996.
16. V.N. Belyi, N.S. Kazak, N.A. Khilo, Quant. Electron., Vol.25, p.537, 1998.
17. L.Niggl, M.Maier, Opt. Lett., Vol.22, p.910, 1997.
18. L.R.Marshall, A.Kaz, JOSA, Vol.B10, p.1730, 1993.
19. J.D.Bierlein, H.Vanherzeele, JOSA, Vol.B6, p.622, 1989.

New method for simulation of nonlinear semiconductor microcavities

S.V.Fedorov[a] and M.A.Kalitieevsky[b],

[a]Vavilov State Optical Institute, 199034, St.Petersburg, Russia,
[b]Ioffe Physics and Technology Institute, 4021, St.Petersburg, Russia.

ABSTRACT

It has been designed and applied the method of transfer matrix for layered structures with second order nonlinearity, as new technique to simulate spectral characteristics of semiconductor microcavities. The nonlinearity of single layer is simulated by transfer matrix with 4x4 dimensions. Light intensity distributions and spectral dependencies for generator of second harmonic have been calculated. It has been shown that the most effective direction of second harmonic wave is not coincide with direction of incident wave. It is demonstrated the universality of suggested algorithm and capability to extend it for other types of cavities and nonlinearities.

Keywords: transfer matrix, cascade nonlinearity, vertical cavity, semiconductors

1. INTRODUCTION

For last decade there is growth interest in the semiconductor optical microcavities. It presents self layered semiconductor structure with central layer situated between two Bragg reflectors. These cavities[1] of extremely high finesse now can be grown thanks to the progress of semiconducting growth control. The main part of energy of resonant electromagnetic field is concentrated in thin, one-$\lambda/2$ central layer of microcavity. This peculiarity is condition on large perspective to use microcavities in creation of different electric microdevices, such as vertical cavity semiconductor lasers,[2] or light modulators. However the enhancement of the electric field inside the cavity due to the resonance effect could also be used for second-harmonic generation. The purpose of this article is to develop adequate, universal, mathematical, and numerical method to simulate nonlinear semiconductor microcavities, and arbitrary nonlinear layered structures at all. We demonstrated this method by simulation of second harmonic generator (SHG) on base of vertical microcavity with central layer obeyed the second order nonlinearity.

2. METHOD OF TRANSFER MATRIXES FOR NONLINEAR LAYERED STRUCTURES

Method of transfer matrix[3] is widely used method to modeling of optical properties of linear layered structures. For layered medium the problem of propagation of light throw it and calculation of optical and polariton modes results in production of matrixes for transmission throw single layers. For linear medium transfer matrixes have the 2x2 dimension. Particular form of matrix is defined by two parameters (the basis) describing

electromagnetic field. The most frequently it is used the basis of tangent components of electric and magnetic field (relatively the bound surface of layered medium), or amplitudes of two waves propagating in contrary directions. In case of mixing of few waves, as result of nonlinear interaction, the dimension of transfer matrix should be equal to double amount of mixing waves.

For description of transmission of perturbation throw nonlinear layer we use the basis of input-output beam: $E_{\pm}$:

$$\vec{E} = \begin{pmatrix} E_+ \\ E_- \end{pmatrix} \tag{1}$$

where $\vec{E}$ is complex vector for amplitude of two beams, in conditions of the beams are plane waves propagating with wave vector $\vec{k} = (k_x, k_y, k_z)$: $E_{\pm} = E_{\pm}(0)e^{\pm ik_z z}$.

The propagation of plane waves in arbitrary linear medium is described by transfer matrix $\hat{M}$: $\vec{E}(z) = \hat{M}(z)\vec{E}(0)$:

$$\hat{M}_{k_z z} = \begin{pmatrix} e^{ik_z z} & 0 \\ 0 & e^{-ik_z z} \end{pmatrix}; \tag{2}$$

$$k = k_0 n/n_0; \qquad k_z = k\cos\varphi = \frac{2\pi}{\lambda}\sqrt{n^2 - n_0^2 \sin^2\varphi_0}, \quad n_0 \sin\varphi_0 < n, \tag{3}$$

where φ_0 is the angle of beam tilt in outer medium with index n_0.

Let us consider layered structure and incident wave having frequency ω, amplitude $\tilde{E}_1$, and falling on structure. There are layers doubling the frequency of light in composition of structure.

Amplitude coefficients of reflection r_1, r_2, and transmission t_1, t_2 of light on frequencies ω, and 2ω consequently, can be found as the solution of linear equations set:

$$\begin{pmatrix} t_1\tilde{E}_1 \\ 0 \\ t_2\tilde{E}_1 \\ 0 \end{pmatrix} = \hat{T} \begin{pmatrix} \tilde{E}_1 \\ r_1\tilde{E}_1 \\ 0 \\ r_2\tilde{E}_1 \end{pmatrix} \tag{4}$$

Here matrix of transition throw total structure $\hat{T} = \hat{L}\hat{N}$ is the production of matrixes of transition throw single linear layers $\hat{L}_j$, throw bounds between layers $\hat{B}_j$: $\hat{L} = \prod_j \hat{L}_l \hat{B}_j$, and throw nonlinear layers: $\hat{N} = \prod_j \hat{N}_j \hat{B}_j$, following behind of linear layers.

Transfer matrix throw single nonlinear layer with cascade nonlinearity is defined by the solution of differential equation set:

$$\begin{cases} \alpha_1 \dfrac{dE_{\pm 1}}{dz} = \pm i\alpha_1 k_1 E_{\pm 1} - i\eta\dfrac{\omega}{c} E_{\pm 1}^* E_{\pm 2}, \\ \alpha_2 \dfrac{dE_{\pm 2}}{dz} = \pm i\alpha_2 k_2 E_{\pm 2} - i\eta\dfrac{\omega}{c} E_{\pm 1}^2. \end{cases} \tag{5}$$

where $E_{\pm 1,2}$ are the amplitudes of two waves $E_{1,2}$: $\vec{\mathcal{E}}_{1,2} = \vec{e}\ \mathrm{Re}\left\{E_{1,2}e^{-i\omega_{1,2}t}\right\}$. Here $\vec{\mathcal{E}}_{1,2}$ is the strength of electrical field for two beams separately, $\vec{e}$ is the ort for linear polarization of field, which is parallel to bounds, $\omega_2 = 2\omega_1$, $\omega \equiv \omega_1$. We have also $\alpha_1 = k_1/(\omega/c)$, $\alpha_2 = \frac{1}{2}k_2/(\omega/c)$ (for ordinary waves only), $k_{1,2} = \frac{\omega_{1,2}}{c}\sqrt{n^2(\omega_{1,2}) - n_0^2(\omega_{1,2})\sin^2\varphi_{1,2}}$ is z component for wave vectors $\vec{k}_{1,2}$ in nonlinear medium with linear index $n(\omega)$, and $\varphi_{1,2}$ are tilts for two harmonic in outer medium with index $n_0(\omega)$. $q = k_2 - 2k_1$ is detuning of synchronism which defines phase mismatch, and which is zero only for nondisperse media: $n(\omega_2) \neq n(\omega_1)$. At

last $\eta(\omega) = \frac{1}{2}\varepsilon_{i,kl}(\omega,\omega)e_i e_k e_l$ is the small nonlinear parameter which is proportional the sum of components for tensor of nonlinear second order susceptibility $\varepsilon_{i,kl}$.

If nonlinearity is small, so amplitudes is small changing for one trip of layer, then the solution of (5) can be written:

$$\begin{cases} E_{\pm 1} = e^{\pm ik_1 z}\Big(E_{\pm 10} - i\eta_{\pm 1}(z)E^*_{\pm 10}E_{\pm 20}\Big), \\ E_{\pm 2} = e^{\pm ik_2 z}\Big(E_{\pm 20} - i\eta^*_{\pm 2}(z)E_{\pm 10}E_{\pm 10}\Big), \end{cases}$$

$$\eta_{\pm 1,2}(z) = -\frac{\eta(\omega/c)}{\alpha_{1,2}}\left(e^{\pm iqz} - 1\right)/\pm iq, \quad \eta^*_{\pm} = \eta_{\mp}.$$

where $E_{\pm 10,20}$ are amplitudes of field at the left side of nonlinear layer. So transfer matrix for single nonlinear layer with thickness d_j is not diagonal :

$$\hat{N}_j = \begin{pmatrix} C_{+1}e^{ik_1 d_j} & 0 & -i\eta_{+1j}E^*_{+10}e^{ik_1 d_j} & 0 \\ 0 & C_{-1}e^{-ik_1 d_j} & 0 & -i\eta_{-1j}E^*_{-10}e^{-ik_1 d_j} \\ -i\eta_{+2j}E_{+10}e^{ik_2 d_j} & 0 & C_{+2}e^{ik_2 d_j} & 0 \\ 0 & -i\eta_{-2j}E_{-10}e^{-ik_2 d_j} & 0 & C_{-2}e^{-ik_2 d_j} \end{pmatrix} \tag{6}$$

where $\eta_{\pm 1j,2j} \underset{\text{def}}{=} \eta_{\pm 1,2}(d_j)$, and $C_{\pm 1,2} = 1$ for $|\eta z E_{\pm 10}| << 1$. In common case, when nonlinearity is large, values $C_{\pm 1,2}(z, E_{\pm 10}, E_{\pm 20})$ can be defined from explicit solution of (5). Nevertheless, the structure of matrix (6) will not be changed.

For definition of transfer matrix for each layer (6), and total matrix $\hat{T} = \hat{L}\hat{N}$ also, we should express values of amplitudes $E_{\pm 10}$, and $E_{\pm 20}$ falling on nonlinear layer throw incident amplitude $\tilde{E}_1$ falling on total structure. However, it is possible if we know amplitudes of reflected waves $r_{1,2}\tilde{E}_1$, because there is:

$$\begin{pmatrix} E_{+10} \\ E_{-10} \\ E_{+20} \\ E_{-20} \end{pmatrix} = \hat{L}\begin{pmatrix} \tilde{E}_1 \\ r_1\tilde{E}_1 \\ 0 \\ r_2\tilde{E}_1 \end{pmatrix}. \tag{7}$$

The same time, coefficients of reflection $r_{1,2}$ is defined from solution of (4), where it is need to know the matrix $\hat{T}$ of total structure.

To solve this collision we use theory of perturbations on small parameter η. In zero approach we have linear theory, and transfer matrix for single layer degenerates to a diagonal matrix. So matrix for total structure $\hat{T}^{(0)}$, and coefficients of reflection $r^{(0)}_{1,2}$ and transmission $t^{(0)}_{1,2}$ are not dependent on values of amplitudes $E_{\pm 10}$, and $E_{\pm 20}$.

After definition of matrix for total structure $\hat{T}^{(n)}$ in n-order of the approach, we define $r^{(n)}_{1,2}, t^{(n)}_{1,2}$ from (4). Further, we can define amplitudes of incident beams falling on single layers, consequently along structure, in $n+1$-order of the approach:

$$\begin{pmatrix} E^{(n+1)}_{+10} \\ E^{(n+1)}_{-10} \\ E^{(n+1)}_{+20} \\ E^{(n+1)}_{-20} \end{pmatrix} = \hat{L}\begin{pmatrix} \tilde{E}_1 \\ r^{(n)}_1\tilde{E}_1 \\ 0 \\ r^{(n)}_2\tilde{E}_1 \end{pmatrix}, \tag{8}$$

$$\begin{cases} E^{(n+1)}_{\pm 1,2}(d_1) = \hat{N}^{(n+1)}_1 E^{(n+1)}_{\pm 10,20}, \\ E^{(n+1)}_{\pm 1,2}(d_j) = \hat{N}^{(n+1)}_{j-1} E^{(n+1)}_{\pm 1,2}(d_{j-1}), \end{cases} \quad \begin{cases} \hat{N}^{(n+1)}_1 = \hat{N}^{(n+1)}_1(d_1, E^{(n+1)}_{\pm 10,20}), & j = 1 \\ \hat{N}^{(n+1)}_j = \hat{N}^{(n+1)}_j(d_j, E^{(n+1)}_{\pm 1,2}(d_{j-1})), & j > 1. \end{cases} \tag{9}$$

As the last step we should substitute (8) in (6) to define single matrixes $\hat{N}_j^{(n+1)}$ and total matrix $\hat{T}^{(n+1)}$ in $n+1$-order of the approach. Convergence of this iterative process in $n \to \infty$ is provided under the condition $\eta z \sum_j d_j |\tilde{E}_1| < 1$. As result we solve the equation set of type (4) relatively unknown amplitudes of field into nonlinear layers.

In conclusion it is need to note the universal character of suggested algorithm, which can be lightly extended on other type of nonlinearity and arbitrary schemes of cavities.

3. VERTICAL CAVITY WITH SECOND ORDER NONLINEARITY

To demonstrate the capability of suggested technique, in comparision of[4], we consider vertical cavity combined of two linear Bragg reflectors and one nonlinear layer between them. Each from two symmetrical reflectors consist of m double semiconductor layers with linear index of reflection $n_a = 3$, and $n_b = 4$. Thus reflectors can be grown for example as GaAs/AlAs heterostructures, and can reflect intensity of light with $R = 0.9 - 0.999$ efficiency depending on number of layers $m = 8 - 16$.

For the central layer of microcavity we use real optical parameters of GaAs crystal. Refraction index on fundamental frequency ($\lambda = 1.0582\ mkm$) is $n(\omega) = 3.479$, and on double frequency $n(2\omega) = 4.352$. Second order nonlinearity is defined by value of electromagnetic susceptibility $2\varepsilon_{x,yz}(\omega)/n^2(\omega) = 1.4 \times 10^{-12}\ m/V$. The thickness of central layer is $\lambda/2$, that is there is vertical microcavity. Working interval of incident fields for semiconductor microcavities is $I = |\tilde{E}_1|^2 = 10^7\ W/cm^2$. So the parameter of nonlinearity changes in diapason $\eta\lambda|E_{10}| \sim 10^{-4} - 10^{-2}$ for different values of field into microcavitiy. Second harmonic wave runs out of cavity with intensity $10^2 - 10^5\ W/cm^2$, that is enough for registration.

Fig.1 demonstrates common spectral dependencies of amplitude value of reflection and transmission in empty microcavity described here. Central peak in curve of transmission of fundamental wave is resonance part of TE00 mode. It is clear that we consider disperse layer because of 2ω peak is not in explicit resonance.

Fig.2 shows the resonance part of spectrum for fundamental wave and the part of second harmonic spectrum corresponding of fundamental spectrum in condition that second harmonic wave is tilted so as detuning of phase synchronism is zero: $q(\varphi_2) = k_2(\varphi_2) - 2k_1 = 0$ (where $k_2(\varphi_2) = \frac{2\pi}{2\lambda}\sqrt{n^2(2\omega) - n_0^2(\omega)\sin^2\varphi_2}$). Thus condition is the most natural condition for direction of SGH, although there should be interval of angles for generation of second harmonic. Note, that if cavity is in resonance on fundamental harmonic it can not be commonly in resonance on second harmonic for the most favorable direction of generation. *tilt2* is tilt of second harmonic.

Fig.3 presents as spectra of fundamental and intensity of harmonic wave depends on number of double layers m in Bragg reflectors. Consequent values of cavity finesse and reflection on intensity are $f_\omega = 4.12$, 11.8, 36.3, 358.2, $R = 0.870$, 0.957, 0.986, 0.9986 $m = 8$ (1), 10 (2), 12 (3), 16 (4). Tilt of second harmonic wave changes on spectrum on interval $\varphi_2 = 0.644 - 0.646$.

Fig.4 presents as spectra of fundamental and intensity of harmonic wave depends on intensity of incident wave. Consequent values of incident intensity are $I = 10^7$, 2×10^7, $3 \times 10^7\ W/cm^2$.

Fig.5 shows dependencies of reflected and transmitted intensities on intensity of incident wave for different

values of cavity finesse. This dependencies are putting in case of saturation of second order nonlinearity: $\eta\frac{\lambda}{2}|E_{10}| = 0.13$. Cavity parameters are $m = 3$, $n_b = 2.0$, $n_a = 2.0$ (1), 3.6 (2),4.0 3), 4.26 (4), 4.47 (5). Cavity finesse $f_\omega = 1.002$ (10), 3.29(2),5.73(3), 8.17 (4), 10.62 (5).

4. CONCLUSION

We have expand linear method of transfer matrixes on the case of arbitrary layered structure with second order nonlinearity. It is destined at the first order for simulation of microcavities where paraxial approach is not valid and can be used for simulation of multimode regime of generation in wide-aperture lasers (see, [5]). Method has been demonstrated on example of SHG on base of vertical semiconductor microcavity. In particular, it has been shown that the most effective direction of second harmonic wave is not coincide with direction of incident wave.

5. ACKNOWLEDGEMENTS

This work was supported by Russian Foundation for Basic Research, project 97-02-18341.

6. REFERENCES

[1] L.Jewell, V.H.Lee, S.I.McCall, J.P.Harbigon, and T.Floretz, Appl. Phys. Lett. **53**, p.640, 1988.

[2] L.Jewell, V.H.Lee, A.Sherer, J.P.Harbigon, and T.Floretz, IEEE J.Quantum Electron. **QE-15**, p.1332, 1991.

[3] M.A.Kalitieevskiy, A.V.Kavokin, Solid State Physics. **37**, p.2721, 1995.

[4] E.Rosencher, B.Vinter, and V.Berger. "Second-harmonic generation in nonbirefrigent semoiconductor optical microcavities", Appl. Phys. **78**, pp.6042-6045. 1995.

[5] S.V.Fedorov, N.N.Rosanov, Opt. Spectrosk. **72**, p. 1394, 1992.

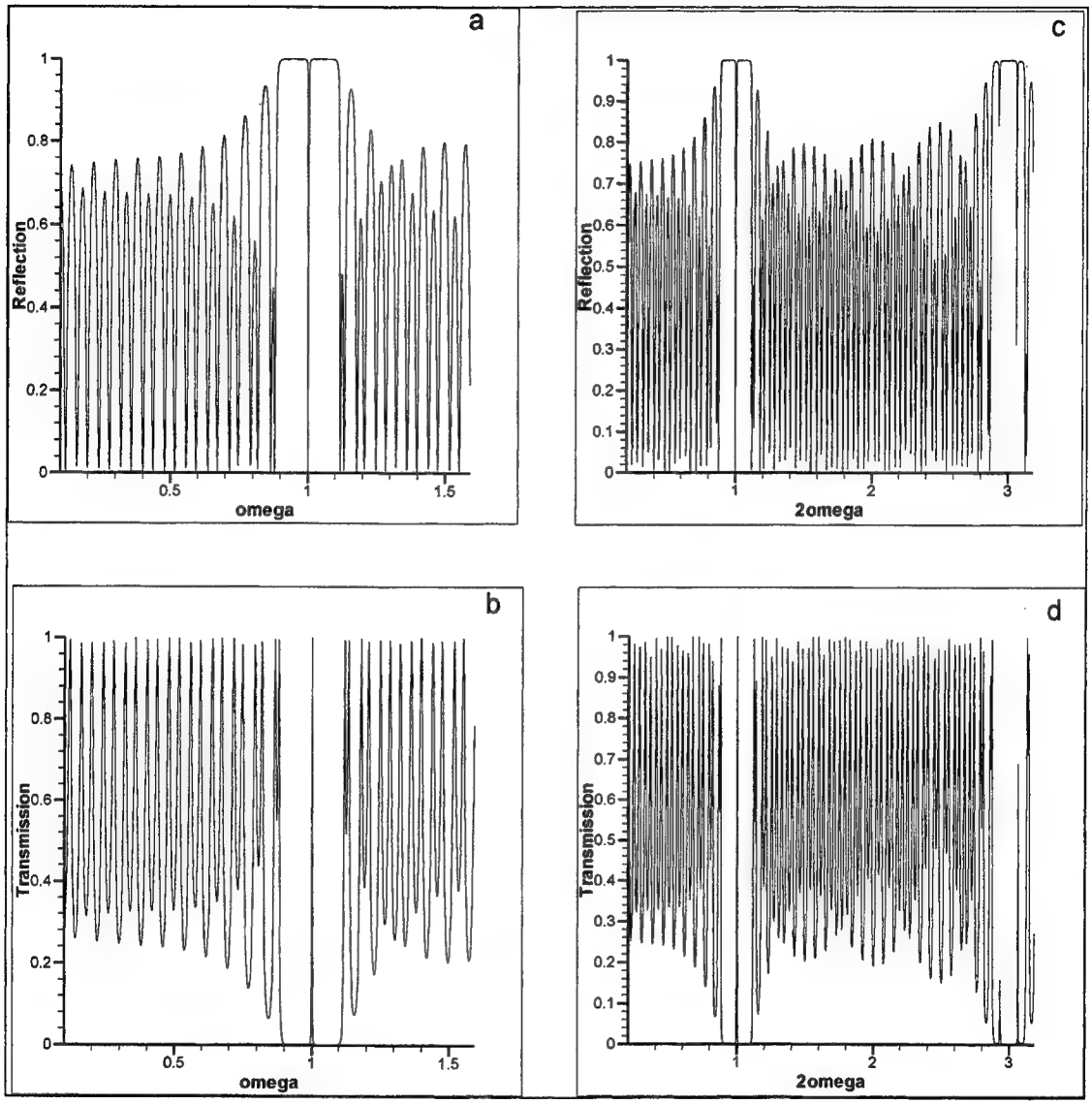
a
Reflection
omega
c
Reflection
2omega
b
Transmission
omega
d
Transmission
2omega

Figure 1:

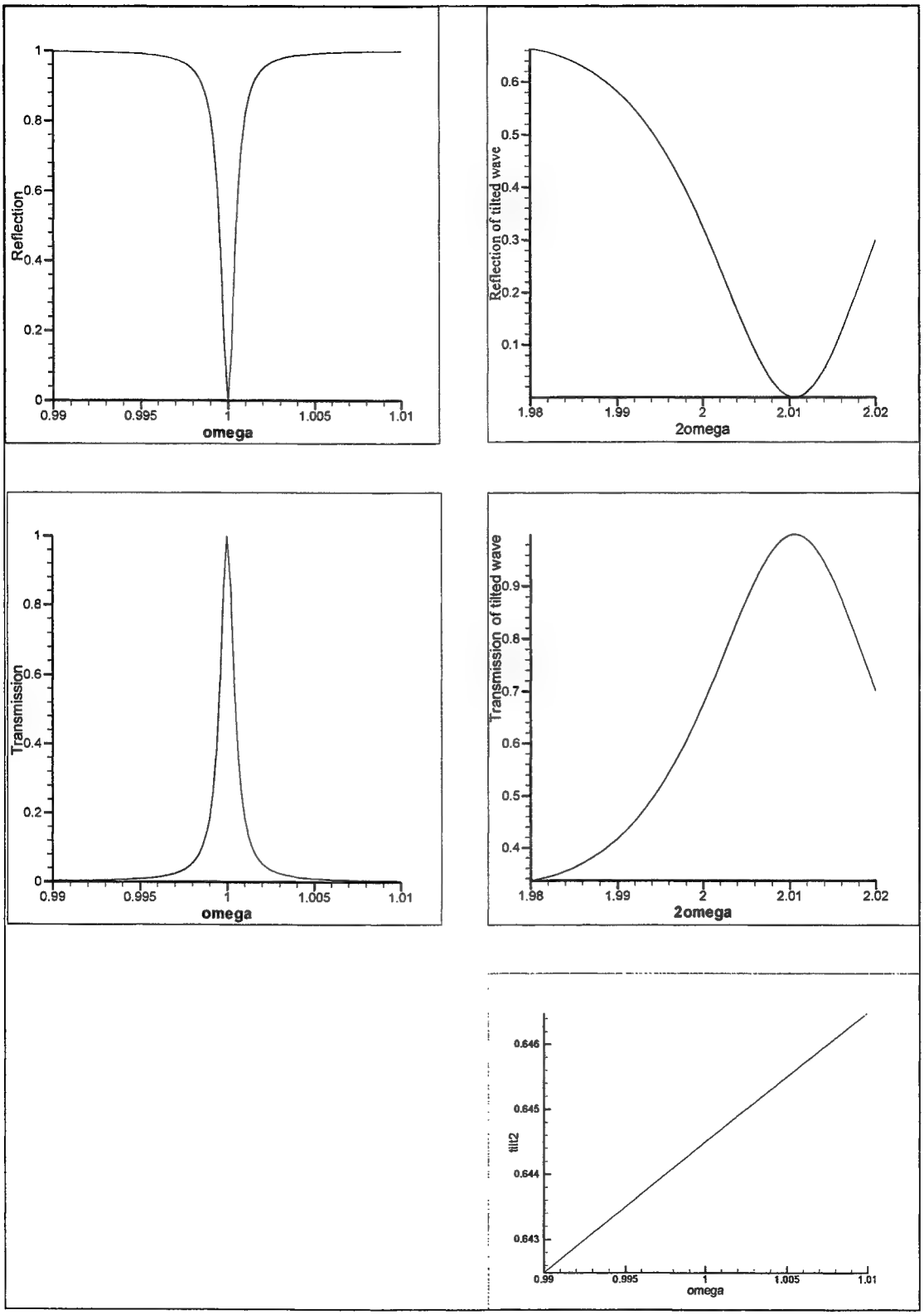
Reflection
omega
Reflection of tilted wave
2omega
Transmission
omega
Transmission of tilted wave
2omega
tilt2
omega

Figure 2:

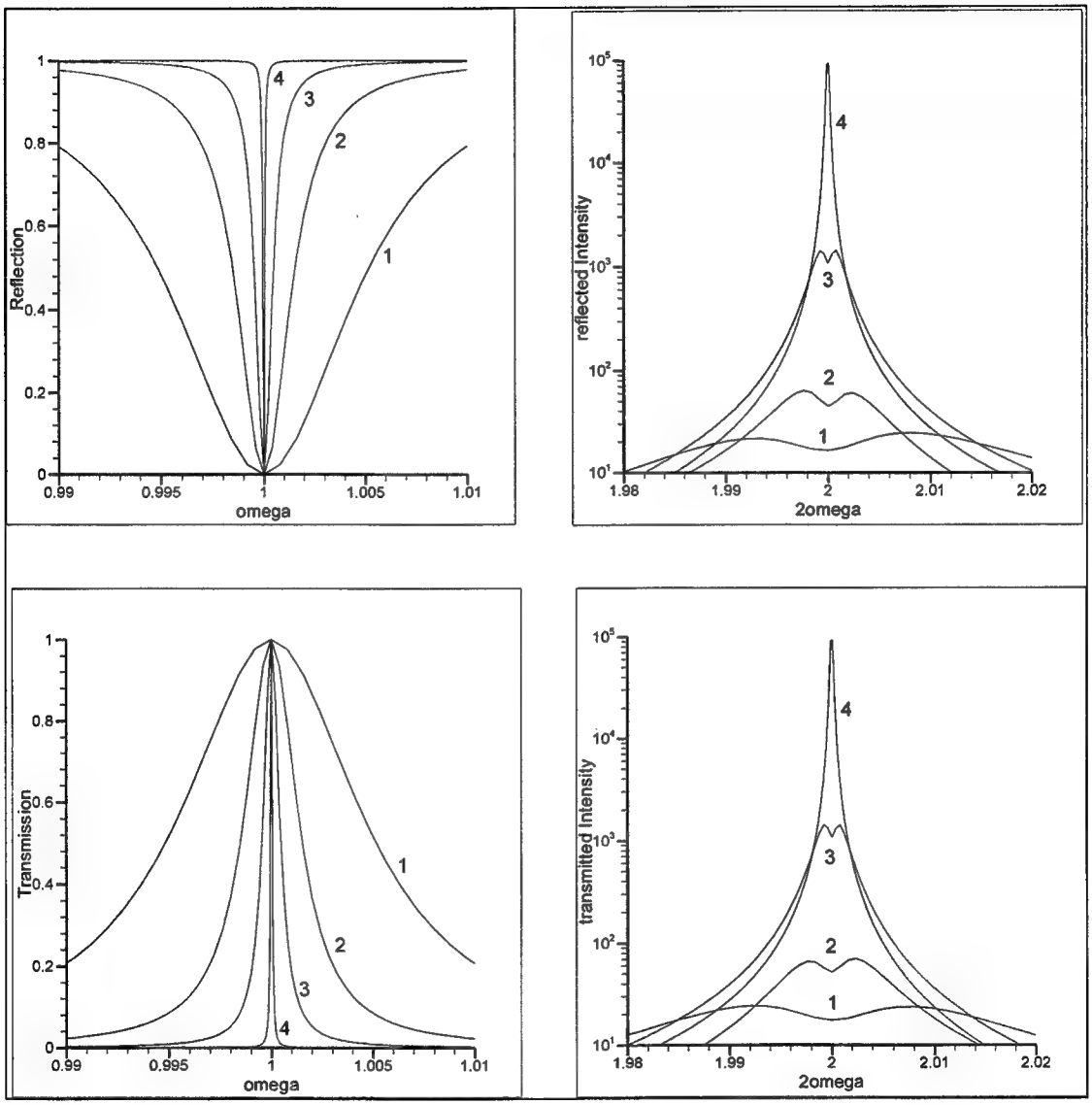
Reflection
omega
reflected Intensity
2omega
Transmission
omega
transmitted Intensity
2omega

Figure 3:

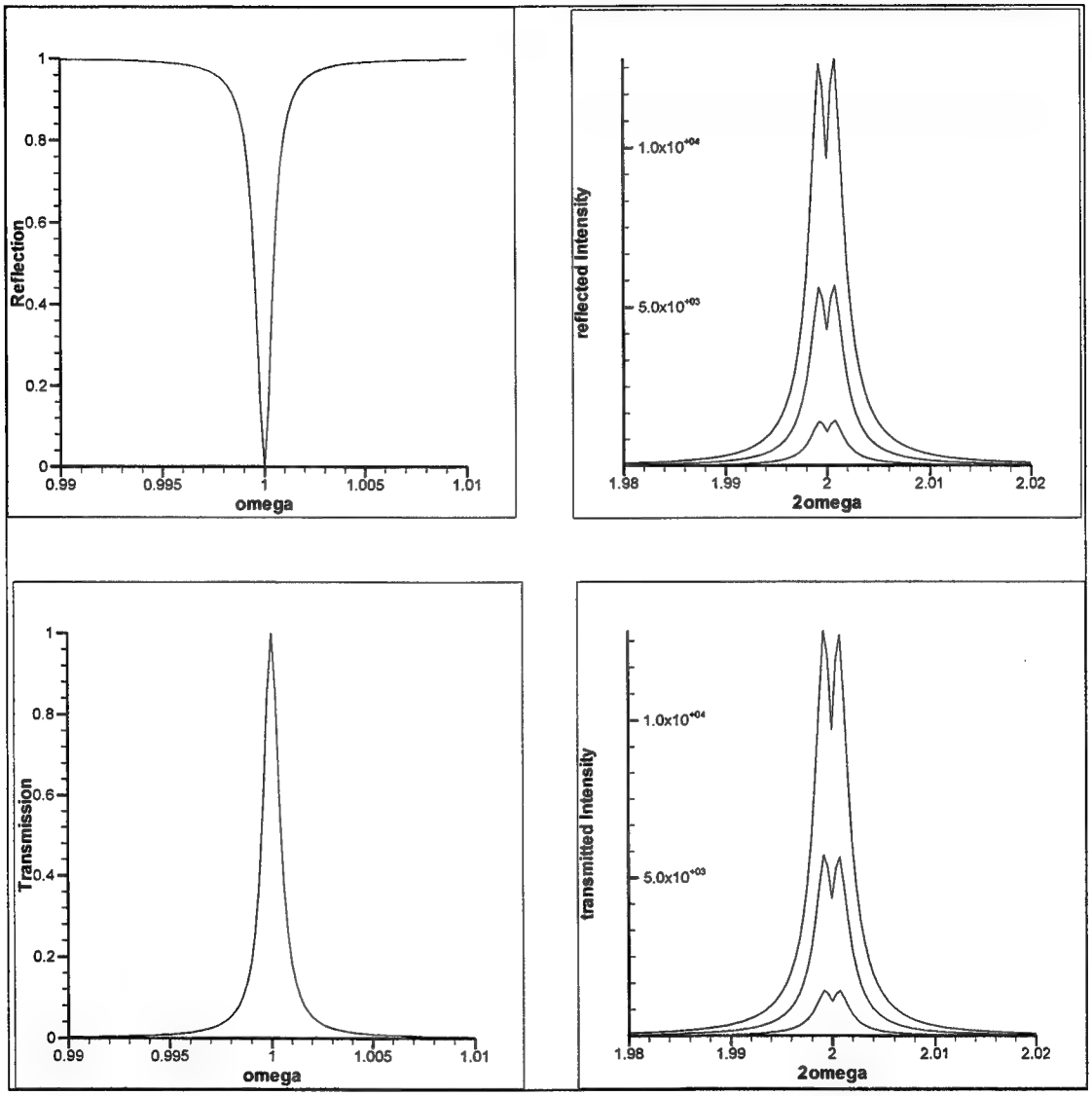
Reflection
omega
reflected Intensity
2omega
Transmission
omega
transmitted Intensity
2omega

Figure 4:

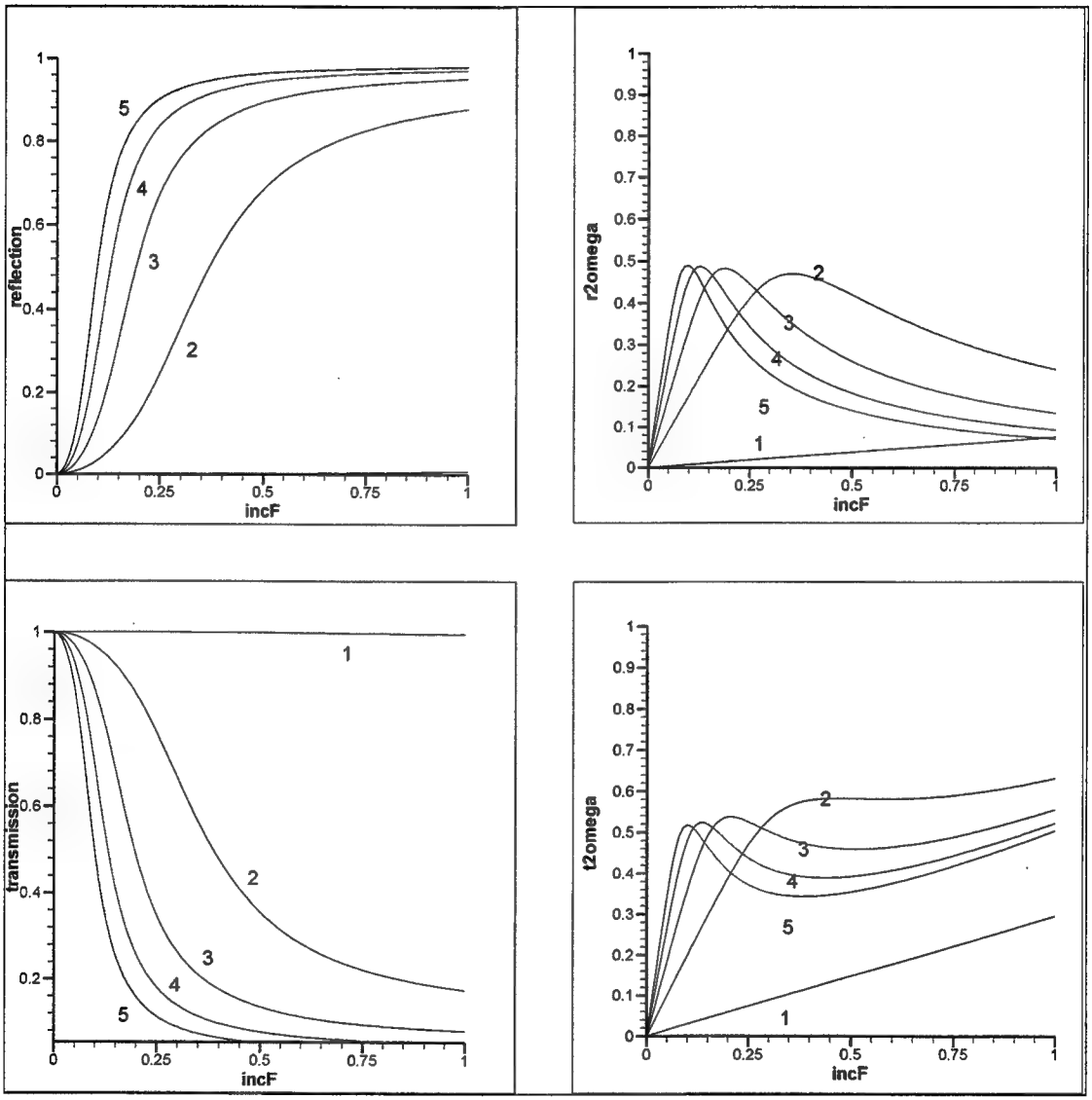
reflection
incF
r2omega
incF
transmission
incF
t2omega
incF

Figure 5:

SESSION 4

Quantum Optics

Generation of sub-Poissonian light via the correlated absorption of photons by the dressed atom

Michael Z. Smirnov

Laser Center
of the St.-Petersburg State Institute for Fine Mechanics & Optics
14 Sablinskaya str., St.-Petersburg, 197101, Russia.

ABSTRACT

Here we study the open modification of the Jaynes-Cummings model that is the coupled system of the dressed atom and the quantized mode. The mode is initially in the coherent quantum state exhibiting the Poissonian photon statistics. When the quasienergy levels of the dressed atom cross the mean number of photons $\langle n \rangle$ in the mode undergoes high-amplitude oscillations. Numeric results show that each time the value of $\langle n \rangle$ falls the photon statistics becomes more regular. Instantaneously, the statistics can become sub-Poissonian with the Fano factor $F \equiv \Delta n^2 / \langle n \rangle$ being many times as small as unity. The above observation provides the evidence that the photons undergo correlated absorption, i.e., they tend to disappear in twos, in threes, etc.

Keywords: Jaynes-Cummings model, dressed atom, quasienergy levels, squeezed states of light

1. INTRODUCTION

The experiments with both the one-atom maser[1,2] and the ion-trap laser[3] have revived the interest of researchers to the Jaynes-Cummings model (JCM) that is the coupled system of the two-level atom and the quantized mode of the electromagnetic field. Being a simple quantum system which allows a thorough theoretical study the JCM exhibits some phenomena playing an important role in both the nonlinear optics and the laser physics, particularly, nonlinear oscillations of the atomic and field variables and generation of the squeezed light[4-8]. Here, we focus our attention on the latter effect considering the sub-Poissonian photon statistics as the manifestation of squeezing[9].

Assuming the quantized mode to start its time evolution from the coherent quantum state the conventional JCM can show only a moderate degree of the transient squeezing[7,8]. To make clear the nature of the above limitation let us plot the mean variation, $\langle n \rangle - n_0$, and the scaled dispersion, $F \equiv \Delta n^2 / \langle n \rangle$, of the photon number in the quantized mode against dimensionless time $\xi = \kappa t$ (Fig. 1). Here, the initial state of the quantized mode is the coherent state $|\nu\rangle$, $n_0 = |\nu|^2 = 6.25$ is the mean number of photons at the time origin, and κ is the coupling constant. Both ν and κ are assumed to be real. Parameter F called the Fano factor quantifies the deviation of the photon statistics from Poissonian and it becomes less then unity for the sub-Poissonian light. In calculation of the above variables we used the theory of the coherent state JCM described elsewhere (see Refs. 4-6, 11).

It is seen from Figure 1 that both the mean variation and the dispersion of the photon number undergo recurring collapses and revivals characteristic for the coherent state JCM (see Refs. 4-6). Instantaneously, the light shows a small degree of squeezing with $F > 0.75$.

SPIE Vol. 3685 • 0277-786X/99/$10.00

In the short-time domain starting at the time origin both $\langle n \rangle$ and F exhibit in-phase oscillations and the deepest minimum of F almost coincides with the deepest minimum of $\langle n \rangle$. The fact that the fall of the mean photon number entails the regularization of the photon statistics can be interpreted in terms of the correlated absorption of photons. Actually, if the photons undergo correlated absorption, i.e. they tend to disappear in twos, in threes, etc., then the photon noise becomes «smoothed out» and the statistics of the remaining photons can become sub-Poissonian[9,10].

The revival domains exhibit the opposite type of correlation as compared to the short-time one, i.e., the mean number of photons and the Fano factor undergo antiphase oscillations.

Clearly, when discussing the photon statistics we apply to the ensemble of the independent quantum systems. The positive or negative correlation between the absorption events in the different systems of the ensemble can occur since as we set one and the same initial conditions for all the systems.

It follows from the above considerations that the degree of the short-time squeezing in the conventional JCM is limited mainly due to the saturation of absorption. The saturation effect can be removed by introducing the open modification of the JCM that incorporates the dressed atom and the quantized mode[12]. Here, the dressed atom is considered to be the coupled system of an atom and the periodically modulated classical field and is characterized by the quasienergy states and the corresponding quasienergy levels[13-16]. If the quantized mode is tuned to resonance with the transition between a pair of the quasienergy levels corresponding to one and the same quasienergy state then the saturation effect does not occur[12]. Therefore, the dressed atom can absorb several photons one after another transferring their energy to the classical field that causes the strong time correlation between the absorption events. We shall demonstrate below that in the latter case the degree of squeezing significantly enhances as compared to the conventional JCM.

In the present paper we consider the particular case when the enhanced degree of the transient squeezing can be obtained by means of the above mechanism. The classical field is suggested to be amplitude-modulated (threechromatic) with its central component tuned to resonance with the atomic transition. The amplitude of the central component is set to be the multiple of the modulation frequency that causes the adjacent quasienergy levels to cross[12, 16, 17-19]. The reason for the above settings is that in the previous paper[12] we have found no enhanced squeezing in case when the frequency separation between the adjacent quasienergy levels is many times as large as the Rabi frequency. Furthermore, we do not concern here the problem of evaluating the maximum degree of squeezing obtainable in the open JCM.

The organization of this paper is as follows: Sec. 2 outlines briefly the theory of the open JCM with the emphasis on the particular case when the quasienergy levels cross. A more detailed presentation of this theory in general case is given in Ref. 12. In Sec. 3 we present numerical results. Finally, Sec. 4 gives a brief summary and the conclusive remarks.

2. THEORY

Consider the dressed atom that is the coupled system of a two-level atom with the upper and lower states denoted by $|0\rangle_a$ and $|1\rangle_a$, respectively, and the amplitude-modulated classical field: $E(t) = \tilde{E} \cdot g(\omega' t) \cdot \exp(i\Omega t) + c.c.$ Here, $\tilde{E}$, Ω, and ω' are the complex-valued amplitude, the optical carrier, and the modulation frequency of the field, respectively. The function of modulation is taken in the following form: $g(\tau) = \exp(i\tau) \cdot [1 + 2a\cos(\tau)]$, where $\tau = \omega' t$ is the dimensionless time, and a is the modulation depth. Therefore, the driving fields spectrum incorporates the central component at frequency $\Omega_0 = \Omega + \omega'$, and the sidebands at frequencies $\Omega_0 \pm 2\omega'$. It is suggested that the central

component is tuned to pure resonance with the atomic transition, $\Omega_0=\omega$, with ω being the transition frequency. The interaction between the atom and the field is described in the dipole and Rotating Wave approximations.

Inasmuch as the classical field is suggested to be of a fixed amplitude the dressed atom is an open quantum system and its energy does not conserve. However, one can introduce the following orthonormalized solutions for the Schrodinger equation[15,16]:

$$\begin{aligned} |\theta_0\rangle_a &= \exp(i\lambda\tau)\cdot\left[\varphi_1(\tau)|0\rangle_a + \exp(-i\Omega t)\varphi_2(\tau)|1\rangle_a\right], \\ |\theta_1\rangle_a &= \exp(i(\delta-\lambda)\tau)\cdot\left[\varphi_2^*(\tau)|0\rangle_a - \exp(-i\Omega t)\varphi_1^*(\tau)|1\rangle_a\right], \end{aligned} \tag{1}$$

which plays somewhat similar role from the point of view of linear spectroscopy as the energy states of the isolated atom and are referred to as the quasienergy states. Here, $\delta=(\Omega-\omega)/\omega'=-1$ is the scaled detuning of the optical carrier from the atomic transition, $\varphi_1(\tau)$ and $\varphi_2(\tau)$ are the coordinate functions given by [16]:

$$\varphi_1(\tau)=\frac{1}{\sqrt{2}}\cdot\exp(i\,a\,\sigma\sin(2\tau)); \quad \varphi_2(\tau)=\varphi_1(\tau)\cdot\exp(-i\tau), \tag{2}$$

with $\sigma\equiv|\mu_{01}\tilde{E}/(\hbar\omega')|$ being the central component Rabi frequency normalized by the frequency of modulation. The eigenvalue $\lambda=\sigma$ determines the positions of the quasienergy levels. Specifically, the lower energy level of the isolated atom splits into two equidistant lattices of quasienergy levels at energies $\hbar\omega'(-\lambda+2n)$ and $\hbar\omega'(\lambda-\delta+2m+1)$ while the upper one splits into the another two lattices at energies $\hbar\omega+\hbar\omega'(\delta-\lambda-(2m+1))$, and $\hbar\omega+\hbar\omega'(\lambda-2n)$. Here, the quasienergy levels labeled by index $n=0,1,2,\ldots$ $(m=0,1,2,\ldots)$ correspond to the quasienergy state $|\theta_0\rangle_a$ ($|\theta_1\rangle_a$). Furthermore, we introduce the transition operator between the quasienergy states $\hat{c}\equiv|\theta_0\rangle_{a\,a}\langle\theta_1|$ and apply Eq. (1) to find relation between $\hat{c}$ and the conventional transition operator $\hat{b}\equiv|0\rangle_{a\,a}\langle1|$:

$$\hat{c}=\exp\left[i(2\lambda-\delta)\cdot\tau\right]\cdot\left[\varphi_1\cdot\varphi_2\cdot\left(\hat{I}-2\hat{b}^+\hat{b}\right)-\exp(i\Omega t')\cdot\varphi_1^{\,2}\,\hat{b}+\exp(-i\Omega t')\cdot\varphi_2^{\,2}\,\hat{b}^+\right], \tag{3}$$

where $\Omega t'\equiv\Omega t+\psi$, $\psi\equiv\arg\left[\mu_{01}\tilde{E}/(\hbar\omega')\right]$, and $\hat{I}$ is the identity operator.

Now, let us turn to the open modification of the JCM by introducing the quantized mode of the electromagnetic field with the creation and annihilation operators denoted by $\hat{a}^+$ and $\hat{a}$, respectively. The Hamiltonian of the whole system incorporating the dressed atom and the quantized mode can be written down as follows:

$$\hat{H}_{JCM}=\hat{H}_a+\hbar\omega_q\hat{a}^+\hat{a}+\hat{V}_{aq}, \tag{4}$$

where $\hat{H}_a$ is the Hamiltonian of the dressed atom including the interaction with the classical field, the second term is the Hamiltonian of the quantized field with ω_q being the eigenfrequency of the quantized mode, and the last term describes the interaction of the atom and the quantized mode. Applying the dipole and Rotating Wave approximations the latter term reads:

$$\hat{V}_{aq} = i\hbar\omega'\kappa\hat{b}\hat{a}^{+} + H.c., \tag{5}$$

where $\hbar$ is the Planck constant, κ is the coupling constant, and H.c. stands for Hermitian conjugation. Then, one can use Eq. (3) to re-arrange the Heisenberg equations:

$$\frac{d}{dt}\hat{b} = -\frac{i}{\hbar}\left[\hat{b}, \hat{H}_{JCM}\right];\ \frac{d}{dt}\hat{a} = -\frac{i}{\hbar}\left[\hat{a}, \hat{H}_{JCM}\right] \tag{6}$$

into the equations of motion of the dressed atom and the quantized mode, yielding:

$$\begin{aligned}\frac{d}{d\tau}\hat{c} = {} & \exp\left(i\delta_q\tau\right)\kappa_q^{*}\left\{\varphi_1^{2}(\tau)\left(\hat{I} - 2\hat{c}^{+}\hat{c}\right)\exp\left[i(2\lambda - \delta)\tau\right] + 2\varphi_1(\tau)\varphi_2^{*}(\tau)\hat{c}\right\}\hat{a}_q + \\ & + \exp\left(-i\delta_q\tau\right)\kappa_q\left\{\varphi_2^{2}(\tau)\left(\hat{I} - 2\hat{c}^{+}\hat{c}\right)\exp\left[i(2\lambda - \delta)\tau\right] - 2\varphi_1^{*}(\tau)\varphi_2(\tau)\hat{c}\right\}\hat{a}_q^{+},\end{aligned} \tag{7}$$

$$\begin{aligned}\frac{d}{d\tau}\hat{a}_q = {} & \exp\left(-i\delta_q\tau\right)\kappa_q\left\{\varphi_1^{*}(\tau)\varphi_2(\tau)\left(\hat{I} - 2\hat{c}^{+}\hat{c}\right) + \exp\left[i(2\lambda - \delta)\tau\right]\varphi_2^{2}(\tau)\,\hat{c}^{+} - \right. \\ & \left. - \exp\left[-i(2\lambda - \delta)\tau\right]\varphi_1^{*2}(\tau)\hat{c}\right\},\end{aligned} \tag{8}$$

where $\delta_q \equiv \left(\Omega - \omega_q\right)/\omega'$, $\kappa_q \equiv \kappa\cdot\exp\left(-i\psi\right)$, $\hat{a}_q = \hat{a}\cdot\exp\left(i\omega_q t\right)$.

Set (7) and (8) can be analyzed the following manner. If the atom does not interact with the quantized mode (κ=0) then operator $\hat{c}$ is the constant of motion of the dressed atom, i.e. $\left(d/d\tau\right)\hat{c} = 0$, while the mode exhibits only a trivial time evolution according to: $\hat{a} = \hat{a}_0\cdot\exp\left(-i\omega_q t\right)$. The interaction can effectively change the dynamics of the system when the field frequency, ω_q, comes close to some transition frequencies between the quasienergy levels listed above. If this is the case some terms in the right-hand part of (7) and (8) oscillate slowly and one can use the second Rotating Wave Approximation by dropping all the other terms. In case of pure resonance the above field and transition frequencies coincide and, therefore, the remaining terms do not vary in time.

Ref. 12 presents the analysis of the particular cases where the approximate analytic solutions of set (7) and (8) are available. It is found that if the quasienergy levels involved into the interaction correspond to different quasienergy states then the equations of motion can be reduced to the similar form as those of the conventional JCM. This case is called as «inelastic interaction». In the opposite limiting case called «elastic interaction» all the quasienergy levels involved into the interaction correspond to one and the same quasienergy state. In this case the populations of the quasienergy states show no saturation and the mean number of photon undergoes an unlimited rise as long as the alteration of the classical field amplitude is negligible. However, if the interaction is pure «elastic» and the quantized mode is initially in the coherent quantum state then the posterior photon statistics becomes either Poissonian or super-Poissonian.

A peculiarity appears when the Rabi frequency becomes the multiple of the modulation frequency so that $\sigma = l = 1, 2, \ldots$ (see also Ref. 17) . If this is the case the quasienergy levels corresponding to the different quasienergy states cross and, therefore, the distinction between the «inelastic» and «elastic» interaction disappear. When the quantized mode is tuned to resonance with the transition between the quasienergy levels, i.e. $\delta_q \equiv \left(\Omega - \omega_q\right)/\omega' = 2m + 1$, $m = 1, 2, \ldots$, both the interaction mechanisms interfere. These results in a comprehensive time dynamics of the open JCM studied below in the present paper.

Suggesting $\sigma = l$, $\delta_q = 2m + 1$ and applying the second Rotating Wave Approximation as described above set (7) and (8) reduces to:

$$\frac{d}{d\tau}\hat{c} = \left(\hat{I} - 2\hat{c}^{+}\hat{c}\right)\cdot\left(\alpha\,\hat{a}_q + \gamma\,a_q{}^{+}\right) + 2\cdot\left(\beta\,\hat{a}_q - \beta^{*}\,a_q{}^{+}\right)\cdot\hat{c}, \tag{9}$$

$$\frac{d}{d\tau}\hat{a}_q = \beta^{*}\left(\hat{I} - 2\hat{c}^{+}\hat{c}\right) + \gamma\,\hat{c}^{+} - \alpha^{*}\,\hat{c}, \tag{10}$$

where $\alpha = (-1)^{l+m+1}\cdot\frac{1}{2}\kappa_q{}^{*}\,J_{l+m+1}(2al)$, (11)

$$\gamma = (-1)^{l-m-1}\cdot\tfrac{1}{2}\,\kappa_q\,J_{l-m-1}(2al), \tag{12}$$

$$\beta = \tfrac{1}{2}\kappa_q{}^{*} \text{ for } m=-1 \text{ , and } \beta = 0 \text{ for } m\neq -1, \tag{13}$$

Then, one can introduce the effective Hamiltonian

$$\hat{H}_{eff} = i\left[\alpha\,\hat{a}_q\,\hat{c}^{+} - \alpha^{*}\hat{a}_q{}^{+}\hat{c} + \gamma\,\hat{a}_q{}^{+}\hat{c}^{+} - \gamma^{*}\hat{a}_q\,\hat{c} + \left(\beta^{*}\,\hat{a}_q{}^{+} - \beta\hat{a}_q\right)\cdot\left(\hat{I} - 2\hat{c}^{+}\hat{c}\right)\right], \tag{14}$$

to represent equations (9) and (10) in the canonical form:

$$\frac{d}{d\tau}\hat{c} = -i\left[\hat{c}, \hat{H}_{eff}\right];\ \frac{d}{d\tau}\hat{a}_q = -i\left[\hat{a}_q, \hat{H}_{eff}\right]. \tag{15}$$

3. NUMERIC RESULTS

Solution of set (9) and (10) (or (15)) can be expressed in an analytic form in the particular cases when $\alpha = \gamma = 0$ or $\beta = 0$. However, our analysis suggests that a high degree of squeezing can be obtained when all the coefficients, α, β, and γ, takes nonzero values. It seems, however, that in general case only numeric results are available. Therefore, in this Section our aim is to calculate numerically the mean number of photons in the quantized mode:

$$\overline{n} = \left\langle \hat{a}^{+}(\tau)\cdot\hat{a}(\tau)\right\rangle = \left\langle \hat{a}_q{}^{+}(\tau)\cdot\hat{a}_q(\tau)\right\rangle, \tag{16}$$

the variance of the photon number:

$$\Delta n^2 = <\hat{n}^2> - \left(\overline{n}\right)^2,\ <\hat{n}^2> = \left\langle \hat{a}^{+}(\tau)\cdot\hat{a}(\tau)\cdot\hat{a}^{+}(\tau)\cdot\hat{a}(\tau)\right\rangle = \left\langle \hat{a}_q{}^{+}(\tau)\cdot\hat{a}_q(\tau)\cdot\hat{a}_q{}^{+}(\tau)\cdot\hat{a}_q(\tau)\right\rangle, \tag{17}$$

and the populations of the quasienergy states:

$$N_1 = \left\langle \hat{c}^{+}(\tau)\cdot\hat{c}(\tau)\right\rangle,\quad N_2 = \left\langle \hat{c}(\tau)\cdot\hat{c}^{+}(\tau)\right\rangle = 1 - N_1, \tag{18}$$

where the angle brackets denote quantum mechanical averaging. The numeric procedure we have developed consists in representing the atomic and field operators and the time evolution operator in the matrix form using the following basis set of the product states:

$$\left|k,\mu\right\rangle \equiv \left|k\right\rangle_f \left|\theta_\mu\right\rangle_a, k = 0,1,2\ldots;\ \mu = 0,1 \tag{19}$$

where $\left|k\right\rangle_f$ are the number states of the quantized mode with k photons. The aforementioned analytic solutions were used in testing the routine. The particular results of calculations for the open JCM are shown in Figs. 2 and 3. In both the figures the dressed atom and the quantized mode are initially in the quasienergy state $\left|\theta_1\right\rangle_a$ and in the coherent state $\left|\nu\right\rangle_f$, respectively.

Figure 2 (a, b, and c) shows the model variables against time for resonance specified by: $l = 1$, $m = -1$. The modulation depth is set to be $a = 0.968$. Both the coupling constant, κ_q, and the initial amplitude of the quantized field, V, are suggested to be real. Curves 1, 2, and 3 correspond to V=3, 6, and 8, respectively. The population dynamics is characterized by the collapses and the revivals of oscillations (Figure 2c). However, in contrast to the conventional JCM the population additionally exhibits slow oscillations of high amplitude those can be attributed to the «elastic» part of interaction between the dressed atom and the quantized mode. The slow oscillations of the same type are exhibited by the mean value and the variance of the photon number in the quantized mode showing the negative correlation with N_1 (Figure 2 a and b). Moreover, the collapses and the revivals of the fast oscillations also occur in the dynamics of both the mean photon number and the Fano factor. However, the amplitude of the latter oscillations falls abruptly with the rise of v.

The effect of the transient squeezing occurs on the time scale of the slow oscillations (Fig 2b). When the dressed atom absorbs several tenths of photons the statistic of the remaining photons becomes sub-Poissonian with the Fano factor being as small as ≈0.3. The time interval while the strong squeezing occurs expands when increasing the field amplitude, v. On the contrary, for the conventional JCM the grow of the field amplitude results in increasing the oscillation frequency (that is the generalized Rabi frequency[11]), and the time of squeezing becomes shorter. Therefore, the open JCM provides the means of obtaining strong squeezing of an intense light for a long time.

It is worth noting that the open JCM can show different types of nonlinear dynamics for various resonances specified by particular values of indices l and m. This is illustrated by Figure 3 (a,b, and c), where we plot the model variables against time for l=1, m=0, a=0.75, and v=2.5. After several transient oscillations the populations of the quasienergy states become almost equal and fixed. Simultaneously, both the mean value and the variance of the photon number grow steadily in time. This type of dynamics except the short-time domain is characteristic for the open JCM with the «elastic» type of interaction as described in Ref. 12

Our numeric results suggest that one can obtain a significant degree of squeezing provided both the «elastic» and «inelastic» interaction mechanisms compete with each other as shown in Fig.2. However, when one of the mechanisms predominates (as in Figs. 1 and 3) only a moderate squeezing should be expected.

4. CONCLUSIONS

We have studied the dynamics of the coupled system of the dressed atom and the quantized mode called the open Jaynes and Cummings model. The dressed atom have been considered as a two-level system driven by a polychromatic classical field with the equidistant spectrum. Specifically, we have performed calculations for the amplitude-modulated (threechromatic) classical field.

It has been found that when the quasienergy levels of the dressed atom cross the model shows a comprehensive time dynamics resulting from the competition of the two interaction mechanisms referred to as the «inelastic» and «elastic» ones. The model variables undergo both fast oscillations and a slow drift. If the quantized mode is initially in the coherent state then the fast oscillations of the atomic populations assume the form of recurring collapses and revivals. The slow variations of the photon number in the quantized mode can be bounded above or not depending on the model parameters.

When the mean number of photons, $\langle n \rangle$, in the quantized mode falls the statistics of the remaining photons becomes more regular. Near the local minima of $\langle n \rangle$ the statistics can become sub-Poissonian with Fano factor $F = \Delta n^2 / \langle n \rangle$ being many times as small as unity. Both the time interval while the squeezing occurs and the degree of squeezing tend to grow when increasing the initial value of the quantized field amplitude.

Finally, the maximum degree of squeezing obtainable by the help of the dressed atom absorption still remains unevaluated and is the subject of the future analysis. Moreover, we believe that an approximate analytical approach can be developed to analyze the particular types of dynamics of the open JCM in the presence of both the «elastic» and «inelastic» interaction mechanisms.

5. REFERENCES

1. D. Meschede, H. Walther, G. Muller, «One-atom maser,» *Phys. Rev. Lett.* **54,** N6, **pp.** 551-554, 1985.

2. G. Rempe, H. Walther, N. Klein, «Observation of quantum collapse and revival in a one-atom maser,» *Phys. Rev. Lett.* **58**, pp. 353-356, 1987.

3. G.M. Meyer, M. Loffler, and H. Walther, «Spectrum of the ion trap laser,» *Phys. Rev. A* **56**, N2, pp. R1099-R1102, 1997.

4. J.H. Eberly, N.B. Narozhny, J.J. Sanchez-Mondragon, «Spontaneous collapse and revival in a simple quantum model,» *Phys. Rev. Lett.* **44, pp.** 1323-1326, 1980.

5. H.-I. Yoo and J.H. Eberly, «Dynamical theory of an atom with two or three levels interacting with quantized cavity fields,» *Physics Reports* **118,** N5, **pp.** 239-337, 1985.

6. N.B. Narozhny, J.J. Sanchez-Mondragon, J.H. Eberly, «Coherence versus incoherence: collapse and revival in a simple quantum model,» *Phys. Rev.* A **23, pp.** 236-247, 1981.

7. P. Meystre, and M.S. Zubairy, «Squeezed states in the Jaynes-Cummings model,» *Physics Letters* **89A**, N8, pp. 390-392, 1982.

8. F.-X. Zhao, M. Orszag, J. Bergou, and S.-J. Zhu, «Enhanced transient squeezing in the Jaynes-Cummings model with atomic coherence,» *Physics Letters* **137A**, N9, pp. 479-484, 1989.

9. D.F. Smirnov, A.S. Troshin, «New phenomena in quantum optics: antibunching and the sub-Poissonian photon statistics, squeezed states,» *Sov. Phys. Usp.* **59, pp.** 628-666, 1987.

10. A. Sizmann, R.J. Horowicz, G. Wagner, and G. Leuchs, 1990, *Optics Communications* **80**, 138 (1990).

11. Allen L. and Eberly J.H., *Optical Resonance and Two-Level Atoms*, 1975 (Wiley, New York).

12. M.Z.Smirnov, «A modified Jaynes-Cummings model for an atom interacting with a classical multifrequency field,» *JETP* **85** (3), pp. 441-446, 1997.

13. C. Cohen-Tannoudji, «Optical pumping and interaction of atoms with electromagnetic field,» in *Cargese Lectures in Physics*, Vol. 2, (M. Levy (ed.), Gordon and Breach, New York), pp. 347-393, 1968.

14. T. Yabuzaki, S. Nakayama, Y. Marakami, and T. Ogawa, «Interaction between a spin-1/2 atom and a strong rf field,» *Phys. Rev.* **A10**, N6, pp. 1955-1963. 1974.

15. M.Z.Smirnov, «Quasienergy spectrum of a two-level atom in the field of high-intensity modulated radiation,» *Quantum Electronics* **25** (9), pp. 871-876, 1995.

16. M.Z. Smirnov, «Nonlinear dynamics of an atom in the quasienergy representation in the presence of a strongly modulated optical field,» *Phys. Rev.* A **52**, pp. 2195-2208, 1995.

17. B. Blind, P.R. Fontana, and P. Thomann, «Resonance fluorescence spectrum of intense amplitude modulated laser light,» *J. Phys. B: Atom. Molec. Phys.* **13**, N 14, pp. 2717-2727, 1980.

18. P. Thomann, «Optical parametric resonances,» *J. Phys. B: Atom. Molec. Phys.* **9**, N 14, pp. 2411-2419, 1976,

19. P. Thomann, «Optical resonances in a strong modulated laser beam,» *J. Phys. B: Atom. Molec. Phys.* **13**, pp. 1111-1124, 1980.

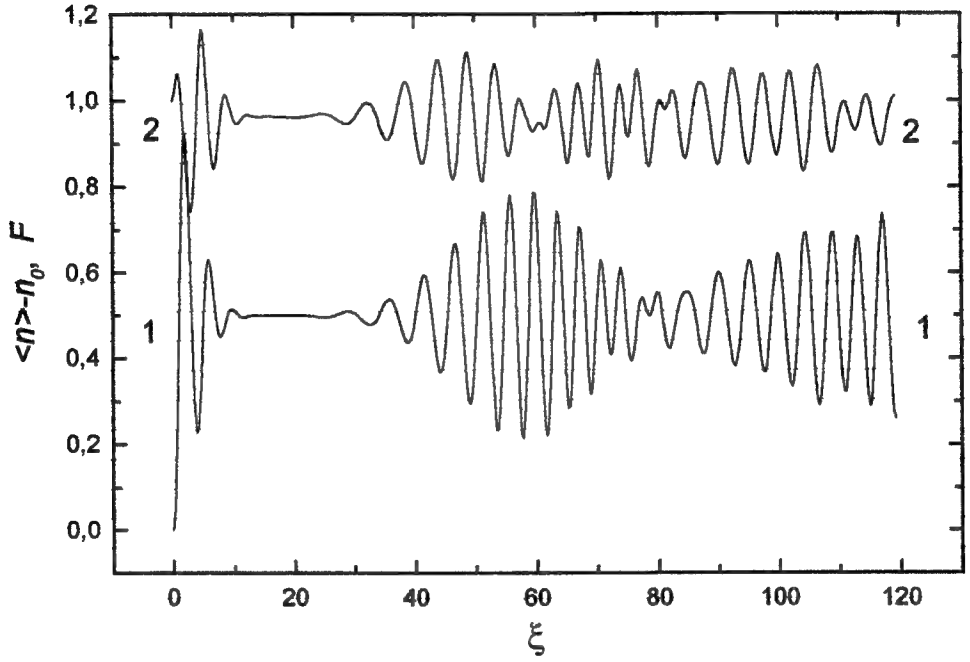

Figure 1 Deviation of the mean photon number, $\langle n \rangle$, from its initial value n_0 (curve 1) and Fano factor F (curve 2) against the dimensionless time, $\xi = \kappa t$, for the coherent state JCM.

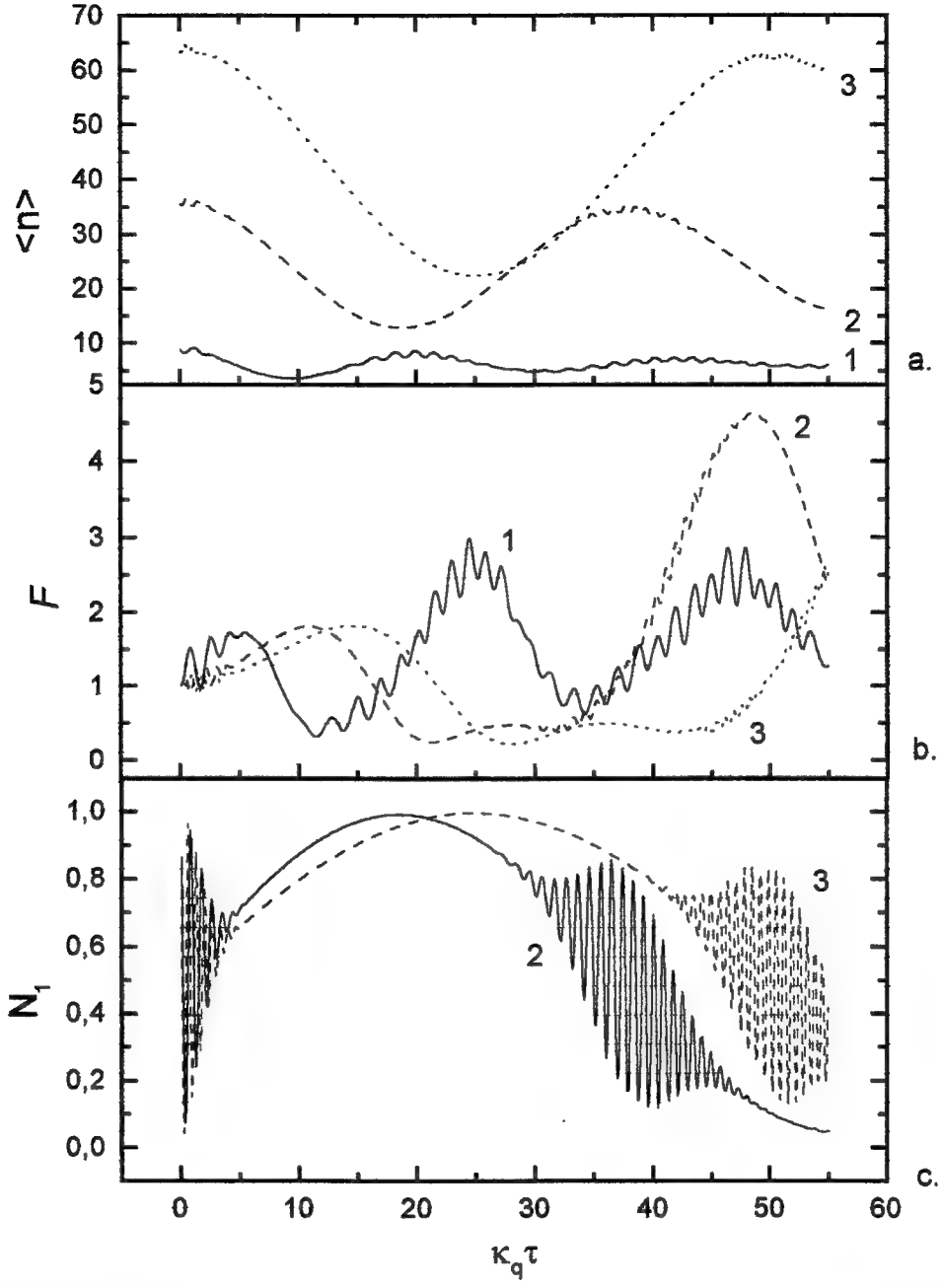

Figure 2 Mean photon number $\langle n \rangle$ (a), Fano factor F (b), and mean population N_1 of quasienergy state $|\theta_1\rangle_a$ (c) against the dimensionless time for the open modification of the JCM at the quasilevel crossing point l=1, m=-1. Coupling constant κ_q is assumed to be real. The modulation depth is a=0.968. The model is initially in the product state $|\theta_1\rangle_a|\nu\rangle_f$, where indices a and f label the dressed atom and the quantized mode, respectively, and $|\nu\rangle_f$ is the coherent quantum state. Curves 1, 2, and 3 correspond to ν=3, 6, and 8, respectively.

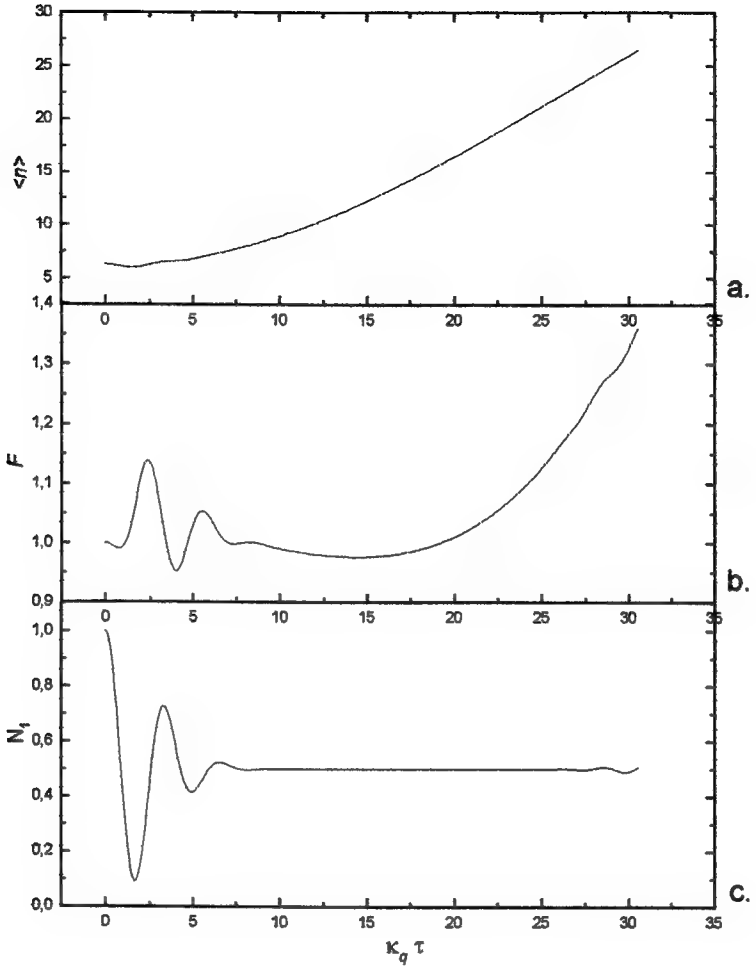

Figure 3 The same as in Fig 2, but for l=1, m=0, a=0.75, and ν=2.5.

Quantum gain and absorption in two color three level V-atom: a dressed state picture

D. Braunstein and R. Shuker*

Department of Physics, Ben Gurion University of the Negev,

84105 Beer Sheva, Israel

Light amplification without population inversion (L.W.I) and absorption with inversion driven by quantum coherent interferences in a closed three level V - type system is studied from the point of view of two color dressed state basis . Approximate analytic time dependent solutions, for coherences and population distribution are derived, and compared with full numerical solutions. Steady state quantities are also calculated, and the conditions under which the system exhibits gain with and without inversion, in the dressed state representation are derived. It is found that for a weak probe laser field light amplification without inversion may occur, for a range of system parameters, in both the bare and the dressed state representations.

*shuker@bgumail.bgu.ac.il

Recently there has been tremendous interest in the study of light amplification and lasing without the requirement of population inversion (LWI), potentially capable of extending the range of laser devices to spectral region in which, for various reasons, population inversion is difficult to achieve. These spectral regions include UV obtained from atomic vapor, and mid-to-far infrared, obtained by intersubband transitions in quantum wells. Many models for LWI have been proposed, mostly three and four level schemes, in Λ and V configurations [1–17]. The dependence of optical gain on system parameters was investigated.

The key mechanism, which is common to most of the proposed schemes, is the utilization of external coherent fields, that induce quantum coherence and interference in multi level systems, though an exception of LWI without the use of coherent fields was also reported [9]. In particular it was shown that if coherence is established between certain atomic states, different

SPIE Vol. 3685 • 0277-786X/99/$10.00

absorption channels may interfere destructively leading to the reduction or even the cancellation of absorption [7,13]. At the same time stimulated emission remain intact, leading to the possibility of gain even if only a small fraction of the population is in the excited state.

Experimental observations of inversionless gain and lasing without inversion have been reported by several groups [18–21]. Inversionless lasers have been shown to have unique properties such as non classical photon statistics and substantially narrow spectral features [22,23]. In a recent paper Y. Zhu [12] analyzed the transient and steady state properties of light amplification without population inversion , in a closed three level V type system, in the bare state basis. Steady state dressed state populations were also calculated, in the limit of strong driving laser.

In this communication we study the same model within the framework of the dressed state basis, and obtain approximate analytic time dependent solutions, as well as steady state solutions for populations and coherences. To our knowledge, this paper details the first calculations of LWI in the dressed state basis, which is valid to some extent to atoms dressed both by the pump and probe lasers. These calculations show the possibility of inversion and inversionless gain in the dressed state scheme as well as gain without inversion in the bare state picture.

Let us consider the closed V-type three level system illustrated in Figure 1. The transition $|a> \leftrightarrow |b>$ of frequency $\omega_{ba}$is driven by a strong single mode laser of frequency ω_L. The transition $|a> \leftrightarrow |c>$ of frequency ω_{ca} is pumped incoherently with a rate Λ. A single mode probe laser(not necessarily weak) is applied to the transition $|a> \leftrightarrow |c>$. γ_b (γ_c) is the spontaneous emission rate from the state $|b>$ ($|c>$).The states $|b>$ and $|c>$ are not coupled.

We have chosen to employ a fully quantum mechanical Hamiltonian, and to obtain the density matrix equations in their semiclassical version. The quantum mechanical Hamiltonian gives rise to a simple picture of the stationary dressed states. The Hamiltonian under the dipole and rotating wave approximation is given by:

$$H = \hbar\omega_{ba}|b><b| + \hbar\omega_{ca}|c><c| + \hbar\omega_L(a^\dagger a + \frac{1}{2}) + \\ + \hbar\omega_p(a'^\dagger a' + \frac{1}{2}) + g(s_+ a + s_- a^\dagger) + g'(s'_+ a' + s'_- a'^\dagger). \qquad (1)$$

g and g' are coupling constants and are assumed to be real. The eigenstates of the unperturbed part of the Hamiltonian form a three dimensional manifold labeled by the atomic indexes, the laser photon number N and by the probe photon number N'.The manifold is written

$$\varepsilon(N,N') = \{|a,N+1,N'+1>, |b,N,N'+1> \\ |c,N+1,N'>\}. \tag{2}$$

In this basis the interaction hamiltonian for the manifold $\varepsilon(N,N')$ takes the form

$$H_{Int} = \begin{pmatrix} 0 & -\Omega & -G \\ -\Omega & -\Delta_1 & 0 \\ -G & 0 & -\Delta_2 \end{pmatrix}. \tag{3}$$

where we have defined the detunigs and the Rabi frequencies, in their quantum form.

$$-g\sqrt{N+1} = \hbar\Omega \ ; \ -g'\sqrt{N'+1} = \hbar G \ ; \\ \Delta_1 = \omega_L - \omega_{ba} \ ; \ \Delta_2 = \omega_p - \omega_{ca}. \tag{4}$$

Here we consider large photon numbers and hence Ω and G do not vary much on the considered nearest neighbors transitions.

We have chosen to work within the framework of the master equation for the atom, since it being an operator equation independent of representation, it can be projected over any basis. We use a generalization of a standard master equation adjusted to account for the scheme described above [24]. The master equation is given by:

$$\dot{\sigma} = -\frac{i}{\hbar}[H,\sigma] - \frac{\gamma_b}{2}[s_+s_-\sigma + \sigma s_+s_-] + \gamma_b s_-\sigma s_+$$
$$- \frac{\gamma_c}{2}[s'_+s'_-\sigma + \sigma s'_+s'_-] + \gamma_c s'_-\sigma s'_+ -$$
$$- \frac{\Lambda}{2}[s'_+s'_-\sigma + \sigma s'_+s'_-] - \frac{\Lambda}{2}[s'_-s'_+\sigma + \sigma s'_-s'_+] + \Lambda s'_+\sigma s'_- +$$
$$+ \Lambda s'_-\sigma s'_+, \qquad (5)$$

here σ is the density operator for the atom + the laser modes system. $s_+(s_-)$, $s'_+(s'_-)$ are the atomic raising and lowering operators, for the $|a> \leftrightarrow |b>$ and $|a> \leftrightarrow |c>$ transitions respectively.

The dressed states are obtained by finding the the eigenvectors of the interaction Hamiltonian given by Eq. (3). To simplify things a little we take both the driving laser field and the probe field to be in exact resonance with the corresponding bare state transitions, i.e. we take $\Delta_1 = \Delta_2 = 0$. When the detunings are set to be zero we notice that the energies in the bare state basis are all degenerate, and in fact equal to zero (in the interaction picture). Carrying out the diagonalization procedure we obtain the eigenstates that correspond to the following eigenvalues

$$E_{|\gamma>} = -\hbar R \quad ; \quad E_{|\alpha>} = 0 \quad ; \quad E_{|\beta>} = \hbar R, \qquad (6)$$

where we have introduced the generalized Rabi flopping frequency $R = \sqrt{\Omega^2 + G^2}$.

Note that for the case $G = 0$ the usual coupling and non coupling dressed states are obtained, while the $|\alpha>$ state which is identical to the $|c>$ state is not involved in the interaction altogether.

Projection of the master equation over the dressed state basis yields particularly simple equations for the first part of equation (5) (the Hamiltonian part of the master equation). However, in the dressed atom basis the relaxation and pump terms of equation (5) give rise to equations that are not simple. In particular couplings between dressed state populations and coherences between two dressed states appear. The equations of motion for the density matrix

elements in the dressed state representation will be given elsewhwere. Here we present only typical ones:

$$\dot{\rho}_{\alpha\alpha} = -(\Gamma_\alpha + \Lambda')\rho_{\alpha\alpha} + \tilde{\Gamma}(\rho_{\alpha\beta} + \rho_{\beta\alpha}) + \tilde{\Gamma}(\rho_{\alpha\gamma} + \rho_{\gamma\alpha}) + \\ + \frac{1}{2}\Lambda'\rho_{\beta\beta} - \frac{1}{2}\Lambda'(\rho_{\beta\gamma} + \rho_{\gamma\beta}) + \frac{1}{2}\Lambda'\rho_{\gamma\gamma} \tag{7a}$$

$$\dot{\rho}_{\beta\gamma} = -(\Gamma_{\beta\gamma} + 2iR)\rho_{\beta\gamma} - (\Gamma_\beta + \frac{1}{2}\Lambda - \frac{1}{2}\Lambda')\rho_{\gamma\beta} + \\ + \tilde{\Gamma}(\rho_{\alpha\beta} + \rho_{\gamma\alpha}) + 2\tilde{\Gamma}(\rho_{\beta\alpha} + \rho_{\alpha\gamma}) - \frac{1}{2}(\Gamma_\alpha + \Lambda')\rho_{\alpha\alpha} - \\ - (2\Gamma_\beta - \frac{1}{4}\Lambda')(\rho_{\beta\beta} + \rho_{\gamma\gamma}) \tag{7b}$$

In obtaining equations (7a) and (7b) we have introduced the following notation

$$\Gamma_\alpha = \frac{1}{R^2}(\gamma_b G^2 + \gamma_c \Omega^2) \ , \ \Gamma_\beta = \frac{1}{4R^2}(\gamma_b \Omega^2 + \gamma_c G^2) \ , \\ \Gamma_{\alpha\beta} = \Gamma_\beta + \frac{1}{2}(\Gamma_\alpha + \Lambda + \Lambda'/2) \ , \ \Gamma_{\beta\gamma} = 3\Gamma_\beta + \frac{3}{2}\Lambda - \Lambda', \\ \tilde{\Gamma} = \frac{G\Omega}{2\sqrt{2}R^2}(\gamma_b - \gamma_c - \Lambda) \ , \ \tilde{\Gamma}' = \frac{G\Omega\Lambda}{2\sqrt{2}R^2} \ , \ \Lambda' = \frac{\Lambda\Omega^2}{R^2}.$$

Γ_α, Γ_β are the spontaneous emission decay rate of the $|\alpha>$, $|\beta>$ and $|\gamma>$ states ($|\gamma>$ also decays with a rate Γ_β). More precisely the state $|\alpha(N)(N')>$ decays by spontaneous emission with a rate Γ_α to the levels $|\beta(N-1)(N')>$, $|\gamma(N-1)(N')>$ and $|\beta(N)(N'-1)>$, $|\gamma(N)(N'-1)>$. Similarly the levels $|\beta(N)(N')>$, $|\gamma(N)(N')>$ decay with the same rate Γ_β to the same levels as $|\alpha(N)(N')>$. The coherences $\rho_{\alpha\beta}$, and $\rho_{\alpha\gamma}$ ($\rho_{\beta\gamma}$) decay with a rate $\Gamma_{\alpha\beta}$ ($\Gamma_{\beta\gamma}$). Λ' is a normalized pump rate which causes population and depopulation of the dressed levels. It also has an important influence on the coherences as can readily be seen from equations (7a) and (7b). $\tilde{\Gamma}$ and $\tilde{\Gamma}'$ are interference terms. The first and second terms in $\Gamma_{\alpha\beta}$ describe damping of the coherence due to radiative transitions of the levels involved to lower levels, and is equal to half the sum of all transition rates starting from $|\alpha(N)(N')>$ and $|\beta(N)(N')>$. The third term in $\Gamma_{\alpha\beta}$ describes coherence damping due to the incoherent pump. The interpretation of $\Gamma_{\beta\gamma}$ is similar except that the $3\Gamma_\beta$ is composed from a $2\Gamma_\beta$ term responsible for the coherence damping due to radiative transition, plus a single Γ_β component resulting from transfer of coherence from higher levels belonging to higher manifolds. Inspection of the full equations

of motion for the elements of the density matrix reveals that $\rho_{\alpha\beta}$ and $\rho_{\alpha\gamma}$ have the same free evolution frequency R, however they oscillate out of phase. The free evolution frequency of $\rho_{\beta\gamma}$ is twice as large, as both levels $|\beta>$ and $|\gamma>$ are contaminated by the bare ground state $|a>$. Note that the closure of the system is satisfied i.e., $\frac{d}{dt}(\rho_{\alpha\alpha}+\rho_{\beta\beta}+\rho_{\gamma\gamma})=0$. Gain or absorption coefficient for the $|j>\rightarrow|i>$ transition is proportional to $Im[\rho_{ij}]$. In our notation amplification will occur if $Im[\rho_{ij}]>0$. Without going into the details of the calculation we disscus here approximate solutions to the equations of motion of the density matrix equations in the dressed state basis in the secular approximation. Both temporal end steady state solutions will be presented graphically. These will be compared with numerical calculations of the full system, i.e., without any approximation.

As mentioned before, the hamiltonian part of the master equation has a simple form in the dressed state basis. The problem arises with the spontaneous emission and pump terms are present in equation (5), giving the complicated couplings appearing in equations (7a) and (7b). Solving exactly the complete set seems to be a formidable task. However the situation can be simplified if the splitting $\hbar R$ between the dressed states of a manifold is large compared with $\hbar\gamma_b$, $\hbar\gamma_c$,$\hbar\Lambda$. We can then ignore the "nonsecular" terms, i.e. couplings between populations and coherences (see [24]).

When the "nonsecular" couplings between populations and coherences are ignored one can obtain reduced equations for the populations while population conservation is still maintained. Solving these equations subject to the condition $\rho_{\alpha\alpha}+\rho_{\beta\beta}+\rho_{\gamma\gamma}=1$ yields temporal solution. Here we present only the steady state populations.

$$\rho^{st}_{\alpha\alpha}=\frac{\Lambda'}{2\Gamma_\alpha+3\Lambda'} \tag{8a}$$

$$\rho^{st}_{\beta\beta}=\rho^{st}_{\gamma\gamma}=\frac{\Gamma_\alpha+\Lambda'}{2\Gamma_\alpha+\Lambda'} \tag{8b}$$

Figure 2 shows a comparison between the exact time dependent solution for $\rho_{\alpha\alpha}$ and $\rho_{\beta\beta}$ (solid line), obtained by solving numerically the non - approximated set of equations, with our approximated analytic solution shown in dashed line. The normalized parameters for the numerical simulation were set to be $\Omega=20\gamma_c$, $\gamma_b=2\gamma_c$, $G=0.1\gamma_c$, $\Lambda=3\gamma_c$, and are the same

as those of Y. Zhu [12], (for the purpose of comparison). We can see that the population $\rho_{\alpha\alpha}$ is a monotonically increasing, oscillating function of time which reaches a steady state value $\rho_{\alpha\alpha}^{st} \approx 0.27$. The behavior of $\rho_{\beta\beta}$ (not shown) is opposite, i.e. it is a monotonically decreasing oscillating function and it reaches the steady state value $\rho_{\beta\beta}^{st} \approx 0.36$. $\rho_{\gamma\gamma}$ is similar to $\rho_{\beta\beta}$, due the choice of parameters made. The approximate solutions describe nicely the envelope of oscillation and the correct expression for the steady state. One can see that $\rho_{\alpha\alpha} < \rho_{\beta\beta} = \rho_{\gamma\gamma}$, for any finite Λ, and hence population inversion do exist in the dressed state basis. For the transitions $|\alpha> \rightarrow |\gamma>$, $|\beta> \rightarrow |\gamma>$ the population difference is negative (noninversion) and it remains to be seen whether this transitions amplify and thus result in lasing without inversion in the dressed state basis. In the strong coupling field limit $\Omega >> G$ the steady state population become

$$\rho_{\beta\beta} = \rho_{\gamma\gamma} = \frac{\gamma_c + \Lambda}{2\gamma_c + 3\Lambda}, \tag{9}$$

and

$$\rho_{\alpha\alpha} = \frac{\Lambda}{2\gamma_c + 3\Lambda}. \tag{10}$$

In this case $|\alpha>$ is the highest excited state of the transition in the manifold and hence we obtain full population noninversion condition in the dressed state basis.

Ignoring the "non secular" couplings between coherences and populations in eq's (7a) - (7b) results in equations that are simpler than the original ones, however they are still very complicated, especially the equations for $\rho_{\beta\gamma}$ and its conjugate, which are coupled to all the other coherences. Based on numerical calculations, we found that $\rho_{\beta\gamma}$ and hence its conjugate are substantially larger than the other coherences, indicating the crucial role these coherences play. In light of the above, we couple each coherence to itself (describing the free evolution) and to $\rho_{\beta\gamma}$ and $\rho_{\gamma\beta}$, acting as the dominant source terms.

Solving the eigenvalue problem of the equations of motion one finds the transient solutions for the coherences , in the strong coupling field limit.

Figure 3 shows the exact coherence $\rho_{\alpha\gamma}$ obtained by solving numerically the equations of motion (solid line), and the corresponding approximate solution (dashed line) based on the

analytic expressions for $\rho_{\alpha\gamma}$ showing absorption despite inversion for the $\gamma \Rightarrow \alpha$. The chosen parameters are the same as in Fig. 2. It can be seen that the exact solutions reach a steady state different from zero, while our approximate analytic solution have zero steady state values. This is compatible with the absence of the population source terms in the approximation. The oscillation frequency is predicted correctly by the approximate solutions.

$\rho_{\beta\gamma}$ has an almost pure sinusoidal form of frequency $2R$. It can be seen from the numerical simulation presented in Figure 3 that the coherences $\rho_{\alpha\beta}$ possesses a definite sign, thus the corresponding transitions between dressed states, being either amplified or attenuated. More precisely $Im(\rho_{\alpha\beta})$ is positive in all the range shown, hence the transition $|\beta > \rightarrow |\alpha >$ is amplified (with population inversion in the dressed state picture). the transition $|\alpha > \rightarrow |\gamma >$ is also amplified ($Im(\rho_{\gamma\alpha}) > 0$), however, without population inversion in this case. Another feature is the strength of the coherence $\rho_{\beta\gamma}$, which is three orders of magnitude stronger than the other coherences. The main deficiency of our approximate equations is the zero steady state predicted by them. The reason for this is the omission of the source terms (populations) in writing in the equations of motion. We have solved (analytically) these equations with the source terms included. The solution obtained was checked against numerical calculations and found to be in excellent agreement. The steady state values are also obtained and are found to be in very good agreement with full numerical results.

As is seen before in the strong coupling field limit (weak probe) $\rho_{\alpha\alpha} < \rho_{\beta\beta} = \rho_{\gamma\gamma}$. We found that amplification of the $|\beta > \rightarrow |\alpha >$ transition occurs in the following two cases:

1. For any incoherent pump rate Λ if $\gamma_b > \gamma_c$.

2. For $\frac{1}{2}\gamma_c < \gamma_b < \gamma_c$, provided that $\Lambda > \frac{\gamma_c(\gamma_c - \gamma_b)}{2\gamma_b - \gamma_c}$.

This gain is "regular" gain, due to population inversion since $\rho_{\beta\beta} > \rho_{\alpha\alpha}$. The transition $|\alpha > \rightarrow |\gamma >$ will be amplified for the same range of parameters. However, this transition is *inversionless*, and it is due to external field induced coherences.

The steady state populations in the bare state basis reduce correctly to the results obtained by Y. Zhu [12].

The probe transition exhibits inversionless gain for $\gamma_b > \gamma_c$ for pump rates satisfying $\Lambda > \frac{\gamma_c^2}{\gamma_b - \gamma_c}$. From the analysis presented above we conclude that for a weak probe , true lasing without population inversion can be realized, both in the bare state and the dressed state basis. For a stronger probe field, but still weaker than that of the coupling laser field, lasing without inversion in the dressed state basis for the $|\alpha> \rightarrow |\gamma>$ transition is found.

SUMMARY

Light amplification without population inversion and absorption with inversion driven by quantum coherent interferences in a closed three level V - type system is studied from the point of view of two color dressed state basis. Approximate analytic time dependent solutions, for coherences and population distribution are derived, and compared with full numerical solutions. Steady state quantities are also calculated, and the conditions under which the system exhibits gain with and without inversion, in the dressed state representation are derived. Transformation to the bare state picture is performed and comparison is made with other bare state results. It is found that for a weak probe laser field light amplification without inversion may occur, for a range of system parameters, in both the bare and the dressed state representations. We also report the occurance of absorption despite the existence of population inversion. This process can be interpreted as constructive interference for the stimulated emission.

[1] S. E. Harris, Phys.Rev. Lett. **62**, 1033 (1989).

[2] M. O. Scully, S. Y. Zhu, and A. Gavrielides, ibid. **62**, 2813 (1989).

[3] G. S. Agrawal, Phys. Rev. A, **44**, R28 (1991).

[4] L. M. Narducci et al., Opt.Comm. **81**, 379 (1991).

[5] O. Kocharovskaya, P. Mandel, and Y. V. Radeonychev, Phys. Rev. A, **45**, 1997 (1992).

[6] Y. Zhu, Phys. Rev. A, **45**, R6149 (1992).

[7] G. Grynberg and C. Cohen - Tannoudji, Opt. Comm. **96**, 150 (1993).

[8] G. A. Wilson, K. K. Meduri, P.B. Sellin, and T. W. Mossberg, Phys. Rev. A, **50**, 3394 (1994).

[9] Gautam Vemuri, K. V. Vasavada, and G. S. Agarwal, Pys. Rev. A, **52**, 3288 (1995).

[10] Yang Zhao, Danhong Huang, and Cunkai Wu, J. Opt. Soc. Am. B **13**, 1614 (1996).

[11] N. A. Ansari and A. H. Toor, Journal of modern optics 1996, Vol. **43**, No. 12, 2425 - 2435

[12] Y. Zhu, phys. Rev. A, **53**, 2742 (1996).

[13] G. Grynberg, M. Pinard, and P. Mandel, Phys. Rev. A, **54**, 776 (1996).

[14] Gautam Vemuri and G. S. Agrawal, Phys. Rev. A, **53**, 1060 (1996).

[15] Shi - Yao Zhu, De - Zhong Wang, and Jin - Yue Gau, phys. Rev. A, **55**, 1339 (1997).

[16] Jacob B. Khurgn, and Emmanuel Rosencher, J. Opt.Soc. Am. B **14**, 1249 (1997).

[17] J. L. Cohen and P. R. Berman, Phys. Rev. A, **55**, 3900 (1997).

[18] A. S. Zibrov et al., Phys. Rev. Lett. **75**, 1499 (1995).

[19] Y. Zhu, and J. Lin, phys. Rev. A, **53**, 1767 (1996).

[20] Gautam Vemuri, G. S. Agarwal, and B. D. Nageswara, Phys. Rev. A, **54**, 3695 (1996).

[21] P. B. Sellin, G. A. Wilson, K. K. Meduri, and T. W. Mössberg, phys. Rev. A, **54**, 2402 (1996).

[22] Y. Zhu, A. I. Rubiera, and Min Xiao, Phys. Rev. A, **53**, 1065 (1996)

[23] G. S. Agarwal, Phys. Rev. Lett. **67**, 980 (1991)

[24] Clude Cohen-Tanudji, Jacques Dupont-Roc and Gilbert Grynberg in Atom-Photon interactions p. 428 (John Wiley 1992)

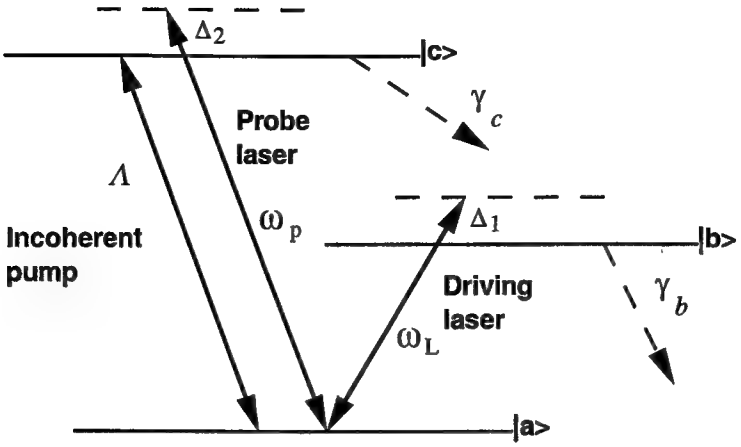

FIG. 1. A three level V - type system for L.W.I

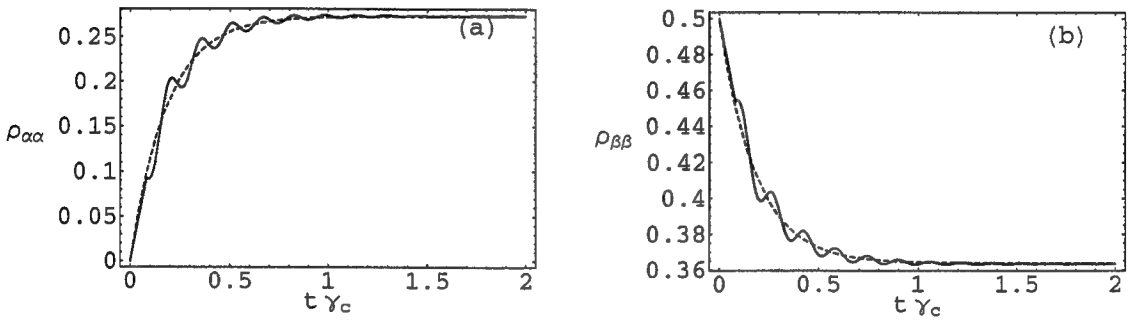

FIG. 2. Normalized time evolution numerical simulation, of dressed state population $\rho_{\alpha\alpha}$ and $\rho_{\beta\beta}$ obtained by solving Eq.s (7a) - (7b) (solid line), and the approximate solution (dashed line). The chosen parameters are: $\Omega = 20\gamma_c$, $\gamma_b = 2\gamma_c$, $G = 0.1\gamma_c$, $\Lambda = 3\gamma_c$

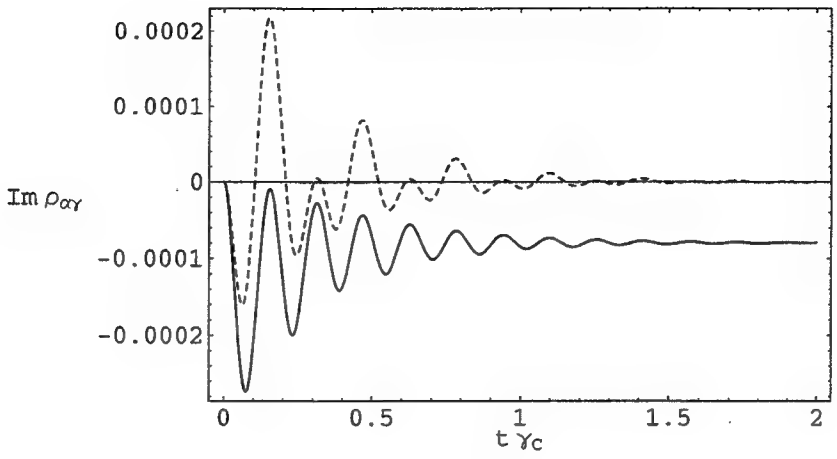

FIG. 3. Normalized time evolution numerical simulation, of dressed state coherenece $\rho_{\alpha\gamma}$ obtained by solving the full set of density matrix equations in the dressed state basis (solid line), and the approximate solution (dashed line) . The chosen parameters are the same as in Fig 2

Generation of non-classical light by electron beams

V. V. Kulagin[a] and V. A. Cherepenin[b]

[a]Sternberg Astronomical Institute, Moscow State University,
Universitetsky prospect 13, 119899, Moscow, Russia

[b]Institute of Radioengineering and Electronics RAS, Mohovaya 18, 103907, Moscow, Russia

ABSTRACT

A process of non-classical (squeezed) light generation by electron beam in a field of a strong external electromagnetic wave is considered. Each electron move in such field along the figure of eight therefore in the direction of the wave vector there is an oscillations of electrons position with a double frequency of the wave. For input noises a degenerate parametric regime is realized therefore a state of an output field can be squeezed. A squeezing coefficient is estimated and for a large amplitude of the input field it can be considerable.

Keywords: Squeezed states of light, free electron systems

1. INTRODUCTION

Nonclassical states of light were generated in experiment more than ten years ago[1–4] but hitherto the experimental squeezing coefficients were modest - about several units. At the same time applications of non-classical light seem to be very promising. Thus, for example in experiments with probe bodies specifically in gravitational wave experiments the sensitivity of installation to external classical force can be considerably increased if the squeezed light is used for the pumping[5–7] . Generally a gain in sensitivity can be proportional to the squeezing coefficient of the input light.

Usually different optical nonlinearities are used for generation of non-classical light and the more the efficiency of nonlinear process the more the squeezing coefficient of the output light. Therefore for example a quadratic nonlinearity is more preferable than a cubic one generally speaking. The most popular processes for generation of an electromagnetic wave in non-classical state are a parametric amplification (a second order nonlinearity) and a four wave mixing (a third order nonlinearity). However a dissipation decreases the squeezing coefficient. As a rule if nonlinear coefficient is large then dissipation is also large and for regimes with small dissipation nonlinear coefficient is modest. That is why a search for physical processes with large nonlinearity and small dissipation at the same time is very important.

The systems with free electrons can be very perspective for squeezed states generation because of small dissipation and high nonlinearity of electron medium. Modern methods of creation of high density electron beams and a possibility to tune the appropriate regime by changing a velocity of electrons give an expectation that a highly squeezed electromagnetic wave can be generated in the electron medium.

In Ref. 8,9 the possibility of squeezed states generation during the process of light reflection from a system of successive free electron mirrors was demonstrated. This process of squeezing is equivalent to the cubic nonlinearity and the bandwidth of squeezing is not large enough. In this paper an analog of degenerate parametric amplification for electron medium is considered.

Other author information:
V.V.K.: E-mail: kul@sai.msu.su
V.A.C.: E-mail: cher@cplire.ru

2. CUBIC OPTICAL NONLINEARITY IN ELECTRON MEDIUM

One of the possible squeezing mechanism in electron medium[8,9] utilizes the fact that under an action of a power electromagnetic wave an electron mirror have a displacement and the greater the amplitude of the wave the greater the displacement of the mirror. Therefore in an output of the system there is a correlation of an amplitude and a phase of reflected wave and consequently this wave is in a squeezed state[10] (an analogous mechanism for resonator with a moving mirror was considered in Ref. 11).

Let a mirror is formed from free electrons and have a thickness l and a constant density of electrons N inside. Then for effective index of refraction one has[12]

$$n = 1 - \omega_c^2/(2\omega_0)^2, \tag{1}$$

where characteristic frequency is $\omega_c^2 = 4\pi Ne^2/m$ (e and m are the charge and the mass of an electron), ω_0 is a frequency of an incident wave. Optimizing the thickness of electron mirror so as to obtain a maximal modulus of amplitude reflection coefficient r_1 of the mirror one has[8]

$$\begin{aligned} r_1 &= (1-n^2)/(1+n^2), \\ t_1 &= 2ni/(1+n^2), \end{aligned} \tag{2}$$

where t_1 is the amplitude transmission coefficient. The thickness of an electron mirror is defined according to the following equation

$$\sin(2nl\omega_0/c) = 0; \qquad l = \lambda_0/4 + m\lambda_0/2; \qquad m = 0, 1, 2 \ldots \tag{3}$$

For optical frequencies one can use a quasi-monochromatic approximation[10] for an incident field E_i from a left side of the mirror and a reflected field E_r

$$\begin{aligned} E_i &= (A + a_1) \cdot \cos\omega_0(t - z/c) + a_2 \cdot \sin\omega_0(t - z/c), \\ E_r &= (B + b_1) \cdot \cos\omega_0(t + z/c) + b_2 \cdot \sin\omega_0(t + z/c), \end{aligned} \tag{4}$$

where A and B are mean amplitude values of incident and reflected pump wave, a_1, a_2, b_1 and b_2 are operators of quadrature components. Then for b_1 and b_2 one has the following equations:

$$\begin{aligned} b_1(\omega) &= r_1 a_1(\omega) - \mid t_1 \mid d_2(\omega), \\ b_2(\omega) &= r_1(a_2(\omega) + 2\omega_0 X(\omega) A/c) + \mid t_1 \mid d_1(\omega), \end{aligned} \tag{5}$$

where d_1 and d_2 are operators of quadrature components of the field in vacuum state which falls on the mirror from the back side (from the right), X is an operator of the coordinate of the mirror (in the reference system where the average speed of electrons is zero). For correlation matrix of spectral densities of a_1 and a_2 one has[10] (we suppose this wave in coherent state)

$$\begin{aligned} < a_1^+(\omega)a_1(\omega') + a_1(\omega')a_1^+(\omega) > /2 &= < a_2^+(\omega)a_2(\omega') + a_2(\omega')a_2^+(\omega) > /2 = N_0\delta(\omega - \omega'), \\ < a_1(\omega')a_2(\omega) > &= < a_1^+(\omega')a_2(\omega) > \approx 0, \end{aligned} \tag{6}$$

where $N_0 = \pi\hbar\omega_0/(cS)$ is a spectral density of vacuum fluctuations, S is a cross section of the laser beam. The correlation matrix of spectral densities of quadratures d_1 and d_2 also satisfies Eq. (6).

In the linear approximation a fluctuating component of a radiation pressure force acting on the mirror due to the incident wave is the following

$$F_p = Sr_1^2 Aa_1/(2\pi). \tag{7}$$

Then for the coordinate of the mirror $X(\omega)$ one can obtain the following expression

$$X(\omega) = -SAr_1^2 a(\omega)/(2\pi M\omega^2), \tag{8}$$

where M is a whole mass of the electron mirror.

Then for the quadratures of the reflected wave one has from Eqs. (5) and (8)

$$\begin{aligned} b_1(\omega) &= r_1 a_1(\omega) - \mid t_1 \mid d_2(\omega), \\ b_2(\omega) &= r_1(a_2(\omega) + \rho(\omega)a_1(\omega)) + \mid t_1 \mid d_1(\omega). \end{aligned} \tag{9}$$

Here the coefficient $\rho(\omega)$ defines a value of correlation of quadrature components in the output wave and has the following form

$$\rho(\omega) = -S\omega_0 A^2 r_1^2/(\pi c M\omega^2) = -8\omega_0 W r_1^2/(Mc^2\omega^2) \tag{10}$$

and W is the power of a laser emiting the incident wave.

For the correlation matrix of quadratures spectral densities for reflected wave one can obtain the following expression according to (9)

$$\begin{aligned} <\mid b_1(\omega) \mid^2> &= N_0, \\ <\mid b_2(\omega) \mid^2> &= N_0(1 + r_1^2 \mid \rho(\omega) \mid^2), \\ < b_1(\omega) b_2^\dagger(\omega) > &= < b_1^\dagger(\omega) b_2(\omega) >^* = N_0 r_1^2 \rho^*(\omega). \end{aligned} \tag{11}$$

Introducing the new quadrature components "rotated" by an angle ϕ with respect to the old quadratures

$$E_r = (B_1 + \tilde{b}_1) \cdot \cos(\omega_0(t + x/c) + \phi) + (B_2 + \tilde{b}_2) \cdot \sin(\omega_0(t + x/c) + \phi) \tag{12}$$

and choosing the phase ϕ so as to maximize the spectral density of for example $\tilde{b}_2$ and minimize of $\tilde{b}_1$, one can obtain from Eqs. (6), (9) and (10):

$$\begin{aligned} <\mid \tilde{b}_1(\omega) \mid^2> &= (1 - r_1^2\rho^2((1 + 4/\rho^2)^{1/2} - 1)/2) \cdot N_0, \\ <\mid \tilde{b}_2(\omega) \mid^2> &= (1 + r_1^2\rho^2((1 + 4/\rho^2)^{1/2} + 1)/2) \cdot N_0. \end{aligned} \tag{13}$$

Therefore the spectral density of the quadrature $\tilde{b}_1$ is smaller than the spectral density of the quadrature component in the vacuum state N_0, and $\tilde{b}_2$ is larger, i.e. the reflected wave is in the squeezed state.

The optimal phase ϕ is defined by an expression

$$tg2\phi = 2\rho(\omega). \tag{14}$$

According to this expression the optimal phase is different for different frequencies therefore one cannot optimize the phase ϕ for considerable frequency band.

The squeezing coefficient g one can define as the ratio of spectral densities for quadrature component of the field in coherent and squeezed states. Then for a value of g one has in this case:

$$g = (1 - r_1^2\rho^2((1 + 4/\rho^2)^{1/2} - 1)/2)^{-1}. \tag{15}$$

Because of a very small electron mass the whole mass of the mirror M can be very small for the thickness l about $\lambda/4$. Therefore the value ρ can be large even for moderate power W of the pumping laser. In this limit for the squeezing coefficient one can obtain

$$g_{\max} = (1 - r_1^2 + r_1^2/\rho^2)^{-1}. \tag{16}$$

Therefore for the small value of r_1 the squeezing $g_{\max}$ is about unity. This means that the vacuum fluctuations from the back (right-hand) side of the mirror admix to the reflected wave and destroy the squeezing of it. The lower the reflection coefficient, the more the vacuum fluctuations pass through the mirror and the weaker the squeezing of the reflected wave. Unfortunately for one electron mirror the value of r_1 is considerably smaller than unity.

To increase the reflection coefficient of the electron medium one has to use several electron mirrors placed one after another[8] at a certain distance L. If the value L is choosen accordingly to the wavelength of the light then this system will reflect the incident electromagnetic wave resonantly. In this case the whole reflection coefficient of composite electron mirror can be about unity for sufficient number of layers and the vacuum fluctuations cannot degrade the squeezing. Optimal period of layers is

$$L = \lambda_0/2 + m\lambda_0/2; \qquad m = 0, 1, 2 \ldots \tag{17}$$

It is necessary to emphasize that the small bandwidth of squeezing is the main shortcoming of this mechanism.

3. QUADRATIC OPTICAL NONLINEARITY IN ELECTRON MEDIUM

Let consider now another nonlinear effect in electron medium. Usual model of a degenerate parametric amplifier is an oscillator with a resonant frequency modulated in time according to the following expression:

$$\omega(t) = \omega_0(1 + \zeta \cos 2\omega_0 t)$$

and ζ is the modulation index.

Each electron in nonrelativistic limit moves in the field of a strong electromagnetic wave along the figure of eight. Actually, for the field $E_x = E_0 \sin\omega_0(t - z/c)$ the component of electron momentum along the x direction for not very large amplitude E_0 will be in the lowest order of V/c

$$p_x = -eE_0/\omega_0 \cdot \cos\omega_0 t,$$

therefore for the z-component of velocity and coordinate $Z(t)$ of the electron one can obtain the following expressions

$$\begin{aligned} V_z &= e^2E_0^2/(4m^2c\omega_0^2)\cos 2\omega_0 t, \\ Z(t) &= Z_0 \sin 2\omega_0 t = e^2E_0^2/(8m^2c\omega_0^3)\sin 2\omega_0 t. \end{aligned} \tag{18}$$

Thus all electrons in the electron mirror move synchronously according to Eqs. (18) (of course the phase of the pumping field E_x is different for the electrons at the front end of the mirror and at the back end therefore there is a phase shift between the displacements of such electrons but for small mirror thickness this phase shift can be neglected). Then the whole mirror will move also according to Eqs. (18) and for the reflection of the incident electromagnetic wave the parametric regime takes place.

Let use again a layer of free electrons with the thickness l and the constant density of electrons N inside for the model of electron mirror. Let the mirror oscillate with amplitude Z_0 in the z-direction with the double frequency of the incident wave which falls perpendicular to the mirror plate. To calculate correctly the statistics of the reflected

wave one have to use the quantum description for the field while for the electrons motion one can use the classical description. Let also suppose that $V_z \ll c$ that implies the inequality $Z_0 \ll \lambda_0$.

There are four waves involved in the process of reflection in this model: first of all these are the incident wave and the reflected wave with frequency ω_0 then it is the transmitted wave from the other side of the mirror also with frequency ω_0 and at last it is the incident wave with the frequency $3\omega_0$ which through the nonlinear interaction is transformed to the frequency band of interest around ω_0. Let consider at first only the waves with frequency ω_0.

For the mirror alone (without resonator) the equations of motion will be algebraic. Taking into account the inequality $V_z/c \ll 1$ ($Z_0 \ll \lambda_0$) one can obtain for the reflected wave with a mean amplitude B and the quadrature components b_1 and b_2 the following equations:

$$\begin{aligned}(B + b_1 + ib_2)\exp(-i\omega_0 t) + \text{ h.c.} &= [r_1(E_0 + a_1 + ia_2)\exp(-i\omega_0 t) + \text{h.c.}] \\ &- [r_1(2V_z(t)/c)(E_0 + a_1 + ia_2)\exp(-i\omega_0 t) + \text{ h.c.}] \\ &- [r_1(2i\omega_0 Z(t)/c)(E_0 + a_1 + ia_2)\exp(-i\omega_0 t) + \text{ h.c.}] \\ &+ [t_1(d_1 + id_2)\exp(-i\omega_0 t) + \text{ h.c.}].\end{aligned} \tag{19}$$

In this expression d_1 and d_2 are the quadrature components of the wave transmitted from the other side of the mirror. This wave is supposed to be in vacuum state with correlation matrix of spectral densities defined according to Eq. (6). The correlation matrix of spectral densities of qudrature components a_1 and a_2 is also defined by Eq. (6).

All terms in right hand side of Eq. (19) have a clear physical meaning. The term in first square brackets is simply the wave reflected from the motionless mirror with reflection coefficient r_1. The term in second square brackets represents the amplitude modulation of the reflected wave due to the amplitude Dopler transformations for the field. The third square brackets term represents the phase modulation of the reflected wave because the phase of the reflected light depends on the position of the mirror (frequency Dopler transformations for the field). The term in fourth square brackets is the wave transmitting through the other side of the mirror.

From Eq. (19) one can obtain a transformation matrix for the quadrature components of the reflected wave

$$\begin{aligned}b_1 &= r_1 a_1 - \nu r_1 a_2 - \mid t_1 \mid d_2, \\ b_2 &= r_1 a_2 - \nu r_1 a_1 + \mid t_1 \mid d_1.\end{aligned} \tag{20}$$

In this equation a parameter ν have the following value

$$\nu = e^2 E_0^2/(8m^2c^2\omega_0^2) \tag{21}$$

and it is considerably smaller than unity acoording to inequality $V_z/c \ll 1$ ($Z_0 \ll \lambda_0$).

One can conclude from Eqs. (20) that the quadrature components of the reflected wave are correlated. Introducing the shifted quadratures according to the Eq. (12) it is easily to obtain for the spectral density of one quadrature component (for example $\tilde{b}_1$) the following expression:

$$<\mid \tilde{b}_1(\omega) \mid^2> = (1 - 2\nu r_1 + \nu^2 r_1^2) \cdot N_0. \tag{22}$$

The minimal value of $<\mid \tilde{b}_1(\omega) \mid^2>$ will be if the reflection coefficient r_1 is close to unity. This condition corresponds to the same optimization as in Eq. (3). Then the spectral density of "quiet" quadrature component is proportional to $(1-\nu)^2$ and the larger the value of ν the smaller the noise spectral density. However the expression (22) is valid only for the small values of parameter ν therefore in the case of ν close to unity one have to take more terms in the decomposition of the exponent in Eq. (19) (take into account the higher nonlinearities in the system) and besides use the relativistic equations for the electron motion.

Equations (19) and (22) were obtained without accounting the transformations of noise from the incident wave with frequency $3\omega_0$ to the output wave. But because of the nonlinear interaction these fluctuations can admix to the reflected wave and degrade the squeezing.

4. TRANSFORMATION OF THE $3\omega_0$ INPUT FLUCTUATIONS IN THE SYSTEM

For the process of reflection of the electromagnetic wave with frequency ω_0 from the mirror oscillating with frequency $2\omega_0$ the lowest order nonlinearity is quadratic. Then the input fluctuations with frequency $3\omega_0$ can be included into the output field through the nonlinear interaction with the movement of the mirror: the product of $2\omega_0$ oscillating term and $3\omega_0$ oscillating term have in the output the ω_o oscillating term (cf. Eq. (19)). To take into account the input fluctuations with central frequency $3\omega_0$ one have to include the following term into the right hand side of Eq. (19):

$$-r_3(2V_z(t)/c + 2i\omega_0 Z(t)/c)(c_1 + ic_2)\exp(-i3\omega_0 t) + \text{ h.c.}, \tag{23}$$

where r_3 is the reflection coefficient of the electron mirror for the incident wave with frequency $3\omega_0$, c_1 and c_2 are the quadrature components of the input mode with central frequency $3\omega_0$. These quadratures satisfy the Eqs. (3) with obvious change of N_0 to $3N_0$. From Eqs. (1) and (2) one can conclude that the reflection coefficient r_3 is nine times less than the reflection coefficient r_1 : $r_3 = r_1/9$.

From Eqs. (19) and (23) one can obtain now the following transformation matrix for the quadrature components of the reflected wave

$$\begin{aligned} b_1 &= r_1 a_1 - \nu r_1 a_2 - \mid t_1 \mid d_2 - r_3 \nu c_2, \\ b_2 &= r_1 a_2 - \nu r_1 a_1 + \mid t_1 \mid d_1 + r_3 \nu c_1 \end{aligned} \tag{24}$$

For the spectral density of the quadrature component $\tilde{b}_1$ one has the following expression:

$$<\mid \tilde{b}_1(\omega) \mid^2> = (1 - 2\nu r_1 + \nu^2 r_1^2 + \nu^2 r_1^2/27) \cdot N_0 \tag{25}$$

and in the limit when r_1 tends to unity and ν tends to unity the minimal spectral density of quadrature component $\tilde{b}_1$ is limited by the value $N_0/27$ and the maximal squeezing coefficient is not larger than 27.

In optical schemes with resonator the fluctuations with frequency $3\omega_0$ are filtrated by the properties of the resonator mirrors (the reflection coefficient of the mirrors near the frequency ω_0 is about unity while this coefficient near the frequency $3\omega_0$ is very small) therefore the effective field of $3\omega_0$ fluctuations interacting with the mirrors is very small. This effect can be utilized also for the electron mirror. Actually one have to adjust the thickness of electron mirror in such a way that the reflection coefficient near the frequency ω_0 will be maximal while near the frequency $3\omega_0$ it will be about zero. For this condition the thickness l of electron mirror must have the following value

$$l_{\text{opt}} = \lambda_0/6. \tag{26}$$

Then in the output of the system (in reflected wave) the fluctuations with frequency $3\omega_0$ will interfere destructively and the reflection coefficient of the mirror for the frequency ω_0 will be only slightly decreased:

$$r_1 = ((3)^{1/2}/2)\exp(-i\pi/6) \cdot (r_1)_{\max}. \tag{27}$$

The squeezing coefficient is defined in this case by the following expression (cf. Eq. (25)):

$$g = (1 - 2\nu r_1 + \nu^2 r_1^2)^{-1}. \tag{28}$$

The squeezing coefficient g is maximal for large value of the reflection coefficient r_1. In experiment this condition means that the concentration of electrons in the electron medium must be high - about the value for metals. This kind of medium can be obtained for example by the evaporation of the matter surface by the power short light pulse.[13] The alternative approach is to use an electron beam with considerably small concentration of electrons. This beam have to be bunched in a certain way so that a system of consecutive electron mirrors will be formed. The

thickness of each mirror have to be defined by the expression (26) and the period of bunching have to be defined by Eq. (17). In this case the squeezing coefficient is defined from Eq. (28) by the following expression

$$g_{\max} = (1 - \nu)^{-2} \tag{29}$$

and can in principal be large for the large value of parameter ν.

5. DISCUSSION

The considered mechanism of squeezed state generation can be useful only if the parameter ν will be close to unity. This condition can be met for very high amplitude of the laser light. Such high amplitude can be achieved for ultrashort laser pulses. Actually for input frequency ω_0 from the optical band and cross section of the light beam about 1 mm^2 the required pulsed power of the laser have to be about 10^8 Wt that is considerable easy to obtain in experiment. The excessive noises of laser light and the noises of electron medium have to be considered in more details for real experiment.

The most advantage of the considered scheme is that the bandwidth of squeezing is independent of frequency. Actually the phase shift is independent of frequency from Eqs. (24) therefore one can adjust this phase shift for considerable frequency bandwidth (the limitation will originate from the effects that are not considered in the model used such as dispersion, higher orders of nonlinearity etc.).

REFERENCES

1. H. P. Yuen, "Two-photon coherent states of the radiation field", *Phys. Rev.* **A13**, pp. 2226-2243, 1976.
2. D. F. Walls, "Squeezed states of light", *Nature (L)* **306**, pp. 141-146, 1983.
3. R. E. Slusher, L. W. Hollberg, B. Yurke, J. C. Mertz, and J. F. Valley, "Observation of squeezed states generated by four-wave mixing in an optical cavity", *Phys. Rev. Lett.* **55**, pp. 2409-2412, 1986.
4. R. Paschotta, M. Collett, P. Kurz, K. Fiedler, H. A. Bachor, and J. Mlynek, "Bright squeezed light from a singly resonant frequency doubler", *Phys. Rev. Lett.* **72**, pp. 3807-3810, 1994.
5. V. B. Braginsky, Yu. I. Vorontsov, K. S. Thorne, "Quantum nondemolition measurements", *Science* **209**, pp. 547-557, 1980.
6. C. M. Caves, K. S. Thorne, R. W. P. Drever, V. D. Sandberg and M. Zimmerman, "On the measurement of a week classical force coupled to a quantum-mechanical oscillator", *Rev. Mod. Phys.* **52**, pp. 341-392, 1980.
7. V. V. Kulagin, V. N. Rudenko, "Non-demolition measurement in the systems with spectral squeezing of vacuum fluctuations", *Sov. Phys. JETP* **67**, pp. 677-687, 1988.
8. V. V. Kulagin, V. A. Cherepenin, "Generation of squeezed states on reflection of light from a system of free electrons", *JETP Lett.* **63**, pp. 170-175, 1996.
9. V. V. Kulagin, V. A. Cherepenin, "Generation of squeezed states of light in the systems of free electrons", *Laser Physics* **7**, pp. 131-134, 1997.
10. C. M. Caves, "Quantum limits of noise in linear amplifiers", *Phys. Rev.* **D26**, pp. 1817-1839, 1982.
11. C. Fabre, M. Pinard, S. Bourzeix, A. Heidmann, E. Giacobino, and S. Reynaud, "Quantum-noise reduction using a cavity with a movable mirror", *Phys. Rev.* **A49**, pp. 1337-1343, 1994.
12. M. Born, E. Wolf, *Principles of Optics*, p. 490, Pergamon Press, New York-London, 1968.
13. R. V. Volkov, V. M. Gordienko, M. S. Dzhidzhoev, M. A. Zhukov, "Control of the properties and diagnostics of a dense femtosecond plasma from modified targets", *Sov. Phys. Quantum Electronics* **24**, pp. 1114-1126, 1997.

SESSION 5

Quantum Nucleonics

Critical analysis of the experiments on the search for induced γ-emission from long-living isomeric states of ^{123m}Te and ^{125m}Te

Andrey V.Davydov
Institute of Theoretical and Experimental Physics,
117259 Moscow, Russia

ABSTRACT

The published experimental works are analyzed in details in which announcements were made of the observation of some effects which might be associated with the phenomenon of induced γ-emission . It is shown that practically in all cases the obtaining of experimental data was accompanied by circumstances which made difficult to interprete them as the indications of the induced γ-emission effect. The exclusion is one of the experiments by S.I.Bondarevskii's group in which they observed a decay acceleration of the ^{123m}Te γ-source cooled down to the liquid helium temperature as compared with decay of other similar γ-source situated at room temperature. However the small magnitude of the observed effect and absence of control measurements require careful repetition of this experiment.

Keywords: Tellurium, isomer, γ-rays, Mössbauer effect, induced γ-emission

1. PREFACE

In 1965 Bulgarian physisists P.Kamenov and Ts.Bonchev proposed to observe the induced γ-emission[1] using as a working media the long-living nuclear isomers with decay scheme like that of ^{125m}Te. On the Fig.1 the decay schemes are shown for two tellurium isomers, ^{123m}Te and ^{125m}Te ; the experiments with these isomers will be discussed below. The proposition[1] is at first sight very attractive. The large life time of the isomer permits to accumulate the excited nuclei in considerable concentration. Fast decay of the intermediate nuclear states, to which the isomeric transitions occurs, corresponds to relatively large width of this level and, therefore, to the broad γ-line emitted in the isomeric transition because the width of this γ-line is determined by the sum of the widths of upper and lower nuclear states[2]. Low energies of emitted photons (88.47 keV for ^{123m}Te and 109.27 for ^{125m}Te) permit to hope to have the relatively high values of the recoilless emission probabilities; large width of γ-line gives a possibility to escape an additional line broadening connected with hyperfine interactions in the gamma source material. Afterwards Bulgarian physicists have published many papers on the theoretical basing of their proposal and we'll refer here

Further author information -
E-mail: davydov@vxitep.itep.ru
Telephone: 7 095 125 94 85; Fax: 7 095 883 96 01

SPIE Vol. 3685 • 0277-786X/99/$10.00

to two more recent of those[3,4], where the interested persons could find the references to the rest of their publications.

Not discussing here the theoretical aspects of this problem which are considered in the works by P.Kamenov et al. and in the series of the papers by B.E.Dzevitskii and G.A.Skorobogatov (the corresponding references may be found in[10–12] and[14]), note that by the generally accepted ideas[5] the ratio of the isomeric state radiative width to the total width of the γ-spectrum emitted in the isomeric transitions must be included as a multiplier into the expression for the cross section of the induced γ-emission process. In the cases of tellurium isomers this ratio is so low that the very process becomes nonobservable.

In the beginning of 80-ths G.A.Skorobogatov and B.E.Dzevitskii in Russia shown the interest in this problem and published in 1984 the paper[6] with the data about an observation of the intensity increase of γ-ray emission with energy of 109.27 keV after cooling the spherical γ-source made of beryllium telluride from room temperature to 77 K. The authors ascribed this effect to the appearance of induced γ-emission when Mössbauer conditions were created in the γ-source after its cooling. Discussing this work (still before its publication in the open printing) with author of present paper G.A. Skorobogatov was told that such interpretation of the observed effect is unconvincing because it might be caused by rather small deformation of the cryostat when being cooled by liquid nitrogen. No control measurements were performed by authors of[6]. It was recommended to G.A.Skorobogatov to change the method and to begin to search for the pairs of photons created in the acts of induced γ-emission (the primary photon and the induced one). These two photons, as we imagined, must be emitted in the same direction and incident simultaneously on the detector creating in it the signal of doubled energy of isomeric transition. Some time later the circumstances turned out in such manner that the collaboration springed up of ITEP scientific group under leadership of the author of present paper and G.A.Skorobogatov and B.E.Dzevitskii to perform the experinent on the search for the pairs of γ-quanta, which, as we assumed, must be emitted after cooling down of the γ-source with sufficient concentration of ^{125m}Te nuclei.

The results of first two experiments performed in the frames of this collaboration (S.K.Godovikov and V.V.Metlushko from Moscow State University took part in the second experiment) were published in[7] and[8]. In both experiments the data were obtained which, as it would seem, shown the appearance of the "double energy peak" ("DEP") in the γ-spectrum of ^{125m}Te after the cooling of the γ-source made of beryllium telluride from room temperature to 4.2 K. However, as it will be shown below, the appearance of this peak was accompanied by some circumstances which did not permit to ascribe it unambiguously to the induced γ-emission process. In the large number of later experiments performed with more perfect apparatus the "double energy peak" were not revealed not once.

In 1989 ITEP group in collaboration with physisists from Moscow State University,

I.V.Kurchatov Atomic Energy Institute and V.G.Khlopin Radium Institute performed the analogous experiment[9] with γ-rays of long-living isomer ^{119m}Sn which decays like ^{125m}Te . The "DEP" was not found in this experiment also, though ^{119m}Sn is a better nuclide for such experiment by its Mössbauer properties as compared with ^{125m}Te .

Then, after the interval of some years, three publications appeared by G.A.Skorobogatov and B.E.Dzevitskii[10–12] in which it was announced again about observation of "DEPs" in the case of ^{125m}Te and of some analogous effects in the case of ^{123m}Te . These papers caused some animation in the scientific circles having an interest in the problem of induced γ-emission. As a result one more experiment was performed in Los Alamos[13] which did not show the presence of wanted effect.

Recently the paper was published by S.I.Bondarevskii et al.[14] in which the results were described of the experiments performed during several years with tellurium and tin isomers. Authors state that they observed steadily the effects which may be connected with induced γ-emission process. Unfortunately the experimental material is expounded too laconically, the descriptions are absent of some important sides of the observed facts. Moreover, there are no figures with measured γ-spectra in the paper, and this all makes it difficult to estimate the work objectively.

We'll try below to analyze in details each experiment performed with tellurium isomers which has shown, as it would seem, the presence of the induced γ-emission. We'll show that in every work the detection of the effects similar to those which might be connected with induced γ-emission process is accompanied by some circumstances which make difficult such interpretation of these effects or exclude the possibility of such interpretation at all.

2. FIRST EXPERIMENT BY B.E.DZEVITSKII AND G.A.SKOROBOGATOV

In this work[6] the γ-source was a sphere of TeBe alloy (95 % ^{124}Te) with diameter of 1.9 mm and mass of 35 mg, which was irradiated during 60 days by thermal neutrons in the flux with density of 1.2×10^{13} cm^{-2}s^{-1} . Let pay attention at once on the funny circumstance: with these dimension and mass the density of the γ-source must be equal to $\sim$ 9.75 g/cm^3 ; however the tabular[15] value of beryllium telluride density equals to 5,09 g/cm^3.

Using the modern data[16] about cross section of ^{125m}Te isomer production in the (n,γ)-reaction (1.12 $\pm$ 0.07 b) one obtains that to the end of the reactor irradiation this γ-source contained 2.14×10^{14} mg^{-1} nuclei of ^{125}Te in the isomeric state. This corresponds to the concentration of these nuclei, ν_{is}, which is equal to 1.09×10^{18} cm^{-3}. After the cooling of the γ-source from room temperature to 78 K the authors have detected the increase of the counting rate by 1.2 $\pm$ 0.1 % as compared with foregoing measurement at room temperature. So far as the time of 84 hours passed between the starts of two measurements and the activity of γ-source decreased via the natural decay of isomeric state, the measured change of the counting rate must correspond to the increase of the γ-emission

intensity by 5.30 ± 0.44 % (authors of[6] give 5.3 ± 0.3 %). Is it possible to connect this large change of γ-ray intensity with induced γ-emission process at aboveindicated concentration of isomeric nuclei in the γ-source material?

The situation is intensified by the fact that only recoilless part of emitted γ-quanta is able to participate in the induced γ-emission process. The probability of recoilless emission f of γ-quantum with energy of 109.27 keV at 78 K in assumption that Debye temperature of TeBe is about 400 K equals to 0.063. If the observed by the authors of[6] increase of the counting rate is really connected with this part of γ-spectrum then the increase of this part intensity would be equal not to 5.3 % now but to 85.5 % !

To determine the upper limit of induced γ-emission cross section on which the authors of[6] could hope on the ground of their formula for radiative width of isomeric level (f-la (8) in[6] which they proposed without demonstration), we shall use the formula for this cross section given in the review[5] (C15, p.725). For monochromatic γ-quanta with energy corresponding to the center of the resonance the cross section is equal to:

$$\sigma(E_{res}) = \frac{\lambda^2}{2\pi} \cdot \frac{\Gamma_r}{\Gamma} \cdot f. \tag{1}$$

Here λ - wave length of γ-radiation, Γ_r - radiative width of isomeric level, Γ - total width of γ-spectrum

The averaging of (1) over the γ-spectrum of Lorentzian form leads to decrease of cross section by two times.

According to[5] the radiative width Γ_r in the case of ^{125m}Te must be accepted as $1/(\tau_{up} \times (1+\alpha_{up}))$. However if one follows[6] then one must accept for Γ_r the expression:

$$\Gamma_r = \frac{1}{(1+\alpha_{up})\tau_{up}} + \frac{1}{(1+\alpha_\ell)\tau_\ell}, \tag{2}$$

and for Γ, correspondingly, the formula:

$$\Gamma = \frac{1}{\tau_{up}} + \frac{1}{\tau_\ell}. \tag{3}$$

In these formulas τ_{up} and τ_ℓ - mean life times of nucleus in the upper and lower nuclear excited states between which the isomeric transition takes place; α_{up} and α_ℓ - total coefficients of inner conversion for isomeric transition and for the following transition to the nuclear ground state correspondingly.

Taking into account that $\tau_{up} >> \tau_\ell$ one obtains from (2) and (3):

$$\frac{\Gamma_r}{\Gamma} = \frac{1}{(1+\alpha_\ell)}, \tag{4}$$

and

$$\Gamma_{ind.} = \frac{\lambda^2}{4\pi} \cdot \frac{f}{(1+\alpha_\ell)}. \tag{5}$$

In the case of ^{125m}Te formula (5) leads to the cross section value:

$$\sigma_{ind.} = 4,8 \times 10^{-22} cm^2. \qquad (6)$$

Mean γ-ray path ℓ in the source is equal by the author's of[6] estimate to 0.0713 cm. If one accept for tellurium density the tabular value 5,09 g/cm^3 then, in the case of source mass equal to 35 mg, this dimension must be increased to 0.0886 cm. It follows from this that the intensity I_γ of Mössbauer part of γ-spectrum emitted by cooled γ-source is increased as compared with intensity I_0 at room temperature in the ratio:

$$\frac{I_\gamma}{I_0} = exp(\sigma_{ind.} \times \nu_{is.} \times \ell) = exp(4,8 \times 10^{-22} \times \nu_{is.} \times \ell) = 1,0000458. \qquad (7)$$

For total γ-intensity the addition equals to 2.9×10^{-6}.

Therefore the observed by the authors of[6] increase of the intensity of γ-quanta registered by detector and connected with cooling of γ-source can not by no means be ascribed to the induced γ-emission process even if one accept for Γ_r the aboveindicated expression (2) from the paper[6].

Note in passing that the paper[6] contains some obviously incorrect statements. So on the first page it is written that the width of Mössbauer γ-line is determined "only by radiative width of nuclear level", although the width of this line coincides in reality with total width of excited nuclear state (in the absence of inhomogenous broadening). The author's reasonings are also incorrect about considering of γ-line broadening connected with excitation and absorption of phonons as homogenous one.

3. THE EXPERIMENTS BY ITEP GROUP.

In the first experiment by this group [7] the γ-source was used of beryllium telluride fabricated by alloying of Te and Be powders in the quartz ampoule at 1100 °C . The shot created inside the ampoule had a view of metallic ignot of oblong form. This sample was irradiated by thermal neutrons in the reactor. After the irradiation the ampoule tail with TeBe ignot was cut and the butt-end of the cut was effaced by hardening cryostable glue VT-200. In such state the γ-source was placed into the cryostat where it was possible to cool it to liquid helium temperature. Two Ge-detectors were used in the experiment, one of which detected the γ-rays emitted in the direction of the long γ-source axis, and the second - in the perpendicular direction. At the beginning the γ-spectra were measured at room temperature during 3 hours each run being of 15 min duration. Then the cryostat was filled by liquid helium and the weak peak appeared near 218.54 keV in the γ-spectrum measured in the direction of long γ-source axis. On the Fig.2 the fragments of summary γ-spectra are shown and the magnitude of the effect is seen. Such peak was not observed in the limits of errors in the spectrum measured at angle 90° with respect to the source axis. One couldn't ascribe the appearance of "DEP" to the chance pile-up pulses corresponding

to the total absorption peak of 109.27 keV γ-rays, as it was done in[17]. The intensity of the pile-up pulse spectrum (in which "DEP" takes the small part of its total area[20]) must grow as a square of the counting rate of single energy pulses. However in our case this counting rate decreased in the transition from room temperature to 4.2 K. This was connected probably with a compression of the γ-source material owing to its cooling.

"DEP" was being observed in 15 spectra measured during 15 min each, that is about 4 hours, and then disappeared. That time we ascribed this disappearance to the decomposition of nonpersistent beryllium telluride under the chemical influence of the glue which was used to seal the γ-source container. Really, when the quartz ampoule was cut some time later, the powder was found in it of dark, almost black colour, instead of metallic ignot.

The experiment[8] by ITEP group was performed under some better background conditions than[7] because γ-source was transferred after the irradiation into the nonactive ampoule. The observation of wanted effect in this experiment was accompanied by strange circumstances. The peak sought for appeared after cooling of the source not at the double energy of isomeric transition but about 20 keV lower and it was moving gradually in time to the 218.54 keV point and it was fixed at that point at last. This movement of "DEP" observed in one of the experiments is shown on the Fig.3. In the series of experiments which were being performed during one week "DEP" was moving in opposite direction when the cryostat was being warmed up and disappeared. There were some measurements however when this peak stayed on his place after warming up of the cryostat. This obviously gave evidence that "DEP" was not of Mössbauer origin. This looked as if we had to do with some apparatus effect simulating the wanted phenomenon. When we changed the electronic equipment and began with using of more perfect amplitude analyzer Nokia LP 4900B, we did not observe "DEP" in no one of numerous experiments. It was assumed that the observed hitherto effect might be connected with a rise of some parasitic ways in the binary structure of previously used analyzer (AI-1024) after its warming up, in which the forming of double pulse amplitudes could take place with low probability. Note that in both ITEP experiments the observed magnitude of "DEP" was too large as compared with that which one could expect basing on even the maximal possible cross section of induced γ-emission. The described circumstances lead us to the decision not to publish these doubtful results in scientific journals. So the only publications of these data are two short abstracts of our reports at XXXVII Conference on nuclear spectroscopy and atomic nucleus structure in Jurmala (Latvia) in 1987[8,18]. At the same time we couldn't state categorically (and we can not do it now) that our latter experiments proved the impossibility of the observation of the induced γ-emission in the experiments with ^{125m}Te , because the γ-sources used in these experiments were made by the technology which slightly differed as compared with that used in our first works. Namely, the annealing temperature at which TeBe alloy was being synthesized was decreased in last experiments from 1100 ^{0}C to 900 ^{0}C. The X-ray structure

analysis of obtained samples shown that they are of cubic lattice with interatomic distance equal to the value typical for beryllium telluride. The signes of presence of free beryllium and tellurium were not found. However it was not possible by means of such analysis to reveal the presence of amorphous tellurium which did not reacted with beryllium. Henceforth we performed the measurements[19] of Mössbauer factor f for γ-rays ^{125}Te with energy of 35.5 keV in the TeBe samples obtained at the annealing temperature of 900 ^{0}C . It was found that this factor corresponds to Debye temperature Θ_D = 206,5 $\pm$ 5,0 K (after correction - 209 $\pm$ 5 K) in contradiction with expected value of $\sim$ 400 K. If the chemical compound of Te and Be which was synthesized at 900 ^{0}C had such low Debye temperature then we couldn't see "DEP" in the limits of our experimental errors. So far as the X-ray structure analysis shown that the main phase of obtained compound was however the beryllium telluride, the low value of Θ_D might be connected with a presence of nonreacted amorphous tellurium which Debye temperature was not larger than 150-160 K. The estimation of relative part of this admixture based on assumption of Θ_D (TeBe) = 400 K gave the value of 30 %. If one assume that namely such favorable conditions took place in our first experiments then in the last ones we could observe the "DEP" of 4/9 area as compared with the data of first experiment. However we did not see even the traces of "DEP". Therefore the situation was unclear and demanded the further study.

4. THE PUBLICATIONS BY G.A.SKOROBOGATOV AND B.E.DZEVITSKII 1996-1997

The attentive reading of these works[10–12] causes a perplexity and formes a paintful impression at last. Let begin from the indication that the papers[10,11] which were published practically simultaneously in two different journals almost totally coincides textually but have different titles. Although the phenomenon discussed in both papers is the same, it is called in one paper[10], as far as one could judge basing on the title, as "collective nuclear superradiation", and in the second paper[11] - as "induced emission of Mössbauer radiation". Evidently these two phenomena are quite different.

It was indicated in the description of the experiment with ^{125m}Te that Ge(Li)-detector was used with resolving power of 0.6 keV in the energy range from 10 to 300 keV. However Ge(Li)-detectors with such properties do not exist. It is possible to fabricate germanium detector, for example, of high purity germanium, which would have a resolution at 10 keV energy much better than 0.6 keV. However at 300 keV even such good detector would have a resolution more than 1 keV. Commercial Ge(Li)-detectors used in Russia are not sensitive to γ-rays of such low energy as 10 keV at all because they have thick "dead" layer on their surface. Note at last that one can see from Fig.2 of[10,11] that the resolution of the detector was not better than $\sim$ 4 keV.

Authors of[10,11] state that under the conditions of their experiment, when the counting rate in the channel of analyzer corresponding to γ-ray energy of 109 keV was equal to 3800 pulse/s (this means that in full photopeak shown on Fig.2 of[10,11] the

counting rate was not lower than 15000 pulse/s) the probability of chance simultaneous detection of two photons was not larger than 10^{-7} per s. Author of the present paper, having large experience of work with analyzer Nokia LP 4900B and being one of coauthors of paper[20] related to study of forming process of the pile-up pulse spectrum in the circuitry of the semiconductor γ-ray detector, may state that under the conditions described in[10,11] total counting rate of pile-up pulses must not be lower than 0.03 of the counting rate corresponding to the photopeak area of 109.27 keV γ-line, that is about 450 pulse/s. Note that we never exceeded in our own experiments the total counting rate about 1000 pulse/s.

At last the main thing: the fragments of γ-spectra shown in[10,11] on Fig.2 and corresponding to the measurements at room temperature and at 4-10 K (sic) are not the results of a new experiment performed by authors of[10,11] as one could think reading the titles of these papers ("New observations..." and so on). They were borrowed from the afore-mentioned work of ITEP group[8] performed in collaborarion with G.A.Skorobogatov and B.E.Dzevitskii. In our short publication[8] the same fragments of γ-spectra were presented corresponding to the "DEP" region. However the correlation of the scales along the coordinate axes was other as compared with that of[10,11] (and therefore with that of original ITEP report from which it was transferred to[10,11]). So at first sight the pictures seem differently (See Fig.4a). On the Fig.4b,c both pair of fragments are shown in the same scales. It is possible to make certain of full identity of the data published in[8] and as if new results presented in[10,11]. It means that authors of[10,11] tried to present the old and very doubtful results as a new sensational ones.

Further reading of[10,11] in its part concerned to the experiments with ^{123m}Te leads to the sad conclusions also. Authors wrote that they observed in the ^{123m}Te γ-spectrum after the cooling of γ-source the increase of the counting rate in the energy region corresponding to the simultaneous hits to the detector of two γ-quanta with energy 88.46 keV (from primary and induced isomeric transitions) and one photon of 159 keV (from the transition to the ground state after the isomeric transition). It is not clear why the authors refused to detect the "DEP" (2×88,46 кэВ). Their statement that the background in this area was as if high contradicts to the data of our own experiments with ^{123m}Te (unpublished) in which we tried to detect the "DEP" but unsuccessfully. The background near 177 keV was sufficiently low. It is written in[10,11] that a γ-source was used with activity of 0.40 ± 0.08 Curies of ^{123m}Te . This corresponds to $\sim 1{,}5\times10^{10}$ Bq. The counting rate did not exceed 10^5 s^{-1}. Therefore the geometrical factor together with detector efficiency was not larger than $\sim 0{,}84\times10^{-5}$. Under these conditions the counting rate of chance triple events caused by simultaneous detection of 3 γ-quanta with energy 159 keV would be about 3000 s^{-1}, if one works with amplitude analyzer Nokia LP 4900 (as authors of[10,11] did) which does not permit to obtain the resolving time lower than 1 mcs. Amplitude spectrum of these chance triple pile-up pulses must stretch from a point located some higher than 159 keV up to 477 keV, corresponding to the data of[20], that

is in the energy range of $\sim$ 318 keV. So the background counting rate in the energy interval of 1 keV must be equal to $\sim$ 9.4 s^{-1}. It is stated in[10,11] that 12 channels of analyzer was assigned to search for a peak corresponding to simultaneous detection of three afore-mentioned quanta, that is a peak with energy position of 336 keV. It is seen from Fig.2 of[10,11] that these 12 channels corresponds roughly speaking to the width of a γ-line 109.27 keV at its base. From the same Fig.2 one can obtain the energy equivalent of 12-channel interval - $\sim$ 18.4 keV. In this energy interval the background counting rate caused only by chance triple pile-up pulses of 159 γ-rays must be equal to $\sim$ 170 s^{-1} or $\sim$ 14 s^{-1} channel $^{-1}$. However authors of[10,11] give for total background counting rate the value of 0.6 s^{-1}. This disagrees with the rest of their own data about experimental conditions. As a matter of fact the contradiction lies much deeper between the initial conditions of the experiment described in[10,11] and the results which authors as if obtained. They note that the detected part of the events like γ(88 keV) + γ(88 kev) + γ(159 kev) equals to $\sim$ 0.0016 of the total number of the 88 keV γ-quantum pairs produced via the induced emission process. This part may be presented as

$$0,0016 = \Omega^2 \times \epsilon^2(88) \times \epsilon(159). \qquad (8)$$

Here Ω - relative solid angle from the gamma-source to the detector, ϵ(88) and ϵ(159) - the detection efficiencies for γ-rays of 88.46 and 159 keV correspondingly. Authors of[10,11] do not distinguish ϵ(88) from ϵ(159) and speak about rather incomprehensive efficiency which is larger than 0.5. Let ϵ(88) be 0.9, then ϵ(159) would be equal to 0.27. We have then from (6): Ω=0.0728. In this case the counting rate of single pulses of 159 keV must be equal to $\sim 2.4\times10^8$ s^{-1} (!) for indicated γ source activity. If one accept a value 0.5 for ϵ(88) than this counting rate would be equal to $\sim 3.3\times10^7$ s^{-1} . The analyzer Nokia LP 4900 can not work at such large counting rates. It is seen that author's statement that counting rate did not exceed 10^5 s^{-1} does not pack with their own initial data. Therefore one can not consider the data presented in[10,11] as the scientific results deserving any attention.

Now let turn to the last publication by G.A,Skorobogatov and B.E.Dzevitskii[12]. The text following the declarative introduction repeats with insignificant variations the content of [10,11] and include the same absurd statements about properties of used Ge(Li)-detector, the level of counting rate of chance pile-up pulses etc. On the figure presented in[12] (See Fig.4d) which shows the γ-spectrum of $Be^{125m}Te$ source measured at 4-10 K the total absorption peak of 109.27 keV γ-line is taken wholly from the spectra presented in[10,11] (that is from the report of ITEP group at Jurmala Conference 1987). The second peak on the same drawing of[12], that is "DEP", did not figure in[10,11]. It is depicted by obviously other "handwriting" and by no means it couldn't appear in such position as result of real measurement. Indeed, as the experiments by ITEP group [8] and recent measurements by Los Alamos group[13] show, there is a significant pedestal in the γ-ray spectra from ^{125m}Te γ-sources in the region of 218 keV - the wide distribution of pulse amplitudes caused apparently

by higher energy γ-lines of other tellurium isotopes, of some impurities and by outer background. So "DEP', if it is really detected, must lie on this pedestal, not on the abscissa axis*) as it is shown in[12].

One is forced therefore to recognize that γ-spectrum shown on the Fig.1 of[12] couldn't be considered as result of any new measurement performed by authors of[12].

All our notes relating to connected with ^{123m}Te parts of[10,11] remain valid and in respect of[12]. The situation is somewhat intensified by authors's note that they used detector BDRK which, as they stated, had an efficiency equal to 0.5. However BDRK is made of silicium not of germanium. Its working volume has a thickness less than 5 mm. Such detector would have an efficiency for 88 keV γ-rays not larger than 0.2 and for 159 keV quanta - < 0.15. It must be added that the overwhelming part of γ-ray interactions with silicium at indicated energies takes place via the Compton scattering, not through the photoeffect. Composing the description of their experiment with ^{123m}Te authors forgot that they already used the BDRK detector in their work[6] and just in connection with its low efficiency. Summing up this section note that in no one work by G.A.Skorobogatov and B.E.Dzevitskii (including[6]) relating to the experiments with ^{123m}Te and ^{125m}Te any proofs were obtained of the possibility to observe the induced γ-emission by these isomers. More of that, the serious doubts arise about real performance of experiments[10–12].

5. THE EXPERIMENTS BY S.I.BONDAREVSKII'S GROUP

We had in our disposal only one publication by this group[14] related to description of the experiments with ^{123m}Te and ^{119m}Sn . Unfortunately many sides of the experiments are described insufficiently clear in the text of this paper. Moreover the illustrations are absent, in particular, γ-spectra are not shown measured at different temperatures. One may notice the series of contradictions between some experimental results described in[14].

Relatively low γ-ray energy of isomeric transition in ^{123m}Te (E_{is} = 88.46 keV) permits to perform the experiments at liquid nitrogen temperature and this possibility lightens the work and reduces its price. One may divide the experiments of[14] in two parts: a) the traditional searches for γ-lines with energies which are the multiples of the isomeric transition energy, and b) the original experiments on the comparison of the halflives of two γ-sources one of which is situated at 77 K and the other - at room temperature.

Authors write in particular about the first group of the experiments: "Depending on the experimental conditions the increases of pulse counting rate of the working samples γ-radiation were observed in wide energy range in different regions of amplitu-

*) "DEP" could be placed in the position shown on the drawing of[12] if the aforementioned pedestal would be subtracted from the corresponding region of γ-spectrum. However nothing is said about such procedure in[12].

de spectrum, and, in the first place, in those corresponding to the energies which were the multiples of the resonant transition energy". One may realized from this that the "increases of counting rates" took place also in the spectrum areas not coincided with multiple values of the isomeric transition energy E_{is}. One may ask how could the induced γ-emission process stimulate the appearance of these increases in such regions of the spectra? Further, it is written that in the experiment with ^{119m}Sn the weak but highly broadened γ-line was revealed in the energy near $2E_{is}$. According to our conceptions "DEP" must not be broadened; one may rather expect a lower relative width of "DEP" as compared with that of the single photon γ-line because the number of the carriers in the semiconductor detector become larger in the case of "DEP' detection. Both these circumstances, evidently contradicting to the conception of the effects related to the induced γ-emission, are not commented in[14]. Authors write also without sufficient explanations about their observations of the influences on the effects being measured of such factors as the chemical composition, geometrical form and linear dimensions of γ-sources, the type and the volume of the detector, the presence of the X-ray filter - even not describing the very essence of the effects observed when the corresponding experimental conditions were changed. The number of important detailes is only briefly mentioned in the paper without presentation of any illustrative material.

Authors give two examples of their experiments one of which relates to the traditional version of a work with tellurium isomers. The integral numbers of counts were measured in the spectrum regions corresponding to the γ-ray energies near $3E_{is}$, $4E_{is}$ and to the various combinations of the isomeric and the following transition energies. Authors found in the spectrum area near $\sim 4E_{is}$ the increase of the counting rate by 22 ± 7 % when the γ-source was cooled from 300 to 80 K. It is not clear what was the subject relatively which these 22 % were given. Are they given with regard to the sum of a background and the part of the γ-spectrum connected with a contribution of high energy γ-lines or to the pure γ-spectrum? It would be correct to calculate this increase relatively to the single photon counting rate. Note that in the case of a detection of an induced γ-emission by the observation of the $4E_{is}$ peak, the peaks must be observed also of much larger intensities in the areas near $3E_{is}$ and $2E_{is}$. Taking into account the detector efficiency (0.7 in[14]) one obtains yet the doubling of a $2E_{is}$ peak as compared with that of $4E_{is}$. However the probability of the creation of induced photon (which is much lower than 1) must play more important role (this probability is small even if one accept as correct the authors's hypothesis about large value of a radiative width of the isomeric state). However authors of[14] say nothing about the appearance of counting rate increase near $2E_{is}$ and $3E_{is}$ with more intensive peaks than that at $4E_{is}$.

Then the authors write about use of ^{123m}Te 159 keV γ-line of the transition to the ground state after the isomeric transition as a reper. They state that its intensity kept constant with 0.2 % accuracy when γ-source was cooled from 300 to 80 K.

However this line can not serve as a reper because its intensity must change when the conditions appear for induced γ-emission (each isomeric transition, primary and induced, must be followed by the transition to the ground state with energy 159 keV). Authors of[14] would be able to detect this change if the rest of effects was really connected with induced γ-emission. One had to determine for this goal the necessary level of precision, and this may be done knowing the relative amplitude of the $4E_{is}$ peak and the detector efficiency.

On the strength of these contradictions the results of[14] related to the traditional method of work with ^{123m}Te can not be recognized as convincing ones. It is possible that we could come to other conclusion having in our disposal the illustrative material (γ-spectra) and more detailed description of very experiments.

The second example, presented by authors of[14] is much more interesting. Authors compared during a long time (150 days) γ-activities of two sources which were situated at different temperatures: 80 and 300 K. They found that to the end of the 159-day period of keeping the sources under these conditions the difference arose between the source activities equal to 0.30 ± 0.06 %; that is the cooled γ-source decayed quicker than the warm source. It must be so, in particular, if the conditions exist in the cooled source permitting to the induced γ-emission to take place. Authors concluded that their measurements proved the presence of such conditions.

Note that there is a point of view[21] (not indiscutable) that induced photon must not be emitted without fail just in the moment of the primary photon action on the nucleus in the excited state. According to[21] it may be emitted much more later on the scale of the mean life time of excited nuclear state. If it is so then the simultaneous hit of two photons bound by process of induced γ-emission on the detector is very improbable. Therefore the performance of the experiments on the determination of isomeric state halflives is very interesting because the results wouldn't depend on the time intervals between the hits of the primary and induced γ-quanta on the detector.

6. CONCLUSION

Thus we see that the results of almost all works in which it was announced about observation of the induced γ-emission in the sources fabricated of nuclear isomers like ^{125m}Te , either contain obvious contradictions, or rough errors (as in[6]), either they were obtained by the way which can not be considered as scientific one.The only exclusion is the experiment by S.I.Bondarevskii's group on the observation of a difference between the halflives of cold and warm γ-sources. However the small value of the found effect requires the performance of additional experiments and careful control measurements. Note that one can determine the decay constant of isomer instead of long measurements of halflives, measuring the yield of X-rays or comparing the counting rates from two sources situated at different temperatures. The results of all versions of experiment must have the same relative value.

7. ACKNOWLEDGEMENTS

Author thank Dr. Yu.N.Isaev for his help in the work under this paper.

8. REFERENCES

1. P.Kamenov and T.Bonchev, "Induced radiation of gamma quanta and two-photon photoeffect", *Compt. Rend. de l'Academie Bulgare des Sciences*, T.18, N 12, p.1103-1106, 1965.
2. W.Weisskopf and E.Wigner, "Berechnung der natürlichen Linienbreite auf Grund der Diracschen Lichttheorie", *Z. Phys.*, v.63, N 1, p.54-73, 1930.
3. P.S.Kamenov, A.Petrakiev and A.Apostolov, "Cross sections for stimulated transisions of gamma quanta applications",*Nucl. Instr. and Meth.*, v.**A353**, p.615-618, 1994.
4. P.S.Kamenov, A.Petrakiev and A.Apostolov, "Simultaneous Mössbauer experiments and gamma laser emission",*Nucl. Instr. and Meth.*, v.**A353**, p.623-626, 1994.
5. G.C.Baldwin, J.C.Solem and V.I.Goldanskii, "Approaches to the development of gamma-ray lasers", *Rev. Mod. Phys.*, v.53, N 4, Part 1, p.687-744, 1981.
6. G.A.Skorobogatov and B.E.Dzevitskii, "Partial radiactive width of nuclear emission lines and new possibilities in nuclear γ-resonance", *Izvestiya AN SSSR, ser. phys.*, v. 48, N 10, p. 1934-1939, 1984.
7. V.G.Alpatov, G.E.Bizina, A.V.Davydov et al., "Observation of $(\gamma\ ,\ 2\gamma)$-reaction on the nuclei of long-living isomer ^{125m}Te",*Izvestiya AN SSSR, ser. phys.*, v.50, N 10, p. 2013-2015, 1986.
8. V.G.Alpatov, G.E.Bizina, S.C.Godovikov et al., "New data on the course of the $(\gamma\ ,\ 2\gamma)$-reaction on ^{125m}Te nuclei", *Report Abstracts of XXXVII Conference on nuclear spectroscopy and structure of atomic nucleus, Jurmala (Latvia), 1987,* "Nauka", Leningrad Division, p. 224, 1987.
9. V.G.Alpatov, A.A.Antipov, G.E.Bizina et al., "Search for the lines of combined energies in γ-spectrum of ^{119m}Sn", *Izvestiya AN SSSR, ser. phys.*, v.53, N 10, p. 2052-2054, 1989.
10. G.A.Skorobogatov and B.E.Dzevitskii, "New observations of collective nuclear superradiation in the isomeric transitions ^{125m2}Te $\rightarrow$ ^{125m1}Te + h ν (109,3 keV) and ^{123m2}Te $\rightarrow$ ^{123m1}Te + h ν (88,46 keV)", *Laser Physics*, v.5, N 2, p.258-267, 1995.
11. G.A.Skorobogatov and B.E.Dzevitskii, "New observations of stimulated emission of Mössbauer radiation in the isomeric transisions ^{125m2}Te $\rightarrow$ ^{125m1}Te + h ν (109,3 keV) and ^{123m2}Te $\rightarrow$ ^{123m1}Te + h ν (88,46 keV)", *Nuovo Cim.*, v.**17D**, N 6, p.609-626, 1995.

12. G.A.Skorobogatov and B.E.Dzevitskii, "Collective polynuclear superradiance emission of Mössbauer radiation from ^{125m2}Te and ^{123m2}Te", *Hyperf. Interact.*, v.107, p.401-411, 1997.
13. R.S.Rundberg, M.M.Fowler, R.D.Taylor and J.B.Wilhelmy, "Cross section for the stimulated emission of 109.28 keV gamma rays from ^{125m}Te ", *Technical Digest for First Intern. Induced Gamma Emission Workshop (IGE-97), Predeal, Romania, 1997*, RC-IGE Foundation, Bucharest-Magurele, Romania, p.107-108, 1997.
14. S.I.Bondarevskii, B.E.Dzevitskii and V.V.Yerjomin, "Observation of nuclear gamma resonance at the induced gamma emission on M4-type transitions of long-lived nuclear isomers", *Proc. Intern. Conf. on Lasers'96, Portland, USA, 1996*, STS Press, McLean, VA., USA, p.261-265, 1997.
15. D.M.Chizjikov and V.P.Schastlivyi, *Tellurium and tellurides*, "Nauka", Moscow, 1966.
16. V.G.Alpatov, A.V.Davydov, G.R.Kartashov et al., "Production of long-living tellurium isomers in (n,γ)-reactions", *Physics of Atomic Nuclei*, v.58, N 1, p. 13-19, 1995. (Russian version: *Yadernaya Fizika*, v.58, N 1, p. 15-22, 1995.).
17. G.C.Baldwin and J.C.Solem, "The futility of observing stimulated gamma-ray emission from a long-lived isomeric state", *Nuovo Cim.*, v.**16D**, N 6, p.627-630, 1994.
18. V.G.Alpatov, G.E.Bizina, S.C.Godovikov et al., "Movement of a "double energy peak" in the gamma spectrum of ^{125m}Te", *Report Abstracts of XXXVII Conference on nuclear spectroscopy and structure of atomic nucleus, Jurmala (Latvia), 1987*, "Nauka", Leningrad Division, p. 242, 1987.
19. V.G.Alpatov, A.V.Davydov, Yu.N.Isaev et al., "Measurement of the Mössbauer factor f for ^{125}Te γ-rays in beryllium telluride", *Technical Digest for First Intern. Induced Gamma Emission Workshop (IGE-97), Predeal, Romania, 1997*, RC-IGE Foundation, Bucharest-Magurele, Romania, 1997, p.45-46.
20. A.V.Davydov, M.M.Korotkov and A.A.Sadovskii, "Forming of the pile-up pulse amplitude spectrum in the circuitry of semiconductor γ-spectrometer", *Izmeritel'naya Tehnika*, N 6, p.63-66, 1993.
21. J.C.Solem and G.C.Baldwin, "Time dependence in stimulated gamma-ray emission: implications for GRASERs", *Nuovo Cimento*, v.**17D**, N 10, p. 1131-1138, 1995.

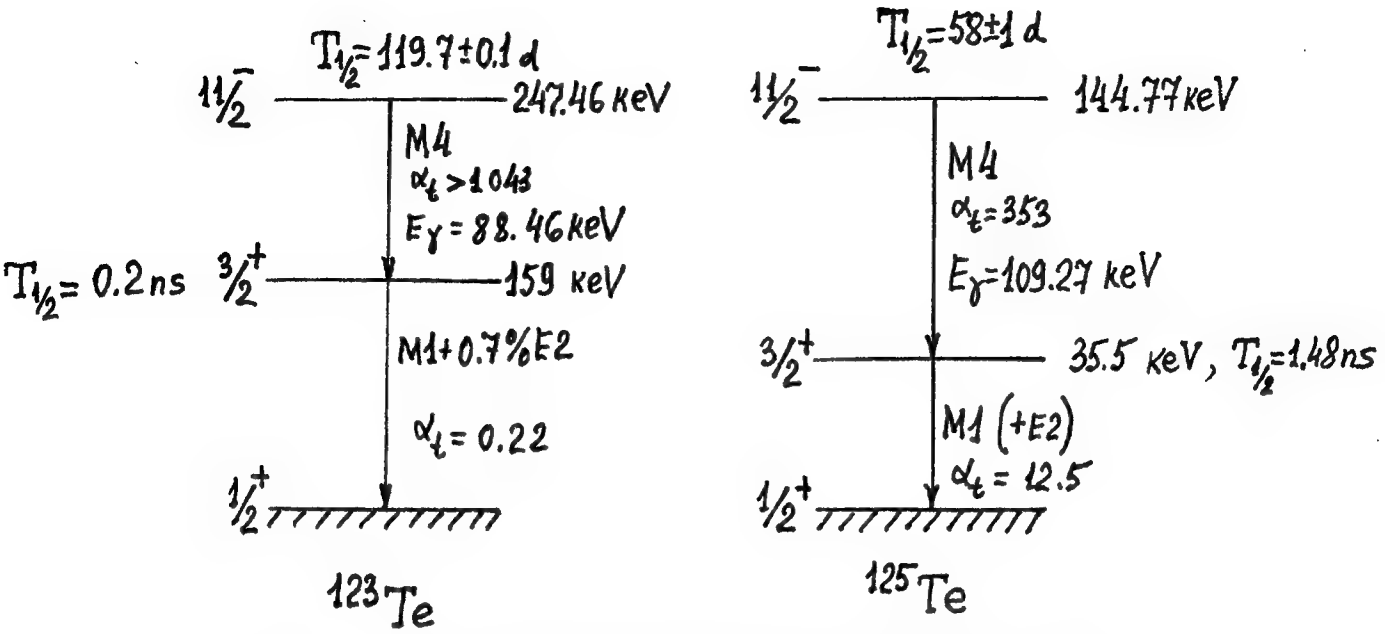

Fig.1. Decay schemes of long-living ^{123m}Te and ^{125m}Te isomers

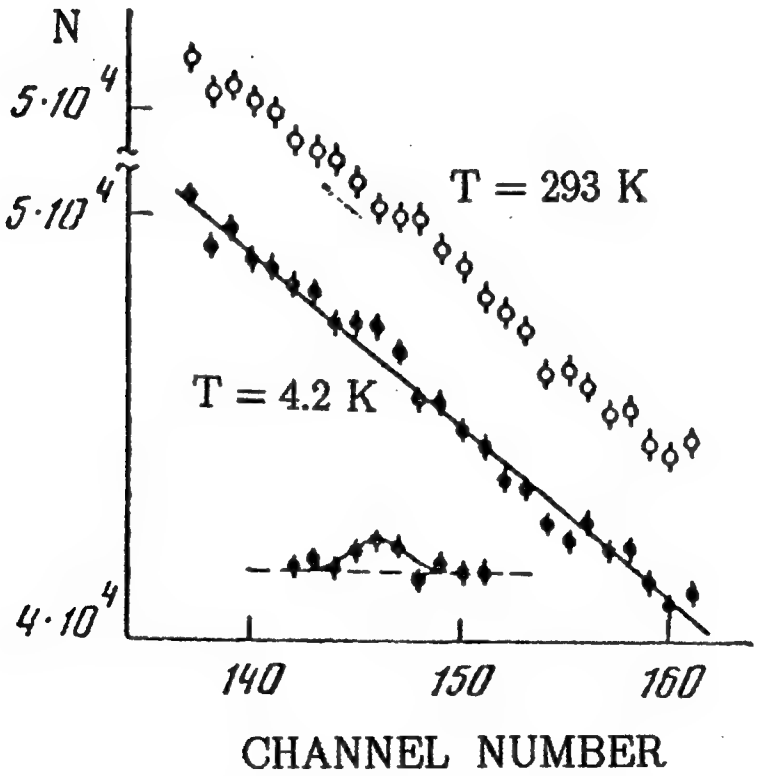

Fig.2. Results of first experiment of ITEP group on the search for "double energy peak" in the γ-ray spectrum of ^{125m}TeBe γ-source cooled down from room temperature to 4.2 K.

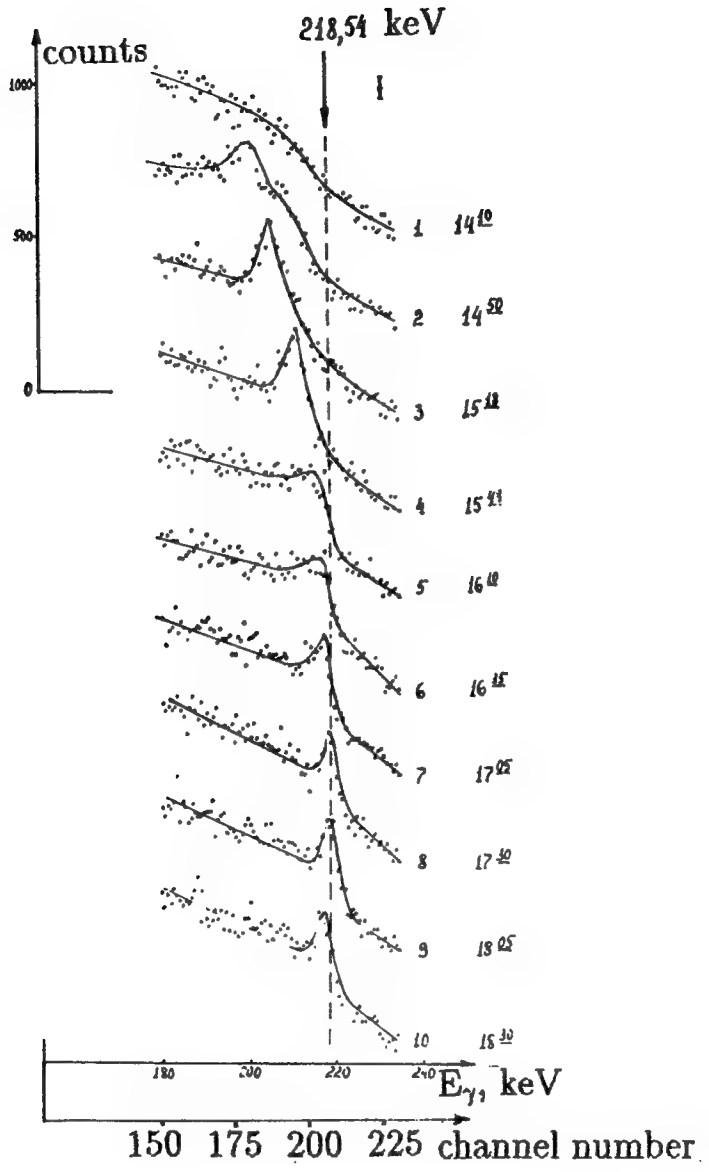

Fig.3. Movement of "double energy peak" found in the second set of ITEP experiments. The successive spectra were measured during 15 min each.

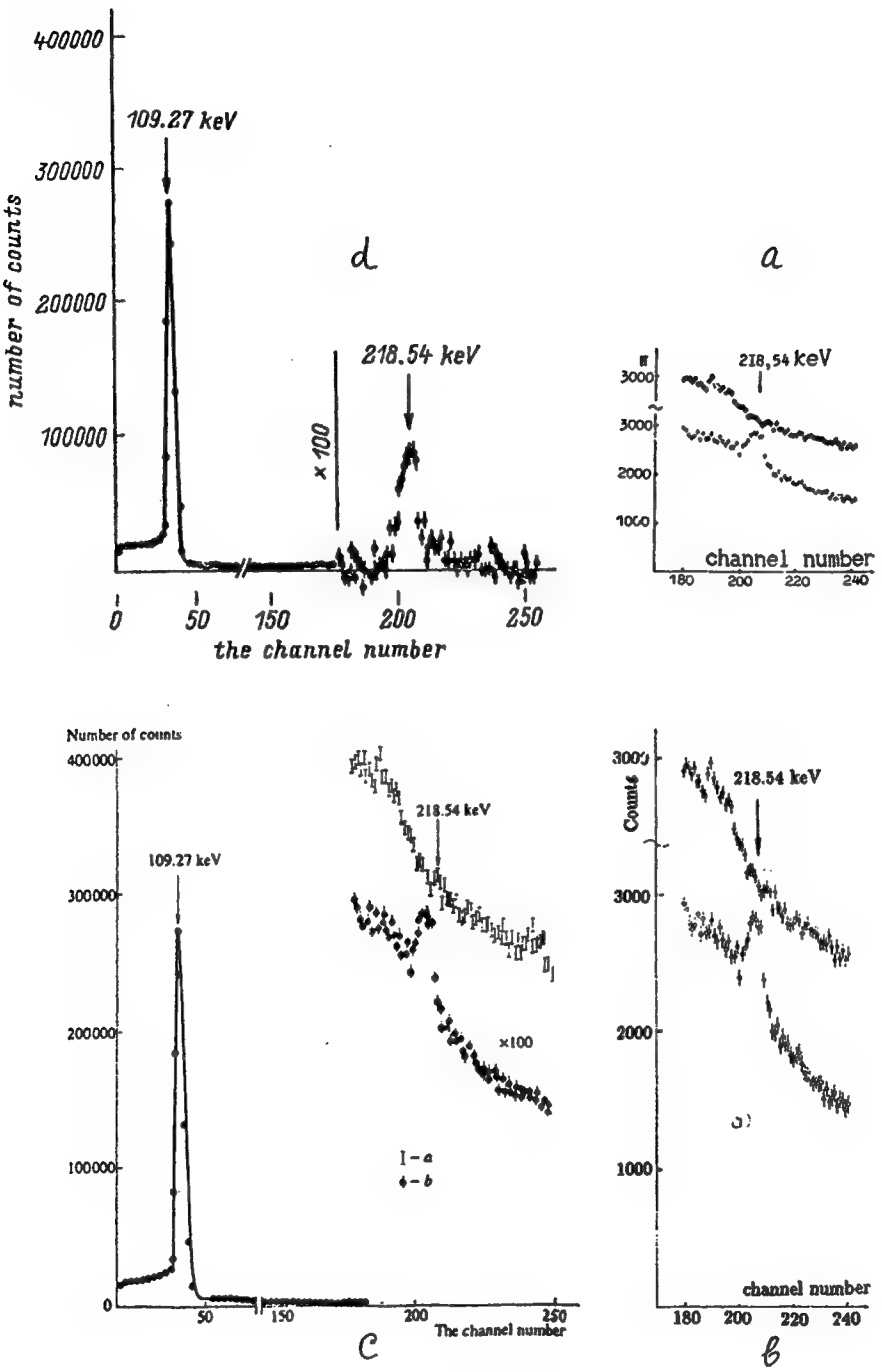

Fig.4. "a": The fragments of γ-spectra detected in the experiments by ITEP group[8] and shown in the scales along coordinate axes, which were accepted in this publication.
"b": The same spectra shown in the scales along coordinate axes accepted in paper[10].
"c": The fragments of γ-spectra from[10].
"d": Spectra of ^{125m}Te γ-rays presented in paper[12].

Gamma-ray solid laser: amplification without inversion and microplasma of active medium

Some results in substantiation for a feasible γ-lasing experiment

S.V.Karyagin

N.N.Semenov institute of chemical physics, Russian Academy of Sciences (ICP RAS)
Prospect Kosygina 4, Moscow, GSP-1, Russia
e-mail: ANN@agrobio.msk.su , fax: (095)-137-8318; Tel:(095)-939-7265

ABSTRACT

Some results in substantiating for a *feasible γ-lasing experiment* are considered. *Self microplasma (SM) existence* in active medium (AM) is set up. SM-density at other pumping types is more by several orders than one at *soft prompt transplantation of excited nuclei* (SPTEN). Hence schemes of *amplification without inversion* (AWI) are broken down by the SM. Types of *AWI and γ-lasers steady against SM* are revealed. *Distance* L'*-effect* on Moessbauer spectrum and on a γ-lasing is predicted. *Radiation-heat regimes and γ-lasing conditions (induced, super-radiant)* are studied. Difficulties of gas-AM (in beams) are analyzed. *New candidate* ^{58}Co (28.1 KeV, 1.51 10^{-5} s) is suggested. SPTEN efficiency is drastically increased on base of new device, so called "atomic (molecular) multi-beam emitter" (AMMBE) proposed also *for industrial laser isotope separation.*

Keywords: gamma-ray solid laser, cooling of active medium, isomeric transitions, quantum nucleonics, selective resonant pumping, amplification without inversion, Borrmann effect, collapse of Moessbauer spectrum by motion of charged carriers

INTRODUCTION

From early works (1961,Rivlin; 1963,Baldwin et al.) up to nowadays a big world experience in *γ-laser* (GL) is stored. A crisis in GL-problem was happened just before 1980-th: no real nuclei-candidates, "heat death" of GL, etc. That crisis stimulated creation of a hybrid model[1-9] on joint of a row GL-directions adopted with all world GL-experience account. In works[1-9] and here a feasible model of **gamma-ray solid laser** *on short-lived isomers* using a method of so called *soft prompt transplantation of excited nuclei* (**SPTEN**)[3-9] is developed. Active medium (**AM**) is creating during the short time of isomer-implantation with kinetic energy of ions less than 0.5 KeV. So the AM is created with list heating and negligible substrate destruction. Theory and computer simulation show[3,5,6,9,19] that just after such pumping a big density of *excited lasing-active nuclei* (**ELAN**) $n_+ > 10^{21}$cm^{-3}, a high relative population $n_+/n > 0.9$ and more than sufficient amount of ELAN $N_+ = n_+V_{AM} > 10^{13}$ in active medium (AM) of volume $V_{AM} \sim 10^{-8}$cm^3 could be reached. At SPTEN an existence of resolved hyperfine structure (**HFS**) for working transition is not necessary. Moreover, a collapse of HFS (see **1.6**) is beneficial for γ-lasing[1-5,7].

1.1 Candidates for gamma-ray solid laser

This model[1-9] is able to use a plenty of different working nuclei-candidates arisen in many reactions, including photo-processes, non-elastic (e.g., Coulomb) scattering of particles on parent nuclei, non-elastic (e.g., Coulomb) scattering of parent nuclei passed through crystal, particle-exchange, etc. Widely known *nuclide* ^{181}Ta is only the most studied "satisfactory" candidate. However even such candidate answers all *in situ* and *ex situ* demands of a real experiment[3-7].

Here *a new candidate* "^{58}Co" is suggested. In this case a working transition (WT) has energy $E_\gamma = 28.1$ KeV; wave-length $\lambda = 4.41\ 10^{-9}$ cm. Time-life (decaying by factor $e^{-1} = 0.368$) $\tau_1 = 1.51\ 10^{-5}$ s. Internal conversion coefficient $\alpha = 1.5$. In *diamond matrix* (IIa-type) Debye temperature $T_D = 1860$ K. Case of ^{58}Co in diamond is marked as ^{58}Co/Di. At temperatures $T << T_D$ a factor of recoilless emission $f' = 0.86$. Both working levels (WL), upper "+" and lower "-", are excited. Branching ratio of WT is $w = 0.999$. *Adopted here* time-ratio $\tau_1/\tau_2 = 1.1$. A total width of WT $\tau_2^{-1} = \Gamma_{tot}$ is *"effected by distance"*, see **2.1**. Nuclear moments of WL are $j_+ = 4^+$ and $j_- = 5^+$. The time-life of lower WL is $\tau_- = 4.78\ 10^4$ s. The time-life of ground state is $\tau_{gr} = 8.83\ 10^6$ s. The ratio of statistical weights $g = (2j_+ +1)/(2j_-+1) = 9/11 = 0.818$. *Conventional* resonant cross-section (at ratio $\tau_1/\tau_2 = 1$, in a frequency-maximum, without HFS) is $\sigma_0 = 1.1\ 10^{-18}$cm^2. *Conventional* cross-section of resonant self-absorption $\sigma_{sa} = g\,\sigma_0 = 8.75\ 10^{-19}$ cm^2. Cross-section of self non-resonant losses on Co-atoms $\sigma = 1.2\ 10^{-21}$cm^2. Cross-section of non-resonant losses on C-atoms of diamond $\sigma' = 5.63\ 10^{-24}$ cm^2. *Exited laser-active nuclei* (ELAN) ^{58}Co* could be created (as recoiled nuclei) in so called "converters" [3-5], e.g., at reactions ^{58}Ni(n,p)^{58}Co* or ^{59}Co(n,2n)^{58}Co* with cross-section $\sigma^* = (0.5 - 0.8)\ 10^{-24}$ cm^2. Even at such small value of σ^* the SPTEN can fit $N_{max} \sim 10^{13} - 10^{14}$ of ELAN at AM site[3-9]. There are many types of AM-body forms[2]. The simplest one has a quadrate in its cross-section with a side **d**, and a length L. AM has dispersed micro-profile (see **1.4**) with external (visible) volume $d \times d \times L$. Let concentration of working

nuclei (WN) is $n = 9\ 10^{20} cm^{-3}$, its total number $N_o = 2\ 10^{11} << N_{max}$ and content of ELAN at the initial moment is 0.9. Then a length of AM is L = 0.32 cm, $d = 3.8\ 10^{-5}$ cm, and AM gives $2.5\ 10^7$ induced gamma-quanta (see **2.1**). The portion of super-fluorescent gamma-radiation in this case is negligibly small (see **2.2**). The heat release in this AM is

$$q = n E_\gamma \alpha / ((1+\alpha)\, \tau_1) = 1.6\ 10^{11}\ W/cm^3. \quad (1)$$

At these conditions the *self-consistent method* gives the estimation $T_{AM} = 27.3$ K for the *quasi-temperature*[2,4] of AM. Such low temperature is oblige to the fulfillment of the *condition for efficient cooling*

$$\Lambda_e, \Lambda_{ph} >> d. \quad (2)$$

where values Λ_e, Λ_{ph} are the free paths of non-equilibrium electrons and phonons correspondingly. Indeed, for the diamond of II-a type at 27.3 K the free paths are $\Lambda_e = 8.5\ 10^{-4}$ cm = 22.4 d >> d, $\Lambda_{ph} = 0.028$ cm = 737 d >> d.

1.2 Balance energy equations for AM, self-consistent method

Balance energy equations for AM (1983,1995, Karyagin) were derived and used in works[2-5,7]

$$(d/dt)Q_e = q - (\tau_{ep}^{-1} + \tau_e^{-1})Q_e, \quad (3a)$$

$$(d/dt)Q_{ph} = -\tau_{ph}^{-1} Q_{ph} + \tau_{ep}^{-1} Q_e, \quad (3b)$$

$$q = 1.6\ 10^{11} W/cm^3, \tau_e = 3.2\ 10^{-13}\ s, \tau_{ph} = 2\ 10^{-11}\ s, \quad (4)$$

where Q_e is energy-density (ED) of non-equilibrium (NE) charged carriers, Q_{ph} is the ED of NE-phonons; $\tau_e = d/v_e$ is time of free exit of charged NE-carriers from AM; $\tau_{ph} = d/v_s$ is a time of free exit of NE-phonons from AM; $v_e \sim 10^8$ cm/s is a mean velocity of charged NE-carriers with energy ~ 1 – 5 eV. For a diamond of II-a-type[18] sound velocity is $v_s \sim 1.6\ 10^6$ cm/s. Time of electron-phonon relaxation τ_{ep} is found from a trial electron-hole mobility[18] $\mu = e\tau_{ep}/m \sim 1.8\ 10^{15}\tau_{ep}$. Here μ is used in $cm^2V^{-1}s^{-1}$ and τ_{ep} in seconds. The decisions for (3a,b) are (5a,b) or (6a,b), (7) in a stationary limit $t >> \tau_{ep}, \tau_e, \tau_{ph}$:

$$Q_e = (q/(\tau_{ep}^{-1} + \tau_e^{-1}))\,(1 - \exp(-(\tau_{ep}^{-1} + \tau_e^{-1})t)), \quad (5a)$$

$$Q_{ph} = (q\tau_{ph}/(1+(\tau_{ep}/\tau_e)))\,\{1 - \exp(-t/\tau_{ph}) - [[\exp(-t/\tau_{ph}) - \exp(-(\tau_{ep}^{-1} + \tau_e^{-1})t)] / [(\tau_{ep}^{-1} + \tau_e^{-1})\tau_{ph} - 1]]\}, \quad (5b)$$

$$Q_e = q/(\tau_{ep}^{-1} + \tau_e^{-1}), \quad (6a)$$

$$Q_{ph} = q\tau_{ph}/(1 + (\tau_{ep}/\tau_e)). \quad (6b)$$

$$Q_e = 0.051\ J/cm^3, \quad Q_{ph} = 0.012\ J/cm^3. \quad (7)$$

The values (7) are achieved by the *self-consistent method*[2,4,7]. The value τ_{ep} is a function[18] of a quasi-temperature[4] $T = T_{AM}$ which at $T << T_D$ is proportional to $Q_{ph}^{1/4}$ with the factor 82.1 K for diamond[4] (Q_{ph} is taken in J/cm^3):

$$\tau_{ep}(T) = \tau_{ep}(50\ K)\,(50/T)^{1.5} = 3.4\ 10^{-11}(50/T)^{1.5}\ s, \quad (8)$$

$$T = 82.1\ (Q_{ph})^{1/4}. \quad (9)$$

Substitution (8), (9) into (6) gives non-linear equations, which lead to self-consistent results (7) - (10):

$$T = 27.2\ K, \ \tau_{ep} = 8.5\ 10^{-11}\ s \text{ and mobility } \mu = 1.5\ 10^5\ cm^2\ V^{-1}s^{-1}. \quad (10)$$

A more accurate procedure with the self-consistent accounting of non-equilibrium carriers in the rest part (around the AM and further) of previously cooled crystal (T~10K) leads to a more precise estimation of quasi-temperature $T = T_{AM}$ in AM

$$T_{AM} = 27.3\ K. \quad (10a)$$

Good coincidence of results (10) and (10a) shows accuracy of simple equations (3), (3a) when condition (2) is fulfilled. *An active medium of solid cold γ-laser contains a self-microplasma* (1995,Karyagin). The existence of self-microplasma was first predicted and theoretically set up in works[4,7]. A density of charged carriers n_e is set at *energy for the creation of pair of charged carriers* ε_0 (13.3eV = 2.1 10^{-18}J for diamond[18]):

$$n_e = 2\,Q_e/\varepsilon_0 = 4.8\ 10^{16}\ cm^3, \qquad (11)$$

So, it is proved that the gamma-generation is not suppressed by heat *in case of SPTEN*. It is shown[5,7] (also see **1.6**) that **appearance of self-microplasma is beneficient for a gamma-lasing in SPTEN-schemes.**

1.3 Suppression of inhomogeneous Doppler shift in solid AM by a "heat-stress-feedback method"

A *solid* AM differs from active media of other aggregate states by a feasibility of method[1-3] (1980,Karyagin) for the full suppression of the inhomogeneous Doppler shift (IDS). The IDS results from a heat expansion of AM[10] and makes a γ-lasing non-realized. Suggested method[1-3] consists in a preliminary moderate stress (stretch, compression) of AM-body *fasten by the thermostated fixtures.* In such conditions any deviation in forces due to the temperature is exactly compensated by the opposite prompt deviation of fixture stress-reaction. Otherwise, in method[1-3] a deep feedback through the fixture stress-reaction is used. The use of "heat-stress feedback method" in other aggregate states is too problematically.

1.4 Developed oriented (e.g., comb-like) micro-profile (DOCLMP) of AM for effectiveness of all solid γ-laser types

Developed oriented (e.g., comb-like) micro-profile (DOCLMP) of AM was suggested and elaborated[2,3-5,7] (1983, 1995, Karyagin) for the effective cooling of AM. E.g., DOCLMP can be engraved on surface of single-crystal as line row of teeth. Each tooth is characterized by transversal width d , transversal high (or depth) h and longitudinal size (thickness) d_o. A size d_o is measured at half of a high h. Hence the thickness at the bottom (foot) of tooth is $2d_o$. The distance between the tops of two nearby teeth (period of DOCLMP along active medium) is $2d_o$. Fulfill number of teeth is $N_{th}=L/2n_o$. E.g., in considered case (see**1.1**) L= 0.32 cm, d = h = 3.8 10^{-5} cm, $d_o = 10^{-6}$ cm, N_{th} = 1.6 10^5 and a fractality (denticulation) is $h/2d_o$ = 19. A building of such DOCLMP demands to use modern micro and nano technologies.

Owing to DOCLMP *the demands to pumping, γ-lasing and cooling (energy transfer from AM to crystal-substrate) are in compromise.* In deed in order to avoid diffraction losses it is necessary to have AM with diameter $(\lambda L)^{1/2} \sim 10^{-4}$ cm. Intrusion of heavy atoms to *depth* 10^{-4} cm is possible only in a *hard intrusion* at energies $10^6 - 10^7$ eV. A heat release in such case is more by 2 – 4 orders than q = 1.6 10^{11} W/cm^3 in eq.(1). *Owing to* DOCLMP *it is possible to coinside a soft transplantation in* 1 – 5 *outer surface layers (at energy* ~ 10^2 eV*) with a sufficiently big transversal sise of AM* ~ 10^{-4} cm. A density of heavy atoms n = 9 10^{20} cm^{-3}, see **1.1**, leads to strong scattering of *energy carriers* (**EC**) and so to decreasing of paths Λ_e, Λ_{ph} (see eq.(2)) lower than 10^{-6} cm. Fortunately all working nuclei are sited at near-surface layers (boundaries of DOCLMP) and so its doesn't hinder to free exit of EC (phonons, electrons, holes) from AM. So *owing to* DOCLMP *the paths* Λ_e, Λ_{ph} *are the same as without impurities.* Lastly, a big ratio $d/2d_o \sim 50$ leads to a big distances ~ 3 10^{-7} between near-hood working nuclei and so DOCLMP is beneficial for line narrowing. DOCLMP is necessary element for a construction of AM in all (not only SPTEN) solid γ-lasers. More common types of DOCLMP are regarded in work[2].

1.5 Atomic (molecular) multi-beam emitters (AMMBE)

A more than sufficient amount of ELAN and its density in AM could be reached with help of a specific device (1983,1995, Karyagin) called as "converter" for γ-lasing or as "atomic (molecular) multi-beam emitter" (AMMBE) for some other scientific and practical applications[3,5,6,19]. Owing to these devices with oriented deep micro-relief[3,5,6,19] the effectiveness of laser isotope (isomer) separation (LIS)[33,34] can be increased by some orders at keeping of LIS-quality. Such result for AMMBE is owed to: big amount of atoms in multi-beam, preliminary its cooling and deionization, possibility to clean beam from ions before switch the LIS, weakening of both charge exchange probability and Doppler spread, compactness of device. *Besides:* the efficiency of LIS increases extremely by many orders if isotopes (isomers) are born in surface layers of AMMBE. At this case not only stable isotopes but also short-lived isomers can be more successively separated by laser. The know-haw and some equipment for AMMBE-development are available in Semenov Institute.

1.6 Narrowing effect of self-micro-plasma on γ-lasing in SPTEN-shemes

Free charged carriers (CC) are jumping between the host atoms with frequency $\nu' \approx v_e (n')^{1/3} \approx 10^{16}$ s^{-1}. The CC are trapped by working atoms. Two types of working traps are interesting: 1. – Deep traps with a long time-living t_{tr} of trapped CC, i.e., $t_{tr} >> 1/\nu'$; 2. – Fine traps, when $t_{tr} \sim 1/\nu'$. In case of deep traps of only one type a line broadening can be small and $\Gamma\tau_1 \approx 1$, if homogeneity of crystal-chemical parameters[15] of trap environment exists at going overall AM from trap to trap. In case of

many trap-types the spectrum is dispersed over many peaks multiplied by a number of HFS-peaks. Together with relaxation processes it gives a continuos spectral band with a damping factor $\Gamma\tau_1 >> 1$ adverse for γ-lasing. In case of fine traps the working atoms are recharging, i.e., its charge-state are changing through "+", "0", "-" with a frequency $\nu_r = n_e \nu'/n'$. The line depends on the charge-state of trap and so is running through positions $\omega_+, \omega_o, \omega_-$ with an amplitude $\delta = \sup\{|\omega_+ - \omega_o|; |\omega_- - \omega_o|; |\omega_+ - \omega_-|\}$. If $\delta << \nu_r$, then one single line of a width $\Gamma = \tau_1^{-1} + \Delta\Gamma$ arises instead of "triplet" $\omega_+, \omega_o, \omega_-$. Here $\Delta\Gamma \approx \delta^2/\nu_r \approx (\delta^2\ n'^{2/3}) / (2n_e v_e)$. The broadening $\Delta\Gamma$ can be decreased by the selection of AM (nucleus, substratum) or by regulation of heat-radiate regime, through the changing parameters δ, n', $n_e \sim n_+ d$. At case of a fortunate selection of AM or its parameters *it could be reached* **the effect of spectral "collapse", i.e., the contraction of all lines of an inhomogeneous spectrum with its HFS into one tight singlet with a natural width $\Gamma\tau_1 \approx 1$. This effect is beneficial for γ-lasing, especially in cases $\tau_1 \sim 10^{-4}$c, $\tau_1 > 10^{-4}$c** (but not for too big τ_1). *This narrowing effect was verified.* E.g., in the low-temperature samples (saturated with hydrogen) the narrowing of lines and its collapse into narrow singlet were revealed when temperature was increasing[13].

E.g., for AM of type ^{58}Co/Di at $T_{AM} = 90$ K the appropriate values are: $n_e \approx 5\ 10^{18}$ cm^{-3}; $\nu' \approx 10^{16}$ s^{-1}; $\nu_r = n_e \nu'/n' \approx 3\ 10^{11}$ s^{-1}. Let $\delta = \underline{6.3\ 10^7\ s^{-1}}$, then $\Delta\Gamma = \delta^2 / 2\nu_r = \underline{6.7\ 10^3\ s^{-1}} = 0.1\ \tau_1^{-1}$. A *spectral band* of width $\delta = 6.3\ 10^7$ s^{-1} (without plasma) is collapsed into *single line* of width $\tau_1^{-1} + \Delta\Gamma$, where $\Delta\Gamma = 6.7\ 10^3$ s^{-1} (at micro-plasma). Another words, a spectral band with adverse factor $\tau_1\delta = 958$ is collapsed into line of natural width with a broadening factor $\tau_1\Delta\Gamma = 0.1$. So $\tau_1/\tau_2 = 1.1$, see ch.2.

2. REAL GAMMA-LASING CONDITIONS

Effect of distanse on γ-lasing. For most difficult stage at $t << T_2$ amount of γ-quanta in a lasing mode is small, a phase is absent, propagation of photons could be regarded separatelly from others and a total spectral width Γ_{tot} in γ-lasing mode is

$$\Gamma_{tot} \equiv \tau_2^{-1} = \Gamma + \Gamma'(L', \tau_v),\ \Gamma'(L', \tau_v) = (\tau_v + c/L')^{-1}. \qquad (12)$$

Here $\Gamma = \Gamma_h + \Gamma_{ih}$ is a standard total width, $\Gamma_h + \Gamma_{ih}$ is a sum of homogeneous Γ_h and inhomogeneous Γ_{ih} widths[15,16]. A term $\Gamma'(L', \tau_v)$ depends on free path of photon L'. Path L' is a length along eikonal of photon from place of its arising to a place of its exit from a lasing mode. A *photon is vanishing for a time* τ_v in resonant or non-resonant absorption and scattering. For resonant processes $\tau_v \sim \Gamma^{-1}$; for non-resonant ones $\tau_v << \Gamma^{-1}$. A sum $\tau_\gamma = \tau_v + (c/L')$ is a "time-life" of photon in lasing mode. In rise only $1/\Gamma_{tot}\tau_{rad}$ of photons induce emission. All resonant probabilities must to include "filtering factor"(see **2.1,2.2**)

$$\tau_2/\tau_{rad} = (\tau_2/\tau_1)\ f'w/(1 + \alpha), \qquad (13)$$

The **time $\tau_2 = 1/\Gamma_{tot}$ is differed from standard time $T_2 = 1/\Gamma$** (which is used widely) because always $\Gamma_{tot} > \Gamma_2$. *In optic lasers* due to n-fold reflection of photon by mirrors the normal sizes of optical device are sufficient to have $L' > 10cT_2$ and so $\Gamma' < 0.1\Gamma$, $\tau_1/\tau_2 > 1.1$. But **at non-resonant detector** in *mirror-less γ-laser* $\Gamma' < 0.1\Gamma$ only at *long distance* $L' > 10\tau_1 c$ *between its exit-plate of γ-laser and the detector (or absorbing target).* E.g., $\tau_1/\tau_2 > 1.1$ for ^{58}Co if a distance $L' > 4.5\ 10^6$ sm = 45 km.

In Moessbauer effect experiments a vanishing time $\tau_v \sim \tau_1$ due to big duration of resonant absorption (scattering)[28]. So $L' > \tau_v c$ in other to observe the L'-effect on line width. Deformation of line-form by apparatus depends on a distance L' too. So $\Gamma = \Gamma_{ob}(L') - \Gamma_{ap}(L') - \Gamma$, where $\Gamma_{ab}(L')$ is an observable line width, $\Gamma_{ap}(L')$ is apparatus broadening, and *a true procedure of "subtraction" indeed is the deciding of integral equation* of rolling-type

$$I_{ob}(\omega) = \int_0^\infty I(\omega')\ A(\omega - \omega')\ d\omega'. \qquad (14)$$

I.e., to execute *in deal* subtraction $G_{ob}(L') - G_{ap}(L')$ means to find a true (non-deformed) form of Moessbauer line $I(\omega')$, if the form $I_{ob}(\omega)$ and kernel $A(\omega - \omega')$ are the well-known functions of frequency ω. Here $I_{ob}(\omega)$ is the observable line-form and the kernel $A(\omega - \omega')$ is the apparatus function. A more general form than equation (14) is a linear integral transformation

$$I_{ob}(\omega) = \sum_e \sum_{e'} \iiint_r \iiint_{r'} \iiint_k \iiint_{k'} \int_{\omega'} \rho(\mathbf{r}')\ I(\mathbf{r}', \mathbf{k}', \mathbf{e}', \omega')\ A(\mathbf{r}, \mathbf{r}'; \mathbf{k}, \mathbf{k}'; \mathbf{e}, \mathbf{e}'; \omega, \omega')\ \mathbf{d^3r}\ \mathbf{d^3r'}\ \mathbf{d^3k}\ \mathbf{d^3k'}\ d\omega', \qquad (15)$$

where **r'** is start point of emitted photon in source; **r** is finish point of this photon in detector; **k',ω',e'** are start values (in source) of wave vector, frequency and polarisation correspondingly ; **k,ω,e** are the final (in detector) ones; **{e,e'; r,r'; k,k'; ω'}** is a region of integration; $\mathbf{d^3r} = dx\ dy\ dz$; $\mathbf{d^3r'} = dx'\ dy'\ dz'$; $\mathbf{d^3k} = dk_x\ dk_y\ dk_z$; $\mathbf{d^3k'} = dk'_x\ dk'_y\ dk'_z$; **r** = (x,y,z) is radius-

vector **r** with components x, y, z of final point of photon in detector; **r'** = (x', y', z') is radius-vector **r'** of start point of photon in source; kernel **A(r,r';k,k';e,e';ω,ω')** is not symmetric to the permuting in pairs **r↔r'**; **k↔k'**; **e↔e'**; **ω↔ω'** and is not a function of only differences **r - r'**; **k - k'**; **e - e'**; **ω - ω'**. Kernel **A(r,r';k,k';e,e';ω,ω')** is a *general apparatus functional* which is depended on both : on the self-apparatus properties and on all interactions of photons with media along its eikonals.

The transformation of rolling-type (14) can only to broaden natural line, but it can't to narrow line $I(\omega)$. *In contrary to it a general* ***transformation (15) can make*** *both:* ***to narrow*** *and to broaden* ***form of line.*** In deal, a line more narrow than natural one could be gotten in n-fold Bragg resonant scattering, at some superposition of resonant filters, in amplification. So, there are **yet no evidence for a new effect**[23] *even if observable line* $I_{ob}(w)$ *is more narrow than a natural one*[24].

The "distance-effect" (12) doesn't change the spontaneous time τ_1. But it needs to be accounted in analyses of some Moess bauer trials[21–26]. A significant part of "shielding-effects" (SE)[23–25] can be conditioned or masked by L'-effect (12) and by a disregarding with a general relation (15). Note two remarks: *1.* – A zero-field-nucleus interaction can't to change essentially an internal electron conversion probability. So a new "shielded"[23–25] natural time-life τ_1' can't be more than $(1+\alpha)\tau_1/\alpha$. *2.* – In a strict quantum theory any real value (e.g., width) needs to be invariable to orthogonal normalized (ON) changes in ON complete base of self vectors (functions, modes). But the results of SE-theory[23] break this law and it can lead to artefact.

2.1 Real threshold conditions (RTC) for induced gamma-oscillation in DOCLMP

The parameter p of "reserved amplification" (RA) is introduced through a formal balance equation[1-9]

$$n\,\sigma_0\tau_2/\tau_1 = p\,(n\,\sigma + n'\,\sigma'), \qquad (16)$$

where $n = n_+ + n_-$ is a total density of working nuclei amount (DWNA) averaged over tooth volume; n_+ is DWNA for a level "+"; and n_- is DWNA for a level "-". This definition of RA. The value $L_0 = (n\sigma + n'\sigma')^{-1}$ is length of non-resonant losses in substance of tooth. Appropriate value in DOCLMP equals $2L_0$. Formally RA= $(\tau_2/\tau_1)n\sigma_0L_0$ is a gain on length L_0. *The definition RA (16)* is only a handy combination of basic values and *isn't a real balance equation:* $n_+ < n$ and the induced cross-section reaches limit $(\tau_2/\tau_1)n\sigma_0$ only at time $t >> \tau_2$[16,27]. RA is estimated from a complex of conditions below. By (16) RA has a maximum $p_m = p_0\,\tau_2/\tau_1$ where $p_0 = \sigma_0/\sigma_o = 888$ for ^{58}Co. Another basic value is a density n' of host-atoms. For a diamond $n' = 1.76\ 10^{23}\ cm^{-3}$. The relative impurity concentration n/n', a value ψ, total length L of DOCLMP, relative length $y = L/2L_o$, amount of diffraction modes **m**, all data in **1.1** are the departure values in estimates. Then the *interim values* are derived: RA; cross-size **d** of AM; volume of AM $\mathbf{V = d^2L}$ (for a square form of AM-cross-section); solid angle **Ω** of diffraction mode; total number $\mathbf{N_0 = nV/2}$ (half of comb-like AM is empty) of working nuclei; resonant cross section σ_0, i.e.

$$\psi = (n/n')/((n/n')+(\sigma'/\sigma));\ L_0 = (1-\psi)/(n'\sigma');\ L=2yL_0;\ p = \psi\,p_0\tau_2/\tau_1;\ d = (m\lambda L)^{1/2};\ V = 4\,(L_0y)^2\,m\lambda;\ \Omega = \lambda/L; \qquad (17)$$

$$N_0 = 2\,(m\lambda/n'\sigma'\sigma)\,\psi\,(1-\psi)\,y^2; \qquad (18)$$

$$\sigma_0 = (\lambda^2/2\pi)\,f'w/(1+\alpha). \qquad (19)$$

The number of gamma-quanta arisen in the amplification of stimulated emission (ASE) is

$$N_A(p) = (N_S/y)\int_0^{\infty} e^{-x}\,dx'\,[\exp[[\,pG(x')-1\,]\,y] - 1] / [pG(x')-1]. \qquad (20)$$

Here $\mathbf{x = t/\tau_1}$; $N_S = (pym\tau_1/4\tau_2)\exp(-x_1)$ *is a number of spontaneous γ-quanta emitted for all time in* m *modes in a spectral interval* τ_2^{-1}; $\exp(-x_1) = n_+(0)/n$; $n_+(0)$ is ELAN-amount density at momentum t = 0. A value $pG(x)/L_0$ is a generalized induced gain. According to[27, 16, 10], *a cross-section of induced emission* $\sigma_i(t)$ *equals to zero at the start momentum* t = 0, *when a resonant interaction (of ELAN and a gamma-radiation field) is switched. The value of* $\sigma_i(t)$ *asymptotically grows up to its limit* $\sigma_i(\infty) = \sigma_o$ *during time* $\sim \tau_2$. A correct formula for $\sigma_i(t)$ is not yet derived because of difficulties in transforming of complicated nonlinear decisions of Maxwell-Bloch equations to cross-section concept. As a compromise, a simple approximate formula containing all properties marked above was suggested and used in works[3-5,7-9] for the quick valuations:

$$\sigma_i(t) = (1-\exp(-t/\tau_2))\,\sigma_i(\infty). \qquad (21)$$

Hence a stationary formula $p/L_o = (n_+ - g\,n_-)(\tau_1/\tau_2)\sigma_o$ *for induced gain* need be transformed to the next more complex form

$$pG(t)/L_o = n_+(t)\,\sigma_{+-}(t) - [n_-(0)\,\sigma_{-+}(t) + \int_0^t n_+(t')\,\sigma_{-+}(t-t')\,d(t'/\tau_1)\,]. \qquad (22)$$

Here $\sigma_{+-}(t) = \sigma_{+-}(\infty)\,(1 - \exp(-t/\tau_2))$ is $\sigma_i(t)$ for emission from "+" to "-" state; $\sigma_{+-}(\infty) = (\tau_2/\tau_1)\sigma_o$ is a limit for $\sigma_{+-}(t)$ at infinity great time. By analogy $\sigma_{-+}(t) = \sigma_{-+}(\infty)\,(1 - \exp(-t/\tau_2))$ is $\sigma_i(t)$ for the transition from "-" to "+"state; $\sigma_{-+}(\infty) = (\tau_2/\tau_1)g\sigma_o$ is a limit for $\sigma_{-+}(t)$ at infinity time. *In common case a value* g *can be different from* $(2j_+{+}1)/(2j_-{+}1)$. *E.g.,* $g = 0$ *in case of ideal AWI (ch.3);* $g = 1$ *in case of non-degenerated working levels.* The nuclei arisen spontaneously in a lower state "-" *at momentum t'* are dephased at this time-point t'. So at $t > t'$ a phasing time t_ϕ of these nuclei (or time of growing of its absorption cross-section) is $t_\phi = t - t'$. The value $n_+(t')\,d(t'/\tau_1)$ is a number of "new" nuclei in state "-" in the time-interval dt'. In case of weak generation the populations $n_+(t)$ and $n_-(t)$ are

$$n_+(t) = n_+(0)\exp(-t/\tau_1), \quad n_-(t) = n_-(0) + \int_0^t n_+(t')\,d(t'/\tau_1). \qquad (23)$$

A time-dependent factor G(t) of induced gain function is transferred to the form (25) at a formal denoting (24):

$$\exp(-x_1) = n_+(0)/n;\ n = n_+ + n_- = \text{const};\ n_- = (1 - \exp(-x_1))\,n\,; \qquad (24)$$

$$G(t) = (1 - \exp(-x\tau_1/\tau_2))\,(\exp(-x_1 - x) - g) + g\exp(-x_1)\,(e^{-x} - \exp(-x\tau_1/\tau_2))\,/\,(1 - (\tau_2/\tau_1)); \qquad (25)$$

$$G(t) = (1 - e^{-x} + gx)\exp(-x_1 - x) - g\,(1 - e^{-x}). \qquad (25a)$$

Here (25a) corresponds to a particular case $\tau_1 = \tau_2$. The decisions (25),(25a) satisfy for all initial and limit conditions. The further analysis is based on the approximation of G(t) by a quadratic form $G(\mu) \approx G_m - (\mu - \mu_o)^2 K$, where $\mu = e^{-x}$. The values G_m, μ_o, K depend on basic parameters τ_1/τ_2, g, $\exp(-x_1)$. Puasson's formula leads to

$$N_A(p) \approx (\pi p/yK)^{1/2}\,(m/8)\,(\tau_1/\tau_2)\exp(-x_1)\,\{\{\exp[(pG_m - 1)y] - 1\}\,/\,(pG_m - 1)\},\ p > 1/G_m. \qquad (26)$$

Eq.(26) is valid at $(pG_m - 1)y > 2$ and contains threshold condition for ASE: $\mathbf{p > 1/G_m}$. The roots of *equation* $G(\mu) = 1/p$ are $\mu_+(p) = \mu_o + \Delta(p)$; $\mu_-(p) = \mu_o - \Delta(p)$, where $\Delta(p) = [(G_m - p^{-1})/K]^{1/2}$. The start-time for γ-lasing is $t_+ = -\tau_1 \ln\mu_+$. The end-time for γ-lasing is $t_- = -\tau_1 \ln\mu_-$. At $t < t_+$ and at $t > t_-$ γ-lasing is absent. Time-interval of ASE-generation is $t_+ < t < t_-$ with duration $t_G(p) = t_- - t_+ = \tau_1 \ln(\mu_+/\mu_-)$ and with a maximum of intensity at $t = t_m = -\tau_1 \ln\mu_o$. Eqs.(20),(26) with $p = \psi\, p_0\tau_2/\tau_1$ give an upper limit of N_A. The substitution of decision $\mathbf{p' = p\,t'_G/2\tau_2}$ (instead of p) to (20),(26) gives a lower limit for N_A. Here $t'_G = t_G(p')$. Factor $t'_G/2\tau_2$ **overaccounts** a frequency band $\sim 2(t'_G)^{-1}$ of γ-pulse. The real value N_A is inside interval $N_A(p') < N_A < N_A(p)$. A peak energy flow I_p equals (at appropriate p or p') to the integrand of (20) multiplied by $E_\gamma/(d^2\tau_1)$. A peak saturation parameter $P_s = \tau_2\sigma_o I_p/E_\gamma$ is also used below.

Numerical examples. According to data of **1.1** there are the next values: $\tau_1/\tau_2 = 1.1$; $\exp(-x_1) = 0.9$; $n/n' = 5\ 10^{-3}$; $\sigma'/\sigma = 4.7\ 10^{-3}$; $\psi = 0.515$; $L = 0.321$ cm; $y = 0.329$; $d = 3.8\ 10^{-5}$ cm; $p = 416.5 >> p_o = 1/G_m = 7.25$, p_o is a threshold. So *it is a super-threshold γ-lasing.* Note, that necessary short period $t_i \sim 10^{-8}$s of ELAN-implantation is in touch in SPTEN-method[2-9]. Besides, the prompt shatters with $t_i \sim 10^{-12}$ s could be created[1,2]. Other parameters are: $G_m = 0.138$; $\mu_o = 0.705$; $K = 1.586$; $\Delta = 0.292$; $\mu_+ = 0.997$; $\mu_- = 0.413$; $t_+ = 3\ 10^{-3}\tau_1 = 4.5\ 10^{-8}$s; $t_- = 0.884\tau_1 = 1.33\ 10^{-5}$s; $t_m = 0.35\ \tau_1 = 5.3\ 10^{-6}$s; $t_G = 0.881\tau_1 = 1.33\ 10^{-5}$s; $p' = 200$. The γ-lasing pulse characteristics are: $10^3 < N_A < 1.3\ 10^7$; $5\ 10^{-12} < N_A E_\gamma < 6\ 10^{-8}$ J; *flux* $F = N_A/d^2$: $10^{12} < F < 10^{16}$ cm^{-2}; $3\ 10^{-3} < FE_\gamma < 40$ J/cm^2; *mean energy flow* $I = F E_\gamma/t_G$: $230 < I < 3.0\ 10^6$ W/cm^2; $2\ 10^3 < I_p < 4\ 10^7$ W/cm^2; solid angle of mode is $\Omega = \lambda/L = 1.37\ 10^{-8}$ rad^2; brightness: $1.5\ 10^{10} < I/\Omega < 2\ 10^{14}$ W/cm^{2}rad^2; $2\ 10^{11} < I_p/\Omega < 3\ 10^{15}$ W/cm^{2}rad^2; $10^{-5} < P_s < 0.2$; $16 < N_S < 34$. *The ratio "signal to noise":* $60 < N_A/N_S < 4\ 10^5$ *is more than sufficient for the experimental demonstration* of γ-lasing.[2-5] A total number of working nuclei in AM is $N_o = 2\ 10^{11}$, i.e., less by 2-3 orders than amount of ELAN, which can be put into AM owing to SPTEN-method. Efficiency of γ-lasing in this case: $10^{-8} < N_A/N_o < 10^{-4}$. *More effective results are at further increasing of concentration n/n'.* E.g., at $n/n' = 0.01$ and the same $N_o = 2\ 10^{11}$ the values are: $L = 0.227$cm; $y = 0.352$; $d = 3.2\ 10^{-5}$ cm; $p = 549.5$; $t_G = 0.884\ \tau_1$; $p' = 265$; $4\ 10^4 < N_A < 3\ 10^{10}$; $4\ 10^{13} < F < 3\ 10^{19}$ cm^{-2}, that is less than its p-pulse limit[1] $F_{lim} = (p-1)/(\sigma_0\tau_2/\tau_1) \approx 5\ 10^{20}$ cm^{-2}; $0.2 < FE_\gamma < 10^5$ J/cm^2; $10^4 < I < 10^{10}$ W/cm^2; $2\ 10^5 < I_p < 2\ 10^{11}$W/cm^2; $10^{13} < I_p/\Omega < 10^{19}$ W/cm^{2}rad^2; $10^{-3} < P_s < 660$, and I_p needs be decreased; $26 < N_S < 53$; $1.5\ 10^3 < N_A/N_S < 5\ 10^8$; $2\ 10^{-7} < N_A/N_o < 0.13$, i.e. a high efficiency could be gotten. It is very difficult to keep $\tau_1/\tau_2 \cong 1.1$, because at $n/n' > 0.005$ clustering of atoms leads to a strong line-broadening. These results could be corrected by accounting of noise, saturation, etc.

2.2 Real threshold conditions for the super-fluorescent gamma-oscillation

The decision[31] for the projection R_3 of Bloch's vector R had been generalized (1995,1998, Karyagin) for non-keeping R: [3,33]

$$R_3 = R\,(R - e^{\varphi+\varphi'})/(R + e^{\varphi+\varphi'}). \qquad (27)$$

Here $R = R'\,D_{ph} - (\tau_{mod}/\tau_2)$ is an *effective time-dependent Bloch's vector*; $R' = (ze^{-x} - g)N_o$ is a *time-dependent* ordinary inverse population in AM *generalized on common case of arbitrary nuclear state degeneration*, see **2.1.** Value R' depends on $x = t/\tau_1$ and $z = (1 + g)\exp(-x_1)$. Factor $D_{ph} = (\tau_2/\tau_1)(\beta/y^2)wf'/(1 + \alpha)$ is an effectively phased part of ELAN in AM. Values p, w, f', α, τ_1, τ_2, y, x, etc. see in **2.1.** Time τ_2 depends on length L', see **2.1.** Factor $\beta = 1 - (1 + y)\exp(-y)$ accounts the loss of photons from phasing process. That loss is owed to *scattering* or *non-resonant absorption* in AM. The time $\tau_{mod} = 2\tau_2 N_o y/p = (4\pi L/\lambda)(1 + \alpha)\tau_1/(wf')$. Here τ_{mod}^{-1} is a speed of photon emission by one nucleus ("averaged" over all ELAN) to solid angle $\Omega = \lambda/L$, with an arbitrary polarization, to frequency-band τ_2^{-1}. The selection of photons for phasing in tight band $1/\tau_1$ is accounted in D_{ph} by factor τ_2/τ_1. *Such factor is absent in more simple old formulas*[10,32]. *Because of it that old simple formulas* ***overestime*** *SF-part in γ-lasing.* The main term of dephasing loss τ_{mod}/τ_2 is introduced in accordance with work[32]. It is necessary to fulfil the threshold condition $R'|_{t=0} > \tau_{mod}/(\tau_2 D_{ph})$, which at $D_{ph}=1$ coincides with Andreev's condition[32,10]. A number of effectively phasing "priming" photons for a time t is

$$\varphi = \int_0^t (R/\tau_{mod})\,dt = \int_0^t ((R'D_{ph}/\tau_{mod}) - \tau_2^{-1})\,dt. \qquad (28)$$

The "feedback" phasing addition from the super-fluorescent pulse in axial mode is

$$\varphi' = \int_0^t (\tau/\tau_0)\,I_{SF}\,dt = \int_0^t (I_{SF}/\tau_0)^{1/2}\,dt, \qquad (29)$$

where width τ^{-1} is a logarithmic derivation of function I_{SF} and $\tau_0^{-1} \equiv w/(1+\alpha)\tau_1$ is a radiation width. So $\tau^{-1} \approx (\tau/\tau_0)I_{SF}$ and the integrand in (29) is proportional to $I_{SF}^{1/2}$. This procedure (1995,1998,Karyagin) is approximate equivalent of averaging of resonant interaction "radiation-ELAN" over a time-depending frequency distribution of γ-pulse, evaluated as a Fourier from pulse-form cut after momentum t. In a derivation $\mathbf{dR_3/dt = A_1 + A_2 + A_3}$ the term $\mathbf{A_1 = -\,R\,(R^2 - R_3^2)/(2\tau_{mod})}$ coincides with a right part of standard Bloch's equation. By analogy with[31] it gets

$$I_{SF} = (R^2 - R_3^2)/(2(g+1)\tau_{mod}) = 2R^3\,e^{\varphi+\varphi'}/\,[(g+1)\,(R + e^{\varphi+\varphi'})^2\,\tau_{mod}]. \qquad (30)$$

Term $\mathbf{A_2 = dR/dt \equiv dR'/dt}$ is a natural addition to A_1 from inverse population decay and needs to be adopted in generalized Bloch's equation. Term $A_3 = -\,(1/2)\,(1 - (R_3/R))^2\,dR/dt$ has no apparent nature and can be understood as a deflexion from exact equation $\mathbf{dR_3/dt = -\,(R^2 - R_3^2)\,R/(2\tau_{mod}) + dR/dt}$. At $x < x_c$ a relation $|A_1 + A_2| > |A_3|$ is valid; x_c is *a root of equation* $\mathbf{R'(x) = 0}$. An approximate decision (26) satisfies *to initial condition* $R_3(0) = R(0)$ *and to asymptotic condition* $R_3(\infty) = -\,R(\infty)$. A *maximum* of function I_{SF} is achieved in point $x = x_m$, in which $\mathbf{R(x) = e^{\varphi(x)+\varphi'(x)}}$. It leads to equations

$$\varphi + \varphi' = \ln R;\ \varphi' = \mathbf{C}\,\mathrm{arctg}((e^{\varphi} - 1)/R), \qquad (31)$$

where $\mathbf{C} = (32\pi L/((g + 1)\lambda f'))^{1/2}$. Functions φ(x), R(x) are: $\varphi = (1 - e^{-x})G_1 - xG_2$; $R = (G_1 e^{-x} - G_2)\mathbf{K}$; $G_1 = p\beta wf'z/(2(1+\alpha)y)$; $G_2 = (G_1 g/z) + \tau_1/\tau_2$; $\mathbf{K} = 2(\lambda/n'\sigma'\sigma)\psi(1-\psi)y\tau_2/(p\tau_1)$. At these conditions the amount of γ-quanta in a super-fluorescent pulse is $N_{SF} = y^{-1}(1 - e^{-y})e^{\varphi+\varphi'}/(1+g)$, where $\varphi + \varphi'$ is the decision of eq.(31). Numerical calculations for $N_o = 2\ 10^{11}$ *in case n/n' = 0.005* (see **2.1**) give: G_1=15.516; G_2=8.858; **K**=1.3287 10^8; **C**=68401.6; x_c=0.56055399; $x_m = x_c - 2.93\ 10^{-6}$; $\varphi(x_m) = 1.69$; $\varphi'(x_m) = 8.75$; $N_{SF} = 1.6\ 10^4$; $N_{SF}/N_A = 1.2\ 10^{-3}$. *in case n/n' = 0.01*: G_1=21.614; G_2=11.907; **K**=9.3934 10^8; **C**=57513; x_c=0.59621367; $x_m = x_c - 7.42\ 10^{-6}$; $\varphi(x_m) = 2.61$; $\varphi'(x_m) = 8.72$; $N_{SF} = 7.0\ 10^4$; $N_{SF}/N_A = 2.3\ 10^{-6}$. Calculations show that *in super-threshold regime* $N_{SF} \ll N_A$ at the same parameters for SF and ASE. Only for a weak near-threshold regime (when $N_{SF} \approx 100$) could be $N_{SF} > N_A$, i.e., so called "weak SF"[32]. The results of ch.2 are more realistic than ones of simple theories.

3. SELECTIVE RESONANT PUMPING CASE

3.1 Resonant activation of ELAN

The SPTEN secures the most soft effects of both *radiation and heat* on AM. On the further places towards soften action on AM are all cases *when parents of ELAN are preliminarily sited in AM.* That parents could be transformed into ELAN by many methods of exposure of parent-nuclei by fluxes of different (non-charged or charged) particles from the various sources[1-10,16]. Among this manifold (without SPTEN) the methods of selective resonant pumping[30,1,8,9,16] (SRP) have the most

big efficiency factor and could provide a pumping with rather soft heat-radiation AM-regimes. But towards soften action on active medium SRP is only on the second place after SPTEN among all manifold of γ-lasers.[4,5]

In case of SRP a beam-flux of resonant γ-quanta $F \approx 27/\sigma_o \approx 3\ 10^{18}\ cm^{-2}$ is necessary in order *to create a marked amount of ELAN in AM*. Here the time-dependence of σ_i, see eq.(21), and duration of SRP-pulse-pumping $t_p \approx 0.1\ \tau_1$ were accounted. Due to resonant absorption this flux is a fast decreasing function of length, if a flux-direction coincide with a *longitudinal* direction of AM. So in this case AM could be created only when $L << L_o$. But the ratio $y = L/L_o << 1$ is not effective for γ-lasing, see **2.1** and **2.2.** Hence the *transversal* or *interim* type of SRP is necessary. In interim case a part of AM cold be in the sufficiently good thermal conditions. But a rest part of AM could be heated so as in a *hard transversal pumping*. So the latter is sufficient to regard. A typical case of ^{58}Co in diamond, see **1.1**, is regarded below without loss of proof-community.

A region of crystal-cooler exposed by SRP-beam has cross dimensions $d \times L \approx 4\ 10^{-5}\ cm \times 0.32$ cm and longitudinal size $L_h > (\sigma' n')^{-1} \approx 1$ cm. It is a rectangular plate with sizes $L_h \times L \times d \approx 1cm \times 0.32cm \times 4\ 10^{-5}cm$ submerged in a crystal. The heat-release in such exposed "plate" (owed to photo-effect on host atoms) is $q_p \approx F\sigma' E_\gamma n'/t_p \approx 10^{11}\ J/cm^3$. So $q_p \approx q$, see eq.(1), but condition (1) is strongly broken, because transversal (relative to main heat-flux from AM) sizes are big: $L_h, L >> \Lambda_e, \Lambda_{ph}$. With use of *self-consistent method*, see 1.2, the quasi-temperature of that "plate" and around AM $T_p \approx 700$ - 750K is estimated. It decreases paths $\Lambda_e \approx 5.9\ 10^{-6}$ cm << d, $\Lambda_{ph} \approx 2.8\ 10^{-6}$ cm << d. As a result the speed of energy exit from AM is suppressed by factors $f = \exp(-d/\Lambda)$: $f_e = 0.0015$ (for electrons) and $f_{ph} = 10^{-6}$ (for phonons). **So SRP adiabatically isolates AM from cooler and AM explodes before γ-lasing**. The situation can be changed by Borrmann effect[1,2,10,16,17] at coupling factor $K = 10^{-6} - 10^{-7}$. Note, that in fast pumping and γ-lasing ***all AM of other types (plasma,gas) are always adiabatically isolated***.

3.2 Schemes of amplification "with" and "without" inversion

Note that a selective pumping needs to use schemes for inversion[1,2,10,11] or for amplification without inversion[1,2,10,12] (AWI). But (see **1.2,1.6**) *the active medium of gamma-laser differs from the substance of the Moessbauer sources with the significant concentration of the charged carriers: electrons and holes*[2-5,7-9]. Its typical values are about 10^{16}-$10^{18}\ cm^{-3}$ (e.g., for ^{58}Co/Di). At this condition all electronic and nuclear hyperfine structure (HFS)-levels are in strong stochastic motion and are mixing (see **1.6**). Hence it is important to provide the *steadiness of inversion and AWI schemes to the charge exchange* (**CE**). AWI-schemes[1,2] (1980,Karyagin) are stedy to CE. Its base is stability of electron-state configuration in some superpositions of optical fields to stochastic influence of atomic environment on HFS[14,15]. Sorry, a visual model in that class[1,2] is stable to recharging only for "crystal-chemical narrowing"[15]. This simple AWI is based on selective induction (SI) of optical transition only for atoms (ions) with working nuclei in ground state (WNGS). At such SI the electronic state (ES) of atoms (ions) with ELAN remains unchanged, whereas the ES of atom (ion) with WNGS is converted into a mixture state (e.g., Ruby state) dependent on dynamics of transitions.[1,2] As a result the gamma-absorption line is *shifted in frequency* relative to the γ-emission one. So AWI arises[1,2]. *Note, that at 1980 the word "AWI" was not exist. Instead of it was used the term* ***"optical division" in time*** *of single pumping process into two: excitation of nuclei and damping of self-absorption*[1,2].

4. DIFFICULTIES OF NON-SOLID GAMMA-RAY LASERS

The solid model[1-9,14,15,19] was foregone with testing of non-Moessbauer AM creation on base of *Marcuse's effect*[29]. Some difficulties revealed in that way need be accounted in modern researches, e.g.[20,26,35]. **For γ-lasing in solid plasma (SP):** The ends of AM are spreading more quickly than its middle. *A speed-difference between the ends is* $|\Delta V| > 10^7$ *cm/s.* For $E_\gamma \sim$ 100 keV it leads to Doppler width $\Gamma_D \sim |\Delta V|\ \omega/c > 10^{17}\ c^{-1}$ and to unreality of γ-lasing on SP (cf.,**1.3**). *Besides*: The losses of γ-lasing owing to its scattering on free electrons of plasma needs to be accounted. **For beam γ-lasing (BGL).** There is *a row of steps1-9* in order to qualitatively estimate a beam γ-lasing (BGL). ***Step1.*** Suppose, that gas-AM is somehow cooled. Let at time t = 0 all atoms in beam have equal speeds. But it is impossible to transform *mixed* ***ionized*** *atomic beam* in a gas-lattice with equal inter atomic gaps along AM-axis. The gaps r are spread around $r_{av} = n^{-1/3}$ with dispersion $|\delta r| \sim r_{av}$. In gas-AM electrons (see below) are adhered and so Debye shielding is not valid at fast resets. Interactions of atoms and ions are not strongly shielded in such gas even at *formal* Debye radius $r_D << r_{av} << r$; interaction energy U(r) is random and dispersion of axial atomic speed for t > 0 is $\Delta V_\parallel \approx (t/M)\,|d^2U/dr^2|_{av}\,|\delta r|$. Account of Doppler broadening condition $V_\parallel\ \omega/c < 1/\zeta\tau_1$ leads to

$$|d^2U/dr^2|_{av}\ t\ |\delta r| < Am_p c/(\tau_1 \omega \zeta), \qquad (32)$$

where $\zeta \sim 1$ for atomic beams, but $\zeta << 1$ for free nuclei beams (see *step6*); $t \approx \tau_1$ is a time of acceleration of marked atom in field of one nearest neighbour. Here $m_p = 1.67\ 10^{-24}$ **G** is a proton-mass; A is atomic mass-number; $\omega = 1.52\ 10^{18}\ E_\gamma\ s^{-1}$ is a frequency of γ-quantum (E_γ is in keV). The gas-AM is saturated by ions, because internal conversion initiates creation of Auger electrons ~ 10 - 10^2 and secondary ones ~ 10^2 - 10^3 which adhere to atoms or to walls. At $\tau_1 < 10^{-4}$ s the concentration

of "+" and "–" ions in gas-AM is $C_i > 10^{-3}$. For a free nuclei beam $C_i = 1$. The polarization by ions enhances interaction of atoms with environment. Averaging over atom-atom, ion-ion, atom-ion neibouers gives $|d^2U/dr^2|_{av} \approx e^2nK_i$. Here e is elementary charge $4.8\ 10^{-10}$ CGSE, **n** is a density-amount of atoms, $K_i \approx (10^{-1} - 10^{-2})\ C_i$. Together with (32) it gives:

$$(K_i)^{3/2}n < 5\ 10^{-20}\ [A/\zeta E_\gamma \tau_1^2]^{3/2},\ \text{if}\ \tau_1 < t_{av};\quad (K_i)^3 n < 5\ 10^{-64}\ [A^{1/2}/\zeta E_\gamma \tau_1]^3,\ \text{if}\ \tau_1 > t_{av}. \qquad (33)$$

For $A \approx 200$, $E\gamma \approx 10$ keV, $\tau_1 \approx 10^{-8}$ s, $\lambda \approx 10^{-8}$ cm, $\sigma_o \approx 10^{-18}$ sm^2, $K_i > 10^{-5}$ a gas-density is $n < 10^{14}$ sm^{-3}. Condition $\sigma_o nL \approx 100$ (see ch.2) leads to $L \approx 10^6$ cm, $d = (\lambda L)^{1/2} \approx 0.1$ cm, $N_o = nd^2L > 10^{18}$. It is difficult case. {For SPTEN (see **2.1**) the appropriate values are A = 58; $E\gamma = 28.1$ keV; $\tau_1 = 1.51\ 10^{-5}$ s; $n \approx 10^{21}$ cm^{-3}; $n' = 1.76\ 10^{23}$ cm^{-3}; $d \approx 3\ 10^{-5}$ cm; $N_o = 2\ 10^{11}$; $T_{AM} \approx 30$ K; $N_A = 10^4 - 10^{10}$.} ***Step2.*** *Laser cooling*[35] *uses rarefied non-ionized almost ideal gas* when a force acting on any atom from cooling optical field (COF) is *regular (non-chance)* function **F(r,V)** of its velocity **V** and position **r**. E.g., if $\mathbf{V}_i = \mathbf{V}_j$, $\mathbf{r}_i = \mathbf{r}_j$ for any i-th and j-th atoms, then in ideal gas $\mathbf{F}(\mathbf{r}_i,\mathbf{V}_i) = \mathbf{F}(\mathbf{r}_j,\mathbf{V}_j)$. In case of ionized gas ($C_i > 0.001$) the i-th and j-th atoms are differ owing to various charges or different Starc-effect in field of environment. So $\mathbf{F}(\mathbf{r}_i,\mathbf{V}_i) \neq \mathbf{F}(\mathbf{r}_j,\mathbf{V}_j)$ and $\mathbf{F}(\mathbf{r},\mathbf{V})$ is a *chance* function. A moving for a majority of atoms at force $\mathbf{R} = -\nabla U(\mathbf{r}_i) + \mathbf{F}(\mathbf{r}_i,\mathbf{V}_i)$ is a long auto-oscillations different from fast damping in ideal gas. So *laser cooling of a real gas-AM is strongly decelerated.* ***Step3.*** The recoil force due to spontaneous emission of optical photon is about $F_{sp} \sim 10^{-15}$ dynes and approximately equals to the chance force $F_{ch} = |dU/dr|_{av}$ in gas at $n \sim 10^{14}$ cm^{-3}, see *step 1*. It gives a hope of laser cooling, i.e., damping of axial velocity $V_\parallel \sim c/\omega\tau_1 \sim 0.2$ cm/s with COF-power $q' \sim 10^4\ MnV_\parallel^2/(2\tau_1) \sim 10^{-1}$ W/cm^3 and flux $J' \sim q'd \sim 10^{-2}$W/cm^2. Factor $\sim 10^4$ accounts that *energy transferred from gas to COF is small part of COF*[35]. ***Step4.*** *A heat release from internal conversion* (**HRFIC**) in case above is $q \sim nE_\gamma/\tau_1 \sim 10^7$ Wcm^{-3} and *flux-COF* needs be $J' \sim 10^4 qd \sim 10^{10}$Wcm^{-2}. HRFIC is the main block in gas-AM ***because of its adiabatic isolation***(cf. **3.1**). For arbitrary n (in cm^{-3}) $L \sim 10^{20}\ n^{-1}$ cm, $d \sim 10^6 n^{-1/2}$ cm, $N_o \sim 10^{32}\ n^{-1}$, $q \sim 10^{-7} n$ Wcm^{-3}, $J' \sim 10^4 qd \sim 10^3\ n^{1/2}$Wcm^{-2}. So *if* L~100 cm, *then* $n \sim 10^{18}$cm^{-3}, $d \sim 10^{-3}$cm, $N_o \sim 10^{14}$, $q \sim 10^{11}$Wcm^{-3}, $J' \sim 10^{12}$Wcm^{-2}, i.e., the cooling conditions are more hard than in solid. ***Step5***. Gas-AM has an initial heat energy ~10 - 10^5 eV per atom (recoil-energy in nuclear reaction for ELAN-creation) or $Q_i \sim (10^{-18} - 10^{-14})$ n J/cm^3. This energy need be taken by COF for time $\sim \tau_1$. So additional flux of COF needs be $J'' \sim 10^4 Q_i d/\tau_1 \sim (1 - 10^4)\ n^{1/2}$ Wcm^{-2} $\sim 10^9 - 10^{13}$ Wcm^{-2}. So *steps 4-5* give a no go. ***Step6***. In case of free nuclei beam: $K_i = 1$, $\zeta \sim \sigma_{fn}/\sigma \sim (10^{-10} - 10^{-12})Z^2 \sim 10^{-6} - 10^{-8}$, where $\sigma_{fn} \sim (e^2Z^2/Am_pc^2)^2 \sim 10^{-32}Z^2$ cm^2 is Compton cross-section for *free nucleus*, Z is number of protons in nucleus, $\sigma \sim (10^{-22} - 10^{-20})$ cm^2 is a usual cross-section of non-resonant losses, see ch.**1**,**2**. Hence condition (33) is changed into $n < (10^{-4} - 10^{-1})\ [A/(\tau_1 Z)^2 E_\gamma]^{3/2}$ with *numerical results* (A ~ 200, Z ~ 100, see *ste1*) : $n < (10^{16} - 10^{18})$ cm^{-3}, $L \sim 100/\sigma_o n \sim 10^4 - 10^2$ cm, $d \sim (10^{-2} - 10^{-3})$ cm, $N_o \sim 10^{16} - 10^{14}$. It seems as eligible case. But it needs to account ***step5***: $J'' \sim (10^8 - 10^{13})$ Wcm^{-2} supposing that efficiency of COF is the same for both: atoms and free nuclei. But it is not so: efficiency for free nuclei is less by many orders. So a real $J'' >> 10^{15}$ W/cm^2. It's no go again. ***Step7.*** A dilution of free nuclei by free electrons (Z per nucleus) changes factor ζ into $\zeta' \sim Z\sigma_{fe}/\sigma \sim 1 - 10^{-2}$, where σ_{fe} is Thomson cross-section. Fast shielding by free electrons returns effective factor $K_i > 10^{-5}$ **with all rest results of step1**. Relativistic factor in ζ' don't change sufficiently these results. ***Step8***. Difficulties in steps 1 – 7 could be soften by use of AMMBE[3,5,6,19], which can decrease the values C_i, q, Q_i, J'' by some orders. ***Step9***. ***SPTEN is a hybrid of beam and solid γ-lasers***. In this hybrid the functions of gas-AM are separated in space: the initial stage (creation of ELAN and high inversion) is sited in a beam, but the further functions (generation, cooling) are cited in solid. The results (theory, methodology, trial, technique) in elaboration of BGL independently on its practice could be useful for SPTEN.

5. PROGRAM-CONCEPTION FOR DEVELOPMENT AND CREATION OF GAMMA-LASER

The *concept* as a single complete regarding of ways for the experimental *feasibility* of γ-laser and a detailed *program for the gamma-laser materialization* are ready to experimental examination. Some topics of concept are reflected in present work.

6. CONCLUSION

Model-SPTEN is feasible. For a long period (1980 – nowadays) it is steady to a plenty of difficulties. Such steadiness is based on main property of cold solids: quasiparticles (phonons, electrons, holes, *but not atoms!*) effectively provide the transferring of energy and charges. Another media have no such useful property. Many ways are revealed for experimental feasibility of γ-laser: devices for effective SPTEN-pumping on base of existing technique; modi to keep AM frozen during γ-lasing; effective nuclei-candidates with appropriate matrixes; theory and handy formulas for analyses of real threshold conditions, heat and radiation regimes; analyses of further difficulties in gas and plasma AM; hot micro plasma in cold AM; conditions for the collapse of working inhomogeneous spectrum into one narrow line; AWI and inversion schemes steady against micro plasma; L'-effect on τ_2; prospect of high powerful γ-lasers[8,9]; usefulness of some results (AMMBE, DOCLMP) in nowadays practice, ets. It needs a wide collaboration in this field.

7. ACKNOLEGEMENTS

Author express his gratitude to V.I.Gol'danskii for support of direction and R.V.Khokhlov, Yu.B.Khariton, A.A.Rukhadze, V.S.Letokhov, G.C.Baldwin, Y.M.Kagan, J.J.Carroll, C.B.Collins, A.N.Starostin, L.A.Rivlin for discussions in divers times.

8. REFERENCES

1. S.V.Karyagin, "On Possibility of Low-Temperature Gamma-Laser", Zh.Eksp.Teor.Fiz.**79**(1980)730-750.
2. S.V.Karyagin, "On the Possibility of Generation in the Short Wave-Length (Moessbauer) Range at Low-Temperatures", Available from VINITI, **No.2797-83Dep.**(1983)1-61 (Russ).
3. S.V.Karyagin, "Low-Temperature Gamma-Ray Lasers with Combined Pulse Pumping from an Aperiodic Reactor", Laser Phys.**5**(2)(1995)343 - 354.
4. S.V.Karyagin, "Gamma-Ray Solid Laser: the Heat Problem and Means of Solution", Hyp.Int.**107** (1997)449-463.
5. S.V.Karyagin, "Gamma-Ray Solid Laser: Realization of Pumping", ib., 465-480.
6. A.A.Sysoev, I.V.Shchekina and S.V.Karyagin, "Gamma-Ray Solid Laser: Ion-Optical System for Fast High-Quality Focusing of Powerful Non-Paraxial Ion Beams of Large Format Enriched with Excited Nuclei", ib., 481-492.
7. S.V.Karyagin, "Gamma-Ray Solid Laser: Steadiness Against both Self-Radiation Defects (Micro-Plasma) and Self Heating", The 1st Int. Induced Gamma Emission Workshop, Predeal, Romania, August 16-20, Technical Digest(1997)97.
8. S.V.Karyagin, V.I.Gol'danskii, "Gamma-Lasers", Proc.Nauch.Tech.Conf.Las.Syst., GNILS,Rainbow(1996)39-43.
9. S.V.Karyagin, "Feasibility of gamma-Laser Based on the Modern Technology and the Existing Technique", ib., 43-44.
10. V.I.Vysotskii, R.N.Kuz'min, "Gamma-Lasers", MGU(1989)1-176 (Russ).
11. D.F.Zaretskii and S.B.Sazonov, "The Coherent Repopulation of Hyperfine Levels and Induced Gamma-Emission", The 1st Int. Induced Gamma-Emission Workshop, Predeal, Romania, August 16-20, Technical Digest(1997)69.
12. O.Kocharovskaya, "Lasing Without Inversion: Problems and Prospects", Hyp. Int.**107**(1997)187.
13. A.Heidemann, G.Kaindl et al., Phys. Rev.Let. **36**(1976)213.
14. S.V.Karyagin, "On Possibility of Regulation of Hyper-Fine Structure Over Many Parameters", Pis'ma v Zh.Tekh.Fiz.**2**(1976)500-504; Sov.Tech.Phys.lett.**2**(1976)196-198.
15. S.V.Karyagin, "On the Ways of Suppression of Inhomogeneous broadening of Moessbauer spectral lines", Proc.Int.Conf.Moessb. Spectr., Bucharest, Vol.**2**(1977)1-34, inv. lect. (Russ).
16. G.C.Baldwin, J.C.Solem, V.I.Gol'danskii, "Approaches to Development of γ-Lasers", Rev.Mod.Phys.**53**(1981)687-744.
17. J.T.Hutton, G.T.Trammell and J.P.Hannon, AIP Conf. Proc., Advances in Laser Science-II,**160**(1987)55.
18. V.S.Vavilov, A.A.Gippius, E.A.Konorova,"Electronic and optical processes in diamond", Nauka(1985)1-120 (Russ).
19. S.V.Karyagin, "Atomic (Molecular) Multi-Beam Emitters with Oriented Micro-Relief for Laser Isotope (Isomer) Separation", Abstr.VI Int.Conf. ILLA'98; ed. by V.Panchenko, V.Golubev; Shatura, NICTL RAN(1998)72.
20. L.A.Rivlin,"Gamma-Ray Lasing by the Free Nuclei: Concept for the Feasible Experiment", Proc. of IX-th Conf. on Laser Optics'98, Technical program, Symposium on Quantum Nucleonics, St. Petersburg, June 22-26(1998)69.
21. A.V.Davydov, "Critical Analyses of the Experiments on Search for Induced Gamma-Emission from Long-Living Isomers Te-123m, 125m", ib., 69.
22. G.A.Skorobogatov, B.E.Dzevitskii, "Experimental Technique for Detection of Induced Gamma Emission in Transition $Te(125_{m,2}) \rightarrow Te(125_{m,1}) + h\nu(109.27\ KeV)$", ib., 71.
23. V.I.Vysotskii, "The Theory of Controlling the Nuclear Gamma-Decay in Quantum Nucleonics", ib., 69.
24. V.I.Vysotskii, S.I.Reiman, "The Experimental Realization of the Effect of Controlling Life-time of Gamma-radioactive Isotopes and the Problems of Quantum Nucleonics", ib.,71.
25. S.K.Godovikov, "Deceleration of the Radioactive Decay by Means of the Moessbauer Scattering (Sn 119m)", ib.,71.
26. V.V.Samartsev, S.N.Andrianov, "Superradiance of Laser Cooled Nuclei", ib.,73.
27. B.V.Chirikov, ZhETF**44**(1963)2016-2022; Sov. Phys.-JETP**17**(1963)1355-1359.
28. F.J.Lynch, R.E.Holland, M.Hamermesh, Phys.Rev.,**120**,No.2(1960)513-520.
29. D.Marcuse, Proc. IEEE**51**(1963)849.
30. V.I.Gol'danskii,Yu.Kagan and V.A.Namiot, ZhETF Pis'ma**18**(1973)34-35; Sov.Phys. - JETP Lett.**18**(1973)34-35.
31. R.Bonifacio and L.A.Lugiato, Phys.Rev.**A11**(1975)1507;**A12**(1975)587.
32. A.V.Andreev, Pis'ma Zh.Eksp.Teor.Fiz.**3**(1977)779.
33. V.S.Letokhov, JETP **64**(1973)1555-1557; Sov.Phys.- JETP**37**(1973)787-793.
34. V.S.Letokhov, "Nonlinear selective photo processes in atoms and molecules", M.: Nauka(1983)408p.
35. A.P.Kazantsev, G.I.Surdutovitch, V.P.Yakovlev, "Mechanical Action of Light on Atoms", M.: Nauka(1991)190p.

Recent experiments on induced gamma emission under isomeric transition

$$^{119m_2}Sn \rightarrow ^{119m_1}Sn + h\nu(65.66keV)$$

Svjatoslav I. Bondarevskii, Boris E. Dzevitskii,
Vjacheslav V. Eremin, and German A. Skorobogatov

Department of Chemistry, St. Petersburg State University, Universitetskii prosp., 2
198904 St. Petersburg, Russia. E-mail: gera@mail.moss.pu.ru

ABSTRACT

An induced gamma emission (IGE) upon the transition $Sn(119m_2) + h\nu_{res}(65.66$ keV) $\rightarrow Sn(119m_1)+2h\nu_{res}$ was triggered in the polycrystal matrix $^{119m_2}SnO_2$ by its cooling to a temperature of 78K. A measured relative value of the IGE output ($\varepsilon(SnO_2)$=0.00014 and $\varepsilon(SnO)\leq 0.000012$) strongly correlates with corresponding recoilless fraction: $f_M(78K) = 0.235$ for $^{119m_2}SnO_2$ and $f_M(10K) = 0.021$ for $^{119m_2}SnO$.

Key words: Mössbauer effect, induced gamma emission, co-operative phenomena, nuclear superradiance.

1. INTRODUCTION

Over many years, an **induced gamma emission** (IGE) have been considered as impossible for the long-lived nuclear isomers because of very small magnitudes of the IGE cross-section: $\sigma_{IGE}\leq 10^{-15}$ b. This estimation follows from the standard model [1] for independent radiators:

$$\sigma_{IGE} = \frac{\Lambda^2}{4\pi}\cdot\frac{\Gamma_\gamma}{\Gamma_{tot}}, \qquad (1)$$

where Λ is a gamma-quantum wave-length, Γ_γ is the partial recoilless radiation width, Γ_{tot} is the total line width. Contrary to these expectations, we found experimentally that IGE is possible under proper conditions upon M4-isomeric transitions of the tellurium-$125m_2$ [2-5], tellurium-$123m_2$ [3, 5], and the tin-$119m_2$ [6]:

$$^{125m_2}Te + h\nu\,(109.3\ keV) \xrightarrow{78K} {}^{125m_1}Te + 2h\nu\,(109.3\ keV) \qquad (2)$$
$$\downarrow 1.48ns$$
$$^{125}Te + h\nu\,(35.5\ keV)$$

$$^{123m_2}Te + h\nu\,(88.46\ keV) \xrightarrow{10K} {}^{123m_1}Te + 2h\nu\,(88.46\ keV) \qquad (3)$$
$$\downarrow 0.196ns$$
$$^{123}Te + h\nu\,(159.0\ keV)$$

SPIE Vol. 3685 • 0277-786X/99/$10.00

$$^{119m_2}Sn+h\nu\,(65.66\ keV)\xrightarrow{78K}\ ^{119m_1}Sn+2h\nu\,(65.66\ keV)\quad(4)$$
$$\downarrow 18.08ns$$
$$^{119}Sn+h\nu\,(23.87\ keV)$$

A realization of the IGE process (2) is reproduced in an independent laboratory [7, 8]. Nevertheless, some literature [9, 10] has evolved also which reports the unsuccessful effort to realize the process (2) and (4). That is why, we carried out again an experimental study of the IGE transition (4) with the aim to establish the conditions favorable to the IGE performing.

2. EXPERIMENTS WITH $^{119m_2}SnO_2$

A metallic tin containing 93% of *Sn*-118 was exposed to activation by thermal neutrons of 10^{15} n·cm^{-2}s^{-1} flux for 1 year. The activated tin was allowed to stand for 2 months and then was transformed into the cylindrical radioactive source possessing a diameter *d*, a height *h*, a weight *m*, and a polycrystal structure with chemical composition $^{119m_2}SnO_2$. A temperature dependence of gamma spectrum of the $^{119m_2}Sn$-source was recorded with the use of the gamma-spectral assembly shown in Fig. 1. A measured absolute activity of the starting tin-$119m_2$ was equal to 0.87 Ci/g. This gives a calculated value of the isomer concentration in dioxide SnO_2 equal to

$$\left[^{119m_2}Sn\right]=(6.4\pm0.6)\cdot10^{18}\,cm^{-3}.\quad(5)$$

Experiment №1 Counting interval equals to Δt = 4160 s. Detector «5» of the *BDEG-10V* type with *Na(Tl)I* as scintillating phosphor is at a distance *l* = 10-20 cm. The absorbing filter «7» is a pure iron of 1 mm thick. The source «1» (*h* = 0.02 cm, *d* = 0.7 cm, *m* = 0.041 g) is thermostated with ethanol at 300K, and with $l.N_2$ at 78K.

Experiment №2 The source «1» is the same as in Exp. №1 except its greater age (by 43 days) and different position (up-edged respect to detector «5»). Counting interval equals to Δt = 1200 s; detector «5» is of the *BDEG-8V* type.

Experiment №3 The source «13» (*h* = 1.2 cm, *m* = 0.039 g, θ = 0°) is thermostated with liquid ethanol at 300K, and with solid ethanol at 78K. Detector «5» is of the *BDEG-8V* type with *l* = 10-14 cm, Δt = 5640 s. . The absorbing filter «7» is a pure iron of 1 mm thick.

Experiment №4 The detector «5», filter «7», and source «13» are the same as in Exp. №3 except that a temperature control is performed through the lead refrigerating line. Δt = 1640 s.

Experiment №5 The source «1» (*h* = 0.7 cm, *m* = 0.039 g, *l* = 5 cm) is thermostated with ethanol at 300K, and also at 78K. Detector «5» is of the *DGR* type based on a germanium semiconductor. Δt = 1200 s. An efficiency of the detector *DGR* equals to η = 0.05 at the line E_γ = 65.66 keV contrary to high efficiency (η = 1) of the detector *BDEG*-10(8)*V*.

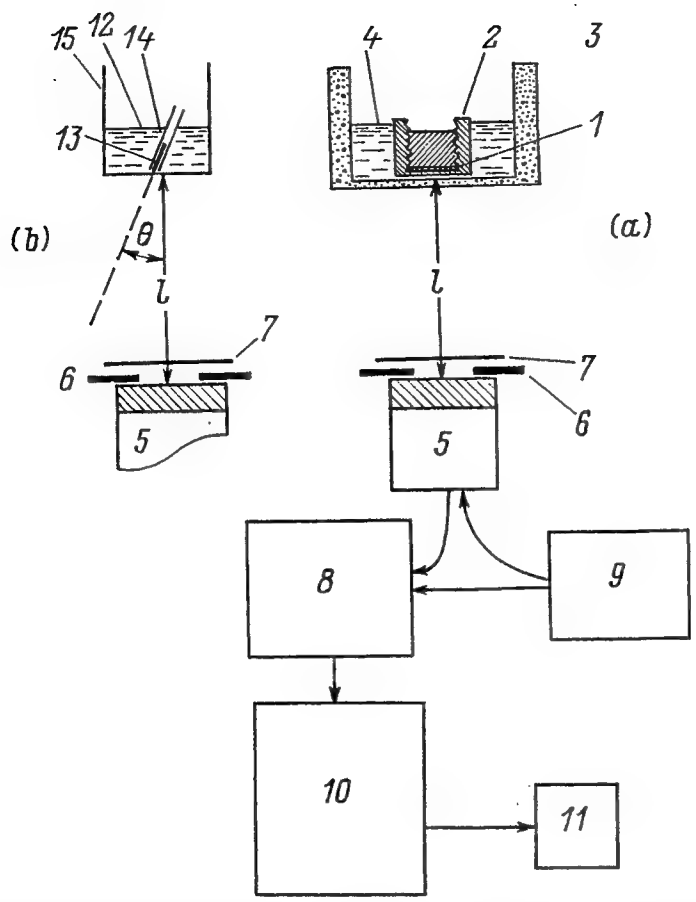

Fig. 1. Experimental setup for investigation of temperature dependence of γ-spectrum of the polycrystalline $^{119m}SnO_2$ source.

(a): «1» is the source in the form of flattened cylinder with height h and diameter d;
«2» is a *PTFE*-container with thin bottom; «3» is a foam plastic thermostat;
«4» is a thermostatting medium; a detector «5» is situated distance *l* from the source;
«6» is a copper (or lead) collimator; «7» is a copper (or iron) soft X-ray-shielding;
«8» is the energy spectrometer *SEG*-06; «9» is a voltage regulator;
«10» is the pulse-height analyzer *AM-A*-02*F*1; «11» is a printer.

(b): «12» is a thermostatting medium;
«13» is the source in the form of elongated cylinder with height h and diameter d;
«14» is an evacuated quartz ampoule with thin bottom (ca. 1 μm);
«15» is a thermostat; θ is an angle between the cylinder «13» symmetry axis and the detector «5» symmetry axis.

The recorded gamma-spectra at 300K and also at 78K are presented in Table 1. It is seen from Tabl. 1 that a background counting level (N) in the (42-91)-keV pedestal of Exp. №1 has a ratio $N(78K)/N(300K) = 0.896 \pm 0.007$ which almost equals to the electron density (e. d.) ratio

$$\frac{e.d.(l.N_2)}{e.d.(l.ethanol)} = 0.911 \qquad (6)$$

of thermostating liquids. This coincidence shows that the overall background radiation in the range of 40-90 keV is mainly a scattered bremsstrahlung from the conversion electrons. Furthermore, a counting level (N_γ) at the line $E_\gamma = 65.66$ keV has a ratio

$$N_\gamma(78K)/N_\gamma(300K) = 0.995 \pm 0.001 \quad (7)$$

which almost equals to the inverse absorption factor (μ^{-1}) ratio

$$\frac{1/\mu(78K)}{1/\mu(300K)} = 0.994 \quad (8)$$

Indeed, an absorption factor (μ) equals to 28.4 cm^{-1} [11] for tin dioxide SnO_2 at 300K under a quantum energy E_γ = 65.66 keV. Hence, a mean free path of the E_γ quantum equals to μ^{-1} = 0.035 cm what is comparable to height h = 0.02 cm in magnitude. It follows that the source «1» is optically thick one, that is, its gamma emittance at the line E_γ is bound to decrease under lowering of source temperature because of attendant increase of factor μ. This is consistent with Experiment №2 wherein even lower ratio

$$N_\gamma(78K)/N_\gamma(300K) = 0.960 \pm 0.002 \quad (9)$$

is recorded on measurement of a gamma spectrum on the end face of the same source. In the end, the results of experiments №1 and 2 revealed an essential dependence of measured gamma-spectrum in the range 40-120 keV on the source temperature and environmental conditions. That is why we used a temperature dependence of gamma-spectrum intensity in the neighbourhood of line $E_{2\gamma}$ = 131.32 keV as a method for the IGE (4) detection

A resolving time of the *BDEG*-10*V* detector equals to t_{res} = 2.5 μs. Hence, at a counting level of 671 pulses/s under the E_γ-quanta recording, the double chance coincidences are bound to give about 5000 pulses per 4160 s in the channel of $E_{2\gamma}$ = 131.32 keV. This is just recorded during the experiment №1 at room temperature. It is seen from Eq. (7) that the level of double chance coincidences is bound to decrease down by 50 pulses under lowering of the source temperature. Instead, the recorded counting level in the $E_{2\gamma}$-channel equals to 6938 pulses per 4160 s at a temperature of 78K. The obtained difference (about 2800 pulses) may be ascribed only to the IGE (4) possessing a relative yield of $\varepsilon_{2\gamma}$ = (0.10±0.04)% (cf. Table 1). In experiment №2, the same procedure gives a relative yield of $\varepsilon_{2\gamma}$ = 0.036±0.04 %.

In order to reduce the relative measurement error ($\Delta\varepsilon_{2\gamma}$), we performed the more elaborated experiments №3, 4, and 5 (cf. Table 1). In experiments №3 and 4, we increased the accumulated pulses number (N_γ) by a factor 2-3 in comparison with experiments №1 and 2. Next, in experiments №3 and 4, we used optically thick source «13» in order to increase the relative output of the IGE (4) process. Furthermore, in experiments №3 - 5 we applied the fixed thermostating media (ethanol, or lead) under all temperatures in order to exclude any temperature dependence of the intensity of a background bremsstrahlung radiation. Finally, in experiment №5, we used the detector

DGR with low efficiency ($\eta = 0.05$ at the line E_γ) in order to reduce a counting load and exclude appropriately the double chance coincidences in the $E_{2\gamma}$-channel

Table 1. Electromagnetic radiation spectrum of the polycrystal source $^{119m}SnO_2$ depending on its temperature.

Experiment № [a]	Spectral range, keV	Pulses number (N) in a time Δt		N (78 K)/N (300 K)	$\varepsilon_{n\gamma}=\Delta N_{n\gamma}/N_\gamma$(300 K) [b]
		N (300 K)	N (78 K)		
1	42-91 pedestal	1141841	1022762	0.896±0.007	
	42-91 E_γ peak	2791760	2776578	0.995±0.001	-0.005±0.001
	92-110 pedestal	92305	93767	1.016±0.007	
	92-110 peak	665	-1580		
	111-165 pedestal	243064	240855	0.991±0.004	
	111-165 $E_{2\gamma}$ peak	4147	6938		0.0010±0.0004
2	36-95 pedestal	495413	472587	0.954±0.010	
	36-95 E_γ peak	1254391	1204048	0.960±0.002	-0.040±0.002
	96-121	34331	34136	0.994±0.011	
	122-167 ($E_{2\gamma}$)	57752	58210		0.00036±0.00038
3	42-96 pedestal	1082749	1083872	1.001±0.007	
	42-96 E_γ peak	3237026	3228857	0.998±0.001	-0.002±0.001
	113-142 ($E_{2\gamma}$)	9933	12179		0.0007±0.0003
4	43-99 pedestal	1586043	1562087	0.985±0.006	
	43-99 E_γ peak	4179682	4193179	1.003±0.001	0.003±0.001
	110-157 ($E_{2\gamma}$)	25962	26818		0.0002±0.0001
5	36-58	100457	96525	0.961±0.063	
	62-69 pedestal	12078	11542	0.956±0.025	
	62-69 E_γ peak	124511	123010	0.988±0.007	-0.012±0.006
	72-125	1779	1683	0.946±0.045	
	128-134 ($E_{2\gamma}$)	128	139		0.00009±0.00017
A theory model [5]	E_γ peak			0.99998	-0.000020
	$E_{2\gamma}$ peak				0.000020
model [12]	E_γ peak			0.999935	-0.000065
	$E_{2\gamma}$ peak				0.000065

([a]) A counting rate within the E_γ(65.66 keV) channel equals to 671, 1045, 574, 2549 and 104 pulses/s in experiment № 1, 2, 3, 4 and 5 respectively.

([b]) $\Delta N_{n\gamma}=N_{n\gamma}(78K)-N_{n\gamma}(300K)$, where $N_{n\gamma}$ is the pulses number accumulated within the channel $E_{n\gamma}=n\cdot E_\gamma=n\cdot 65.66$ keV in a time Δt.

The above-listed improvements in the investigation techniques were resulted in near-constant counting level in all temperatures in the neighbourhood of E_γ-line (cf. Table 1, experiments №3-5). Hence, in all cases, a level of the double chance coincidences in the neighbourhood of $E_{2\gamma}$-line was bound to be temperature independent within the experimental error. Instead, in all experiments №3-5, we obtained a sensible enhancement of counting level in the $E_{2\gamma}$-channel as the temperature decreases down to 78K (cf. Table 1). In our opinion, the IGE (4) is the sole cause of this enhancement. In units of standard deviation (σ), the obtained value of the IGE relative output ($\varepsilon_{2\gamma} = \Delta N_{2\gamma}/N_\gamma(300\text{K})$) equals to $\frac{10}{4}\sigma$, $\frac{36}{38}\sigma$, $\frac{7}{3}\sigma$, 2σ and $\frac{9}{17}\sigma$ in experiment №1, 2, 3, 4 and 5 respectively. It follows that the combined magnitude of the IGE (4) relative output equals to

$$s = \left(\frac{10}{4} + \frac{36}{38} + \frac{7}{3} + 2 + \frac{9}{17}\right)\sigma = 8.3\sigma \tag{10}$$

3. DISCUSSION

We calculated a theoretical value of the IGE relative output

$$\varepsilon_{2\gamma} = \frac{\Phi_{2\gamma}(78\text{K}) - \Phi_{2\gamma}(300\text{K})}{\Phi_\gamma(300\text{K})} \tag{11}$$

using the co-operative model of Ref. [5]

$$\varepsilon_{theor} = \frac{2\pi}{3}[{}^hX]\prod_{i=1}^{3} Min\left(l_i, \frac{1}{\mu}\right)\frac{f_M(T)\tau_l}{(1+\alpha_h)(\tau_h+\tau_l)}, \tag{12}$$

or the refined co-operative model of Ref. [12]

$$\varepsilon_{theor} = \frac{1}{2}[{}^hX]\prod_{i=1}^{3} Min\left(l_i, \frac{2\pi^{1/3}}{\mu}\right)\frac{f_M(T)\tau_l}{(1+\alpha_h)(\tau_h+\tau_l)}. \tag{13}$$

Here $\Phi_{n\gamma}(T)$ is a flux of photons with energy of $E_{n\gamma} = n{\cdot}h{\cdot}\nu$, $[{}^hX]$ is a concentration of nuclear isomer X in the high-lying state (h), l_i is the source linear dimension along i-th co-ordinate, $f_M(T)$ is the Mössbauer factor at temperature T, τ_h (τ_l) is a lifetime of nuclear isomer at the high(low)-lying level, α_h is a conversion factor in the decay of high-lying level. In the transition (4) one has $\alpha_h = 4999$, $\tau_h = 293$ d. [13], and $f_M(78\text{K}) = 0.235$ for a matrix SnO_2 [14]. The theoretical IGE output ($\varepsilon_{2\gamma}$) we calculated by Eqs. (12), (13) with using the concentration (5) (cf. Table 1).

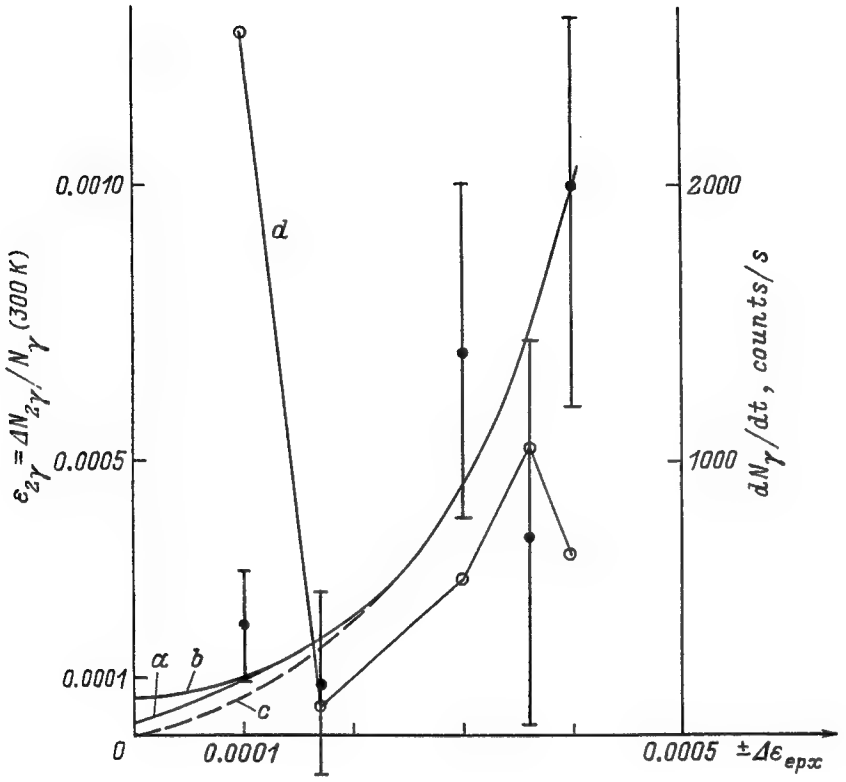

Fig. 2. Experimental values of IGE (4) output ($\varepsilon_{2\gamma}$) as a function of the experimental standard error ($\pm\Delta\varepsilon_{exp}$), from the Table 1. Under reducing of standard error ($\Delta\varepsilon_{exp}$) the curves «a», «b» and «c» approaches the theoretical magnitudes $\varepsilon_{2\gamma} = 0.00002$ (Ref. [3]), $\varepsilon_{2\gamma} = 0.000065$ (Ref. [12]) and $\varepsilon_{2\gamma}=0$ (Ref. [1]), respectively. The curve «d» connects the points (0) corresponding to right-hand vertical scale (dN_γ/dt, a counting rate in the channel $E_\gamma = 65.66$ keV).

The data for the IGE output both experimental and theoretical are shown also in Fig 2. It is seen from the latter that a measured value of $\varepsilon_{2\gamma}$ reduces under reducing of standard deviation ($\Delta\varepsilon_{exp}$) and approaches the theoretical magnitude 0.000065 rather than zero (cf. curve «b» at Fig. 2). Furthermore, as opposed to the random noise, a measured values of $\varepsilon_{2\gamma}$ take the positive magnitudes only. As this takes place, the probability of Poisson noise giving a random combined signal as large as (10) equals to 10^{-15}. At the same time, the non-random occurrence of this signal as a result of double chance countings in the $E_{2\gamma}$ channel is excluded on the basis of the lack of any correlation between the measured $\varepsilon_{2\gamma}$ magnitude and a counting load in the E_γ channel (cf. curve «d» at Fig. 2). As a consequence we consider the IGE (4) as the sole cause for the signal (10) occurrence.

Table 2. Results of searching for an induced gamma emission in M4-transition $^{119m2}Sn \longrightarrow {}^{119m2}Sn+h\nu$ (65.66 keV)

Source of information	Present work	Ref. [10]
Activity of metallic *Sn*	0.9 Ci/1 g	0.5 Ci/1 g
solid matrix	SnO_2	SnO
$[^{119m2}Sn]$, atom/cm^3	$6.5*10^{18}$	$4.3*10^{18}$
T_{exp}	78 K	10 K
$f_M(T_{exp})$	0.24	0.021
μ(65.66 keV), cm^{-1}	28.4	34.1
$\varepsilon_{coll.} \sim f_M[^*Sn]\mu^{-3}$, Eq. (13)	0.007%	0.0002%
$\varepsilon_{exp.}=\Phi_{2\gamma}(T_{exp})/\Phi_{\gamma}(300K)$	(0.014±0.005)%	≤ 0.0012%

In the Table 2, the characteristics of our experiments are listed as opposed to experiment of Ref.[10]. As may be seen from Table 2, the radioactive source of Ref.[10] had a low factor f_M, the reduced concentration $[^{119m_2}Sn]$ and reduced permeability μ_0^{-1} in contrast to our source. As a result, the theoretical value (13) of the IGE output for our source in 35 times that of Ref. [10]. That is why the experiment of Ref. [10] gives no way of detection the IGE process (4). The poor quality of the radioactive source is the reason why work [10] has led to negative result.

5. ANTI-ACKNOWLEDGEMENTS

This work is performed without any financial support from capitalistic Russia.

6. REFERENCES

1. G.C. Baldwin, J.C. Solem, and V.I. Gol'danskii, *Rev. Mod. Phys.*, **53**, pp. 687-744, 1981.
2. G.A. Skorobogatov, and B.E. Dzevitskii, *Izvestija Acad. Sci. USSR, ser. phys. (Russ.)*, **48**, pp. 1934-1939, 1984.
3. G.A. Skorobogatov, and B.E. Dzevitskii, *Laser Physics*, **5**, pp. 258-267, 1995.
4. G.A. Skorobogatov, and B.E. Dzevitskii, *Il Nuovo Cimento (D)*, **17**, pp. 609-626, 1995.
5. G.A. Skorobogatov, and B.E. Dzevitskii, *Hyperfine Interactions*, **107**, pp. 401-411, 1997.

6. S.I. Bondarevskii, B.E. Dzevitskii, and V.V. Yeremin, *Proceedings of the Intern. Conf. on LASERS' 96 (Dec. 2-6, 1996, Portland, OR)*, pp. 261-265, STS Press, McLean, VA, 1997.
7. V.G. Alpatov, G.E. Bizina, A.V.Davydov, B.E. Dzevitskii, G.R. Kartashov, M.M. Korotkov, G.V. Kostina, A.A. Sadovskii, and G.A. Skorobogatov, *Izvestija Acad. Sci. USSR, ser. phys. (Russ.)*, **50**, pp. 2013-2015, 1986.
8. V.G. Alpatov, G.E. Bizina, S.K. Godovikov, A.V.Davydov, B.E. Dzevitskii, G.R. Kartashov, M.M. Korotkov, V.V. Metlushko, A.A. Sadovskii, and G.A. Skorobogatov, *Proceedings of 32th Conf. Nucl. Spectr. and At. Nuclear Structure (Apr. 14-17, 1987, Yurmala) (Russ.)*, p. 224, Nauka, Leningrad, 1987.
9. R.S. Rundberg, M.M. Fowler, R.D. Taylor, and J.B. Wilhelmy, *Technical Digest of 1st Intern. Induced Gamma Emission Workshop (Aug. 16-20, 1997, Predeal, Romania)*, pp. 107-108, ICIGE, 1997.
10. V.G. Alpatov, A.A. Antipov, G.E. Bizina, S.K. Godovikov, A.V.Davydov, G.R. Kartashov, M.M. Korotkov, P.A. Polozov, B.I. Rogozev, A.A. Sadovskii, I.A. Suvorov, and A.N. Cheltsov, *Izvestija Acad. Sci. USSR, ser. phys. (Russ.)*, **53**, pp. 2052-2054, 1989.
11. E. Storm, and H.I. Israel, *Nuclear Data Tables*, **A7**, p. 565, 1970.
12. G.A. Skorobogatov, and G. Preparata, *in press*.
13. R.L. Auble, *Nuclear Data Sheets*, **26**, pp. 207-279, 1979.
14. P. Boolchand, *J. Quant. Spectrosc. Radiat. Transfer*, **40**, pp. 777-795, 1988.

Laser nucleosynthesis of radioactive isotopes and isomers

G. M. Chumak
Russian Scientific Center "Applied Chemistry"
St.Petersburg, Russia, 197198

ABSTRACT

I have investigated analitical simulation of the possibility of application superstrong, ultrafast laser radiation for nucleosyntesis of ^{26}Al, $^{26}Al^{m}$ (Al-Mg-cycle) in cosmic regolith using products of the reaction $^{3}He(d,p)^{4}He$, and other light accelerated charged particles. It may be laser propulsion with annihilation of cosmic propillents a matter.

1. INRODUCTION

By this report J'd like to mark the 80th anniversary of my father, M. A. Chumak (1916-1993) – geologist, and my teacher, academic, G. I. Budker (1918-1977) – a physicist. For me, They both are as the best examples of a fortitude, honesty and a great professionalism. Through my life J thought hardly about how to connect a physics of high energy density and a geology thgether into one work to publish. As always, the decision came suddenly. At last time J work at modification high energy excimer lasers in subnanosecond and terawtt regime, tranformation the UV lasing in EUV, VUV, and X-ray lasing, search a matter for a pillet. The picture of a moonstone of the "Apollo-11"'s expedition (july 1969) ais always on my desk. At thist moment (july 1969) J became a father of my first child, my doughter Helen. Once all these have been sumed together. Results of it you'll see below. The autor understads clearly that a decision of this problem has a nuance of science-fiction but no more than other projects on the same subject. However, the author supposes that today is a time to come to this subject. It might seem to be impossible to find.synchronization laser propulsion.today, but some experience received during the may be usful us the future to work with this problem (om the more high level of physical and technical knowledges).

Superstrong, ultrashort light fields with a certain polarisation generated by excimer or solid state systems allow to extend optical physics methods to nonlinear quantum electrodynamics, plasma physics and high energy physics. When laser beams of such an energy and duration interact with matter, self-focusing and self-channeling take place by the influence of nonlinear (ponderomotive) forces (for example, the Kerr effect) and relativistic effects /1, 2/. This results in generating spontanious magnetic fields of 20-250 MGs; in excitating shock pulses with pressure of 0.6Mbar-1 GBar; generating ions and charge particle with energy of 3-200 Mev; generating harmonics and X-ray emission in the wide energy range of 0.0001-5 Mev being sufficient for electron-positron pairs formation; in transforming nuclears of some elements into their isomer states because of the interaction of several laser-excited atomic electron shells with nuclear levels.

SPIE Vol. 3685 • 0277-786X/99/$10.00

Further we discuss the possibility of using laser radiation for the nucleosynthsis of radioactive isotopes of elements in the middle the periodic table. Searchig the target material suitable for effective complex application of the above-mentioned effects of the interaction of superstrong light field with matter for the convertion of light field energy into other forms of energy has culminated at last in choose in a superficial (3-6 mm) layer of a fine-graihed, loosely-bound lunar regolith /3/. The formation velocity of the regolith is about 1 mm per 1 mln years. The solar wind and flashes action is responsible for the enlarged content of inert gases (He^3, He^4, Ne, Kr, Xe); the cosmic ray action manifests itself as a presence of nuclear splitting products, as a decay and formation of numerous rare isotopes including radioactive ones. As a target we suppose to use rombic crystals $(Mg,Fe)Ti_2O_3$ and the mineral $MgAl_2O_3$. The similar superficial content is also inherent to other cosmic bodies in the absence of the atmosphere.

From the W. Fowler's works on nuclear astronomy /4/ of is known, that in the Early universal ^{26}Al (the fundamental state is $5+(^{26}Al)$ with the β^+- half-life period of 1 mln years and the isomeric state $0+(^{26}Al^m)$ with β^+ - half-life period of 6.3 s which was formed in the reaction $^{25}Mg(p, \gamma)^{26}Al$ (fig.1.) in Al-Mg-cycle (fig.2.)), was of considerable importance as energy source for the interstellar ionization (see in /4a/ the map of the gamma-ray line emission at 1809 keV from aluminium-26 decay as measured by the ComptonTelescope(COMPTEL) indtrument).

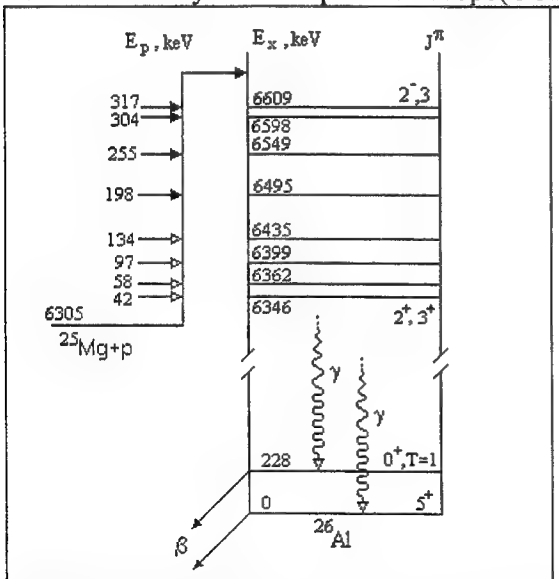

Fig.1. The diagram of power levels of a nucleus ^{26}Al near to a threshold of proton disintegration. The resonances were observed down to the minimal energy Ep = 198 keV /4/.

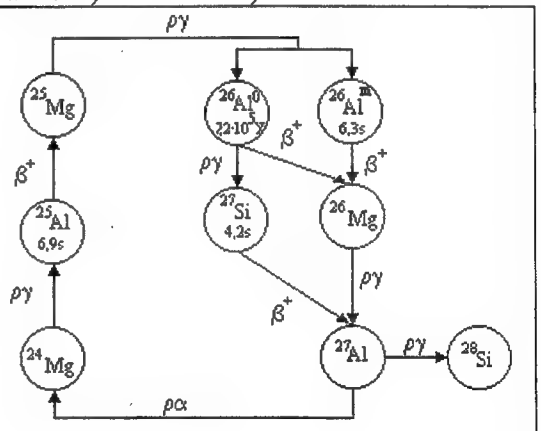

Fig.2. A sequence of nuclear reactions and β^+-disintegrations for Mg-Al-cicle /4/. The periods of half-disintegration of all radioactive isotopes are specified. The reaction ^{27}Al (p, g) ^{28}Si results in outflow of nucleuses from Mg-Al-cicle.

Probably, the Nature has prepared for our interplanetary and inter- galactic cosmic flights the optimal, ecologically clean working body for lasers and laser propulsion of the new generation: relict minerals with the necessary isotopic ratio Mg, Al for Al-Mg-cycle and for the conversion of laser radiation into γ- and x-ray radiation, saturated by a thermo-nuclear fuel with clean nuclear reactions $^3He(d,p)^4He$, $D(d,p)^3He$, $^3He(\alpha,\gamma)^7Be$..... Besides, here electron and positron annihilation will at first make a weighable contribution to the positive energy balance.

2. Ultrashort powerful laser matter interaction

The basic issues affecting the laser-plasma interaction are considered, including: the different absorption mechanisms; the formation of transient, nonequilibrium, asymmetric electron distribution function; the energy losses; the role of instabilities and the ponderomotive force; ion expantion and acceleration; and surface wave propagation along the boundary of the plasma /5/.

The new generation of lasers with power exceeding the terawatt level that have been developed in recent years have possibilities for studying laser-matter interaction physics. In contrast to other powerful (up to 200 TW) but massive installations developed for the laser-fusion program (ICF) /6 /, laser impuls space propulsion (LIPS) / 7 /, (ORION) /7a/, free-electron power beaming of energy (SELENE /8/) through the atmosphere to a satellite, the high power level of these new lasers is achieved by shorting the pulse duration down to the subnanosecond - femtosecond ranges, and thus the total energy of the pulse is 0.1-500 Joules /9/. This lasers, therefore, are relatively compact and flexible devices that can operate at repetition rates from several Hertz to several kilohertz and with contrast ratios of more than 10^{10}. It is possible to produced states of the medium with relaxation times (e.g., time for expantion, collision time, life time of excited states, ets.) exceeding the laser pulse duration. Furthermore, a very high electric field amplitude can be achived in focal spot, much higher, than the magnitude of the atomic field $E_a = 5.1\times10^9$ V/cm. This high field amplitude can be achived in a lineary polarized laser beam with intensity /10/:

$$I_a = cE_a^2/8\pi = 3.5\times10^{16}\ W/cm^2 \qquad (1)$$

Laser-matter interactions occurring at intensities $I>I_a$ will result in direct ionization of the material and production of highly stripped ions.

The parameter characterizing the ionization process in a strong field is known as the Keldish parameter /11/. It equals the ratio of the ionization potential I_i to the electron oscillation energy in a laser electric field ε_{os}

$$\Gamma = I_i/2\varepsilon_{os} \qquad (2)$$

For example, for ionization of a K-shell electron from an atom with charge Z, one obtains $I_i = Z^2/I_H$, where I_H is ionization potential for hydrogen. The oscillation energy reads

$$\varepsilon_{os} = e^2E_a^2(1 + \alpha^2)/4m_ew^3, \qquad (3)$$

where w is the laser frequency and α is the polarization parameter ($\alpha = 0$ for linear polarization, and $\alpha = 1$ for circular polarization). It is convenient to represent Γ and ε as functions of the laser parameters in the form

$$\Gamma^2 = 0.73Z^2/I_{14}\lambda\mu_m^2(1 + \alpha^2)$$
$$\varepsilon_{os} = 9.3(1 + \alpha^2)I_{14}\lambda_{\mu m}^2 \ (eV) \qquad (4)$$

where I_{14} is the laser intensity in units of 10^{14} W/cm2 and λ is the laser wavelength in microns. For intensity $I > 10^{14}$ W/cm2 and $\lambda < 1$ μm one obtains from equation (4) that $\Gamma^2 > 1$. This means that multiphoton ionization takes place. The ionization rate (probability of ionization of one atom per unit time) in multiphoton limit is

$$w_n = w_0n^{3/2}(\varepsilon_{os}/I_i)^n \qquad (5)$$

which depends on the number of absorbed quanta, $n = I_i/hw_0$; the ionization potential, I_i; and the laser intensity (via ε_{os}). Equation (5) was derived under the assumption $\varepsilon_{os} << I_i$. Thus one can conclude that multiphoton ionization is important for short wavelength lasers at relatively low intensities (10^{14} W/cm^2). Multiphoton ionization can compete with collisional ionization only in rarefied gases. The latter mechanism dominates in solids. Its probability is

$$w_c = \nu_{in}\,\varepsilon_{os}/I_i \qquad (6)$$

where ν_{in} in is the frequency of an inelastic collision. The probability depends weakly on the laser intensity.

At $I > I_a$ ($\Gamma^2 << 1$) tunnel ionization occurs. The probability for tunnel ionization is

$$w_i = (I_i/h)\exp[-(u/3)(I_i/hw_0)(I_i/\varepsilon_{os})^{1/2}], \qquad (7)$$

which becomes comparable with the probability for collisional ionization (6).
At laser intensities $I = 3\times10^{16}$ W/cm^2 (when $E = E_a$) the term in the square brackets in (7) becomes equal unity. Therefore, the atoms become ionized during a time less than one period of the laser wave. One can consider the ionization of a solid target under the action of a high-intensity laser in two stages. First, atoms are ionized by the laser field, and, second, by the impact of the electrons accelerated and heated by the laser field. The final degree of the ionization depends mainly on the average electron energy rather than the laser intensity. Finally, if laser radiation with a high contrast ratio hits the solid target, a plasma layer with the electron density $n_e \geq 10^{24}$cm^{-3} and high conductivity will form in a few femtoseconds. The electron concentration in this layer is much higher than the critical density $n_e = mw_0^2/4\pi e^2$. Thus the laser-matter interaction proceeds in the skin-effect regime. Absorption of the electromagnetic radiation in the

overcritical plasmas ($n_e >> n_c$) may occur in regime of either the normal or anomalous skin effect, depending on the relationship between the electron mean free path, skin depth, laser frequency, collision frequency, and electron thermal velocity.

In the case the relatively low intensities ($I \leq 10^{16}$ W/cm^2) and low electron temperatures, the normal skin effect takes place. The electric properties of the plasma in this case can be characterized by the dielectric permeability

$$\varepsilon = 1 + i4\pi\sigma / w_0 , \qquad (8)$$

which is more conveniently expressed in the form associated with the Drude model /12/

$$\varepsilon = 1 - w_{pe}{}^2 / w_0(w_0 + i\nu_{eff}) \qquad (9)$$

where $w_{pe} = (4\pi e^2 n_e / m_e)^{1/2}$ is the electron plasma frequency and ν_{eff} is the effective frequency of the electron collisions. Note that in the case considered, $w_{pe} >> w_0$;$\nu_{eff} >> w_0$, i.e., Re $\varepsilon < 0$.

The skin depth in / 5 / reads

$$l_s = (c / w_{pe}) (\nu_{eff} / w_0 \cos\vartheta_0)^{1/2} \qquad (10)$$

For normal incident ($\cos\vartheta_0 = 1$) of the electromagnetic wave the energy dissipation (and absosorption coefficient), relate to the real part of the surface impedance ξ, are

$$\mathrm{Re}\,\xi = \frac{\omega_0}{c} l_s ; A \cong 2\,\mathrm{Re}\,\xi = \frac{2\omega_0}{\omega_{pe}} \left(\frac{\nu_{eff}}{\omega_0} \right)^{1/2} = 2 \left(\frac{n_e \nu_{eff}}{n_e \omega_0} \right)^{1/2} \qquad (11)$$

When n_e / n_c , Re $\xi << 1$ and $A << 1$. For the case of the oblique incidence of the laser beam at an angle ϑ_0, the solution of Maxwell's equation results in the Fresnel formula /12/:

$$R_s = \left| \frac{\sin(\Theta_0 - \Theta_t)}{\sin(\Theta_0 + \Theta_t)} \right|^2 ; R_p = \left| \frac{tg(\Theta_0 - \Theta_t)}{tg(\Theta + \Theta_t)} \right|^2 \qquad (12)$$

where $\vartheta_t = \arcsin[\sin\vartheta_0 / \varepsilon^{1/2}]$ is the complex refraction angle. The indices s and p correspond respectively to the cases when electric field vector lies in the plane perpendicular to the planes of the incidence (s) or (p). At laser intensities $10^{12} - 10^{14}$ W/cm^2 the thermal energy of the electron is relatively low (up to ten of electronovolts), the plasma proves to be nonideal ($\nu_{eff} = w_{pe}$). At the laser intensity grows, the plasma electron temperature increases, affecting decrease of the electron collision frequency and absorption coefficient. At present time electron temperature of 300 to400 eV at intensities of $10^{14} - 10^{15}$ W/cm^2 for pulse duration $\leq$0.4 ps have been obtained experimentally.

The physics of the interaction changes qualitatively in excess of 10^{16} W/cm^2, when the plasma temperature exceeds 1 keV. The ionization rate increases due to tunnel effect, and the charge of the ions increases because of the higher temperature. The electron mean free path is now larger than the skin depth, $l_{ei} > l_s$. The distance the electron penetrates during the wave period is larger than skin length, i.e., $\upsilon / w_0 >> l_s$. Thus, all the conditions for the anomalous skin effect to be valid are fulfilled. Let us introduce the effective frequency of the electron interaction with the field as $\nu_{eff} = \upsilon_{th} / l_{as}$, *where* υ_{th} is the electron thermal velocity. Inserting this equation into (10) one can obtain the field penetration depth for the anomalous skin effect l_{as} in the well-known form /12a/:

$$l_{as} \sim (c/w_{pe})[(\upsilon_{th}/c)(w_{pe}/w_0)]^{1/3} \qquad (13)$$

For a normally incident electromagnetic wave, the absorption coefficient is also proprtional to the real part of the surface impedance /12/:

$$A_{as} \cong (8/3\sqrt{3})(w_0 l_{as}/c) \qquad (14)$$

One can estimate from equation (10) and (13) that $l_{as} > l_{ns}$. *That is true for conditions appropriate to the classical anomalous skin effect* /12/. In the case of the interaction of an ultrashort intense laser pulse with matter, the electron distribution function proves to be transient, non-Maxwellian, and asymmetric /13/. Thus, the field and the plasma parameters in this case are independent and change in time and space during the interaction time.

When the laser intensity is further increased ($I >> I_a$) another physical threshold is reached, which corresponds to the oscillation energy becoming equal to the electron rest energy $E_{os} = mc^2$. The corresponding (relativistic) values of the laser intensity and field amplitude are

$$I_i = 4n_e m_e c^3 = 1.14 \times 10^{19} \lambda_{\mu m}^{-2}$$
$$E_r = 2m_e c w_0 / e = 12.87 E_a / \lambda_{\mu m} \qquad (15)$$

Her $n_e = m_e w_0^2/4\pi e^2 = 10^{21}\lambda^{-2}$ [cm-3] is the critical electron density of the plasma at the frequency w_0 (wavelength λ). At intensities above the relativistic threshold, plasmas with the relativistic electrons may be produced. The laser-matter interaction at relativistic intensities become strongly nonlinear. The first nonlinear effect that one has take into account is due to the light pressure on the surface of the solid target /5/:

$$P_{light} = (1 + R)E_0^2/8\pi = (1 + R)I/c = 3.3\times10^{-2} I_{14} \text{ [Mbar}\} \qquad (16)$$

where I_{14} is the reflection coefficient. It follows from equation (9) that the light pressure at relativistic intensity $I_r = 10^{19}$ W/cm^2 (λ = 1 μm) reaches 3.3×10^3 Mbar. This pressure is comparable to the thermal pressure in the central core of a heated and compressed laser-fusion target. The light pressure can lead to direct heating of ions. It can also induce a Rayleigh-Taylor instability at the plasma-vacuum interface because at this boundary the "light liquid"(photons) accelerates the heavy ions. Such a plasma may also be used as a source of stripped ions and for particle accelerators. The laser

beam at such intensities (10^{20}–10^{21} W/cm^2) act like a piston on a solid target producing strong shok wave, and large part of the absorbed energy is transferred to ions.

In the paper /14/, which is based on steady-state paraxial theory by Akhmanov /15/ and Sodha /16/, relativistic self-focusing of Gaussian laser beams for arbitrary large nonlinearity is presented. The dielecctric constant of the plasma is given by

$$\varepsilon_0 = (1 - w_{pe}^2 / w^2) \qquad (17)$$

The expression for w_{pe} *have* to be generalized relativistically with respect to the oscillattion of the electrons within the elecromanetic field the ganerates maximum kinetic energies ε_{kin} of relativistic magnitude /17/:

$$\varepsilon_{kin} = m_0 c^2 \left[\left(1 + \frac{e^2 E^2}{m_e \omega^2 c^2} \right)^{1/2} - 1 \right] \qquad (18)$$

where E is the actual maximum electric field of laser beam, I is its actual irradiace, and w is the laser frequency. The relativistic general expression for plasma frequency w_{pe} is then,

$$w_{pe}^2 = (4\pi n_e e^2/m_e)[m_e c^2/(m_e c^2 + \varepsilon_{kin})]$$

$$= \begin{cases} 4\pi n_e e^2/m_e [1 + (I / I_{rel})]^{-1} & \text{if } I << I_{rel} \\ 4\pi n_e e^2/m_e [1 + (I / I_{rel})^{1/2}]^{-1} & \text{if } I >> I_{rel} \end{cases} \qquad (19)$$

Using equation (17) equation (19) and following /16/, a nonlinear self-focusing medium can be described by an intensity –dependent effective dielectric constant as

$$\varepsilon = \varepsilon_0 + \Phi(I) \qquad (20)$$

where ε_0 is the linear part of the dielectric constant, and

$$\Phi = \begin{cases} (w_{pe}^2 / w^2)[1 - (1 + I / I_{rel})^{-1}] & \text{if } I << I_{rel} \\ (w_{pe}^2 / w^2)[1 - \{ 1 + (I / I_{rel})^{1/2} \}^{-1}] & \text{if } I_i >> I_{rel} \end{cases} \qquad (21)$$

is the nonlinear relativistic term. The effective dielectric constant for an arbitrary large magnitude of nonlinearity can written as /14/

$$\varepsilon = \varepsilon_0' - \varepsilon_1(f) r^2 \qquad (22)$$

where $f(z)$ is the dimensionless beamwidth parameter and ε_0' and ε_1 represent, respectively,
the linear and nonlinear dielectric constants for an arbitrary magnitude of nonlinearity.

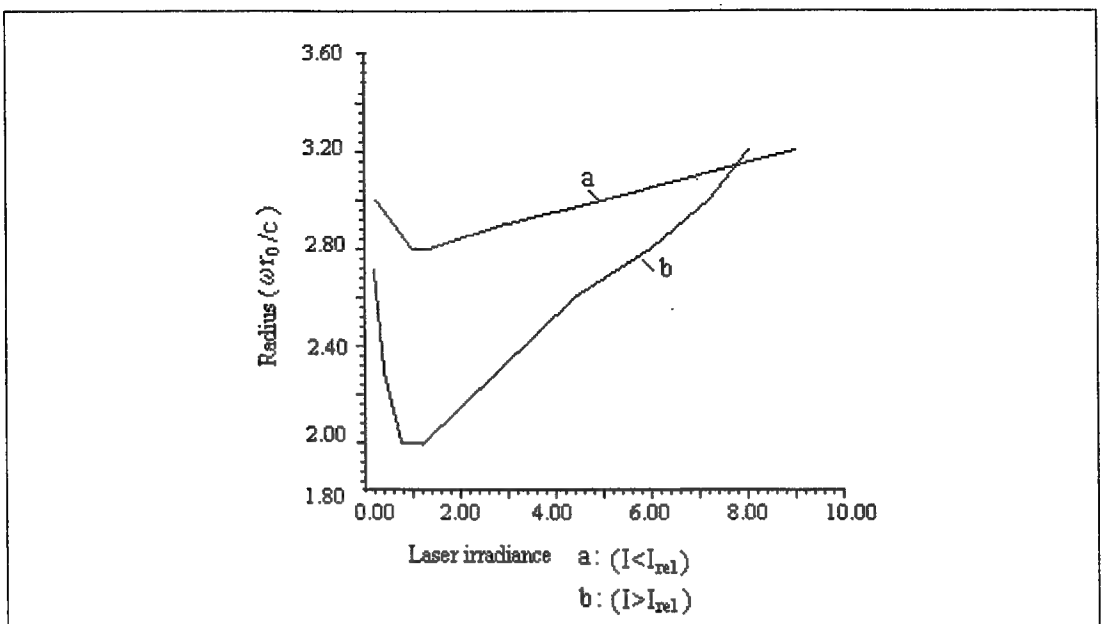

Fig.3. Variation of dimensionless radius with lser irradiance for *a)* $I < I_{rel}$, , b) $I > I_{rel}$/v./14/.

Fig.3 shows the dielectric increase for a Neodymium glass laser, with irradiences exceeding 10^{18} W/cm^2. Due to the saturating nature of the nonlinear dielectric constant, we obtain two velues of critical powers, P_{cr1} and P_{cr2}. The variation of beam radius with laser irradiance is shown in fig.4. The theory /14/ predict the formation of oscillatory waveguide when certaine condition are satisfied, and the present results are valid for all values of z (fig.5, 6).

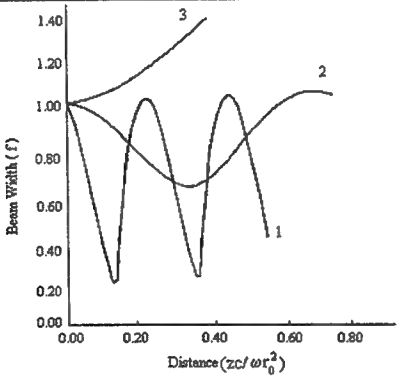

Fig.4. Variation of beamwidth parameter (f) with distance of propagation for $I < I_{rel}$.
Curves I, II, III are for I/I_{rel} = 10, 100, and 1000, respectively.

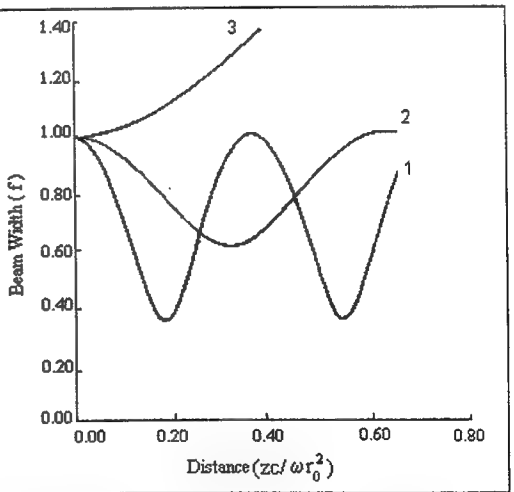

Fig.5. Variation of beamwidth parameter with distance of propagation for $I > I_{rel}$.
Curvees I, II, and III are for $I / I_{rel} = 10^3$, 10^4 , and 10^6 , respectively

This results have shown relativistic self-focusing lengths and critical power.

Recently the concept of fast ignition for inertial confinement fusion /18/ raised attention to the problem of magnetic field generation /19/, which may have a significant effect on the stability of a plasma channel dug by a laser pulse on the shape of the electron distribution function and other phenomena. Self-generated magnetic fields could also have an effect on laser beam propagation and on particle trajectories in laser wakefield and beat wave accelerators. One mechanism of magnetic field generation involves the vortex part of the ponderomotive force /20/. It is effective if the gradien of plasma density is not colliniar with the gradient of laser beam intensity. This situation is common in an overdense plasma and ponderomotive plasma density /21/. It can also work in an underdense inhomogeneous plasma for the amplitude modulated laser beam /19/.Another mechanism for the magnetic field generation that can operare in homogeneous plasma has been discussed in /22, 18/. It is related to the inverse Faraday effect /23, 24/ induced by a circularly polarized laser pule in underdense plasmas. The high-frequency electron motion in the laser field should be treated relativistically, but we may neglect the effect of low-frequency magnetic field on it assuming that $<B><<E_0$. The nonlinear electron current is

$$j_{NL} = -i\frac{e\omega_{pe}^{\ 2}}{16\pi m\omega_0^{\ 3}}\gamma^{-1}E_1 div(\gamma^{-1}E_1^{\ *}) + c.c. \quad (24)$$

In the relativistic case , $I \geq I_{rel}$, the magnetic field approaches the magnitude of $B \sim 1$, or in dimensional units

$$<B_z> \sim w_{pe}^{\ 2}mc/4ew_0 \quad (25)$$

The radial component of magnetic field, $<B_r>$, is $c\tau_0/r_0$ times smaller than the axial component. Acording to equation (25), in the relativistic limit the magnitude of magnetic field saturates at a level $<B_z> \approx 25n_e/\lambda_0 n_c$ MG, where λ_0 is in microns. For a laser wavelegth 0.35 μm and electron density $n_e \approx 10^{21}$ cm^{-3} this estimate predicts a magnietic field about 8 MG for the relativistic laser intensity of 10^{19} W/cm^2. For example, the gyroradius of relaativistic electron in the magnetic field of 10 MG is about 30 μm, which comparable to the characteristic radius of the laser pulse.

3. DISSIPATION OF LASER ENERGY IN PLASMA

With heating the plasma by pulse methods – the laser radiation, the beam of electrons - the energy originally is transfered langmuirts to fluctuations. Thus there is a condition with a high level of excitation langmuir of the waves - langmuir turbulece of plasma. A turbulence in continuous environments is divided on weak and strong /25/.

The weak turbulence /26/ describe by the kinetics to the equations for quasiparticle (langmuir plasmons), the kind of this equation is determined by the mechanism of interaction quasiparticles. Thus turbulence represents a superposition monochromatics of flat waves with various wave vectors, phase of these waves, to within the small members, random and statistically are independent. For laangmuir turbulence effect breaking weak turbulence a picture, is the effect of formation of areas of localization strong electrical RF- fields. From these areas of cavities or cavitons plasma is pushed

out by RF-pressure, so density of plasma in them is lowered. In result the RF-field appears closed in the field of lowered density. The level of energy of a RF-field in these areas can on some orders surpass average in volume. The RF-field is located in cavities, which initial scale has the order of length langmuir of a wave. Then the cavities fast are compressed, achieving the sizes several r_D, then because of strong attenuation Landau penetrated the RF-energy, made in them.

The theory strong turbuence (laangmuir) /27/ can be used for an explanation of the mechanism withouth scattering of absorption of a powerful electromagnetic wave in non-uniform plasma with research pulse of fusion reactions in plasma D-T, D $-^3$He etc. targets. Absorption of an electromagnetic wave and the plasmas basically are located in of a so-called critical point, in which the frequency of electromagnetic radiation, falling on plasma, coincides with plasma frequency wave. In this area the mechanism dissipation of energy of electromagnetic radiation in plasma is connected with turbulence plasma , ignition by an electromagnetic wave. The presence in a considered task two strongly of differing spatial scales – microscopic of scale plasma turbulence l_1 of the order debye of length r_D and macroscopic of scale l_2 length of an electromagnetic wave $2\pi c/w$ allows to break a task on two parts. The first part - theory plasma turbulence, created in scale turbulence of the electromagnetic pumping. The second part - distribution of an electromagnetic wave in environment with effective dielectric permeability by modified with the account turbulence. The equations for macroscopic of an electromagnetic field should be decided together with the hydrodynamical equations. Describing ablation of a plasma target, use of the concept effective dielectric constant essentially simplifies a task about absorption of electromagnetic radiation in turbulence to plasma, for the first time this concept was applied in work / 26, 27/.

4. KINETICS OF THE CHARGED PARTICLES IN PLASMA

Let's discuss an opportunity get over of difficulties, connected with perforce of use of extremely hot mixes and appreciable decrease of capacity of reaction, by transition to "target" to variant device, in which the reactions will occur between high energy $^3He^{++}$ and enough cooling by deuterium ions /28/ (in this case speed of DD-reaction is very small, that decides a problem radioactivity. With calculations nuclear energy extraction it is necessary to take into account the following basic reactions: D + ^{3}He $\rightarrow$ p(14.8) + α(3.67) + 18.35 Mev; D + D $\rightarrow$ 3He(0.82) + n(2.57) +3.27; D + D $\rightarrow$ T(1.0) + p(3.0) +4.0; D + T $\rightarrow$ α(3.5) + n(14.1) +17

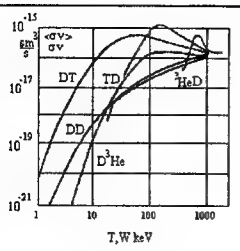

Fig.6. Average on to maxwwell distribution of speed of nuclear reactions and dependence of speed of reaction on energy of a beam with interaction of fast ions ^{3}He and tritium with cold deuterium (shaped curves) /28a/.

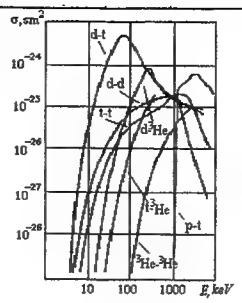

Fig.7. Dependence of section of reactions from tab. 1. from energy of reacting particles in system of centre of inertia /29/.

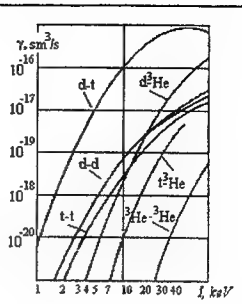

Fig.8. Dependence of speed of reaction <συ> on temperature maxwellian of plasma: 1 - d (d, ^{3}He) n; 2 - d (d, t) p.

The speeds of these reactions in maxwellian to plasma are shown in a fig.6; here is given (to the right above) dependence of size $\sigma_j\upsilon$ on energy of a fast ion ^{3}He in laboratory system of coordinates. It is visible, that the section sharply falls close W » 400 keV. The nuclear reactions proceeding in a mix protons, deuteriums, tritiums and ^{3}He are submitted in table1 /29/. At each reaction the power output (keV) is specified. As a result of reaction two particles will be formed, their energy is defined(determined) by the laws of preservation of energy and pulse. In this case energy of products (in system of centre of weights) is specified in table 1.

Tabl.1. Nuclear reactions in a mix p, d, t, ^{3}He,^{26}Al,^{26}Al^m, ^{27}Al, ^{25}Al, ^{24}Mg, ^{25}Mg, Mg, ^{27}Si.

T + D = α(3512) +n(14072) + 1790
D + T = ^{5}He(817) + γ +166632 = α + n + γ + 17590
D + D =T(1008) + p(3025) + 4033
D + D = 3He (817) +n(2452) + 3269
D + D = α + γ +23843
T + T = α + n + n +11332
T + T = ^{5}He (1729) + n(8645) + 103374 = α +n + n(8645) +11332
T + ^{3}He = D(9547) + α(4774) + 14321
T + ^{3}He = He(1856) + p(9282) +11138 = α + n + p(9282) +12096
T + ^{3}He = α +n + p + 12096
D + ^{3}He = p(14683) + α((3671) + 18354
D + ^{3}He = ^{5}Li + γ + 16384 = α + p + γ +18354
^{3}He + ^{3}He = p + p+ α + 12860
^{3}He + ^{3}He = ^{5}Li(1816) + p(9078) + 10894 = α + p + p(9078) +12860
^{3}He + n = p +T +784
D + p = ^{3}He + γ + 5494
T + p = ^{3}He +n –763
p + ^{24}Mg = ^{25}Al + γ + Q
^{25}Al → ^{25}Mg + e$^+$ + ν + Q
^{25}Mg + p = ^{26}Al^0 (^{26}Al^m) + γ + Q

$^{26}Al^{0} \rightarrow {}^{26}Mg + e^{+} + \nu + 1898$
$^{26}Al^{m} \rightarrow {}^{26}Mg + e^{+} + \nu + 1808$
$^{26}Al^{0} + p = {}^{27}Si + \gamma + Q$
$^{27}Si \rightarrow {}^{27}Al + e^{+} + \nu + Q$
$^{27}Al + p = {}^{28}Si + \gamma + Q$

The sections of reactions are known with good accuracy. With low values energy of reacting particles the size of section is determined by coulomb shielding of nucleuses, which energy $B=\tau Z_1 Z_2 (e^2/hc)(2\mu c^3)^{1/2}$, where m - given weight of reacting particles; Z_1, Z_2 - their charges. Therefore for the description of sections of reactions it is usual

$$\sigma(E) = \frac{S(E)}{E} \exp\left(-\frac{B}{\sqrt{E}}\right) \quad (28)$$

function S (E):

The function S (E) rather smooth, that allows to pick up uniform the functional approximation for the basic reactions of table 1:

$$S(E) = S_0 \frac{1 + a(E - E_0) + b(E - E_0)^2}{1 + c(E - E_0)^2} \quad (29)$$

In a fig.7. the dependences of sections of reactions of table1. in system of centre of weights received with the help of the formulas (28) and (29) are shown. In a fig.8. the dependences the rates of reactions from temperature of ions the maxwellian plasma for some reactions from table 1 are shown. The part of reactions goes with formation of γ-radiation. The experimental measurements have shown, that sections of the channel of reactions with formation of γ-quantums is insignificant and makes of 10^{-4}-10^{-7} complete sections of reaction.

5. EQUIPMENT, INSTRUMENTS, METHODS.

When the energy of a guided particle (ion, atom, molecule) exceeds energy of rest of the partner on interaction, a large part of energy to be spent for a movement of general centre of inertia of both particles and only small share on their relative movement. All processes occur in system of centre of inertia; a movement of system as whole, in a task do not enter. To not have ssuch a transition from laboratory of coordinate frame in system of centre of inertia, an idea involuntarily arises to combine these systems, by directing particles of a particle towards each other with equal pulses. Thus even in nonralativistic case for two identical the energy of particle interaction appears twice greater. With occurrence relativistic case the effect sharply grows, giving the following relation:

$$E_{lab} = \frac{2E^2}{mc^2}$$

Where - E_{lab} and E - energy of a particle in laboratory to system of coordinates and in system of centre of inertia, accordingly, and mc^2 - its energy of rest.

It is the fast-ignitor consept for for laser nucleasynthesis of radioactive isotops and isomers in Mg-Al-ccycle.

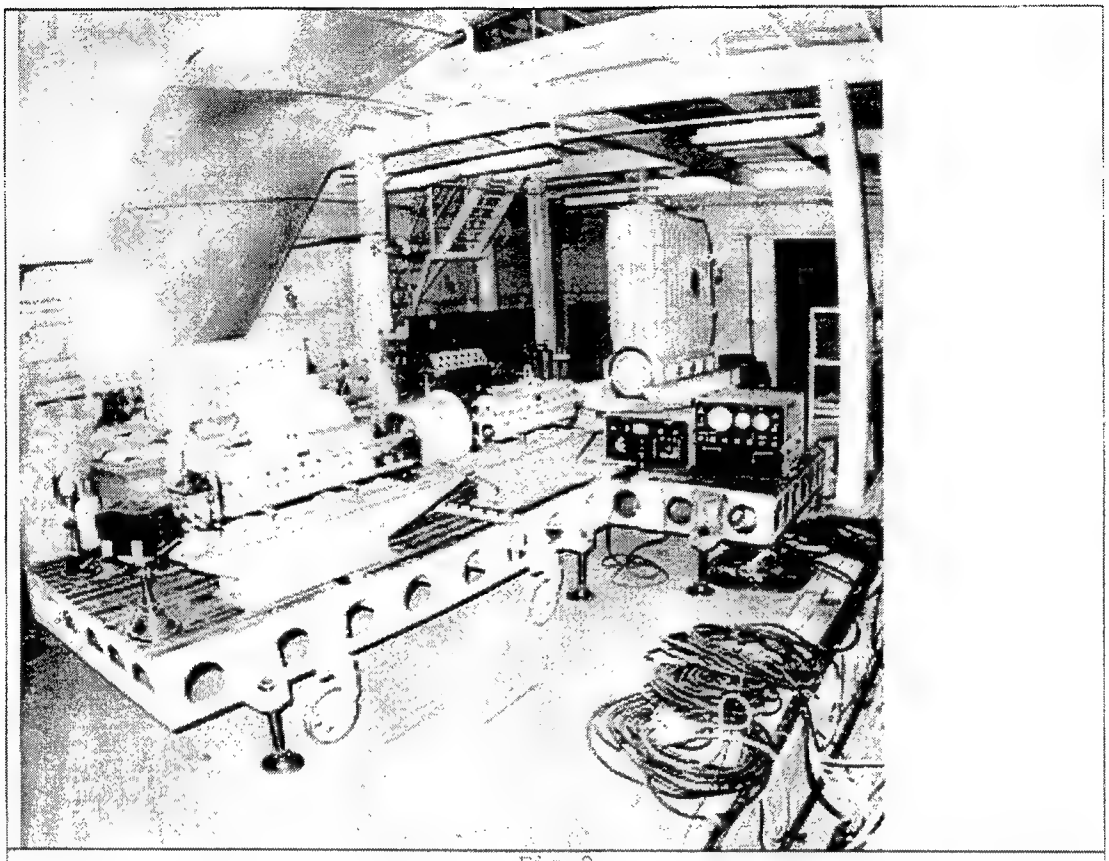

Fig.9

The system was composed of three stage: high repetition-rate discharge generator and first amplifier, second is the wide-aperture discharge with x-ray gun preionizer amplifier, and two crossed electron-beam-pumped lasers (fig.9). The investigation were carried out with a UV-preionized self-sustained discharge laser of ELI series 96. The length of active medium was 65 cm, the distance between electrodes was 2,2 cm. Ratio of buffer volume and active volume was 103. Second had a 15×15 cm aperture 1-m-long discharge chamber with a x-ray gun preionizer. Electron beams with energy (1-2.0 MeV) and current (150-380 kA) are required for the pumping of large laser volumes (0.25×0.25×1 m^3). with these consticted currents it is impossible to ignore of the azimutal self-magnetic field of beam on the electron motion that may lead in the beam self-focusing diode.

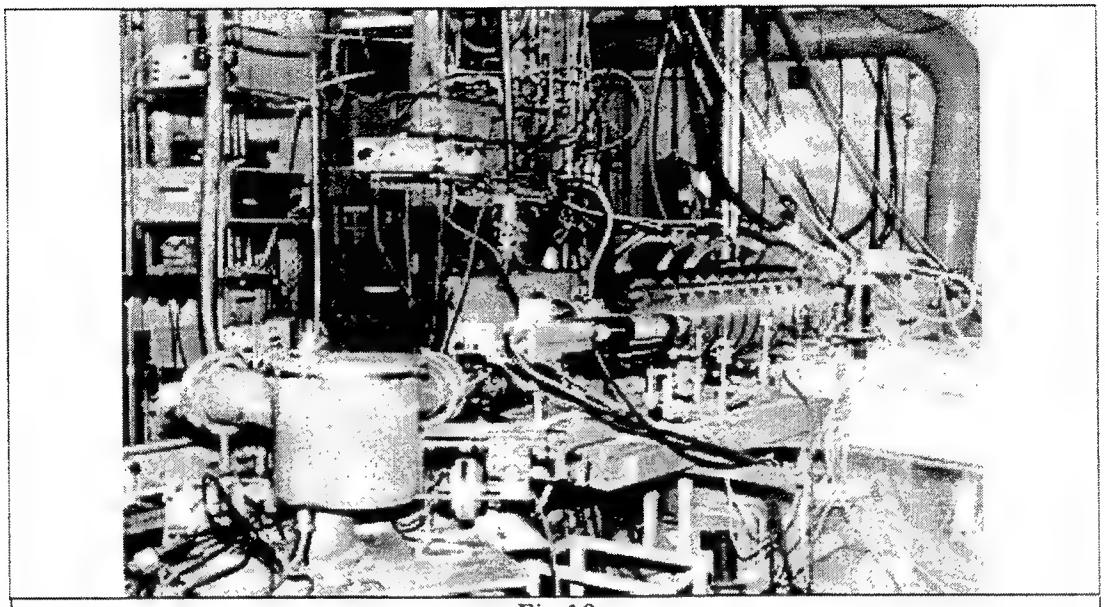

Fig.10

A compact plant (fig.10) (λ - geometry) with parameters: electron beam current 100-150 kA (current density 300-1000 A/cm2), electrons kinetic energy 0.3-0.8 MeV, beam energy 300-1500 J, pulse duration 30 ns, guade masgnetic field 2-10 kG, beam diameter 9 cm, cathod diameter 10 cm, cathode-anode gap 0.6 cm, laser chamber diameter 15 cm, its active length 150 cm have been made for search of control methods of electron beams with supercritical currents wich would be obtined during the laser volumes pumping by beam with apreture about 1 m^2 and more. THe high-density pyrographite were used as a cathode materials. Pyrographitic cathodes were made so that their layers were perpendicular to diode gap and also to power lines of magnetic and electric fields, applied to diode.

The materials of laser camera were selected in consideration of their stability in galogen medium for minimization of fluorine concentration decrease, and also in consideration of their chemical purity for impurities concentration reduction in laser camera, which were formed as a result of chemidesorption and UV stimulated desorbtion from the surface. It turned out possible for a number of materials to improve the surface properties by employment of flioro-polymer coatings. The method of mixture purification in the closed contour which were employed on the plant increased not only the laser mixture lifetime, but also improved essentially the surface condition of laser camera materials in particular while lasing on ArF molecule. The photocell with the oxiden-silver-caesiated photocathode (resolution of time is 0,3 ns) was employed for measurements of puls form. A lasing spectrum and an emission spectrum of plasma of discharge in He were registered by the crossed dispersion spectrograph (spectral range is 220-900 nm, inverse linear dispersion is from 0,4 nm/mm for UV region to 0,8 nm/mm for visible region). The registering of variation of transmission coefficient of laser emission in gas mixture out of discharge region was carried out by the optics elements and by the pyroelectric receiver.The registering of fluorine concentration variation in laser mixture was carried out by optic method through absorption of UV

radiation by molecular fluorine in region of 290 nm. An optical double-ray circuit with time successive registering of signals by one measuring channel was employed (sensitivity of method was 0,25 torr).

REFERENCES

1. H. Hora, *Physics of Laser Driven Plasmas*, Jon Wiley & Sons, New York, 1981
2. A. M. Prokhorov, et.al.Zh. Eksp. Teor. Fiz. **106,** pp.148-160,1994.
3. B. Mason, W.Melson, *The Lunar Rocks*, N-Y,L,S, Toronto, 1970.
4. B^2FH, C. Rolfs, W.S.Rodney, in *Nuclear Astrophysics,* ed. C. Barnes, D. Clayton, D. Schramm, CambUniv.Press, 1982.

4a. N.Gehhrels, and J. Paul, "The New Gamma-Ray Astronomy", Physics Today, pp.26- 32, Feb.1998.

5. E. G. Gamaly, "Ultrashort Powerful Laser Matter Inteeraction", Laser and Particle Beams, **12**,no.2,pp.185-208, 1994.
6. R. E. Kidder, et.al. *Physics of High Energy Density*.Proc of the Int.Schools of Phys."Enrico Fermi", Course XLVIII, eds. P. Caldirola, and H. Knoepfel, Academic Press, N-Y,London, 1971.
7. C. R. Phipps, and M. M. Michaelis, "LIPS: Laser Impuls Space Propulsion", Laser and Particle Beams, **12**, no.12,pp.23-54,1994.

7a. C. R. Phipps, et.al.,"ORION: Cleaning Near-Earth Space Debris Using a 20-kW, Earth-Based, Repetitively Laser, Laser and Particle Beams, **14**, no1,pp1-44,1996.

8. H. E. Bennet, J. D. G.Rather, and E. E.Montgomery IV,"Free-Electron Laser Power Beaming to Satellites at China Lake, California", Proc. SPIE, **2118,** pp135-155, 1994.
9. I. J. Bigio, et.al."MERCURY: a Second-Generation KrF Laser for Inertial Fusion Research", Proc.SPIE, **1810**, pp.405-409, 1992.
10. C. W. Allen, *Astrophysical Quantities*, Univ. Of London, TheAthlone Press,1873
11. L. V. Keldysh, " Ionization in the Field of a Strong Electromagnetic Wave", Zh. Eksp.Teor. Fiz., **49**, pp.1945-1957, 1964.
12. L.D. Landau & E. M. Lifshitz, *Electrodynemic of Continuous Media,* Pegamon,N-Y, 1960. E. M. Lifshitz, & L. P. Pitaevskii, *Physical Kinetic,* Pergamont, Oxford, 1981.
13. A. A. Andreev, et.al, "Heating of a Dense Plasma with an Ultrashort Laser Pulse in the Anomalous Skin-Effect Regime",Zh. Eksp. Teor. Fiz.**101**, pp1801-1826,1992.
14. M. Asthana, M. S. Sodha, & K. P. Maheshwri, " Nonlinear Relativistic Self-Focusing of Laser Radiation in Plasmas: Arbitrary Intensity", Laser and Particle Beams, **12**, no.4,pp.623-632, 1994.
15. S. A. Akhmanov,et.al. Sov. Phys.Usp. **10**, pp.809-689, 1968.
16. M. S. Sodha, et.al. *Self Fokusing of Laser Beam in Dielectrics, Plasmas and Semiconductors*. Tata McGraw-Hill Pabl.Co.Ltd, NewDelhi, 1974.
17. H. Hora in *Laser Interaction and Related Plasma Phenomena,* **3B,** eds. H. Schwarz, and H. Hora, Plenum Press, N-Y, p.803, 1974.
18. R. N. Tabak, et.al, Phys. Plasmas, **1**,p.1626, 1993

19. Y. Yu.Bychenkov & V. T. Tikhonchuk, "Magnetic Field Generation by Shrt Ultraintense Laser Pulse in Underdense Plasmas", Laser and Particle Beams, **14**,no.1 pp.55-62, 1996, R. N. Sudan,Phys. Rev. Lett. **70**, p.3075, 1993, V. K. Tripathi & C. S. Lu, Phys.Plasmas, **1**, p.990, 1994.
20. E. G. Gamaly Phys. Fluids, **B5**, p.3765, 1994.
21. S. C. Wilks, et.al.,Phys. Rev. Lett. **69**, p.1833, 1992
22. A. Sh.Abdulaev, et.al., JETP, **67**, p.507, 1988. S. Eliezer, et.al., Phys. Lett, A **164**, p.416, 1992.
23. R. N. Steiger, & C. H. Woods, Phys. Rev. A **45**, p.1467, 1972.
24. Yu. M. Aliev, et.al., *Non linear Theory of Strong Electromagnetic Wavw-Plasma Interactions,* ed. O. N. Krokhin, Nova Science Pablishers, p.55, 1993.
25. L. A. Arrtsimovich, & R. Z. Sagdeev, *Plasma Physics for Physics*, M. Atomizdat Pablishers, 1979, G. M. Zaslavskii, & R. Z. Sagdeev, *Introduction in Nonlinear Physics,* M. Nauka, 1988.
26. V. E. Zakharov, "Collaps and Self-Focusing Longmuir Wavw", in *Fundamentals of Plasma Physics*, eds.A. A. Galeev, & R. N. Sudan, M. Energoatomizdat, pp.79-117, 1994.
27. V. D. Shapiro, &V. I. Shevchenko, "StrongTurbulence of Plasma Oscilations", in *Fundamentals of Plasma Physics*, eds. A. A, Galeev, &R. N. Sudan, M. Energoatomizdat, pp.119-173, 1884.
28. B. A. Knyazev, & D. D. Ryutov, *Low-Radioactive Open-EndFusion Reactor*, Preprint 89-11,Budker Inst.Nuclear Phys. Russian Acad. Science, 1989
29. S. V. Putvinskii, "Alpha-Particles in Tokamaks",*Questions of Theory Plasmas,* ed. B.B Kadomzev, **18**, 1990.

Spectral projections for induced gamma emission from $^{178}Hf^{m2}$

Hilary E. Roberts

SRS Technologies, 500 Discovery Drive, Huntsville, Alabama 25803, USA

Abstract: Calculations of induced gamma emission (IGE) potential output spectra from the 178Hfm2 isomer are developed assuming three decay modes through the fast Yrast channel, the 78 ns channel and the 4 s channel. Temporal and energy distributions of energy are examined. These spectra are then compared to potential regions of interest for various uses with an emphasis on medical applications.

Key Words: nuclear isomers, induced gamma emission, quantum nucleonics, K-mixing, cobalt-60, cancer, irradiation

1. Introduction

It has been demonstrated by Collins[1] *et al.* that nuclear isomers in the region of mass 180 could be induced to emit the energy stored in isomeric states in the form of gamma radiation. This immediately leads to considerations for the possibility of achieving stimulated emission based upon such metastable isomeric states. We herein consider the potential spectral output of such induce gamma emission (IGE) for one particular isomer, $^{178}Hf^{m2}$, and evaluate estimates of the spectral content for potential applications[2] such as medical irradiation.

2. Background

The process involved in the experiments by Collins' team[3] was a class of photon scattering known as a (γ,γ') reaction. By adding an increment of energy, ΔE, carried by an incident photon to the excited nuclear isomeric state at energy E above the ground state, it was shown to be possible for certain nuclei to raise the energy of the nucleus to a state at an energy of $E + \Delta E$, from which instantaneous decay occurred with the emission of a gamma photon or suite of photons with a total energy of $E + \Delta E$. An excellent published review of the theory and experiment al basis to date was provided by Collins and Carroll[4] in their paper at the GRALAS'95 conference. This work is considered one of the key foundations for a field of study now known as Quantum Nucleonics.[5]

The break through experiment was performed by Collins *et al.* with $^{180}Ta^{m}$. This isomer is the only naturally abundant isomer, with a half-life on the order of 10^{15} years. The long half-life is attributed to the large nuclear spin in combination with the deformation of the nucleus, and the relatively low isomer energy level. The projection of spin on the nuclear symmetry axis requires the deformation quantum number in addition to the usual set of principal, spin, and rotation quantum numbers. This additional quantum number is denoted as K. In general, transitions that require changes in K>1 are strongly forbidden. The $^{180}Ta^{m}$ isomer carries eight units of K, while the ground state is in the usual K=0 state. This large K value, coupled with a large ΔE requirement ($\Delta E >> E$), conspire to provide an unusually long persistence for $^{180}Ta^{m}$.

More recently it has been shown that many isomeric isotopes in the region of mass 180 exhibit similar behavior.[6-9] (This region is nearly mid-way between two magic numbers. In this region nuclides exhibit some of the largest quadrupole moments in the range of +0.4. This indicates a strong assymetry from nuclear sphericity for nuclear systems in this region.) The systematics experiments reported in the literature have shown that the total energy $E + \Delta E$ for the isomer and input photon is in

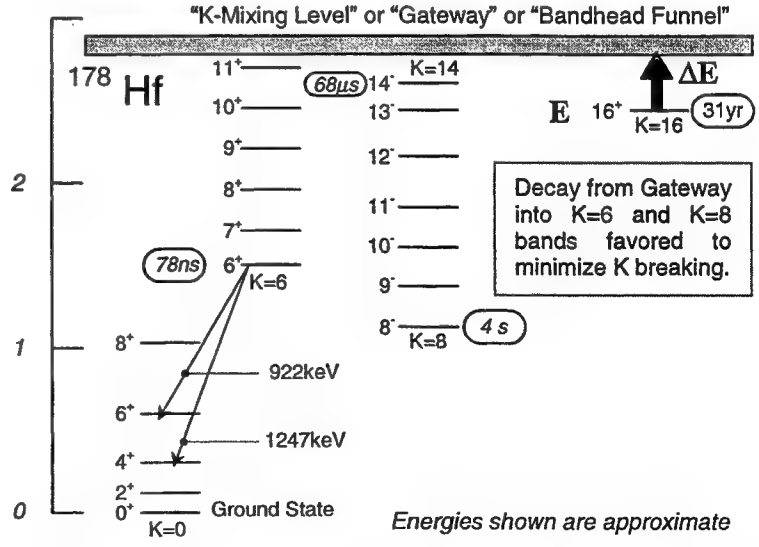

Figure 1: Energy levels for 178Hf shows richness of states conducive to producing a rich cascade spectra from 16+ to ground.

the range of 2.5 to 3 MeV. Typically, with the exception of the aforementioned Ta isomer, isomers in the mass-180 region have relatively short half-lifes on the order of seconds or less. However, there is an isomer in this mass region that is unique: $^{178}Hf^{m2}$ has a moderate half-life of 31 years.

An energy state diagram for ^{178}Hf is shown **in Figure 1.** The m2 isomer state resides at 2.45 MeV and carries sixteen units of K. This arises from a 4-quasi-particle model wherein both a 7/2[514] state and a 9/2[624] state are occupied by unpaired neutrons and similarly by unpaired protons. The unpaired neutrons bring J=9/2 + 7/2= 16/2 of angular momentum. Likewise the unpaired protons bring 16/2 of angular momentum, for a total angular momemtum of 16, all with positive parity. This results in the K=16 band-head for the m2 isomer level. The occurrence of the K=6, K=8, K=14 and other rotational band-heads can be accounted for in similar fashion. Rotational bands are built up from the J=K band-head in units of J=K+1, K+2, etc., where K>0. For K=0, the J's are restricted to even values. As will be seen later, at some energies there can arise a substantial crossing and potential mixing of states as rotational levels of J above any given band-head become matched in energies.

Such a large value of K=16 would ordinarily lead to the expectation that any transitions from the m2 isomer state would be strongly forbidden. The long half-life fits in well with that expectation. However, notice that ^{178}Hf also has a K=8 isomer level, denoted as m1. The m1 isomer has a half-life of four seconds. While this is long for ordinary nuclear states, it raises a question. Why is its half-life so short in comparison to that for ^{180}Ta, which also has a K=8 for the isomer state, with a 10^{15} year half-life. One possible explanation is that there may also exist for this hafnium isotope a nearby state above the K=16 level in the vicinity of 2.5 MeV which allows for transitions back to the ground state. This is variously referred to as a K-mixing state, or a gateway, or a band-head funnel.

Such K-mixing states have been inferred for other isomers in the mass-180 region. This gateway in other isomers appears to be relatively broad, on the order of half an eV. This is enormous in comparison to typical nuclear states which are on the order of a μeV in width, with correspondingly short lifetimes of 10^{-18} seconds or less. One feature of the gateway is apparently its ability to allow for a mixing of K-states within a narrow energy range. Consequently this is also referred to as a K-mixing level. K is not considered a strong quantum number, meaning that transitions of K>1 are not probable and greatly enhance the life time of the associated nuclear state, but that K breaking does indeed occur. As it must, to allow for any decays to ground from these states. At least as far back as 1962, it was known that the assymetries of deformed nuclei generate a very much more complex state level situation.[10] Shown in **Figure 2** are curves produced by Mottelson and Nielson, using their unify theory, for proton states as a function of deformation.[11, 12] It is readily apparent that larger deformations lead to situations where energy levels cross and hence where significant mixing of states as a function of deformation could occur at certain energies. As can be seen from these curves, at

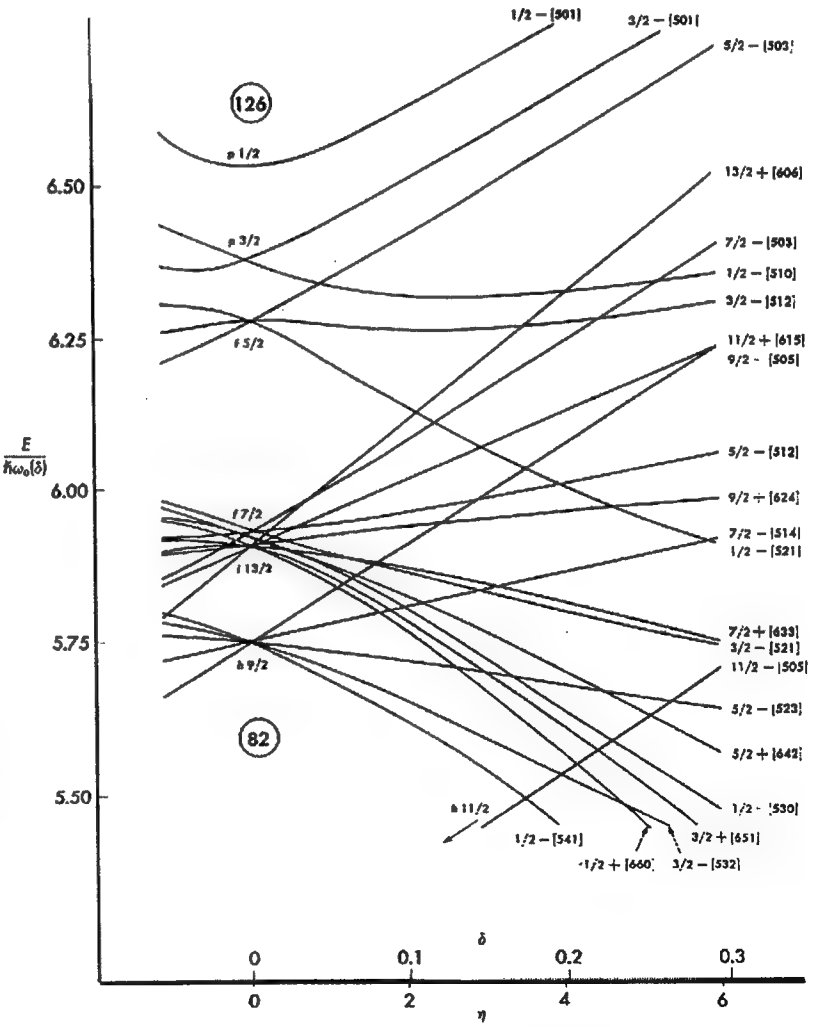

Figure 2: State levels for protons in region between 82 and 126 magic numbers. After Mottelson and Nielson.

deformations of about 0.2 significant state mixings can occur in the energy range of between 2.5 to 3 MeV. Davydov[13, 14] *et al.* have likewise shown via calculated state coefficients that K-mixing occurs in the states of nuclei without axial symmetry, as noted by Preston.

If such a mixing state occurs in $^{178}Hf^{m2}$ in the energy regime of between 2.5 to 3 MeV, upward transitions with a modest energy difference from the isomer level at 2.45 MeV to the gateway could account for the shortened lifetime from such a high K state in comparison to ^{180}Ta. The closer in energy that the mixing region lies to the isomer level, the more the half-life would be expected to be reduced. A 31 year half-life for $^{178}Hf^{m2}$ K=16, compared to a 10^{15} year half-life for $^{180}Ta^{m}$ K=8 indicates, at least heuristically, that such a mixing level might lie very close above the isomer level. Similarly the presence of such a gateway state immediately leads to a possibility for pumping the 16+ isomeric state up to the gateway which would result in a cascade of photons back to the ground state. Such a presumed cascade is the basis for the spectral projection of this analysis.

Notice in Figure 1 that in addition to the 16+ isomeric state, this isotope also exhibits rotational bands built upon K=6 and K=8 (and other not shown) states. Because rotational states are by definition orthogonal to the symmetry axis which defines K, higher rotation states of J at a given K do not add to the K value. These rotation states may connect in a band of states with the K-mixing state. Consequently downward transitions from the mixing state into these rotational bands with intermediate values of K allow for multiple pathways back to the ground state. Upon reaching the band-heads at the 6+ or 8- states, the nucleus decays from these isomer states with the characteristic life-time for those states, 78 ns and 4 s, respectively. The ratio of decays that feed into the K=6 and K=8 is undetermined at this time. Simple comparison of the K values would lead to an expectation that the K=8 band would be favored over the K=6 band. Also, it should be noted that the gateway shown is only the lowest of several such expected gateways at ever increasing energies. The ever increasing complexity of the level crossings as a function of deformation shown in Figure 2 is the basis for the expectation of such multiple gateways at ever-increasing energies.

The verification of this type of process and the actual trigger energy required to initiate induced gamma emission in $178Hf^{m2}$ has been the subject of ongoing experiments at the *Institut National de Physique Nucléaire et de Physique des Particles* and *Center de Spectromètrie Nucléaire et de Spectromètrie de Masse*, Orsay Campus, by Briançon[15] *et al.* These experiments were discussed at the ICIGE97 conference by Briançon. The data is still under analysis by her team. Expectations for a reasonable trigger energy range from a few tens of KeV up to the order of 0.3 MeV (or possibly somewhat higher).

Assuming that such K-mixing transitions can be shown to occur for this isomer, as have been shown to occur in isomers of similar mass, it becomes of interest to consider what the output spectrum of such an emission process would be. As can be seen from Figure 1, most of the transitions down the rotation bands are on the order of a few hundred KeV. However, the transitions from the 6+ state to the Yrast (K=0) band should be on the order of 1 MeV. This is in the range of emission from ^{60}Co sources. Hence, such emissions from Hf may be useful in application processes that employ cobalt as a radiation source.

3. Spectral Projections for Induced Gamma Emission of $^{178}Hf^{m2}$

The potential transitions from the 16+ state through the 8- band are shown in **Table 1**. The numbers in bold are the accepted energies for the m1 and m2 isomeric states as reported in standard references such as the CRC Handbook.[16] As can be seen from Figure 1, decays from both 8- and 6+ will decay through the same series of transitions for the last three steps of the cascade to ground. Likewise, an m2 decay from the 16+ state through the K=8 band would likely lead to populating the 4s m1 state. Hence, m1 and m2 decays should share the same set of decays that arise from m1 only decays. Inspection of Table 1 shows that this seems to be the case. The 574 KeV line corresponds to a 13-,11- transition and the 258 KeV line corresponds to a 11-,10- transition. There remains the need for transitions from the 10- state down to the metastable m1 8- state. There should be corresponding transitions noted for this step as well. However, the reported CRC data do not seem to be able to resolve these transitions. The last four steps of the cascade from the 8-,0+ are reported identically for both m1 and m2 transitions. This is consistent with the expectations arising from Figure 1. Similarly, **Table 2** shows the potential transitions via a cascade through the 78 ns K=6 channel.

16+ to 8-	**1298**
16+, 13-	13
16+,12-	309
14-,13-	140
14-,12-	437
13-,12-	296
13-,11-	**574**
12-,11-	278
11-,9-	495
11-,10-	**258**
12-,10-	536
10-,9-	237
10-,8-	454
9-,8-	217
8- to Grd	**1147**
8-,8+	88
8-,6+	427
6+,4+	**325**
4+,2+	**214**
2+,0+	**93**

Table 1: K=16 via K=8 transitions

The gateways reportedly observed in the mass-180 systematics do not exhibit a measurable life time. In Tables 1 and 2, the upper series of decay transitions corresponds to emissions above the intermediate metastable states at the 6+ and 8- states. These emissions are therefore expected to occur promptly upon triggering a decay from the 16+ m2 isomer state through the gateway. The lower series of decay transitions in Table 1 correspond to delayed transitions which will exhibit the characteristic decay time for the 8- and 6+ states, 4 s and 78 ns, respectively. Thus the expected emission spectrum from pumping the 16+ state will have both an energetic distribution as well as a temporal distribution. The temporal nature of the emission spectrum is important to understand. It is a critical factor in the design of experimental schemes to detect and discriminate induced isomer emission from incipient spontaneous m1 and m2 isomer decays. It also allows the possibility of achieving a significant population of an excited state with a short lifetime of 78 ns. This makes this isomer of particular interest as a system for gamma ray lasing. However, there are other applications where the population of even the 4 second state is very useful. In particular medical applications and other industrial applications would not necessarily be highly sensitive to an energy hang up with a 4 second half-life.

16+ to 6+	**895**
9+,8+	~250
9+,7+	~500
8+,7+	~250
8+,6+	~400
7+,6+	~150
6+ to Grd	**1550**
6+,6+	922
6+,4+	1247
6+,4+	325
4+,2+	214
2+,0+	93

Table 2: K=16 via K=6 transitions

A projected spectrum of the energy distribution arising from 16+ decays through the 4 second channel is shown in **Figure 3**. The relative intensities shown are based on zeroth-order transition probabilities derived from the multipolarities and minimum energy change. In the K=8 and K=6 bands, $\Delta J=1$ transitions are expected to decay by M1 radiations, and $\Delta J=2$ by E2 transitions. The relative transition rates are taken arbitrarily in the ratio M1/E2 = 2 to estimate the line intensities. The solid lines are the expected prompt emission arising from the 16+ state feeding the K=8 band via the K=mixing level. The dashed lines are the delayed emissions arising from decays out of the 8- m1 state to ground. This analysis is expected to be refined to in future calculations using more rigorous transition probability calculations, but these should be adequate for comparison to preliminary experimental data that may soon be available from Collins.

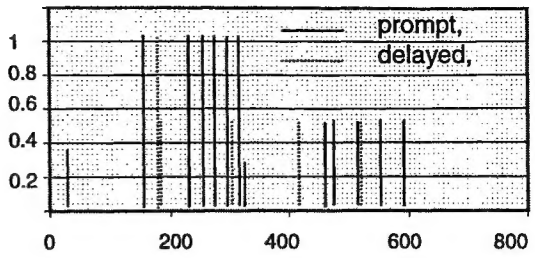

Figure 3: Estimated relative spectral output via 4 s channel to ground for $^{178}Hf^{m2}$.

A similar analysis was used to project the spectral characteristics for emissions feeding the 78 ns channel via 16+ transitions through the gateway down through the K=6 band of rotational states. The projected spectral lines are shown in **Figure 4**. Notice that emission through this channel will be expected to produce two lines in the region of 1 MeV.

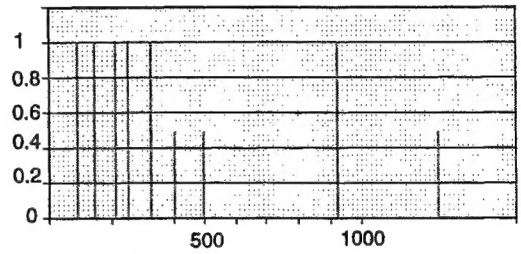

Figure 4: Estimated relative spectral output via 78 ns channel to ground for $^{178}Hf^{m2}$.

The combined emission from the K=8 and K=6 band decays is shown in **Figure 5**. Notice the rich density of lines in the low energy region below 0.5 MeV. Also note that if any of the K=6 band is populated via K=mixing from the K=16 band, there will be at least one line in the region of 1 MeV. From an applications perspective this is the best of both worlds: low energy emission leading to large energy transfers to absorbing media, and higher energy emission leading to higher penetration of the gamma photons before absorption. Also shown for

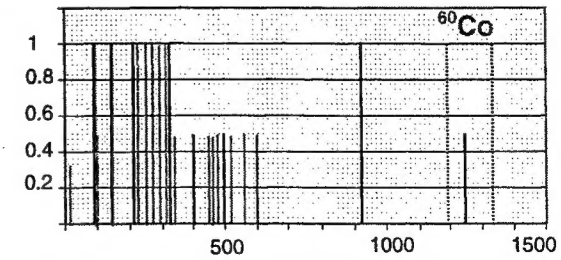

Figure 5: Combined estimates of spectral output via 4 s and 78 ns channels to ground for $^{178}Hf^{m2}$. Comparison to ^{60}Co lines also shown.

comparison on Figure 5 are the two gamma lines (dashed) from a ^{60}Co source.

Now to briefly consider one potential application for the projected spectrum from induced gamma emission for this hafnium isomer.

4. Illustration of a Medical Application for Induced Gamma Emission

Typically medical irradiations use a cobalt source or radiation produced in an accelerator. 60Co has a half-live of 5.27 years and an activity of about 1100 Ci /g. In comparison the hafnium m2 isomer has an activity due to spontaneous emission about 17 times less due to its greater mass density and longer half-life. In addition the isomer emission is of substantially lower energy which means it will absorbed much more readily by tissue and be shielded with significantly less mass. The attenuation coefficient for 0.3 MeV emission into water is about 0.1 whereas the attenuation coefficient at 1.3 MeV is about 0.65.

Because of the reasonable expectation that the isomer can be induced to emit a spectrum of gamma energy that will to some degree resemble that shown in Figure 5, it is instructive to visualize how that might be used in a medical application. In the treatment of cancer, doses in the range of a few tens of Grays (1 Gray = J/kg) are typical. For sterilization of medical equipment and as a bacteriacide, typical doses range from a few to a hundred kGray.

A one gram source of hafnium isomer contains about 1GJ of energy. As is readily apparent, release of even a small fraction of this energy via induced gamma emission would be more than adequate to achieve typical dosages for medical applications. Furthermore, unlike 60Co, the isomer source is able to modulate from its low incipient decay rate to a rate controlled by the trigger source flux. There is a standard methods of treating tumorous cancers wherein a small gamma sources, called seeds, are surgically placed into the cancerous tissue. This delivers the dose directly into the needed tissue with the highest energy density occurring in the diseased tissue and falling off in intensity as other body tissue is encountered. If hafnium isomer were used as such seeds, a low energy x-ray source external to the patient could "turn on" the induced emission from isomer seeds for the desired dosage, then turn off the induced emission. Because of the exceptionally high energy density stored in the hafnium isomer, very much smaller seeds could be used for implantation than is currently feasible. This is just an illustration of some of the potential uses that can be envisioned for induced gamma emission (IGE) should such prove feasible.

5. References

1 C. B. Collins, C. D. Eberhard, J. W. Glesener, J. A. Anderson, Phys. Rev. C **37**, 2267, 1988.

2 H. Roberts, Hyperfine Interactions **107**, 9, 1997.

3 C. B. Collins, J. J. Carroll, T. W. Sinor, M. J. Byrd, d. G. Richmond, K. N. Taylor, M. Huber, N. Huxel, P. von Neumann-Cosel, A Richter, C. Spieler, W. Zeigler, Phys. Rev. C **42**, 1813, 1990.

4 C. B. Collins, J. J. Carroll, Hyperfine Interactions **107**, 3, 1997.

5 L. A. Rivlin, C. B. Collins, J Laser Phys., **6**, 617, 1996.

6 C. B. Collins, J. J. Carroll, T. W. Sinor et al., Phys. Rev C **42** , R1813, 1990.

7 J. J. Carroll, M. J. Byrd, D. G. Richmond et al., Phys. Rev. C **43**, 1238, 1991.

8 C. B. Collins, T. W. Sinor, , D. G. Richmond, Phys. Rev. C **43** (1991) 879.

9 J. J. Carroll, C. B. Collins, K Heyde et al., Phys. Rev C **48** (1993) 2238.

10 M. A. Preston, *Physics of the Nucleus* (Addison-Wesley, Reading, MA, 1962) 240-248.

11 S. G. Nielson, *K. Danske Vidensk. Selsk. mat.-fus. Medd.*, **16**, 29, 1955.

12 B. R. Mottelson, S. G. Nielson, *K. Danske Vidensk. Selsk. mat.-fus. skr.*, **8** 1, 1959.

13 A. S. Davydov, G. F. Fillipov, Nuclear Phys. **8**, 237 1958.

14 A. S. Davydov, V. S. Rostovsky, Nuclear Phys. **12**, 58 1959.

15 Ch. Braincon, *Physics with the 178m2Hf high-spin isomer, presented at International Commission on Induced Gamma Emission*, Technical Digest, 1997, final paper as yet unpublished.

16 N. E. Holden, Handbook of Chemistry and Physics, 74th Edition, ed. D. L. Lide (CRC Press, Boca Raton, FL, 1993) 11-104.

Author Index